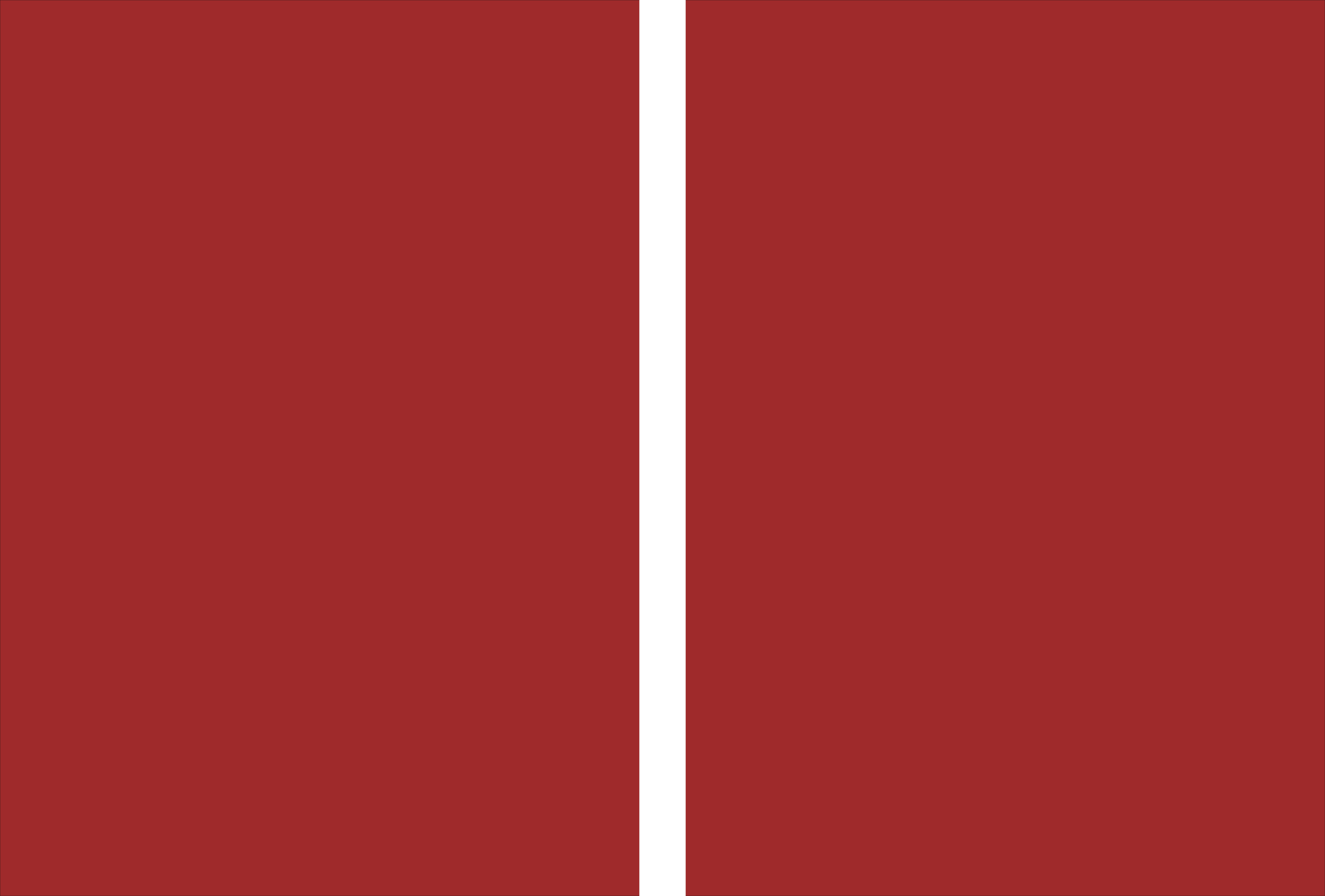**Universidade do Minho**
Escola de Engenharia

Ana Carina Loureiro Mendes

Innovative self-assembled and microfabricated structures to be used in distinct biomedical applications
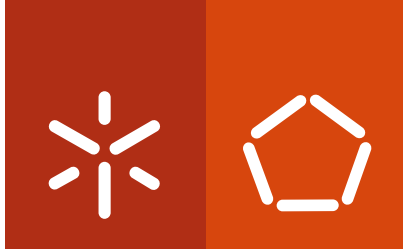
Julho de 2012

Universidade do Minho

Escola de Engenharia

Ana Carina Loureiro Mendes

Innovative self-assembled and microfabricated structures to be used in distinct biomedical applications

Programa Doutoral em Engenharia Biomédica

Trabalho realizado sob a orientação do
Professor Rui Luís Gonçalves dos Reis
e da
Doutora Helena Paula de Sousa Sepúlveda Azevedo

Julho de 2012

TO MY PARENTS

Four years and plenty of intense moments have passed. These have been shared with all those who made this dissertation possible and without whom the following 235 pages would not have come to be. As such, I would like to express my deepest gratitude towards them.

First of all, I would like to thank my supervisor, Prof. Rui Reis, the director of the 3B's Research Group, for giving me the opportunity to be part of his dynamic, international and innovative laboratory as well as for his support on providing me the tools and means to pursue my research; for allowing me to participate in international conferences/courses, the possibility to collect important scientific experience abroad. Thank you for all the experiences I wouldn't have had if I had been assigned to another laboratory.

I am also grateful to my co-supervisor Dr Helena Azevedo, for the valuable discussions about the scientific work; for teaching me about the peptide synthesis and other relevant topics; for providing me with the opportunities to participate in relevant conferences (Gordon and Nature) which proved to be memorable scientific experiences; for creating the opportunity to go to The Nanotechnology Platform Lab in Barcelona and to put so much effort in the correction of the papers and thesis.

I am greatly thankful to Dr Erkan Baran, besides being one of the main mentors of this thesis, he is also a friend. Thank you very much Erkan for extending your hand whenever I was in need of it. Thanks to you I am now able to say that I was a fortunate PhD student to have the opportunity to deal with such a creative, innovative and hard-working scientific mind that brought to me new perspectives and scientific knowledge. For all of that I am deeply grateful.

My gratitude is also extended to Dr Alvaro Mata, for allowing me to work at The Nanotechnology Platform Lab and to guide all the work in such a passionate way. His enthusiasm and strength have certainly increased my motivation to constantly give the best of myself in achieving the main goals as well as providing the opportunity to build distinct work methodologies.

To my dear colleagues and friends of 3B's world-wide, a special thanks for all of the support and good moments spent together. Although not cited here (since there are so many names that

would have deserved to be), everyone contributed in his or her own way to this long journey in 3B´s and for all of that I am truly grateful. To the members of the "Clube Alegria no Coração", thank you for the laughs, advice, support and friendship shared specially during these last months.

Barcelona is where I spent the last year of this PhD and for this reason it also deserves mention. To my dear friends and colleagues from The Nanotechnology Platform Lab: muchísimas gracias por todo! It was a pleasure to have the opportunity to meet you all. I would also like to thank Daniel and Bea for all the support and friendship in C/Saint Pére Mes Baix, to Sergio for the interesting walks from Gracia to Urquinaona and finally to Juan J. for all the patience and good times spent together.

I am greatly thankful to all the people who shared my life beyond the research during my stay in the Minho region. Starting with my "international" friends in Guimarães, the ones from the theatre groups (TIT and CETE), namely Ana Rosa, Elisabete, Isabel and Rita, for the crazy conversations that made me laugh so many times; to Antonio for the longest conversations and philosophic discussions about life and points of view; to Pedro for the sharing of distinct interests in such a enthusiastic way, for every 3 Km running and guitar chords played during this period. Thanks to my dearest Vitor, my human diary over the last two years of this PhD and finally to Analuce for something that I consider a strong friendship.

Many thanks to my dear and good friends Nádia, Tânia, Salomé, Rita, Gariso, Inês, Ana Filipa, Manel, Ana Frangolho, Paula, Saul, Gabriel, and many others (you know who you are) whom have been following my long way and supported me in every moment of need in your own special way.

To my Family,

Como não poderia deixar de ser, as minhas últimas palavras de agradecimento são dirigidas às pessoas que sustentam a minha vivacidade, que sempre me apoiaram incondicionalmente e que seguramente são os que mais compartilharam de cada emoção vivida ao longo deste percurso. Por isso um infindável obrigado ao Miguel e à Matilde, os meus melhores amigos mais jovens. Decididamente todo o entusiasmo e admiração pela tia Ni contribuiram desde sempre para minha motivação, força e avanço. Ao Pedro e à minha querida Né, cujo o âmago, força de carácter sempre me acompanharam e me valeram.

E por último ao Fernando e à Adília, cujas palavras são insuficientes para expressar a minha imensa gratidão por ter uns pais como vocês!

INNOVATIVE SELF-ASSEMBLED AND MICROFABRICATED STRUCTURES TO BE USED IN DISTINCT BIOMEDICAL APPLICATIONS

ABSTRACT

Advances in self-assembly offer new opportunities in molecular design of biomaterials. A major advantage of these systems is their ability to generate similar fibrillar structures to those found in the natural extracellular matrix (ECM) of tissues and to integrate directly into their structure biomolecular ligands for cell signalling. On the other hand, the integration of self-assembly into existing microtechnologies could offer new possibilities to fabricate hierarchical materials with high levels of precision and reproducibility. Therefore, the overall goal of the work presented in this thesis was to develop novel biomaterial systems (microcapsules and membranes) for encapsulation and culture of cells by exploring self-assembly and microfabrication techniques. Towards this goal, this PhD work investigated the application of xanthan gum, an anionic extracellular polysaccharide produced by the bacterium *Xanthomonas campestris*, as potential cell encapsulation matrix, as this polysaccharide remains largely unexplored in this regard. In one first attempt, xanthan was carboxymethylated and the microcapsules were generated by simple ionic crosslinking. To generate stable microcapsules by self-assembly, efforts were made to synthesize xanthan derivatives by conjugation with hydrophobic molecules (palmitoyl and phospholipid) or by combination with multidomain peptides of opposite charge.

A second objective of this PhD work was to produce microcapsules with homogeneous size distribution and micrometer size favorable for mass transfer and easy injects for cell therapy. Different devices (microdroplet generator and microfluidics) and methods (ionic crosslinking, self-assembly) were developed to prepare xanthan-based microcapsules. The microstructure (morphology, molecular organization) and properties (size, membrane thickness, permeability, stability) of the developed microcapsules were investigated in detail.

Using a new microdroplet generator, microcapsules of ionic crosslinked carboxymethylated xanthan (chapter III) and self-assembled palmitoyl xanthan (chapter IV) were generated with an average diameter of 500 and 576 µm, respectively. The self-assembly of phospholipid-xanthan (chapter V) and native xanthan with a positively charged multidomain peptide (chapter VI) was guided in microfluidic device to obtain stable capsular structures with regular spherical shape and controlled size at the microscale. The results of these studies showed that the properties of the developed microcapsules could be easily controlled by manipulating the concentration of

building blocks and assembling conditions. Moreover, capsule forming devices were successful used to guide the formation of capsular structures.

Cell encapsulation experiments were also conducted to corroborate the initial hypothesis. ATDC5 cells (a murine chondrocytic cell line) encapsulated into the developed xanthan based microcapsules remained viable and were observed to proliferate for prolonged culture periods (up to 3 weeks) with enhanced metabolic activity.

In summary, these studies suggested that xanthan polysaccharide can be an alternative to the current cell encapsulating materials but *in vivo* studies are necessary to validate this hypothesis. Additionally, the combination of self-assembly with micro-fabrication techniques demonstrated to be an innovative approach for the fabrication of microcapsules in cell-friendly conditions with controlled properties.

In a distinct work, molecular self-assembly was combined with soft lithography to fabricate patterned self-supporting membranes in a single-step process (chapter VII). A positively charged multi-domain peptide (with or without the cell-adhesive sequence RGDS) was used to self-assemble with the anionic ECM polymer hyaluronic acid. The assembling conditions were optimized to realize membranes with well-controlled properties, including membrane thickness, bioactive epitope availability, and topographical pattern morphology. The resulting self-assembled membranes exhibited a hierarchical structure of nanofibers and surface microtopographies with various densities of RGDS. Rat bone marrow stem cells were shown to recognize the RGDS sequence and the topographical patterns, varying their morphology depending on the concentration of binding motif or specific physical features that were cultured on.

The studies reported in this thesis proved that combining self-assembling materials with microfabrication technologies can be an effective approach to fabricate microcapsules and membranes with increased level of control over their structure, shape, bioactivity and overall performance. The versatility of the combined bottom-up and top-down fabrication processes described here may permit the development of novel hierarchical biomaterials with precise biomolecular and physical properties and the opportunity to better tune them with spatio-temporal control.

AUTO-ORGANIZAÇÃO MOLECULAR E MICRO-FABRICAÇÃO DE ESTRUTURAS INOVADORAS PARA APLICAÇÕES BIOMÉDICAS DISTINTAS

RESUMO

Avanços em química supramolecular têm vindo a constituir novas oportunidades na formulação de novos biomateriais. A grande vantagem destes sistemas é a sua capacidade para gerar estruturas fibrilares semelhantes às existentes na matriz extra-celular dos tecidos e a possibilidade de integração na sua estrutura de grupos bioactivos para interacção celular. Por outro lado, a integração destes processos de auto-organização molecular nas micro-tecnologias existentes possibilita o fabrico de materais hierarquicamente organizados com elevados níveis de precisão e reprodutibilidade. Por consequinte, o trabalho apresentado nesta tese teve como objectivo principal desenvolver novos sistemas de biomateriais (microcápsulas e membranas) para encapsulamento e cultura de células através de técnicas de auto-organização molecular e micro-fabricação. Neste doutoramento investigou-se também a aplicação da goma xanthan, um polissacarídeo poli-aniónico produzido pela bacteria *Xanthomonas campestris*, como potencial matriz para encapsulamento de células. Numa primeira abordagem, o xanthan foi carboximetilado e as microcápsulas geradas por reticulação iónica deste composto. A geração de micro-cápsulas por auto-organização molecular foi conseguida pela síntese de derivados do xanthan pela conjugação de moléculas hidrofóbicas (palmitoil e fosfolípido) através da combinação do xanthan com péptidos com capacidade de auto-organização de carga oposta.

Um outro objectivo deste trabalho, consistiu na produção de cápsulas à escala micrométrica com uma distribuição de tamanhos uniforme, favorável a transferências de massa e facilidade de injecção em terapias celulares. Para tal, foram desenvolvidos dispositivos para fabrico de microcápsulas (gerador de microcápsulas e micro-fluidicos) e métodos químicos (reticulação iónica e a auto-organização molecular) para produzir microcápsulas baseadas em xanthan. A micro-estrutura (morfologia, organização molecular) e propriedades (tamanho, espessura da membrana, permeabilidade, estabilidade) das microcápsulas desenvolvidas foram investigadas em detalhe. Microcápsulas feitas de xanthan carboxymetilado reticulado ionicamente (capítulo III) e por auto-organização molecular do palmitoyl xanthan (capítulo IV) foram produzidas através do gerador de micro-cápsulas com diametro cerca de 500 e 576 µm, respectivamente. A auto-organização molecular do fosfolípido-xanthan (capítulo V) e do xanthan nativo com péptidos de carga oposta (capítulo VI) foram conduzidas através de um dispositivo micro-fluidico para obter estruturas capsulares estáveis com forma esférica regular e tamanho

controlado na escala micrométrica. Os resultados destes estudos mostraram que as propriedades das microcápsulas desenvolvidas podem ser facilmente controladas através da manipulação da concentração dos materiais e condições de organização. Além disso, os dispositivos utilizados foram bem sucedidos para guiar a formação de estruturas capsulares.

Experiências de encapsulamento de células foram também realizadas para corroborar a hipótese inicial. Células da linha celular ATDC5 foram encapsuladas nas cápsulas de xanthan tendo permanecido viáveis. Adicionalmente, foram observadas a proliferar para longos períodos de cultura (até três semanas) com aumento da actividade metabólica.

Em suma, estes estudos sugerem que o polissacárido xanthan pode constituir uma alternativa aos materiais convencionais utilizados em encapsulamento de células. Contudo estudos in vivo serão necessários para validar esta hipótese.

A combinação de processos de auto-organização molecular com técnicas de micro-fabricação demonstrou ser um método inovador para a fabricação de microcápsulas em condições celulares favoráveis e com propriedades controladas.

Por último, auto-organização molecular foi combinada com processos de fotolitografia para fabricar membranas com padrões topográficos (capítulo VII). Foi utilizado um péptido carregado positivamente (com e sem a sequência peptídica de adesão celular RGDS) para interagir com o polímero aniónico ácido hialurónico. As condições de organização molecular foram optimizadas para fabricar membranas com propriedades controladas tais como espessura da membrana, concentração de sequência bioactiva e morfologia do padrão topográfico. As membranas obtidas apresentaram uma estrutura altamente organizada constituida por nano-fibras contendo micro-topografias na superfíce com diferentes densidades de RGDS. Células estaminais da medula óssea de rato reconheceram a sequência RGDS e os padrões topográficas, variando a sua morfologia consoante a concentração de RGDS e morfologia do padrão.

Os estudos apresentados nesta tese demonstraram que a combinação de auto-organização molecular com tecnologias de microfabricação constitui uma estratégia eficaz para fabricar microcápsulas e membranas com maiores níveis de controlo sobre a sua estrutura, forma, bioatividade e desempenho.

Page

SECTION 1-BACKGROUND

Chapter I-Self-Assembly in Nature: Using the Principles of Nature to Create Hierarchical Complex Peptide Structures for Biomedical Applications

SECTION 2- EXPERIMENTAL

Chapter II – Materials and Methods

Chapter VII. Co-assembled and Microfabricated Bioactive Membranes

SECTION 4- CONCLUSIONS AND OUTLOOK

Chapter VIII. General Conclusions and Perspectives

A

A	Adenine
Ala or A	Alanine
ALP	Alkaline Phosphatase
Arg or R	Arginine
Asn or N	Aspargine
Asp or D	Aspartic acid
ATDC5	Mouse condrocyte teratocarcinoma AT805 derived cell line

B

BMP-2	Bone morphogenetic protein-2
BSA	Bovine Serum Albumin

C

C	Concentration
C	Cytosine
C_0	Initial concentration
CAD	Computer-aided design
Calcein-AM	Calcein acetomethyl
CD	Circular dichroism
CMX	Carboxymethyl xanthan
Cys or C	Cysteine

D

DAPI	4',6-diamidino-2-phenylindole dihydrochloride
DMEM	Dulbecoo's Modified Eagle's Medium
DMF	Dimethylformamide
DMSO	Dimethylsulfoxide
DNA	Deoxyribonucleic Acid
DS	Degree of Substitution
DSC	Differential Scanning Calorimetry
DOPE	1,2-dioleoyl-sn-glycero-phosphoetilamine
d-size	Diameter size

E

ECM	Extracellular matrix
EDC	Ethyl(dimethylaminopropyl)carbo diimide
ESI-MS	Electron-spray ionization mass spectrometry

F

FBS	Fetal bovine serum
FGF-2	Fibroblast growth factor
FITC	Fluorescein isothiocyanide
Fmoc	9-fluorenylmethoxycarbonyl
FTIR	Fourier transform infrared (spectroscopy)

G

G	Guanine
GC	Gas chromatography
GF	Growth factor
Gln or Q	Gluyamine
Glu or E	Glutamic acid
Gly or G	Glycine

H

HA	Hyaluronic acid
HBTU	O-(benzotriazol-1-yl)-N,N,N',N'-tetramethyluronium
HEPES	4-(2-hydroxyethyl)-1-piperazineethanesulfonic acid buffer solution
His or H	Histidine
HIV	Human immunodeficiency virus
HMDS	Hexamethyldisilazane
HPLC	High-performance liquid chromatography
H&E	Harris Hematoxylin and eosin staining

I

IgG	Immunoglobulin G
Ile or I	Isoleucine

L

Leu or L   Leucine

Lys or K   Lysine

M

MBHA   4-methylbenzhydrylamine rink amide resin
MDP   Multi Domain Peptides
MES   2-(*N*-morpholino)ethanesulfonic acid (buffer solution)
Met or M   Methionine
mRNA   messenger Ribonucleic Acid

MTT   3-(4,5-dimethylthiazol-2-yl)-2,5-diphenyltetrazolium bromide
Mw   Molecular Weight
MWCO   Molecular Weight Cut-Off

N
NHS   N-hydroxysuccinimide
NMR   Nuclear Magnetic Resonance

P
PA   Peptide Amphiphile

PBS   Phosphate Buffer Saline
PDMS   Poly(dimethyl siloxane)
Phe or F   Phenylalanine
PI   Propidium Iodide
PKA   Protein Kinase A
PLL   Poly-L-Lysine
Pro or P   Proline
PX   Palmitoyl Xanthan

Q
QCM-D   Quartz Crystal Microbalance with Dissipation (monitoring)

R
RNA   Ribonucleic Acid
rMSC   Rat Mesenchymal Stem Cells

S
SEC   Size-exclusion chromatography
SEM   Scanning Electron Microscopy

Ser or S   Serine

SP   Solid Phase

STEM   Scanning Transmission Electron Microscopy

T
T   Temperature

T   Thymine
T   Transmittance

TCP   Tissue Culture Plate

TEFLON   Poly(tetrafluoro ethylene)
TFA   Trifluoroacetic acid
TGF-β   Transforming Growth Factor beta
Thr or T   Threonine
TIS   Triisopropylsilane
TMV   Tobacco Mosaic Virus

Tris-EDTA   Tris(hydroxymethyl)aminomethane- Ethylenediaminetetraacetic acid (buffer solution)

Trp or W   Tryptophan
Tyr or Y   Tyrosine

U
UV   Ultra-violet

V
Val, V   Valine
v/v   Volume/volume
VEGF   Vascular Endothelial Growth Factor
W
WAXS   Wide angle x-ray scattering
Wt%   Weight percentage

w/w   Weight/weight

Others
2D   Two-dimensional
3D   Three-dimensional

SECTION 3- DEVELOPMENT AND CHARACTERIZATION OF SELF-ASSEMBLED AND MICROFABRICATED STRUCTURES

Chapter III. Encapsulation and Survival of a Chondrocyte Cell Line within Xanthan Gum Derivative

Chapter IV. Palmitoylation of Xanthan Polysaccharide for Self-assembly Microcapsule Formation and Encapsulation of Cells in Physiological Conditions

then carried into a gelling inducer solution (phosphate buffer solution, PBS). In PBS, the palmitoyl xanthan droplets self-assemble into capsular gel structure. The hollow capsules were then collected and treated with poly-L-lysine to strengthen the outer surface of the microcapsules.

Chapter V. Guided and Microfluidic Self-Assembly of Phospholipid-xanthan Microcapsules

Chapter VI. Microfluidics Fabrication of Self-assembled Peptide polysaccharide Microcapsules as 3D Environments for Cell Culture

Chapter VII. Co-assembled and Microfabricated Bioactive Membranes

The present thesis is divided into four sections, containing a total of eight chapters, and is based on the format adopted by the 3B´s Research Group, which consist on the compilation of scientific papers published or submitted for publications in international peer-reviewed journals. The contents of each section and chapters are summarized below.

The first section (*Section 1*) includes a review paper about self-assembly in nature and how to use supramolecular chemistry to create highly sophisticated materials for applications in medicine (Chapter I). It aims to provide an introduction to the concepts used in the PhD research and also a literature review on the topic.

Section 2 (Chapter II – Materials and Methods) describes the scientific objectives and experimental approach of the PhD study. In addition, it provides detailed information on the chemicals, materials, methods and techniques used in the experimental work. This section also serves as a complement to the information given in each of the following experimental chapters.

Section 3 contains 5 chapters (chapters III-VII) that describe original research. In Chapter III, a chemical derivative of xanthan gum polysaccharide (carboxymethyl xanthan) was investigated as a new artificial matrix for the encapsulation of chondrocytic cells. A novel micro-droplet generator was developed to produce microcapsules. Xanthan was further modified to obtain an amphiphilic system by conjugation with hydrophobic palmitoyl groups (Chapter IV) and a phospholipid molecule (Chapter V). Chapter VI presents the fabrication of microcapsules by combining a positively charged self-assembling peptide with xanthan.

Chapter VII reports on the fabrication of hierarchical and bioactive self-supporting membranes, integrating physical and biomolecular elements, in a single-step process, that combines molecular self-assembly with soft lithography.

The final section (*Section 4,* Chapter VIII - Conclusions*)* summarizes the significant findings in the experiments presented in the previous section and describes how the conclusions address the initial hypotheses.

Six chapters presented in this thesis are based on the following articles:

Chapter I

A. C. Mendes, E. T. Baran, R. L. Reis, H. S. Azevedo, Self-assembly in Nature: Using the Principles of Nature to create Hierarchical Complex Peptide Structures for Biomedical Applications, *submitted*.

Chapter III

A. C. Mendes, E. T. Baran, R. C. Pereira, H. S. Azevedo, R. L. Reis, Encapsulation and Survival of a Chondrocyte Cell Line within Xanthan Gum Derivative, *Macromolecular Bioscience* 2012, 12(3): 350-359.

Chapter IV

A. C. Mendes, E. T. Baran, C. Nunes, M. A. Coimbra, H. S. Azevedo, R. L. Reis, Palmitoylation of Xanthan Polysaccharide for Self-assembly Microcapsule Formation and Encapsulation of Cells in Physiological Conditions, *Soft Matter* 2011, 7 (20): 9647-9658.

Chapter V

A. C. Mendes, E. T. Baran, R. L. Reis, H. S. Azevedo, Guided and Microfluidic Self-Assembly of Phospholipid-xanthan microcapsules, *submitted*.

Chapter VI

A. C. Mendes, E. T. Baran, P. Lisboa, R. L. Reis, H. S. Azevedo, Microfluidics Fabrication of Self-assembled Peptide-polysaccharide Microcapsules as 3D Environments for Cell Culture, *submitted*.

Chapter VII

A. C. Mendes, K. H. Smith, E. Tejeda-Montes, E. Engel, R. L. Reis, H. S. Azevedo, A. Mata, Co-assembled and Microfabricated Bioactive Membranes, *submitted*.

Section 1

BACKGROUND

Chapter I

SELF-ASSEMBLY IN NATURE: USING THE PRINCIPLES OF NATURE TO CREATE HIERARCHICAL COMPLEX PEPTIDE STRUCTURES FOR BIOMEDICAL APPLICATIONS

SELF-ASSEMBLY IN NATURE: USING THE PRINCIPLES OF NATURE TO CREATE HIERARCHICAL COMPLEX PEPTIDE STRUCTURES FOR BIOMEDICAL APPLICATIONS

ABSTRACT

Self-assembly is a ubiquitous process in biology where it plays numerous important roles. It underlies the formation of a wide variety of complex biological structures, like for example the organization of lipid bilayers in cell membranes which is essential for maintaining the integrity and function of cells. Over the past two decades, materials scientists have aspired to exploit nature's assembly principles to create artificial materials, with hierarchical structures and tailored properties, for the fabrication of functional devices. Towards this goal, both biological and synthetic building blocks have been subject of extensive research in self-assembly. In fact, molecular self-assembly is becoming increasingly important for the fabrication of biomaterials because if offers a great platform for constructing materials with high level of precision and complexity, integrating order and dynamics to achieve functions such as stimuli-responsiveness (pH, ionic strength, temperature, light), environmental adaptation (space confinement) and bioactivity (cell receptor signaling to promote regenerative processes). The importance of peptide self-assembling building blocks has been recognized in the last years, as demonstrated by the literature available on the topic. The simple structure of peptides, as well as their facile synthesis, makes peptides an excellent family of structural units for the bottom-up fabrication of complex nanomaterials. Additionally, peptides offer a great diversity of chemical (specificity, intrinsic bioactivity, biodegradability) and physical properties (small size, conformation, stability) to form self-assembled structures with different molecular configurations. The motivation of this review is not only to provide an overview on the design principles for peptide self-assembly but also to demonstrate how these principles have been applied to manipulate their self-assembly across the scales with numerous illustrative examples about such an exciting research. Applications of self-assembling peptides as biomaterials, including carriers for drug delivery, hydrogels and 3D networks for cell culture and tissue engineering, are also described

_____

## 1.	SELF-ASSEMBLY DEFINITION

Molecular self-assembly, the spontaneous organization of molecules into ordered aggregates due to their mutual interactions (from the non-covalent type) without external control, is of central importance to life (e.g., protein folding, pairing of nucleotides in DNA, formation of lipid bilayers - Figure I.1.). It generates much of the functionality of the living cell and provides the basis of supramolecular chemistry where the instructions of how to assemble larger entities are coded in the structural motifs of individual molecules[1].

The definition of molecular self-assembly still remains ambiguous, being used many times improperly. For instance, self-assembly and self-organization are two concepts that are often confused or even misunderstood. Halley and Winkler[2] distinguish self-organization from self-assembly based on thermodynamic principles, where self-organization implies a non-equilibrium process and self-assembly is reserved for spontaneous processes tending toward equilibrium. Two main classes of self-assembly have been considered: static and dynamic. Static self-assembly is related with the local or global equilibrium of the systems without dissipation of energy[3-5]. In dynamic self-assembly, the formation of structures through supramolecular interactions only take place if the system is dissipating energy [3-5].

## 2.	BIOLOGICAL SELF-ASSEMBLIES

Biology is replete with examples of highly functional complex nanoscale structures formed by self-assembly[6]. The importance of self-assembling in biological and biochemical activities can be easily understood considering the low consumption of energy required in the non-covalent interactions. It is a process that operates in the thermodynamic minimum.

Figure I.1.A exemplifies one of the most powerful characteristics of biological systems: their ability to assemble individual molecules into large, complex, functional structures. A variety of biological structures, ranging from proteins and nucleic acids to viruses and cell membranes, possess a highly precise organization on the nanometer scale which derives from specific interactions at molecular level being this organization critical for their function. Biological self-assembly uses biomolecular building blocks of precisely defined shape, size, hydrophobicity and spatial distribution.

Protein folding (Figure I.1.A) clearly illustrates the non-covalent interactions involved in the self-assembly in aqueous solution. The peptide sequence (primary structure) is synthesized from the 20 amino acids by translation of a sequence present in a messenger ribonucleic acid (mRNA)..

When viewed in a simplistic perspective, proteins appear to be an assembly of linear covalent strands. Precise folded proteins involve, however, the assembly of prefolded intermediates before yielding perfectly functioning proteins. The secondary structure of proteins may be constituted by α-helices and β-sheets in their backbone. α-Helices occur when peptide bonds are connected by hydrogen bonds and can be visualized when protein chains exhibit a helix motif. The β-sheet tends to form when a protein folds back and forth upon itself.

The formation of protein tertiary structure is mediated by how α-helices and β-sheets bend and pack into each other originating a protein subunit. The conformation of the tertiary structure is provided by the number and type of interactions (e.g. hydrogen bonds, hydrophobic and ionic interactions) and it is at this stage of protein folding that the functional regions of the protein (e.g. catalytic and binding points) become assembled. Lastly, the quaternary structure of proteins is formed when the subunits previously formed are interacting together. Nevertheless, it is the primary structure containing the specific order of amino acids that will dictate exactly how the folding will occur and consequently the same sequence will give every time the same structure, except when disturbance is introduced in the system[4]. These biomolecules play an important role in numerous vital functions in living systems. Besides their structural function, they are also transporting agents, scaffolds of biological catalysis (enzymes), protection agents and hormone receptors[4,7].

A particularly important example of self-assembly is provided by the double-stranded (ds) **deoxyribonucleic acid** (**DNA)** molecule. Two complementary chains of linear DNA strands, composed of millions of nucleotides, constituted of polyphosphate/sugar backbones attached to nucleobase residues (adenine (A), cytosine (C), guanine (G) and thymine (T)) wrap around one another in the familiar double helix (Figure I.1.B). DNA helix has a diameter of approximately 2 nm, a helical repeat of 3.4 nm (10.5 base pairs) and persistent length of about 50 nm[8]. Complementary pairs of nucleobases (A-T and C-G) form strong hydrogen bonds that strongly sustain the strands together, supported by π-π stacking interactions. The stability resulted from the combination between these two pairs of nucleobases is unique and responsible for the effectiveness of DNA replication.

Viruses are protein-based supramolecules, with different shapes and variety of sizes, that manifest their functionality through self-assembly. A typical virus possesses a protein outer shell (capsid) composed of multiple copies of coat proteins arranged in a symmetrical fashion, and housed within the viral genome, which contains all the essential genes to replicate within the host. In general, viruses adopt an icosahedral or helical structure, giving a sphere- rod-shape particle. Many viruses, such as herpes, polio, the human immunodeficiency virus (HIV) adopt the

icosahedral conformation that are confined into a lipidic bilayer designed as envelop. To assemble into an icosahedral geometry, its capsomers, the structural units of this kind of viruses, are distributed symmetrically despite their self-assembly from assymetrical components. For example, the tobacco mosaic virus (TMV), which self-assembles into rod like structures[3-4], represents an excellent example of effective control over size of self-assembled structures. First, the TMV protein forms a two-layer disk, with 17 proteins in each ring. A special initiation sequence in the RNA then binds in the hole at the center. This cause the disk to dislocate, forming a lockwasher shaped ring with 16 1/3 subunits pert turn. The remaining subunits then stack in this structure elongating until the RNA is covered. Thousands of coat proteins (2130 identical protein units each with 158 amino acid residues) self-assemble into 300 nm long cylinder (protein shell - capsid) around a single RNA molecule (that comprises ~6400 nucleotides) which acts as a template (Figure I.1.C). The length of the assembly is determined by the length of the enclosed RNA template. In the absence of the RNA template, the TMV coat proteins assemble into cylinders with the same diameter (18 nm) as the untemplated capsids but with variable length. The RNA template limits the self-assembly of the capsid proteins through specific molecular interactions. The head-to tail assembly of TMV represents a superb example of a biological system that takes advantage of the natural assembly pathway. One of the interesting features of the TMV is that if the virus is broken into its sub-unities, when re-mixed in physiological conditions, the virus has the ability to self-assemble exactly into the previous structure constituting a full replica.

The **cytoplasmic membrane** (Figure I.1.D) is a phospholipid bilayer which serves to separate the inside environment of the cell from the outside. The phospholipid bilayer is arranged so that the polar ends of the molecules (the phosphate and glycerol portion of the phospholipid that is soluble in water) form the outermost and innermost surface of the membrane while the non-polar ends (the fatty acid portions of the phospholipids that are insoluble in water) form the center of the membrane This membrane is stable enough to serve as a barrier to the transport of water soluble ions (Na^+, K^+, Ca^{2+}) and molecules and has the fluidity to allow the entrance of particles inside the cell by endocytosis (the process by which cells take in solutes or particles by enclosing them in vesicles or vacuoles pinched off from the cytoplasmic membrane).

The previously described examples clearly show how sophisticated self-assembly can be and how nature's assembly principles can be used to create supramolecular materials.
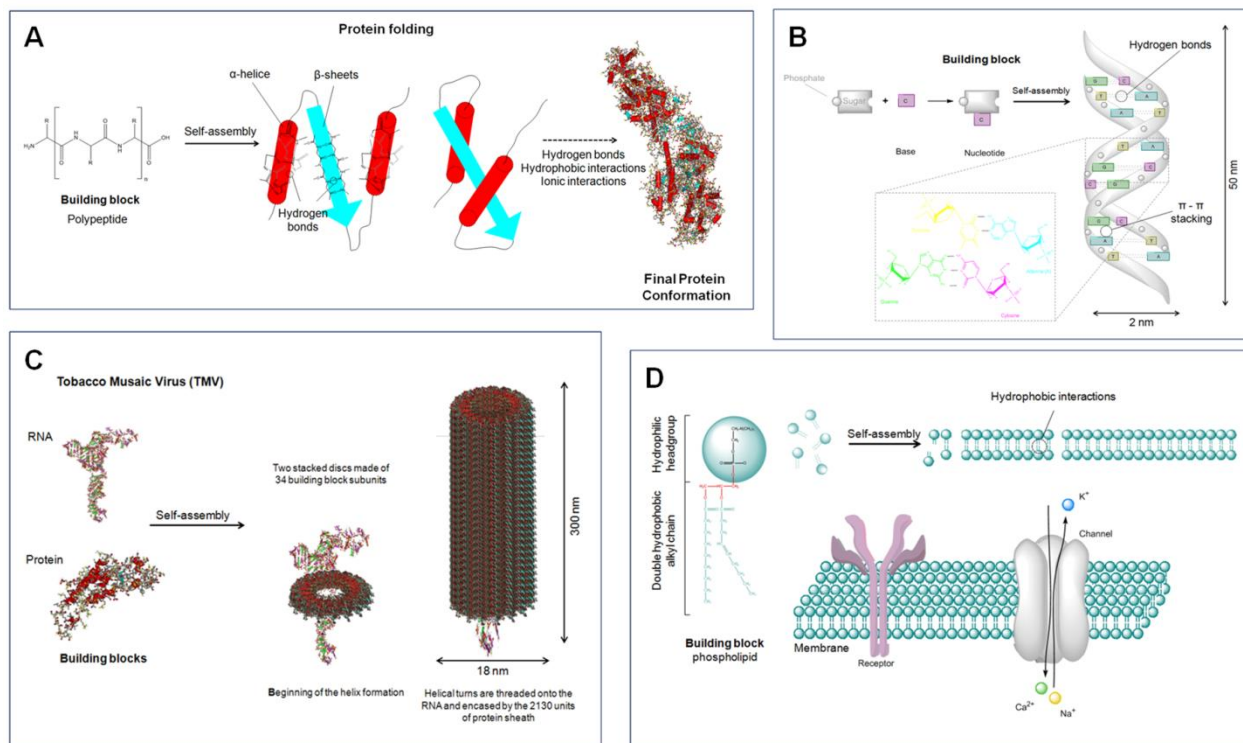
Figure I.1. Examples of biological self-assembled structures showing the building blocks and the relevant interactions involved in the self-assembly process. **(A)** Protein folding; **(B)** ds-DNA; **(C)** Tobacco mosaic virus (TMV); **(D)** Cell membrane.

3.   DESIGN OF SUPRAMOLECULAR MATERIALS

From a materials science point of view, self-assembly is a simple and low cost bottom-up process to fabricate functional supramolecular materials from pre-existing components (building blocks) involving a reduced number of steps. Different building blocks (biological and synthetic, Table I.1.) have been extensively studied for this purpose. These building blocks can be atoms, molecules or macromolecules, and be designed (chemical nature of the blocks, composition, length, molecular architecture) to contain all the necessary information to direct their self-assembly into complex materials for specific applications. In most cases, their self-assembly is reversible and allows the combination of different building blocks. While the instructions for assembly lie in the molecular structures (recognition, chirality) of the **building components** and on the precise positioning of functional groups that provide the **intra- and intermolecular interactions**, the nanostructures that emerge through self-assembly are controlled by the **environment** and the **driving force**. Each of these characteristics of the self-assembling system is described in detail in the following sections.

3.1. Self-assembling building blocks

According with Whitesides[9], the components of a self-assembling system consists of a group of molecules or segments of a macromolecule that interact with one another. These molecules or molecular segments may be the same or different. Their interaction leads from some less ordered state (a solution, disordered aggregate or random coil) to a final state (a crystal or folded macromolecule) that is more ordered.

Proteins and DNA are not only examples of self-assembled biological structures, but these macromolecules have been used as building blocks for fabricating complex assemblies (Table I.1.). A wide range of different molecules can be used to form supramolecular nanostructures in a variety of different assembling conditions. The molecules must have the potential to form multiple non-covalent interactions with itself in a given solvent. In addition, certain structural features (e.g. helicity) and their persistence length are also key parameters.

Amino acids are naturally occurring molecules being the molecular constituents of peptides and proteins. **Peptides** are versatile assembly components owed their intrinsic functional diversity, being chemically more diverse than DNA, and have been widely exploited as self-assembling building blocks. Their self-assembly has been studied in detail and will be the focus of this review.

Lipids are the most important building blocks of cell membranes. Generally, they are composed of a hydrophilic head group and a hydrophobic tail region[3,10]. Due to the large variability in the head group and tail chemistries, lipids are often categorized into polar and non-polar. The hydrophobic nature and rigid structure of lipids creates a tendency of these molecules to aggregate into larger structures in which the position and orientation of the molecules is organized. In addition, the structural diversity of lipids (fatty acids, triglycerides, phospholipids, cholesterol) with different polarities, charged groups and lengths allows the formation of dynamic (e.g. monolayers, bilayers) and compartmentalized (e.g. micelles, vesicles) structures in water, acting as barriers, within isolated processes can occur.

High molecular weight **saccharides** (polysaccharides) are produced annually by a broad variety of plants and microorganisms with remarkable chemical (neutral, charged, linkage type) and structural diversity (linear or branched, random coil or helical conformation). Polysaccharides contain multiple OH groups capable of hydrogen bonding. In addition, with their single molecular recognition functionality, polysaccharides are highly adaptable and can introduce densely-charged templates into nanostructured assemblies[11].

In biology, **nucleic acids** (DNA and RNA) are fundamental molecules of life as carriers of molecular information. They play essential roles in gene heredity, regulation and expression. DNA's base sequence stores and imparts instructions, while RNA's sequence plays the role of a

messenger and a regulator of gene expression. As biological polymers, nucleic acids possess recognition capabilities and interesting chemical properties which depend on their base sequence. Nucleic acids can be synthesized with a nearly infinite number of sequences[8]. The nucleobases present in DNA and RNA molecules can form hydrogen bonds and π-π stacking interactions and these interactions can be engineered for the bottom-up fabrication of a variety of nanostructures. DNA double helix is inherently a nano-scale object. Although being more chemically labile, RNA molecules have structural components that are very similar to DNA. In addition, most RNAs are single-stranded molecules with nanoscale motifs that mediate precise intra- and inter-molecular interactions. Two strands of DNA or RNA with completely complementary sequences can bind to each other and form a fully bases-paired duplex structure.

Table I.1. Biological and synthetic building blocks used for the supramolecular self-assembly into complex structures and their potential biomedical applications[6,12-16].

CPMV-cowpea mosaic virus; λ phage-lambda bacteriophage; hHPBV- human hepatitis B virus

Viruses have been used as robust building blocks in nanosciences due to their canonical shape (rod or sphere) and size uniformity. The surface properties of viruses can be manipulated genetically or chemically without disrupting their integrity and morphology. They have been employed to generate long-range ordered assemblies for biomaterials development.

Synthetic block copolymers, with their easily controllable properties (molecular dimension, composition, solubility, stability, stimulus responsive behavior) have been widely used for fabricating a variety of organized assemblies with distinct morphologies (micelles, vesicles, tubes) depending on the relative volume fractions of the blocks. **Dendritic** molecules (e.g. dendrons) are synthetic molecules which have a well defined (monodisperse) 3D branched architecture. Dentritic building blocks can assemble into more complex nanoscale assemblies (nanoparticles, nanofibers) by non-covalent interactions[17].

Surfactants are compounds that consist of a hydrophobic (usually a long hydrocarbon chain) and a hydrophilic (ionic or polar group)[18]. Examples of surfactants are the well-known sodium dodecylsulfate (SDS) and sodium oleate. Numerous studies have demonstrated that surfactants self-assemble in aqueous solution into micellar, vesicle and multilayer structures.

3.2.   Supramolecular interactions

The interactions relevant in molecular self-assembly are non-covalent forces (electrostatic, hydrophobic, hydrogen bonding, van der Waals, aromatic stacking, metal coordination) that are individually weak (2-250 kJmol^{-1}) when compared with to covalent bonds (100-400 kJmol^{-1}) but collectively, if in sufficient number, they can generate highly stable assemblies and their subtle balance govern the shape and function of the final assembly (Figure I.2.).

Electrostatic interactions

Coulombic interactions are long range non-selective interactions that can result in attractive or repulsive effects. Ionic self-assembly has been employed as straightforward and reliable method for the organization of different building blocks (polyelectrolytes, charged surfactants, peptides and lipids, DNA). Charged groups, including phosphate of nucleic acids or carboxylates and amino groups on protein side chains, can interact with counterions and combined to form new materials. Binding of charged surfactants with oppositely charged polyelectrolytes is a typical example of ionic self-assembly[19].

Hydrophobic effects

The hydrophobic effect is a unique organizing force, based on repulsion of solute by the solvent instead of attractive forces at the site of organization. Non-polar molecules tend to avoid a non aqueous surrounding. Hydrophobic effects are responsible for the folding of proteins and the aggregation of amphiphiles into micelles and vesicles.

Stacking effects (π-π stacking)

In chemistry, pi stacking (also called π-π stacking) refers to attractive, noncovalent interactions between aromatic rings. π-π stacking is a popular chemistry concept describing how aromatic molecules are stabilized when oriented face-to-face as in a stack of coins. It explains how certain supramolecular structures are formed and especially in biology it explains the finer points of base pairing in DNA. π-π stacking between aromatic units, for example between aromatic side chain of certain aminoacids (e.g. tyrosine-tyrosine, tryptophan-phenylalanine interactions) mediate protein folding and are responsible for intermolecular stability.

Hydrogen bonding

Hydrogen bonds are formed between atoms such as oxygen or nitrogen that have electronegativity larger than hydrogen. The atom to which the hydrogen is connected is referred as hydrogen-bond donor and the other atom is called hydrogen-bond acceptor (Figure I.2.). Hydrogen bonding (H-bonding) interactions are highly directional and can be of either short- or long-range nature, leading to secondary structures such as α-helices and β-sheets in proteins. The strength of single hydrogen bonds depends mainly on the nature of donor or acceptor, although it is influenced by a larger extent by the solvent. Combining several hydrogen bonds in a functional assembly strengths the interaction and their spatial arrangement enhances its specificity. In DNA, H-bonding is responsible for highly specific molecular recognition.

Tuning the strength and directionality of interactions among building blocks is the key feature that defines the field of supramolecular materials[20]. The interactions that provide high degree of directionality to the assembly process of the different building blocks are favorite elements in the design. By controlling the multiple interactions during assembly will lead to a wide range of ordered structures (ribbons, tapes, tubes, helices). For example, repulsive forces, due to ionic interactions, can be neutralized due to changes in pH, or addition of multivalent ions or charged polymers.
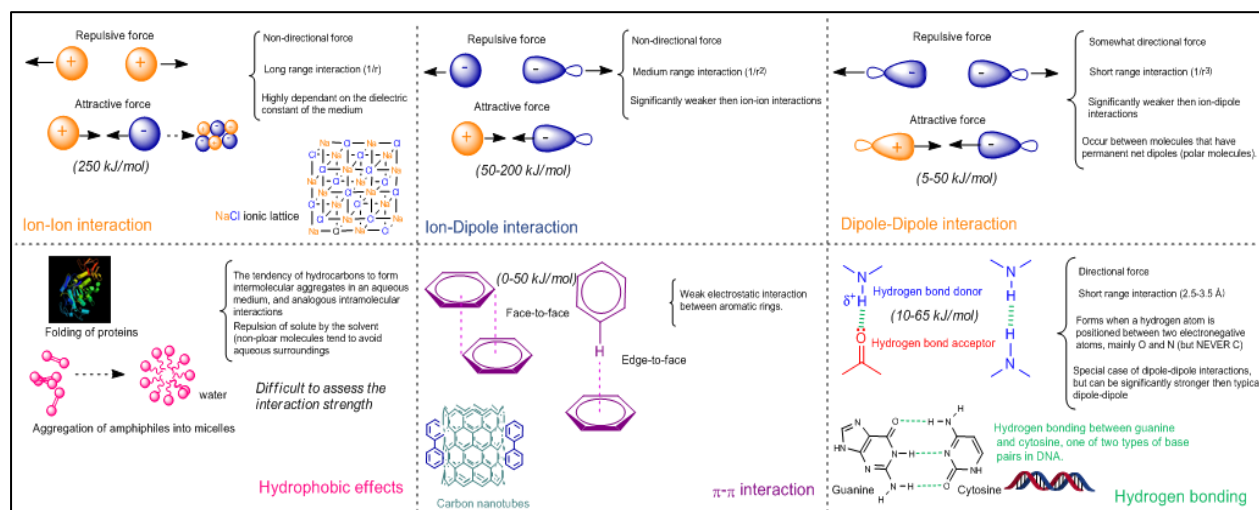
Figure I.2. An illustration showing the non covalent interactions involved in supramolecular chemistry and their strength[21]

3.3. Molecular recognition

The way in which one molecule recognizes and binds to another is a fundamental process that is important in many biochemical pathways (e.g. selective substrate recognition by specific enzymes) and also in analytical chemistry (e.g. receptor binding to particular analytes). Molecular recognition, the specific noncovalent association of one molecule with another, underlies the entire field of self-assembly and the chemical recognition information that is programmed into each molecule offers the potential for constructing supramolecular architectures.

3.4. Chirality

Chirality is a geometric property of a molecule (or spatial arrangement of atoms) of being non-superposable on its mirror image; it is an important property in many biomacromolecules which results from the inherent chirality of the molecular building blocks (e.g. amino acids, nucleotides). Peptides are chiral, which can lead to the generation of materials of a particular handedness which in turn can add another level of recognition[22]. It has been predicted that the formation of lipid tubules is driven by the chirality of the bilayer, and the tubule diameter depends on magnitude of the chirality, i.e., the magnitude of the favored twist in the molecular packing[15].

3.5.   Environment and the driving force

The self-assembly needs an environment in which it will occur and it is often related with a driving force. The driving force causes the movement of the system through the different possible configurations of the system on its way to the ordered final state.

The self-assembly of molecules is normally carried out in solution or at an interface to allow the required motion of the components. The interaction of the components with their environment can strongly influence the course of the process. For self-assembly to occur, molecules must be mobile. In solution, thermal motion provides the major part of the motion required to bring the molecules into contact. Therefore one of the challenges consists on assuring the mobility of the components; as they become larger than molecules, Brownian motion rapidly becomes irrelevant, and gravity and friction become important. The concentration of self-assembling units is expected to influence the diffusion and the mobility of the components. Increasing the concentration will drive assembly of larger structures.

For self-assembly to generate ordered structures, the association either must be reversible or must allow the components to adjust their positions within an aggregate once it has formed. The strength of the bonds between the components, therefore, must be comparable to the forces tending to disrupt them. For molecules, the forces are generated by thermal motion.

3.6.   Controlled self-assembly

There are many pathways to trigger and/or drive the self-assembly by changing gradually the environmental conditions (e.g. building block concentration, pH, temperature, ionic strength, solvent), or by an external input (e.g. light, enzyme activity, magnetic or electric field). The presence of ions in solution, as well the pH and solvent polarity, are significant factors that affect the non covalent interactions and hence the assembly routes. The pH environment can modulate the degree of protonation/deprotonation of amino acids with ionizable groups (carboxyl and amino side chains, Table I.2.) in peptides and proteins and thus control their electrostatic interactions (attraction/repulsion). Similarly, ionic strength also affects the charge state of molecules. Charge screening effects by counterions have been widely used to drive the formation of peptide assemblies. In addition to their role as solution entities, ions are also important components in many self-assembly processes. Bulk self-assembly of small molecules frequently yields structures that exhibit a high degree of order on the nanometer scale, whereas at the micrometer scale they exhibit more disordered morphologies. A method to dynamically control the self-assembly process consist on designing self-assembling molecules that are sensitive to external stimulus, such as light or catalytic activities. This external stimulus can

convert a non-assembling precursor into self-assembling element which is produced locally. A major challenge in self-assembling is to control the kinetics of the process (nucleation and growth) and avoid defects in the formed assemblies. There is, therefore, a need to design self-assembling systems (building blocks and assembling pathways) that allow the spatio-temporal control of the process.

Temperature is also known to play a role on the kinetics of self-assembly by regulating the formation and size of ordered aggregates[23]. An interesting study reporting the use of temperature control on peptide amphiphile assembly at the micro and macroscale has been demonstrated by Stupp and co-workers by the formation macroscopic bundles of aligned nanofibers[24]. Light-triggered self-assembly was also demonstrated by the Stupp group by conjugation of a 2-nitrobenzyl group with the amide nitrogen of the amino acid closest to the hydrophobic segment (alkyl tail) of peptide amphiphile (PA)[25]. This chemical configuration protects the amide nitrogen from hydrogen bonding. The 2-nitrobenzyl group can be cleaved photochemically (upon light irradiation at 350 nm) restoring a standard PA.

The highly- to non-specific activities of enzymes have been also explored in the context of dynamic self-assembly by designing self-assembling building blocks that are sensitive to enzymatic activities under controlled conditions of pH, temperature and ionic strength. Enzyme-directed self-assembly can be achieved either by catalyzing the synthesis of a self-assembly molecules, or by removing a blocking from the molecules[13]. For that, several enzymes have been used, including proteases, phosphatases and esteresases, which catalyze hydrolysis reactions (formation of supramolecular assembly via bond cleavage) or by transferase enzymes (kinases) which might generate supramolecular assemblies via bond formation. A peptide amphiphile (PA) was designed containing a sequence which is a substrate of a protein kinase A (PKA)[26]. Upon treatment with PKA, the PA molecules became phosphorylated causing the disassembly of the cylindrical structures. Subsequent treatment with alkaline phosphatase enzyme, which cleaves the phosphate groups, resulted in PA reassembly. Another example of enzyme mediated self-assembly[27] employs the natural enzyme alkaline phosphatase (ALP) and a phosphorylated, anionic nanofiber gel matrix to template, in 3D, hydroxyapatite nanocrystals. ALP liberates phosphates necessary for hydroxyapatite mineralization from organic phosphates. The gradual nature of this enzymatic process provides critical regulation of free phosphate concentration, preventing rapid, uncontrolled nonspecific mineralization in the incubating medium.

The laboratory of Ulijn has provided very interesting examples on enzymatically controlled self-assembly[28-31]. They have used a protease enzyme (subtilisin) to produce building blocks in a

reversible and spatially confined manners using aromatic peptide amphiphile (Fmoc-dipeptide methyl esters) as self-assembling precursors. Subtilisin catalyses the hydrolysis of these esters to yield a Fmoc-peptide that self-assembles into hollow nanotubular structures[28]. Because the rate of formation of the self-assembling building blocks is determined by the kinetics of the enzymatic reaction, different folded structures may be formed offering additionally the possibility of controlling the mechanical properties.

These parameters play a key role in the thermodynamics and kinetic of the self-assembly process, thus acting on the morphology of the resulting assemblies.

Templated self-assembly

In templated self-assembly, a prefabricated template (2D substrate chemically or mechanically patterned) orients and directs the assembling components to (i) create structures with better long-range order than their non-templated counterparts, (ii) control the morphology of the resulting assemblies, and/or (iii) form novel structures/phases that would not favorable in the absence of the template[32]. The patterned substrate interacts selectively with the assembling components and their organization near the substrate is governed largely by the patterns on the template and this organization is propagated into the bulk of the assembling structure via the interaction between the components. Another approach towards templated self-assembly is the use of geometric confinement to orient bulk structures or to induce the formation of novel morphologies not found in bulk systems. Templated self-assembly can be used to hierarchically organize self-assembled structures for higher order assemblies.

In the template self-assembly approach, specific physical and chemical interactions of the molecules and components with the surfaces are the driving forces for the formation of stable organized films at solid substrates. Vertical and horizontal segregation of components, their chemical binding and anchoring density determine supramolecular organization in a self-assembled film.

Guided self-assembly

Another method to introduce hierarchical organization in supramolecular materials consists on using external forces, such as mechanical[33], magnetic[34] and electric forces for orientation. Like physical templates, externally applied fields can also be used to direct the self-assembly process. Field-directed self-assembly has the added advantage that fields can be switched on/off and tuned dynamically. Therefore, these external forces can be used to template assemblies with improved long-range order and controlled orientation. Time varying fields can

be used to agitate an equilibrium structure in order to allow energetically unfavorable defects to be removed from the system or to establish and sustain a dynamically self-assembled system. For example, the van Hest group has shown the alignment of diacetylene-containing PA nanofibers in presence of a strong magnetic field (20 T)[34]. A highly aligned morphology was observed where the fibers were oriented parallel to the applied magnetic field. Furthermore, the alignment on a molecular level was passed on to the high-molecular-weight chains that formed upon light-induced polymerization of the diacetylene groups and was reflected in optical properties of the material. This study shows that through a convenient hierarchical build up of self-assembling materials, structural information on a molecular scale is transferred to macroscopic properties, allowing the development of new materials that are well defined on all dimension scales. Later, the same group reported the patterning of a solid film using polarization holography (variation of the light polarization direction) and diacetylene-containing PA fibers aligned in a strong magnetic field, with no template, mask, or mechanical contact with the film[35]. Using polarized light, spatially confined polymerization was achieved because polymerization only took place at positions where the polarization of the incident light was parallel to the fiber orientation, yielding a polymer pattern.

X-ray irradiation was also shown to induce the crystallization of like-charge supramolecular peptide filaments by repulsive forces, but this phenomenon only occurred at low peptide concentrations ($\leq$ 1 wt%; beyond this concentration the crystallization is spontaneous)[36]. The x-ray triggered organization of peptide filaments from a disordered state to a hexagonally ordered state was attributed to an increase in charge density caused by x-ray irradiation leading to enhanced electrostatic repulsions among filaments. Addition of ions that screened the charges on the filaments suppressed the formation of crystalline structures. More recently, Stupp and co-workers reported the effect of an electrical field during the dynamic self-assembly of a negatively charged polyelectrolyte and a positively charged peptide amphiphile in water leading to the formation of an ordered membrane[37]. The superposition of an external electric field during molecular co-assembly and diffusion of the charged species allowed controlling both growth rate and directionality of the fibrils that made up the membrane. Depending on the strength and orientation of the field, they observed a significant increase or decrease of up to nearly 100% in membrane thickness, or the controlled rotation of nanofiber growth direction by 90 degrees, which led to a significant increase in mechanical stiffness. These results suggest the possibility of using electric fields to control structure in self-assembly processes that involve the diffusion of oppositely charged molecules.

4.   PEPTIDES AS SELF-ASSEMBLING BUILDING BLOCKS

The unique self-assembling properties of peptides and their ability to form emergent structures are increasing being exploited for the development of new bioactive biomaterials. The successful synthesis of self-assembling peptides with different molecular designs and the pathways used to drive their supramolecular assembly are discussed in the following sections. A number of very important physiological and biochemical functions of life are influenced by peptides. For example, peptides are involved in receptor-mediated signal transduction, influencing cell-cell communication upon interaction with receptors. Another important feature of peptides is related with their aggregation state and its implications in human diseases. Long, unfolded polypeptides have an innate tendency to form aggregates, such as amyloid fibrils which are known to be involved in Alzheimer´s disease. The self-assembly process involved in collagen fibrillogenesis is also determinant for proper animal development and may be associated with certain pathological situations. The isolation of peptides from natural sources is often problematic and the demand of synthetic peptides in biological applications is steadily increasing. Peptides can be obtained through chemical synthesis or genetic engineering.

Synthetic routes include conventional synthesis in solution or solid phase chemistry which allows for the synthesis of short peptides (2-30 amino acids). Several reviews covering solid-phase peptide synthesis have been published[38-40]. The easy preparation of short peptides by solid phase has provided ample opportunities for peptide design and to study the effect of molecular design on their properties.

There are 20 natural (L-form) amino acids that are used by cells to synthesize peptides and proteins. The names, three-letter and one-letter codes, and structures of the 20 α-amino acids are given in Table I.2. With the exception of glycine (G), all amino acids are chiral and have the same basic structure, a central alpha carbon atom to which a hydrogen atom, an amino group, a carboxyl group and side chain R group are attached. The nature of their side chain (charged, polar, non-polar, aliphatic, aromatic, Table I.2.) contributes to their biochemical mode of action and dictates the conformation assumed by peptides and proteins. The aliphatic residues (A, I, L, M, V) provide a hydrophobic environment while amino acids with aromatic (F, W, Y) side chains can be engaged in π-π stacking. Neutral polar residues (N, Q, S, T) can be involved in the formation of hydrogen bonding through OH (S, T) or CONH (N, Q) groups. Basic (H, K, R) residues can be positively charged and acidic amino acids (D, E) can carry a negative charge. The presence of charged groups in these residues can be used to create electrostatic interactions that are important to drive (attractive forces) or to prevent (repulsive forces) the self-assembly process.

Table I.2. The twenty gene-coding/natural L amino acids: structure and properties (nature and pKa values for the ionizable side chains and their tendency for α-helix-promoting/breaking and β-structure promoting/breaking. Neutral: 0.8-1.00, no tendency either way)[13].
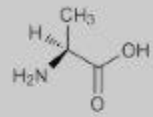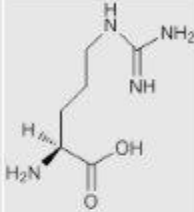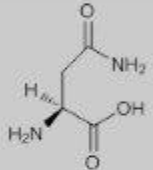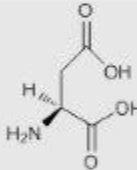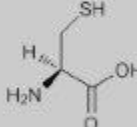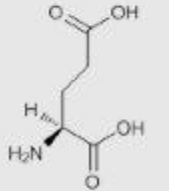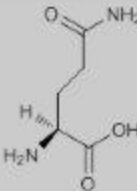
Amino acid	Three/One-letter code	Structure	Nature/pKa side chain	α-Helix promoting/breaking	β-Sheet promoting/breaking
L-Alanine	Ala (A)		Hydrophobic Aliphatic	1.45 (promoting)	0.97 (neutral)
L-Arginine	Arg (R)		Hydrophilic Basic (+) pKa ~ 12.4	0.79 (neutral)	0.90 (neutral)
L-Asparagine	Asn (N)		Polar Neutral	0.73 (breaking)	0.65 (breaking)
L-Aspartic Acid	Asp (D)		Hydrophilic Acidic (-) pKa ~ 3.8	0.98 (neutral)	0.80 (neutral)
L-Cysteine	Cys (C)		Polar Can form disulfide bond upon oxidation pKa ~ 8.2	0.77 (neutral)	1.30 (promoting)
L-Glutamic Acid	Glu (E)		Hydrophilic Acidic (-) pKa ~ 4.2	1.53 (promoting)	0.26 (breaking)
L-Glutamine	Gln (Q)		Polar Neutral	1.17 (promoting)	1.23 (promoting)

Table I.2. (cont.)
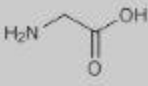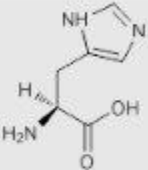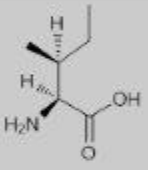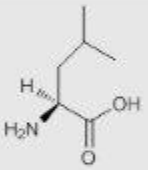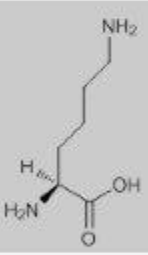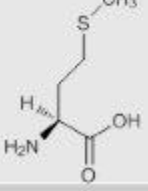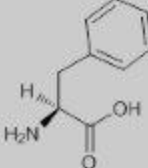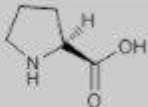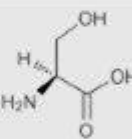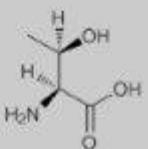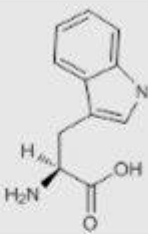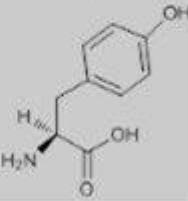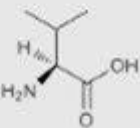
Amino acid	Three/ One- letter code	Structure	Nature/pKa side chain	α-Helix promoting/ breaking	β-Sheet promoting/ breaking
Glycine	Gly (G)			0.53 (breaking)	0.81 (neutral)
L-Histine	His (H)		Hydrophilic Basic (+) pKa ~ 6.1	1.24 (promoting)	0.71 (breaking)
L-Isoleucine	Ile (I)		Hydrophobic Aliphatic	1.00 (neutral)	1.60 (promoting)
L-Leucine	Leu (L)		Hydrophobic Aliphatic	1.34 (promoting)	1.22 (promoting)
L-Lysine	Lys (K)		Hydrophilic Basic (+) pKa ~ 10.5	1.07 (neutral)	0.75 (breaking)
L-Methionine	Met (M)		Hydrophobic Aliphatic	1.20 (promoting)	1.67 (promoting)
L-Phenylalanine	Phe (F)		Hydrophobic Aromatic	1.12 (promoting)	1.28 (promoting)

Table I.2. (cont.)

Amino acid	Three/ One-letter code	Structure	Nature/pKa side chain	α-Helix promoting/ breaking	β-Sheet promoting/ breaking
L-Proline	Pro (P)			0.59 (breaking)	0.62 (breaking)
L-Serine	Ser (S)		Polar Neutral	0.79 (neutral)	0.72 (breaking)
L-Threonine	Thr (T)		Polar Neutral	0.82 (neutral)	1.20 (promoting)
L-Tryptophan	Trp (W)		Hydrophobic Aromatic	1.14 (promoting)	1.19 (promoting)
L-Tyrosine	Tyr (Y)		Hydrophobic Aromatic pKa ~ 10.1	0.61 (breaking)	1.29 (promoting)
L-Valine	Val (V)		Hydrophobic Aliphatic	1.14 (promoting)	1.65 (promoting)

There are other amino acids that contain functional groups with the ability to bind other compounds. For example, cysteine (C) can bind to gold surfaces and histidine (H) has high affinity for binding Ni^{2+} ions. Additionally, Cys contains thiol groups (SH) available for the formation of intra and inter-molecular disulfide bonds (crosslinking) upon oxidation, while serine (S), threonine (T) and tryrosine (Y) provide chemical groups for chemical or enzymatic modification (e.g. OH groups in serine can be phosphorylated to yield phosphoserine). The

absence of a side chain in glycine (G) allows a higher degree of flexibility compared with other residues. On the contrary, proline (P) having its side chain attached to the amino terminus, can add structural rigidity due to its locked conformation[13].

Amino acids are therefore simple building blocks that provide relevant non-covalent interactions to build complex supramolecular assemblies. Peptides are formed by linking a series of amino acids by peptide (amide) bonds. Just using natural amino acids, the number of possible combinations that can be obtained for a single peptide or protein is extremely large (20^n, where *n* is the number of amino acids in the sequence).

As self-assembling building blocks, peptides are readily accessible through chemical synthesis; the information required for their self-assembly is encoded within their sequence; their self-assembly is usually spontaneous (simple method to develop nanostructured materials), instantaneous (milliseconds) and reproducible (defined stable structures). Furthermore, by varying systematically the chemical structure (e.g. sequence size and nature of the amino acid side groups) during synthesis it is possible to adjust the self-assembling properties of the building blocks as well as to produce a variety of diverse nanostructures (e.g. micelles, fibers, vesicles)[41].

4.1. Classes of self-assembling peptides

α-helix forming peptides

α-helical coiled coil motifs are highly diverse, in terms of structure and function, and are therefore excellent starting units to form fibrous structures[42]. Most coiled coils are based on heptad sequence repeat (**abcdefg**). The first and fourth positions (**a** and **d**) are usually hydrophobic residues and the remaining sites largely polar. This configuration results in a rope-like assembly that measures $\sim$ 1nm per heptad. Replicating the helical structure of collagen is very appealing. For example, Chaikof[43] and Hartgerink[44] have developed a strategy that employs electrostatic interaction to guide the self-assembly of hetetrimeric triple helices using aminoacid triplets (Pro-Arg-Gly)$_n$, (Glu-Hyp-Gly)$_n$, (Pro-Hyp-Gly)$_n$ on their peptide chain design. In a recent paper, Hartgerink[45] described the synthesis of collagen mimetic peptides (Pro-Lys-Gly)$_4$(Pro-Hyp-Gly)$_4$(Asp-Hyp-Gly)$_4$ that was shown to replicate the self-assembly of collagen (from peptide chain to triple helix formation to nanofiber and finally to a hydrogel). This finding demonstrates the utility of electrostatic interactions for stabilizing triple helices.

β-sheet fibrillizing peptides

A wide range of natural proteins possess intrinsic propensity to self-assemble into fibrillar nanostructures that are rich in β-sheet secondary structure[46]. The β-strands in the nanofibrils are organized perpendicularly to the fibril axis and connected through a dense hydrogen-bonding network between amides and carbonyls in the protein backbone[47]. Most β-sheet forming peptides share a common motif of alternating hydrophobic and hydrophilic residues. Another example of β-sheet fibrillizing peptide consist of a 11-residues sequence rich in glutamine, containing arginine and glutamic acid at positions 3 and 9 ($AcQ_2RQ_5EQ_2-CONH_2$). This peptide system is known to form anti-parallel β-sheets that at higher concentrations (~0.01 mM) form semi-flexible tapes[48].

Knowles et al.[49] demonstrated a scalable self-assembly approach for fabricating free-standing nanostructured films using from amyloidogenic proteins (polypeptides molecules capable of self-assembly into β-sheet rich linear aggregates).

Amphiphilic peptides

Amphiphilic peptides are beginning to attract great interest in bionanotechnology due their versatility and potential to form bioactive nanostructures by self-assembly. Their self-assembly properties have been investigated and exploited by several groups and a recent review on the topic scrutinized the existence of ~ 100 to 200 papers by May 2011[50]. The laboratory of Stupp has given important contributions in understanding the self-assembly of peptide amphiphiles and the state-of-the art on self-assembling peptides described here is focused on the molecular design of Stupp's PAs. The first element of design relies on its amphiphilic nature[51]. The peptide segment is covalently bond to a very hydrophobic segment, which can be a simple alkyl tail found in ordinary lipid molecules, or more complex aromatic-aliphatic segments, or even a steroid structure such as cholesterol. Their surfactant nature orients the more hydrophilic peptide segment into the water interface, and the hydrophobic segment to the interior of the supramolecular assembly. The peptide sequence can be further subdivided into three regions[52]. The peptide region close to the hydrophobic segment drives β-sheet formation (second element of design). There is strong theoretical evidence that β sheet formation between PAs is the driving force imposing a cylindrical geometry. This evidence is greatly supported by spectroscopic studies, which revealed a β-sheet secondary structure in which hydrogen bonding tends to be aligned along the long axis of fibers (with some degree of twisting or disruptions)[53]. The third element of design in PAs is the presence of net charge in the peptide sequence. The introduction of charged segments into the self-assembling peptide block not only enhances their

solubility in aqueous solutions but also suppress their self-assembly as a result of coulombic repulsion. The net charge also endows the PA responsive to pH variations and electrolyte addition and drives their self-assembly into cylindrical nanofibers upon neutralization or charge screening. As self-assembly proceeds, a network of bundled fibers is formed and gives origin to a self-supporting gel matrix. The fourth element of design is the epitope, a bioactive peptide sequence that bears a biological signal. This region of the peptide sequence is placed on the other extreme of the PA molecule, so it will be facing the water environment upon self-assembly, being accessible to be recognized by or to recognize other biomolecules. The nature of the cylindrical assembly of the PA system allows the presentation of high density of biological signals perpendicular to the long axis of the nanofiber, an external presentation that is favorable for cell signaling[54]. The Stupp lab has designed a variety of PA molecules with high control over their supramolecular shape and functionality. The amino acids in the peptide segment and the monomers in the alkyl tail can be varied to change the pathway of self-assembly and the physical features of the final self-assembled structure. β-sheet forming segment determines the geometrical features of PA assemblies, as well as the nanofibres internal order and cohesion.

Self-complementary peptides

The group of Zhang at MIT has developed a class of self-assembling peptides termed as self-complementary ionic peptides inspired by the segment $(RERERKRK)_2$ found in the Z-DNA binding protein zuotin[55]. The 16 amino-acid peptides, termed as RAD16-I $(RADA)_4$, KLD-12 $((LKLD)_3)$, EAK16-II $((AE)_2(AK)_2(AE)_2(AK)_2)$ are composed of alternating hydrophilic and hydrophobic amino acids residues, present β-sheet configuration and ability to form hydrogels through changes in ionic strength or pH (addition of salts or buffers[56]). These self-assembling peptide hydrogels have been shown to be effective in bone and optical nerve repair, drug delivery and as mediators to improve cardiac therapies[56]. Moreover, they have the ability to be functionalized to create cell-instructive scaffolds[57].

β-hairpin peptides

β-hairpin peptide sequences have been explored[58-59] by Schneider and Pochan, due to their ability to self-assemble into gels by its intramolecular folding propensity. The design of β-hairpin peptides comprises a tetra-peptide turn sequence $(-V^DPPT-)$ and two neighboring β strands of alternating hydrophobic valine (V) residues and hydrophilic lysine (K) residues $(VK)_4V^DPPT-(KV)_4-NH_2)$[59-60]. This initial peptide sequence has been referred as MAX1. At acidic pH, the lysines are protonated preventing peptide self-assembly. Neutralizing the charge, by addition of counterions or increase of pH, results in the formation of self-supporting rigid hydrogels by self-

assembly. Replacing the lysine residue at position 15 with a negatively charged glutamic acid (E) residue (VK)$_4$V^{D}PPT-K(VE)(VK)$_2$V-NH$_2$), the gelation kinetic of the resultant peptide (MAX8) increased significantly in response to identical cell culture conditions[61]. It has been demonstrated that the gel properties (e.g., gelation kinetics, stiffness, network mesh size) of the β-hairpin peptides have the ability to be modulated for cell encapsulation[61] or controlled release[62] purposes by changing the peptide sequence, concentration, ionic strength and/or temperature[63].

Multidomain peptides

Hartgerink's group has proposed a distinct design of peptides termed as multi-domain peptides (MDP). The MDP consists of an ABA block motif[64-66] in which the B block is composed of alternating hydrophilic and hydrophobic amino acids (glutamine or serine and leucine, respectively) surrounded by the charged flanking A blocks (e.g. glutamate or lysine). K$_2$(QL)$_6$K$_2$, K$_2$(SL)$_6$K$_2$, E(QL)$_6$E, E(SL)$_6$E are examples of MDPs investigated by the Hartgerink group. The A block provide water solubility and counteract fiber assembly via electrostatic repulsion. This design allows all glutamine or serine side chains to lie on one face of the peptide and leucine side chains on the other. In aqueous environment there will be a significant driving force for two of these hydrophobic faces to pack against one another forming a hydrophobic sandwich which consequently stabilizes the fully extended conformation. An intermolecular β-sheet hydrogen-bonding network can then be created between two or more pairs of these sandwiches. Different variations of these multidomain peptides[66-68] have been previously synthesized and demonstrated to self-assemble into well-defined nanofibers[64] with various bioactive epitopes[67,69](Table I.3.) and form self-supporting gels when the charge is screened (e.g. in presence of multivalent anions such as phosphate)[65].

4.2. Methods and techniques for the characterization of self-assembling peptides

There are a number of techniques that have been used to characterize the structural properties of self-assembling peptides and the formation of supramolecular assemblies. CD, NMR spectroscopies can provide information about the self-assembly behavior (folding) of peptides in solution while AFM and TEM have been used to provide high-resolution information on the size and nanoscale morphology of the nanostructures (Figure I.3.).
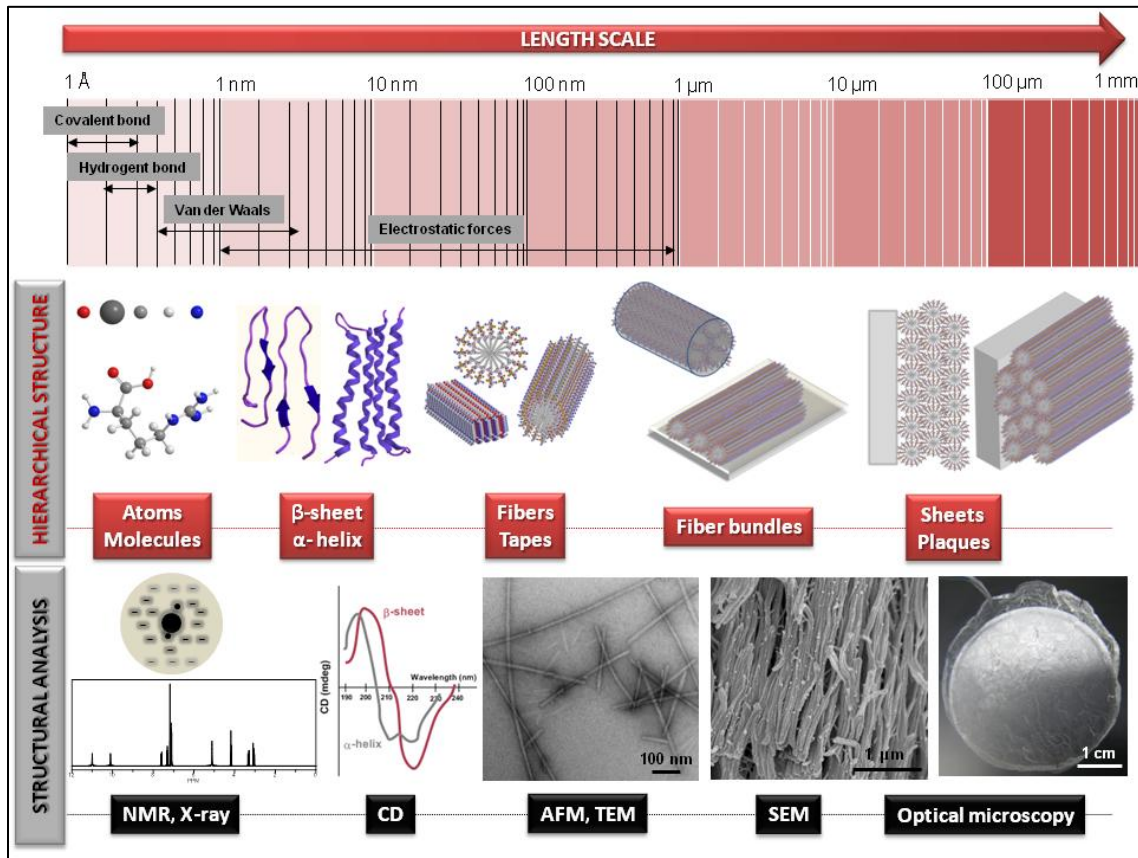
Figure I.3. Length scales of the forces involved in self-assembly[70] (*first panel*) and the hierarchical complex structures generated by peptide self-assembly (*second panel*) Spectroscopy and microscopy techniques used for structural characterization of peptide molecules and assemblies from the nanometer to centimeter length scales (*third panel*). NMR: Nuclear magnetic resonance; X‑ray: X‑ray diffraction; CD: Circular dichroism; AFM: Atomic force microscopy; TEM: Transmission-electron microscopy; SEM: Scanning-electron microscopy.

Summarizing, the network of nanofibers formed by peptide self-assembly are remarkably reminiscent of the filamentous structures found in the extracellular matrix (ECM). Cell-adhesion or macromolecular-binding sequences can be incorporated into the peptide structures and are natural choices to recreate bioactive artificial ECMs. Peptide nanofibers can display high epitope densities that facilitate receptor clustering for signaling and simultaneously maximize successful binding. Peptide self-assembly technology can further provide additional routes for the spatial and temporal program of selective binding of relevant biological molecules to nanofiber networks. For effective display of these signals on the nanoscale it is also necessary a careful synthetic design for presenting the peptide signals in a proper supramolecular setting that allows better interaction with target cell receptors.

5. APPLICATIONS OF SELF-ASSEMBLING PEPTIDE BIOMATERIALS IN REGENERATIVE MEDICINE

The extracellular matrix (ECM) of tissues is a dynamic and hierarchically organized nanocomposite that regulates essential cell functions such as adhesion, migration, proliferation and differentiation. Engineering complex tissues requires biomaterial scaffolds that recapitulate the structure and composition of ECM to provide cells with physical and biochemical signals that are important for tissue development and organization (functional tissue). 3D scaffolds, in which cells are randomly distributed, offer limited control over spatial cell organization and tissue architecture. Microscale control over cell position and ECM composition may enable improved regulation of biochemical signaling, interactions between cells and ECM and cell-cell contacts.

To recreate the structure and function of natural ECMs, and to promote cell-matrix interactions at the molecular level, self-assembly allows to create scaffolds based on a network of interwoven nanofibers. The nanofibers can have diameters as small as 10 nm (significantly smaller that those obtained by electrospinning, a top-down fabrication technique) and be designed with bioactivity to provide cells with instructive cues towards tissue formation.

Materials that provide temporary function, while stimulating and guiding tissue regeneration, would be useful throughout medicine. At sufficiently high concentration, the fibrillization of peptides is accompanied by gelation. Nanofibers obtained by self-assembly can become entangled to form network hydrogels that have a variety of applications including artificial matrices for cell culture, controlled drug delivery and tissue engineering. This part of the review will focus on the application of self-assembling peptides as biomaterials and highlights the most relevant works that the authors considered of particular interest and significance in the field. Several excellent reviews are cited that are sources of more detailed descriptions and discussions.

5.1. Peptide hydrogels for 3D cell culture

Traditional cell culture is performed on 2D plastic surfaces which are far from the complex 3D environment where cells naturally reside. 3D environments provide another dimension for external mechanical and chemical inputs, which dramatically affects integrin ligation, cell contraction and associated intracellular signaling. Furthermore, 3D models might help to isolate and investigate specific cell-cell and cell-ECM interactions. Well-defined synthetic 3D systems require control not only of cell adhesion sites and matrix viscoelasticity, but of nano and microporosity (which regulates cell motility and the transport of soluble molecules), growth-factor binding and matrix degradation. Peptide hydrogels offer significant potential to recreate 3D cell

culture biomimetic environments because the formation of these self-assembled matrices occurs under physiological and cytocompatible conditions enabling the direct encapsulation of cells in a 3D environment. Zhou and co-workers, developed a peptide-based bioactive hydrogel as 3D scaffolds for anchorage-dependent cells[71]. This hydrogel is formed through self-assembling of two aromatic short peptide derivatives: Fmoc-FF (Fluorenylmethoxycarbonyl-diphenylalanine) and Fmoc-RGD (arginine-glycine-aspartate) and exhibited a highly hydrated, stiff and nanofibrous network comprising bioactive ligands at the fiber surface, mimicking some features of the extracellular matrix. Encapsulated dermal fibroblasts were observed to adhere, spread and proliferate within this hydrogel, suggesting the use of these self-assembled matrices as suitable model scaffolds for 3D cell culture.

Several works describing the use of self-assembled peptide hydrogels for cell encapsulation and 3D cell culture (Table I.3.) have been reported in the literature[13,72]. Some examples will be also described in the topic peptide hydrogels as scaffold for tissue engineering.

5.2. Peptide hydrogels for delivery of bioactive factors

Peptide-based matrices have also been used for the delivery of therapeutic agents such as proteins and small molecules (e.g. drugs). Physical encapsulation/entrapment of proteins (e.g. lysozyme, trypsin inhibitor, bovine serum albumin (BSA), and Immunoglobulin (IgG) was reported by Koutsopoulos using self-complementary ionic peptide gels (Table I.3.)[73]. It was demonstrated that the protein release through the peptide hydrogels was dependent on the protein size and the density of the peptide nanofibers. Similar strategy was applied by Branco and co-workers[74] for entraping proteins, BSA, IgG, lysozyme, α-lactalbumin, myoglobin and lactoferrin within β-hairpin gels. The release rate of the protein was shown to be dependent on the charge density of the protein.

These systems have also been used for the controlled release of small drugs. Herein, the drug is encapsulated by physical entrapment within the gel, as reported by Altunbas et al[62] in the encapsulation of the hydrophobic polyphenol curcumin within β-hairpin gel. The release rate was modulated as function of peptide concentration. Webber[26] also demonstrated the ability to encapsulate chemotherapeutics, such as doxorubicin (cancer drug) in the core of peptide amphiphiles nanofibers. The drug was released through the disassembly of peptide nanofibers triggered by enzymatic phosphorylation of a serine residue.

Self-assembling peptides have also been designed to act as reservoir for the local and temporal release of growth factors (GFs) through the incorporation of GF binding sequences. Stupp and co-workers found peptide sequences by phage display with binding affinity for BMP-2 (e.g.

YPVHPST[75] and TGF-β1 (e.g. LPLGNSH)[76] growth factors with potential use in bone and cartilage regeneration, respectively. The use of heparin binding peptide sequences has been also applied for the controlled release of angiogenic growth factors for therapeutic applications in islet transplantation and cardiovascular disease[77].

5.3. Peptide hydrogels as scaffolds for tissue repair

Bone

Despite four decades of research on bone regeneration therapies, the gold standard in bone replacement therapy is still the use of autografts (patient's own bone) or allografts (donor bone). However, both approaches present drawbacks such as morbidity and severe pain complications at the donor-site of harvesting, risk of septic complications, viral transmission or disease transfer and limited bone volume at donor site[78]. In that respect, there is an enormous need for synthetic replacements for bone repair and regeneration. The use of self-assembling peptides for bone repair applications has been reviewed[56,79]. Several studies demonstrated the potential of these materials for bone regeneration. For example, 3D self-assembled peptide nanofibers were shown to enhance significantly the *in vitro* proliferation and osteogenic differentiation of mesenchymal stem cells when compared with conventional cell culture plate[80]. Moreover, it was found that self-assembling peptide sequences containing the phosphoserine (S(P)) residue and the RGD cell adhesion sequence ($C_{16}O$-$C_4G_3S(P)RGD$) have the ability to induce hydroxyapatite mineralization in 2D[81]. Later, this combination of signaling epitopes (5% RGDS and S(P) 95%) simultaneously with pre-osteoblastic cells were loaded as a gel into a porous titanium foam in order to increase biocompatibility of typical metallic implants[82-83]. The ability of these amphiphilic self-assembled matrices ($GS(P)E_2L_3A_3$-OC_{16} and $SDGRK_2L_3A_3$-OC_{16}) to induce faster bone regeneration at tissue interfaces was demonstrated. The same nanofiber matrix was tested in a rat femoral critical size defect and showed significant bone formation[84]. In another study, peptide functionalized with RGDS ($CH_3(CH_2)_{14}CONH$–GTAGLIGQ–RGDS) and DGEA ($CH_3(CH_2)_{14}CONH$–GTAGLIGQ–DGEA) sequences were investigated as an ECM-mimicking biomaterial to provide an instructive microenvironment for osteogenic differentiation of human mesenchymal stem cells[85], showing osteogenic differentiation with and without the addition of osteogenic media. Additionally, self-assembled nanostructures consisting of BMP receptor-binding peptides[86-87], as mentioned previously, have been explored due to its osteoinductive potential to be applied in bone repair therapies. RAD16 peptide based gels have also been demonstrated to be valuable in enhancing of bone regeneration[56,88-89].

Cartilage

Cartilage is an avascular tissue with low capacity of self-repair mainly due to the reduced availability of chondrocytes and absence of progenitor cells in cartilage tissue, and restricted mobility of chondrocytes in the dense ECM. Cartilage lesions, caused by trauma or disease, results in the loss of partial or complete tissue functionality. Thus, one of the approaches in regenerative medicine for repairing cartilage defects consist on the use of an injectable system capable of gelling in situ, to deliver autologous chondrocytes and stimulating cells to produce cartilage. Significant advances have been made in developing self-assembling gels for creating well-controlled 3D environments for encapsulating chondrocytes to foster the formation of cartilage. For instance, a self-assembling KLD-12 peptide hydrogel was used as a 3D scaffold for encapsulation of chondrocytes[90]. This self-assembling matrix was found to support cell survival and to retain the chondrocytic phenotype with increased production of glycosaminoglycans and type II collagen (components of cartilage ECM). Moreover an increase in dynamic stiffness of the matrix material during the culture period was observed. In another study, bone marrow stromal cells were encapsulated within a self-assembling peptide hydrogel containing two peptide sequences (KLD-12 and RADA16-I) known to enhance chondrogenic differentiation [91]. Chondrogenesis in these self-assembling peptide matrices was shown to be superior when compared with agarose hydrogels, as shown by extracellular matrix production, DNA content, and aggrecan molecular structure.

Also in the context of cartilage repair using self-assembling peptide hydrogels, a peptide amphiphile (Table I.3.) was designed to form nanofibers for cartilage regeneration and displaying a high density of TGFβ-1 binding sequence. These materials were shown to support the survival and promote the chondrogenic differentiation of MSCs[76]. Moreover, regeneration of articular cartilage in a full thickness chondral defect treated with microfracture in a rabbit model, with or even without the addition of exogenous growth factor, was also observed.

Central nervous system

The central nervous system (CNS) is a dynamic organ which is prone to injury and degeneration. Stimulation of the central nervous system to regenerate after trauma (e.g. after spinal cord injury, SCI) both structurally and functionally, still remains a significant challenge due to the inherent complexity of the adult CNS, as well as the inability of the central neurons to regenerate correct axonal and dendritic connections. Strategies for regenerating the adult CNS include cellular replacement, neurotrophic factor delivery, axon guidance and removal of growth inhibition, manipulation of intracellular signaling, cellular bridging and artificial substrates, and

modulation of the immune response[92]. Artificial substrates may be useful for repair of lesions where cellular bridging is necessary. The ideal artificial substrate will have a molecular composition that is easily manipulated and immune tolerant, and will contain a porous structure for nerve regeneration and cell repopulation that will be easily absorbed by the CNS. Different types of self-assembled peptide hydrogels have been investigated for CNS repair. A peptide amphiphile containing the IKVAV epitope (Table I.3.) and able to form three-dimensional networks of nanofibers by self-assembly, was used to encapsulate neural progenitor cells. The IKVAV sequence is derived from the protein laminin responsible for neurite growth[54]. This artificial nanofiber scaffold was shown to induce very rapid differentiation of cells into neurons, while discouraging the development of astrocytes comparatively to laminin. These findings had led the same authors to use a similar PA molecule containing the IKVAV epitope ($C_{16}O$-$(SL)_2A_3EIKVAV$) *in vivo* using a mouse model of SCI[93]. The peptide solution was injected at the site of injury where gelation took place. It was found that treatment with the PA reduced astrogliosis, reduced cell death and increased number of oligodendroglia at the injury site. In addition, the IKVAV based peptide gel promoted the regeneration of injured motor and sensory axons, while in injured spinal cords treated with peptide gel (without IKVAV sequence) axons were unable to traverse the lesion. Later, using two SCI models (compression and contusion) and two different species (mice and rats), the injection of IKVAV PA on the animal functional recovery was investigated[94]. This study confirmed the regeneration potential of the IKVAV PA in improving behavioral outcome by stimulating axon regeneration through the lesion.

Peptide hydrogels, formed by self-assembly of ionic self-complementary peptides (($RADA)_4$ and ($RARADADA)_2$) at physiological conditions, were also shown to perform successfully in neurorepair strategies[95]. It was demonstrated the ability of these gels to support neuronal cell attachment, differentiation and extensive neurite outgrowth, being permissive substrates for functional synapse formation between the attached neurons. The authors postulated that the bioactivity of these peptides is due to the similarity of the tripeptide arginine-alanine-aspartate (RAD) sequence in the peptide with the RGD motif which is known as a binding site for some cell integrins. The ability of these peptide hydrogels for brain repair was also demonstrated using a severed optic tract in a hamster model. Injection of peptide solution at the lesion site created a permissive environment for regenerated axons to reconnect to target tissues with sufficient density to promote functional recovery, as demonstrated by a return of lost vision[96]. In another study, ($RADA)_4$ peptide was used as a scaffold for transplantation of neural progenitor cells and Schwann cells into the transected dorsal column of spinal cord of rats to evaluate its potential for spinal cord injury repair[97]. The self-assembled matrix was shown to promote survival, migration and differentiation of both cells. In addition, migration of host cells, growth of blood vessels and

axons into the scaffolds was also observed. The same hydrogels were also investigated on the reconstruction of acutely injured brain. Increased brain tissue restoration was observed in groups treated with this hydrogel[98].

Revascularization therapies

Angiogenesis, the process of new blood vessels formation, assumes great relevance in wound healing. Heparin based molecules have shown to play an important role in angiogenesis due to their ability to bind, stabilize, and protect proangiogenic proteins such as vascular endothelial growth factor (VEGF) and basic fibroblast growth factor (FGF-2). Based on this knowledge, heparin was used to trigger the self-assembly of peptide amphiphile molecules[99-100] containing heparin binding sequences ($C_{16}O$-A_4G_3-LRKKLGKA) demonstrating the ability of these systems to stimulate new blood vessel formation *in vivo*. In diabetes type I, loss of vascular networks during islet isolation from donor tissue is common. However, implanting heparin-containing peptide gels delivering VEGF, FGF-2 in diabetic mouse significantly increased vascular density in the transplant site and improved islet engraftment, as evidenced through the higher cure percentages and shorter times to achieve normoglycemia[101]. These heparin binding peptide nanofibers with heparin displayed on their surfaces has shown to increase islet survival and insulin secretion and if combined with angiogenic growth factors lead to enhanced levels of islet endothelial cells sprouting[102] that may be valuable in islet transplantation to treat diabetes type I.

There is a need of cell-based therapies for ischemic tissue repair in cardiovascular diseases, as result of limited regeneration of cardiomyocytes[103]. To overcome this limitation, a biocompatible matrix is normally required to support cell functions during the transplantation, once the direct cell transplantation (embryonic stem or endothelial progenitor cells) results in low cellular viability and minimal retention[104]. A scaffold constituted of self-assembled peptide nanofibers containing fibronectin-derived RGDS cell adhesion epitope was used to encapsulate bone marrow-derived stem and progenitor cells *in vivo*[104]. Enhanced viability, proliferation and adhesion of encapsulated cells suggested the potential of these materials to be applied in cell therapies for ischemic diseases. Self-assembled RAD16 based gels have also shown to support the survival of encapsulated endothelial and myocardial cells[105] and the potential to create a 3D micro-environment when injected in myocardium by recruiting both endogenous endothelial and smooth muscle cells with stimulation of vascularization[103].

Heparin binding peptide nanofiber gels were observed to have binding ability for paracrine factors from hypoxic conditioned stem cell media[106]. When injected in coronary artery ligation, the preservation of hemodynamic function in a mouse ischemia (reperfusion model of acute

myocardial infarction) was observed and revascularization in chronic rat ischemic hind limb models was stimulated.

Peptide nanostructures containing bioactive signals offer exciting novel therapies with potential impact in regenerative medicine. Table I.3. display some examples of self-assembling peptide structures containing different biological epitopes for specific applications.

Table I.3. Self-assembling peptide biomaterials presenting different epitopes for a variety of regenerative applications.

Peptide sequence/design Self-assembling block + epitope	Supramolecular material Self-assembling mode	Application	Reference
$C_{16}O$-A_4G_3E**IKVAV** Negative PA + Laminin-derived cell adhesion sequence	Gel formed by addition of culture medium	Selective differentiation of neural progenitor cells.	[54]
$C_{16}O$-$V_3A_3E_3$**RGDS** Negative PA + Fibronectin-derived cell adhesion sequence	Gel formed by the addition of Ca^{2+} ions.	Cell delivery in cell-based therapies.	[104]
HSNGLPLGGGSEEEAAAVVV(K)-$CO(CH_2)_{10}CH_3$ TGFβ1 binding sequence + Reverse negative PA	Gel formed by the addition of Ca^{2+} ions.	Cartilage regeneration	[76]
$C_{16}O$-$V_2A_2K_3$**GKLTWQELYQLKYKGI**-NH_2 Positive PA + VEGF-mimetic peptide	Non-assembled material	Ischemic tissue repair	[107]
RGDSKKLLA(K)-(COC_8H_{16})-diacetylene-(C_2H_{25}) Fibronectin-derived cell adhesion sequence + Positive diacetylene PA	Patterned gel formed by diffusion of NH_4OH vapor and further polymerized by UV radiation.	Substrate to study behavior of human mesenchymal stem cells	[108]
$C_{16}O$-**GTAGLIGQE**RGDS Negative PA + Enzymatic (MMP-2) cleavage sequence+ Fibronectin-derived cell adhesion sequence	Gel formed by the addition of Ca^{2+} ions.	Dental tissue regeneration	[109]
Ac-**K(SL)$_3$SLRG(SL)$_3$K**RGDS-CONH$_2$ Positive MDP + Enzymatic cleavage sequence (MMP-2) + Fibronectin-derived cell adhesion sequence	Gel formed by the addition of phosphate or heparin	Dental pulp tissue engineering	[110]
Ac-G**GRDS**GGG**QQKFQFQFEQQ**-	Microgel formed by the addition of	Cell encapsulation.	[111]

$CONH_2$ Fibronectin-derived cell adhesion sequence + β-sheet fibrillizing peptide Ac-GG**IKVAV**GGG-(Q$_{11}$)-$CONH_2$ Laminin-derived cell adhesion sequence + β-sheet fibrillizing peptide	PBS in a water-in-oil emulsion. Hydrogel formed by the addition of PBS.	Defined matrices for endothelial cells growth.	
Ac-G**RGDS**PG-G(RADA)$_4$-$CONH_2$ Fibronectin-derived cell adhesion sequence + Self-complementary peptide Ac-**YIGSR**GG(RADA)$_4$-$CONH_2$ Laminin-derived cell adhesion sequence + Self-complementary peptide	Gel formed by addition of hepatocyte culture medium. Gel formed by addition of PBS.	Peptide immobilized on syntethic membranes for hepatocyte culture. Substrate for endothelial cell culture	57,56,112
Fmoc-FF, Fmoc-**RGD** Fmoc-protected dipeptide + Fibronectin-derived cell adhesion sequence	Gel formed by pH and temperature changes	Cell encapsulation/ 3D culture	71

TGFβ1- Transforming growth factor beta 1 (chondrogenesis promoter protein); VEGF- Vascular endothelial growth factor (angiogenic signaling protein).

6. SUMMARY AND OUTLOOK

The exciting findings on peptide self-assembly suggest that this bottom-up technology can offer tools to the three-dimensional assembly of supramolecular objects at scales and with geometrical complexity and regularity not accessible to top-down technologies. Despite the level of precision, there has been difficult to construct these self-assembling systems across length scales. Hierarchical structures are of great advantage for tissue engineering applications as they provide a more natural environment for cells to grow and develop into tissues. In addition, the mechanical properties of materials intimately reflect the nature of the intermolecular interactions that held together their building units into large-scale hierarchical systems. Understanding how to control the fabrication and organization of matter across multiple length scales is of growing interest to construct complex materials with practical utility namely as complex biomaterials for applications in tissue regeneration, drug delivery and cell culture.

REFERENCES

1. Boncheva M, Whitesides GM. Making things by self-assembly. Mrs Bulletin 2005;30(10):736-742.

2. Halley JD, Winkler DA. Consistent Concepts of Self-organization and Self-assembly. Complexity 2008;14(2):10-17.

3. Pelesko JA. SELF ASSEMBLY, The Sciense of Things That Put Themselves Togheter: Taylor & Francis Group; 2007.

4. Steed JW. Core concepts in supramolecular chemistry and nanochemistry / Jonathan W. Steed, David R. Turner, Karl J. Wallace. Chichester, England ; Hoboken, NJ :: John Wiley; 2007.

5. Whitesides GM, Grzybowski B. Self-Assembly at All Scales. Science 2002;295(5564):2418-2421.

6. Whitesides GM, Mathias JP, Seto CT. Molecular Self-Assembly and Nanochemistry - a Chemical Strategy for the Synthesis of Nanostructures. Science 1991;254(5036):1312-1319.

7. Bhagavan NV. Medical Biochemistry: Harcourt/Academic Press; 2002.

8. Li HY, LaBean TH, Leong KW. Nucleic acid-based nanoengineering: novel structures for biomedical applications. Interface Focus 2011;1(5):702-724.

9. Whitesides GM, Boncheva M. Beyond molecules: Self-assembly of mesoscopic and macroscopic components. Proceedings of the National Academy of Sciences of the United States of America 2002;99(8):4769-4774.

10. Collier JH, Messersmith PB. PHOSPHOLIPID STRATEGIES IN BIOMINERALIZATION AND BIOMATERIALS RESEARCH. Annual Review of Materials Research 2001;31(1):237-263.

11. Capito RM, Azevedo HS, Velichko YS, Mata A, Stupp SI. Self-assembly of large and small molecules into hierarchically ordered sacs and membranes. Science 2008;319(5871):1812-1816.

12. Scanlon S, Aggeli A. Self-assembling peptide nanotubes. Nano Today 2008;3(3-4):22-30.

13. Ulijn RV, Smith AM. Designing peptide based nanomaterials. Chemical Society Reviews 2008;37(4):664-675.

14. Zayed JM, Nouvel N, Rauwald U, Scherman OA. Chemical complexity-supramolecular self-assembly of synthetic and biological building blocks in water. Chemical Society Reviews 2010;39(8):2806-2816.

15. Schnur JM. Lipid Tubules - a Paradigm for Molecularly Engineered Structures. Science 1993;262(5140):1669-1676.

16. Bromley EHC, Channon K, Moutevelis E, Woolfson DN. Peptide and protein building blocks for synthetic biology: From programming biomolecules to self-organized biomolecular systems. Acs Chemical Biology 2008;3(1):38-50.

17. Smith DK. Dendritic supermolecules - towards controllable nanomaterials. Chemical Communications 2006(1):34-44.

18. Reynhout IC, Cornelissen JJLM, Nolte RJM. Synthesis of Polymer-Biohybrids: From Small to Giant Surfactants. Accounts of Chemical Research 2009;42(6):681-692.

19. Faul CFJ, Antonietti M. Ionic self-assembly: Facile synthesis of supramolecular materials. Advanced Materials 2003;15(9):673-683.

20. Aida T, Meijer EW, Stupp SI. Functional Supramolecular Polymers. Science 2012;335(6070):813-817.

21. Hoeben FJM, Jonkheijm P, Meijer EW, Schenning APHJ. About supramolecular assemblies of pi-conjugated systems. Chemical Reviews 2005;105(4):1491-1546.

22. Smith DK. Lost in translation? Chirality effects in the self-assembly of nanostructured gel-phase materials. Chemical Society Reviews 2009;38(3):684-694.

23. Keum JW, Hathorne AP, Bermudez H. Controlling forces and pathways in self-assembly using viruses and DNA. Wiley Interdisciplinary Reviews-Nanomedicine and Nanobiotechnology 2011;3(3):282-297.

24. Zhang SM, Greenfield MA, Mata A, Palmer LC, Bitton R, Mantei JR, Aparicio C, de la Cruz MO, Stupp SI. A self-assembly pathway to aligned monodomain gels. Nature Materials 2010;9(7):594-601.

25. Muraoka T, Koh CY, Cui HG, Stupp SI. Light-Triggered Bioactivity in Three Dimensions. Angewandte Chemie-International Edition 2009;48(32):5946-5949.

26. Webber MJ, Newcomb CJ, Bitton R, Stupp SI. Switching of self-assembly in a peptide nanostructure with a specific enzyme. Soft Matter 2011;7(20):9665-9672.

27. Spoerke ED, Anthony SG, Stupp SI. Enzyme Directed Templating of Artificial Bone Mineral. Advanced Materials 2009;21(4):425-+.

28. Hirst AR, Roy S, Arora M, Das AK, Hodson N, Murray P, Marshall S, Javid N, Sefcik J, Boekhoven J and others. Biocatalytic induction of supramolecular order. Nature Chemistry 2010;2(12):1089-1094.

29. Roy S, Ulijn RV. Exploiting Biocatalysis in the Synthesis of Supramolecular Polymers. Enzymatic Polymerisation 2010;237:127-143.

30. Williams RJ, Mart RJ, Ulijn RV. Exploiting Biocatalysis in Peptide Self-Assembly. Biopolymers 2010;94(1):107-117.

31. Williams RJ, Smith AM, Collins R, Hodson N, Das AK, Ulijn RV. Enzyme-assisted self-assembly under thermodynamic control. Nature Nanotechnology 2009;4(1):19-24.

32. Grzybowski BA, Wilmer CE, Kim J, Browne KP, Bishop KJM. Self-assembly: from crystals to cells. Soft Matter 2009;5(6):1110-1128.

33. Carnall JMA, Waudby CA, Belenguer AM, Stuart MCA, Peyralans JJP, Otto S. Mechanosensitive Self-Replication Driven by Self-Organization. Science 2010;327(5972):1502-1506.

34. Lowik DWPM, Shklyarevskiy IO, Ruizendaal L, Christianen PCM, Maan JC, van Hest JCM. A highly ordered material from magnetically aligned peptide amphiphile nanofiber assemblies. Advanced Materials 2007;19(9):1191-+.

35. van den Heuvel M, Prenen AM, Gielen JC, Christianen PCM, Broer DJ, Lowik DWPM, van Hest JCM. Patterns of Diacetylene-Containing Peptide Amphiphiles Using Polarization Holography. Journal of the American Chemical Society 2009;131(41):15014-15017.

36. Cui HG, Pashuck ET, Velichko YS, Weigand SJ, Cheetham AG, Newcomb CJ, Stupp SI. Spontaneous and X-ray-Triggered Crystallization at Long Range in Self-Assembling Filament Networks. Science 2010;327(5965):555-559.

37. Velichko YS, Mantei JR, Bitton R, Carvajal D, Shull KR, Stupp SI. Electric Field Controlled Self-Assembly of Hierarchically Ordered Membranes. Advanced Functional Materials 2012;22(2):369-377.

38. Albericio F. Orthogonal protecting groups for N alpha-amino and C-terminal carboxyl functions in solid-phase peptide synthesis. Biopolymers 2000;55(2):123-139.

39. Alvarez M, Isidro-Llobet A, Albericio F. Amino Acid-Protecting Groups. Chemical Reviews 2009;109(6):2455-2504.

40. Chan WC, White PD. Fmoc solid phase peptide synthesis - a practical approach. Oxford: Oxford University Press; 2000.

41. Gazit E. BIOINSPIRED CHEMISTRY Diversity for self-assembly. Nature Chemistry 2010;2(12):1010-1011.

42. Bromley EH, Channon K, Moutevelis E, Woolfson DN. Peptide and protein building blocks for synthetic biology: from programming biomolecules to self-organized biomolecular systems. ACS Chem Biol 2008;3(1):38-50.

43. Rele S, Song YH, Apkarian RP, Qu Z, Conticello VP, Chaikof EL. D-periodic collagen-mimetic microfibers. Journal of the American Chemical Society 2007;129(47):14780-14787.

44. Fallas JA, O'Leary LER, Hartgerink JD. Synthetic collagen mimics: self-assembly of homotrimers, heterotrimers and higher order structures. Chemical Society Reviews 2010;39(9):3510-3527.

45. O'Leary LER, Fallas JA, Bakota EL, Kang MK, Hartgerink JD. Multi-hierarchical self-assembly of a collagen mimetic peptide from triple helix to nanofibre and hydrogel. Nature Chemistry 2011;3(10):821-828.

46. Gazit E. Self-assembled peptide nanostructures: the design of molecular building blocks and their technological utilization. Chemical Society Reviews 2007;36(8):1263-1269.

47. Knowles TPJ, Buehler MJ. Nanomechanics of functional and pathological amyloid materials. Nature Nanotechnology 2011;6(8):469-479.

48. Collier JH, Rudra JS, Gasiorowski JZ, Jung JP. Multi-component extracellular matrices based on peptide self-assembly. Chemical Society Reviews 2010;39(9):3413-24.

49. Knowles TPJ, Oppenheim TW, Buell AK, Chirgadze DY, Welland ME. Nanostructured films from hierarchical self-assembly of amyloidogenic proteins. Nature Nanotechnology 2010;5(3):204-207.

50. Hamley IW. Self-assembly of amphiphilic peptides. Soft Matter 2011;7(9):4122-4138.

51. Cui HG, Webber MJ, Stupp SI. Self-Assembly of Peptide Amphiphiles: From Molecules to Nanostructures to Biomaterials. Biopolymers 2010;94(1):1-18.

52. Webber MJ, Kessler JA, Stupp SI. Emerging peptide nanomedicine to regenerate tissues and organs. Journal of Internal Medicine 2010;267(1):71-88.

53. Jiang HZ, Guler MO, Stupp SI. The internal structure of self-assembled peptide amphiphiles nanofibers. Soft Matter 2007;3(4):454-462.

54. Silva GA, Czeisler C, Niece KL, Beniash E, Harrington DA, Kessler JA, Stupp SI. Selective differentiation of neural progenitor cells by high-epitope density nanofibers. Science 2004;303(5662):1352-1355.

55. Zhang S, Holmes T, Lockshin C, Rich A. Spontaneous assembly of a self-complementary oligopeptide to form a stable macroscopic membrane. Proceedings of the National Academy of Sciences 1993;90(8):3334-3338.

56. Semino CE. Self-assembling Peptides: From Bio-inspired Materials to Bone Regeneration. Journal of Dental Research 2008;87(7):606-616.

57. Wu J, Mari-Buye N, Muinos T, Borros S, Favia P, Semino C. Nanometric self-assembling peptide layers maintain adult hepatocyte phenotype in sandwich cultures. Journal of Nanobiotechnology 2010;8(1):29.

58. Hule RA, Nagarkar RP, Hammouda B, Schneider JP, Pochan DJ. Dependence of Self-Assembled Peptide Hydrogel Network Structure on Local Fibril Nanostructure. Macromolecules 2009;42(18):7137-7145.

59. Schneider JP, Pochan DJ, Ozbas B, Rajagopal K, Pakstis L, Kretsinger J. Responsive Hydrogels from the Intramolecular Folding and Self-Assembly of a Designed Peptide. Journal of the American Chemical Society 2002;124(50):15030-15037.

60. Rughani RV, Schneider JP. Molecular Design of beta-Hairpin Peptides for Material Construction. Mrs Bulletin 2008;33(5):530-535.

61. Haines-Butterick L, Rajagopal K, Branco M, Salick D, Rughani R, Pilarz M, Lamm MS, Pochan DJ, Schneider JP. Proc. Natl. Acad. Sci. U.S.A. 2007;104:7791.

62. Altunbas A, Lee SJ, Rajasekaran SA, Schneider JP, Pochan DJ. Encapsulation of curcumin in self-assembling peptide hydrogels as injectable drug delivery vehicles. Biomaterials 2011;32(25):5906-5914.

63. Yan C, Mackay ME, Czymmek K, Nagarkar RP, Schneider JP, Pochan DJ. Injectable Solid Peptide Hydrogel as a Cell Carrier: Effects of Shear Flow on Hydrogels and Cell Payload. Langmuir 2012;28(14):6076-6087.

64. Dong H, Paramonov SE, Aulisa L, Bakota EL, Hartgerink JD. Self-assembly of multidomain peptides: Balancing molecular frustration controls conformation and nanostructure. Journal of the American Chemical Society 2007;129(41):12468-12472.

65. Dong H, Paramonov SE, Aulisa L, Bakota EL, Hartgerink JD. Self-Assembly of Multidomain Peptides: Balancing Molecular Frustration Controls Conformation and Nanostructure. Journal of the American Chemical Society 2007;129(41):12468-12472.

66. Aulisa L, Dong H, Hartgerink JD. Self-Assembly of Multidomain Peptides: Sequence Variation Allows Control over Cross-Linking and Viscoelasticity. Biomacromolecules 2009;10(9):2694-2698.

67. Galler KM, Aulisa L, Regan KR, D'Souza RN, Hartgerink JD. Self-Assembling Multidomain Peptide Hydrogels: Designed Susceptibility to Enzymatic Cleavage Allows Enhanced Cell Migration and Spreading. Journal of the American Chemical Society 2010;132(9):3217-3223.

68. Galler KM, Aulisa L, Regan KR, D'Souza RN, Hartgerink JD. Self-Assembling Multidomain Peptide Hydrogels: Designed Susceptibility to Enzymatic Cleavage Allows Enhanced Cell Migration and Spreading. Journal of the American Chemical Society 2010;132(9):3217-3223.

69. Galler KM, Hartgerink JD, Cavender AC, Schmalz G, D'Souza RN. A Customized Self-Assembling Peptide Hydrogel for Dental Pulp Tissue Engineering. Tissue Engineering Part A 2012;18(1-2):176-184.

70. Palermo V, Samori P. Molecular self-assembly across multiple length scales. Angewandte Chemie-International Edition 2007;46(24):4428-4432.

71. Zhou M, Smith AM, Das AK, Hodson NW, Collins RF, Ulijn RV, Gough JE. Self-assembled peptide-based hydrogels as scaffolds for anchorage-dependent cells. Biomaterials 2009;30(13):2523-2530.

72. Collier JH, Rudra JS, Gasiorowski JZ, Jung JP. Multi-component extracellular matrices based on peptide self-assembly. Chemical Society Reviews 2010;39(9):3413-3424.

73. Koutsopoulos S, Unsworth LD, Nagai Y, Zhang S. Controlled release of functional proteins through designer self-assembling peptide nanofiber hydrogel scaffold. Proceedings of the National Academy of Sciences 2009;106(12):4623-4628.

74. Branco MC, Pochan DJ, Wagner NJ, Schneider JP. The effect of protein structure on their controlled release from an injectable peptide hydrogel. Biomaterials 2010;31(36):9527-9534.

75. Behanna HA, Donners JJ, Gordon AC, Stupp SI. Coassembly of amphiphiles with opposite peptide polarities into nanofibers. Journal of the American Chemical Society 2005;127(4):1193-200.

76. Shah RN, Shah NA, Del Rosario Lim MM, Hsieh C, Nuber G, Stupp SI. Supramolecular design of self-assembling nanofibers for cartilage regeneration. Proceedings of the National Academy of Sciences 2010;107(8):3293-3298.

77. Matson JB, Stupp SI. Self-assembling peptide scaffolds for regenerative medicine. Chemical Communications 2012;48(1):26-33.

78. Khan Y, Yaszemski MJ, Mikos AG, Laurencin CT. Tissue engineering of bone: Material and matrix considerations. Journal of Bone and Joint Surgery 2008(90A):36-42.

79. Matson JB, Zha RH, Stupp SI. Peptide self-assembly for crafting functional biological materials. Current Opinion in Solid State & Materials Science 2011;15(6):225-235.

80. Hosseinkhani H, Hosseinkhani M, Tian F, Kobayashi H, Tabata Y. Osteogenic differentiation of mesenchymal stem cells in self-assembled peptide-amphiphile nanofibers. Biomaterials 2006;27(22):4079-86.

81. Hartgerink JD, Beniash E, Stupp SI. Self-assembly and mineralization of peptide-amphiphile nanofibers. Science 2001;294(5547):1684-8.

82. Sargeant TD, Oppenheimer SM, Dunand DC, Stupp SI. Titanium foam-bioactive nanofiber hybrids for bone regeneration. Journal of Tissue Engineering and Regenerative Medicine 2008;2(8):455-462.

83. Sargeant TD, Guler MO, Oppenheimer SM, Mata A, Satcher RL, Dunand DC, Stupp SI. Hybrid bone implants: self-assembly of peptide amphiphile nanofibers within porous titanium. Biomaterials 2008;29(2):161-71.

84. Mata A, Geng Y, Henrikson KJ, Aparicio C, Stock SR, Satcher RL, Stupp SI. Bone regeneration mediated by biomimetic mineralization of a nanofiber matrix. Biomaterials 2010;31(23):6004-12.

85. Anderson JM, Vines JB, Patterson JL, Chen H, Javed A, Jun HW. Osteogenic differentiation of human mesenchymal stem cells synergistically enhanced by biomimetic peptide amphiphiles combined with conditioned medium. Acta Biomater 2011;7(2):675-82.

86. Hosseinkhani H, Hosseinkhani M, Khademhosseini A, Kobayashi H. Bone regeneration through controlled release of bone morphogenetic protein-2 from 3-D tissue engineered nano-scaffold. Journal of Controlled Release 2007;117(3):380-386.

87. Lee JY, Choo JE, Choi YS, Suh JS, Lee SJ, Chung CP, Park YJ. Osteoblastic differentiation of human bone marrow stromal cells in self-assembled BMP-2 receptor-binding peptide-amphiphiles. Biomaterials 2009;30(21):3532-41.

88. Misawa H, Kobayashi N, Soto-Gutierrez A, Chen Y, Yoshida A, Rivas-Carrillo JD, Navarro-Alvarez N, Tanaka K, Miki A, Takei J and others. PuraMatrix facilitates bone regeneration in bone defects of calvaria in mice. Cell Transplantation 2006;15(10):903-10.

89. Horii A, Wang X, Gelain F, Zhang S. Biological designer self-assembling peptide nanofiber scaffolds significantly enhance osteoblast proliferation, differentiation and 3-D migration. Plos One 2007;2(2):e190.

90. Kisiday J, Jin M, Kurz B, Hung H, Semino C, Zhang S, Grodzinsky AJ. Self-assembling peptide hydrogel fosters chondrocyte extracellular matrix production and cell division: Implications for cartilage tissue repair. Proceedings of the National Academy of Sciences 2002;99(15):9996-10001.

91. Kopesky PW, Vanderploeg EJ, Sandy JS, Kurz B, Grodzinsky AJ. Self-assembling peptide hydrogels modulate in vitro chondrogenesis of bovine bone marrow stromal cells. Tissue Eng Part A 2010;16(2):465-77.

92. Horner PJ, Gage FH. Regenerating the damaged central nervous system. Nature 2000;407(6807):963-70.

93. Tysseling-Mattiace VM, Sahni V, Niece KL, Birch D, Czeisler C, Fehlings MG, Stupp SI, Kessler JA. Self-Assembling Nanofibers Inhibit Glial Scar Formation and Promote Axon Elongation after Spinal Cord Injury. The Journal of Neuroscience 2008;28(14):3814-3823.

94. Tysseling VM, Sahni V, Pashuck ET, Birch D, Hebert A, Czeisler C, Stupp SI, Kessler JA. Self-assembling peptide amphiphile promotes plasticity of serotonergic fibers following spinal cord injury. Journal of Neuroscience Research 2010;88(14):3161-3170.

95.   Holmes TC, de Lacalle S, Su X, Liu G, Rich A, Zhang S. Extensive neurite outgrowth and active synapse formation on self-assembling peptide scaffolds. Proceedings of the National Academy of Sciences 2000;97(12):6728-6733.

96.   Ellis-Behnke RG, Liang Y-X, You S-W, Tay DKC, Zhang S, So K-F, Schneider GE. Nano neuro knitting: Peptide nanofiber scaffold for brain repair and axon regeneration with functional return of vision. Proceedings of the National Academy of Sciences of the United States of America 2006;103(13):5054-5059.

97.   Guo J, Su H, Zeng Y, Liang YX, Wong WM, Ellis-Behnke RG, So KF, Wu W. Reknitting the injured spinal cord by self-assembling peptide nanofiber scaffold. Nanomedicine: Nanotechnology, Biology, and Medicine 2007;3(4):311-321.

98.   Guo J, Leung KKG, Su H, Yuan Q, Wang L, Chu TH, Zhang W, Pu JKS, Ng GKP, Wong WM and others. Self-assembling peptide nanofiber scaffold promotes the reconstruction of acutely injured brain. Nanomedicine: Nanotechnology, Biology, and Medicine 2009;5(3):345-351.

99.   Rajangam K, Behanna HA, Hui MJ, Han X, Hulvat JF, Lomasney JW, Stupp SI. Heparin binding nanostructures to promote growth of blood vessels. Nano Lett 2006;6(9):2086-90.

100.   Rajangam K, Arnold MS, Rocco MA, Stupp SI. Peptide amphiphile nanostructure-heparin interactions and their relationship to bioactivity. Biomaterials 2008;29(23):3298-305.

101.   Stendahl JC, Wang LJ, Chow LW, Kaufman DB, Stupp SI. Growth factor delivery from self-assembling nanofibers to facilitate islet transplantation. Transplantation 2008;86(3):478-81.

102.   Chow LW, Wang L-j, Kaufman DB, Stupp SI. Self-assembling nanostructures to deliver angiogenic factors to pancreatic islets. Biomaterials 2010;31(24):6154-6161.

103.   Davis ME, Motion JPM, Narmoneva DA, Takahashi T, Hakuno D, Kamm RD, Zhang S, Lee RT. Injectable Self-Assembling Peptide Nanofibers Create Intramyocardial Microenvironments for Endothelial Cells. Circulation 2005;111(4):442-450.

104.   Webber MJ, Tongers J, Renault MA, Roncalli JG, Losordo DW, Stupp SI. Development of bioactive peptide amphiphiles for therapeutic cell delivery. Acta Biomaterialia 2010;6(1):3-11.

105.   Narmoneva DA, Vukmirovic R, Davis ME, Kamm RD, Lee RT. Endothelial Cells Promote Cardiac Myocyte Survival and Spatial Reorganization. Circulation 2004;110(8):962-968.

106.   Webber MJ, Han X, Prasanna Murthy SN, Rajangam K, Stupp SI, Lomasney JW. Capturing the stem cell paracrine effect using heparin-presenting nanofibres to treat cardiovascular diseases. Journal of Tissue Engineering and Regenerative Medicine 2010;4(8):600-610.

107. Webber MJ, Tongers J, Newcomb CJ, Marquardt KT, Bauersachs J, Losordo DW, Stupp SI. Supramolecular nanostructures that mimic VEGF as a strategy for ischemic tissue repair. Proc Natl Acad Sci U S A 2011;108(33):13438-43.

108. Mata A, Hsu L, Capito R, Aparicio C, Henrikson K, Stupp SI. Micropatterning of bioactive self-assembling gels. Soft Matter 2009;5(6):1228-1236.

109. Galler KM, Cavender A, Yuwono V, Dong H, Shi S, Schmalz G, Hartgerink JD, D'Souza RN. Self-assembling peptide amphiphile nanofibers as a scaffold for dental stem cells. Tissue Eng Part A 2008;14(12):2051-8.

110. Galler KM, Hartgerink JD, Cavender AC, Schmalz G, D'Souza RN. A customized self-assembling Peptide hydrogel for dental pulp tissue engineering. Tissue Eng Part A 2012;18(1-2):176-84.

111. Tian YF, Devgun JM, Collier JH. Fibrillized peptide microgels for cell encapsulation and 3D cell culture. Soft Matter 2011;7(13):6005-6011.

112. Genove E, Shen C, Zhang SG, Semino CE. The effect of functionalized self-assembling peptide scaffolds on human aortic endothelial cell function. Biomaterials 2005;26(16):3341-3351.

Section 2

EXPERIMENTAL

Chapter II

MATERIALS AND METHODS

Scientific objectives and experimental approach

The general aim of the PhD work presented in this dissertation was to investigate alternative self-assembled and microfabricated matrices (microcapsules and membranes) to encapsulate cells and serve as scaffolds for cell culture intended for applications in the biomedical field. The specific aims of this work were:

(i) develop and characterize materials based on xanthan polysaccharide that can undergo gelation (by ionic crosslinking or self- assembly) and evaluate their potential as cell encapsulation matrices;

(ii) develop methods for producing microcapsules based on xanthan derivatives with controlled size and shape;

(iii) demonstrate the ability of xanthan-based microcapsules to support and sustain cell viability and function;

(iv) fabricate self-assembling patterned membranes with characteristics resembling the native ECM;

(v) investigate how microscale features and biochemical signals on self-assembled membranes affect the adhesion and morphology of bone marrow stem cells.

The above mentioned objectives were established based on the following hypotheses:

(i) Xanthan gum could offer very interesting rheological and functional properties for developing encapsulating matrices; this polysaccharide remains largely unexplored as a potential biomaterial;

(ii) Self-assembly can be an advantageous alternative to the conventional crosslinking methods used to fabricate capsular structures for cell encapsulation in mild conditions;

(iii) Biopolymers (xanthan gum and hyaluronan polysaccharides) combined with synthetic self-assembling peptides can lead to innovative biomaterial systems and provide new applications in biomedicine;

(iv) Self-assembly nanofabrication and its integration into existing microtechnologies can offer new possibilities to fabricate highly structured biomaterials with increased level of bioactivity for cell culture and growth in biomimetic environments.

This chapter aims to provide detailed information concerning the used materials, reagents and technologies applied for processing the materials, characterization techniques and the biological assays used in this PhD work. Furthermore, it serves as a complement to the information given in each of the following experimental chapters. The organization of this chapter can be easily understood in Figure II.1..
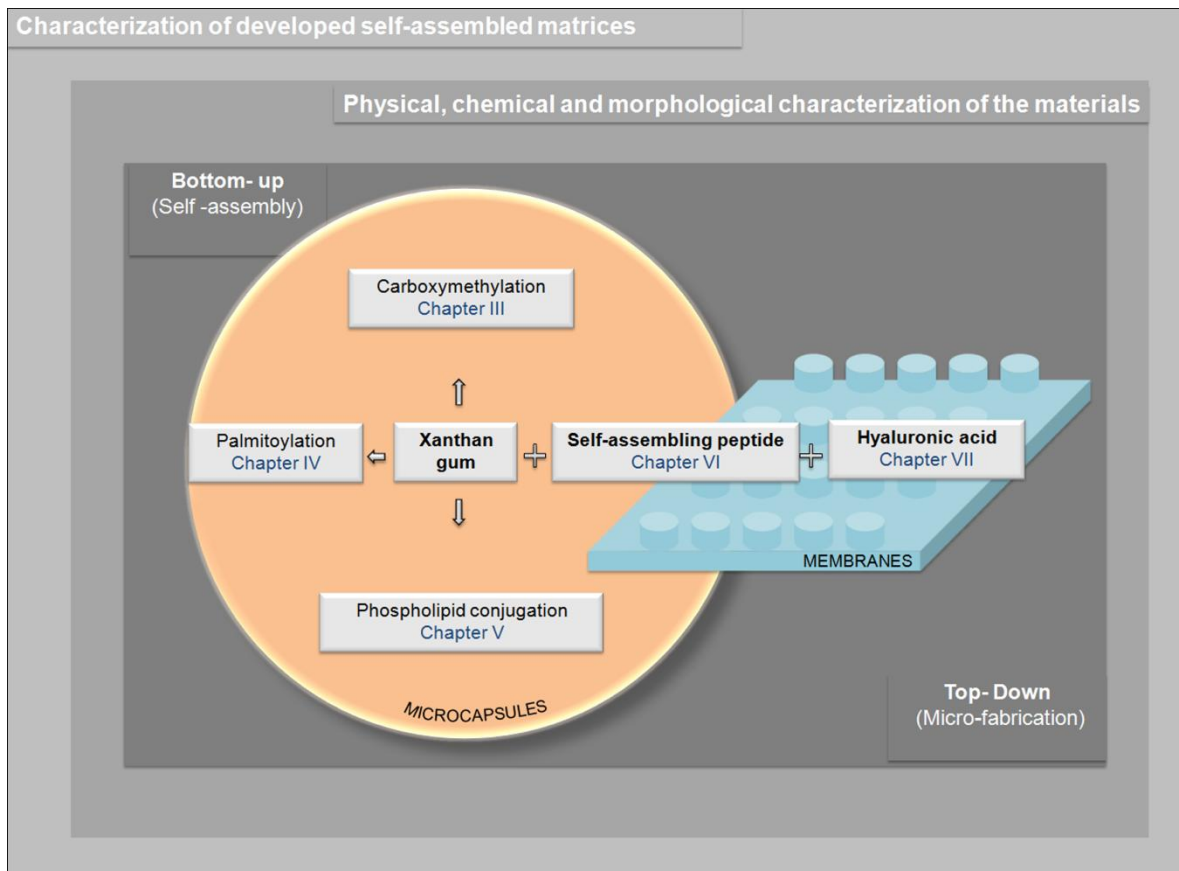
Figure II.1. Schematic overview showing the materials and integration of technologies to fabricate microcapsules and patterned membranes developed in this PhD work.

1. MATERIALS

1.1. General chemicals

The majority of the chemical reagents, unless otherwise noted, was purchased from Sigma-Aldrich (USA) and used as provided. Fmoc-protected amino acids and (2',4'-dimethoxyphenyl-fmoc-aminomethyl)-phenoxyacetamidonorleucyl-4-methylbenzhydrylamine (MBHA-rink amide) resin were purchased from Novabiochem (USA) and O-(benzotriazol-1-yl)-N,N,N',N'-tetramethyluronium (HBTU) from Carbosynth (UK). Reagents and solvents for high-performance liquid chromatography (HPLC) were of HPLC grade and obtained from Fluka (Steinhein, Germany). Similarly, reagents for spectroscopic analysis (e.g. potassium bromide (KBr) for FTIR and deuterated solvents for ^{1}H-NMR) were obtained with the adequate requirements for each technique. Details are presented for each chemical when used for the first time in this chapter.

1.2. Xanthan gum

Xanthan gum is an extracellular polysaccharide produced by the bacterium *Xanthomonas campestris* [1-4]. The primary structure of xanthan consists of $\beta(1\rightarrow4)$-linked glucose units, similar to the structure of cellulose backbone, substituted at O-3 of alternate glucose residues, with a trisaccharide (Figure II.2.). The trisaccharide consists of one glucuronic acid unit between two mannose units. The terminal mannose moiety may carry pyruvate residues linked to the positions 4 and 6 with an unknown distribution. D-Mannose unit linked to the main chain contains an acetyl group at position O-6 [1-5].
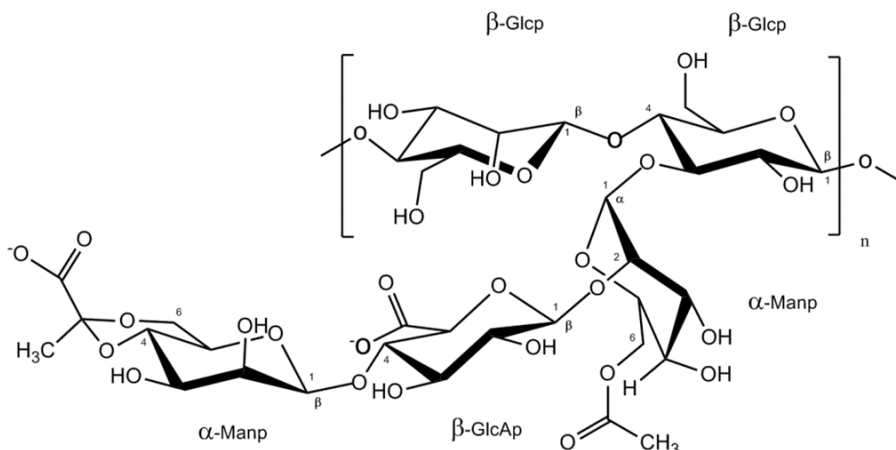
Figure II.2. Chemical structure of xanthan gum repeating unit.

The pyruvic acid content of xanthan can vary substantially depending on the strain of *X. campestris*, resulting in different viscosities of xanthan solutions. Molecular modelling studies

suggest that xanthan gum can assume a helical structure, with the side branches positioned almost parallel to the helix axis and stabilizing the structure [1-3,5]. The presence of acetic and pyruvic acids is the mainly responsible for the polyanionic character of this polysaccharide. Xanthan forms very viscous solutions, and, at sufficiently high polymer concentration, it exhibits weak gel-like properties [1,6]. Furthermore, it was shown to be biocompatible [4], biodegradable being widely used in food, cosmetics and pharmaceuticals because of its encouraging reports on safety [1]. The use of xanthan gum as matrix for the encapsulation of mammalian cells has not been reported in the literature. Based on its intrinsic properties, simultaneously with the opportunity to explore the potential of this biopolymer as cell encapsulation matrix, xanthan gum was selected as starting material in this PhD work.

1.2.1. Characterization of native xanthan (starting material)

The xanthan gum from *Xanthomonas campestris* used in this PhD work was obtained from Sigma/Aldrich (USA) without chemical characterization concerning its molecular weight, monosaccharide, pyruvate and acetate content. Therefore, a significant effort was devoted to characterize the starting material before its chemical modification.

1.2.1.1. Elemental analysis

The carbon, hydrogen, and nitrogen contents of xanthan were determined by elemental analysis using a LECO CHNS-932 (USA) elemental analyser and following the manufacturer's standard procedures.

Table II.1 Elemental composition of native xanthan gum (starting material). The values represent the mean of two replicates with standard deviation.

Sample	%C	%H	%N	%O[a]
Native xanthan	35.660 ± 0.099	5.710 ± 0.098	0.560 ± 0.003	58.070 ± 0.194

[a] by difference

Oxygen was calculated by difference and cafein (C= 49.48%, H=5.19% N=28.85%) was used as standard material. The results are presented on Table II.1.

1.2.1.2. Determination of sugar composition (monosaccharide content)

. The monosaccharide content of xanthan can be appreciated in Table II.2.

Table II.2 Sugar composition of native xanthan gum (starting material). The values represent the mean of three replicates with standard deviation.

Sample	Man (mol%)	Glc (mol%)	GlcA (mol%)	Total sugars (mg/g)
Native xanthan gum	29.1 ± 0.5	56.7 ± 0.8	14.2 ± 0.8	851.3 ± 15.8

Neutral sugars were determined as alditol acetates as described by Coimbra *et al.*[7]. A pre-hydrolysis with 72% H_2SO_4 for 3 h at room temperature was performed in order to solubilise the material. Afterwards, the polysaccharide was submitted to a hydrolysis with H_2SO_4 2 M at 120 ºC during 1 h. 2-Deoxyglucose was used as internal standard. Monosaccharides were reduced with sodium borohydride and acetylated by acetic anhydride using methylimidazole as catalyst. The alditol acetate derivatives formed were analyzed by gas chromatography (GC) equipped with a 30 m column DB-225 (J&W Scientific, Folsom, CA, USA) with i.d. and film thickness of 0.25 mm and 0.15 □m, respectively and using a flame ionisation detector. The oven temperature program used was: initial temperature 200 ºC, a rise in temperature at a rate of 40 ºC/min until 220 ºC, standing for 7 min, followed by a rate of 20 ºC/min until 230 ºC and maintain this temperature 1 min. The injector and detector temperatures were, respectively, 220 and 230 ºC. The flow rate of the carrier gas (H_2) was set at 1.7 mL/min.

Uronic acids were quantified by a modification [7] of the 3-phenylphenol colorimetric method [8]. Samples were prepared by hydrolysis with 72% H_2SO_4 for 3 h at room temperature followed by 1 h in 1 M H_2SO_4 at 100 ºC. A calibration curve was made with D-galacturonic acid. The hydrolysis and analysis of the samples was done in triplicate.

Methylation analysis. Linkage analysis was carried out by methylation as described by Ciucanu and Kerek [9]. Xanthan samples (1-2 mg) were dissolved in 1 mL of anhydrous dimethylsulfoxide (DMSO), then powdered NaOH (40 mg) was added and allowed to react during 30 min, followed by addition of CH_3I (80 µL) that was allowed to react during 20 min. The methylated polysaccharides were hydrolyzed with 2 M TFA at 121 ºC for 1 h, and then reduced and acetylated as previously described for neutral sugar analysis. The partially methylated alditol acetates (PMAA) were separated and analyzed by gas chromatography-mass spectrometry (GC-MS) on an Agilent Technologies 6890N Network (USA). The GC was equipped with a DB-1 (J&W Scientific, Folsom, CA, USA) capillary column (30 m length, 0.25 mm of internal diameter and 0.15 µm of film thickness). The samples were injected in splitless mode (time of splitless 5 min), with the injector operating at 220 ºC, and using the following temperature program: 45 ºC for 5 min with a linear increase of 10 ºC/min up 140 ºC, and standing for 5 min at this

temperature, followed by linear increase of 0.5 ºC/min up to 170 ºC, and standing for 1 min at this temperature, followed by linear increase of 15 ºC/min up to 280 ºC, with further 5 min at 280 ºC. The helium carrier gas had a flow rate of 1.7 mL/min and a column head pressure of 2.8 psi. The GC was connected to an Agilent 5973 mass quadrupole selective detector operating with an electron impact mode at 70 eV and scanning the range m/z 40–500 in a 1 s cycle in a full scan mode acquisition.

1.2.1.3. Determination of acetate and pyruvate degree of substitution of native xanthan

The acetate and pyruvate content (Table II.3) was determined by ^{1}H NMR spectroscopy in a Varian Unity Plus 300 MHz spectrometer (USA) by reference to an external standard (sodium acetate) as described by Hamcerencu [4]. Xanthan was dissolved in D_2O (3 g/L) in presence of Na acetate (3×10^{-3} M). ^{1}H NMR spectra were recorded at 75 °C. Three peaks were considered: two peaks at $\delta = 1.47$ and $\delta = 2.16$ ppm attributed to pyruvate and acetate groups bound to the xanthan and one at $\delta = 1.90$ ppm.
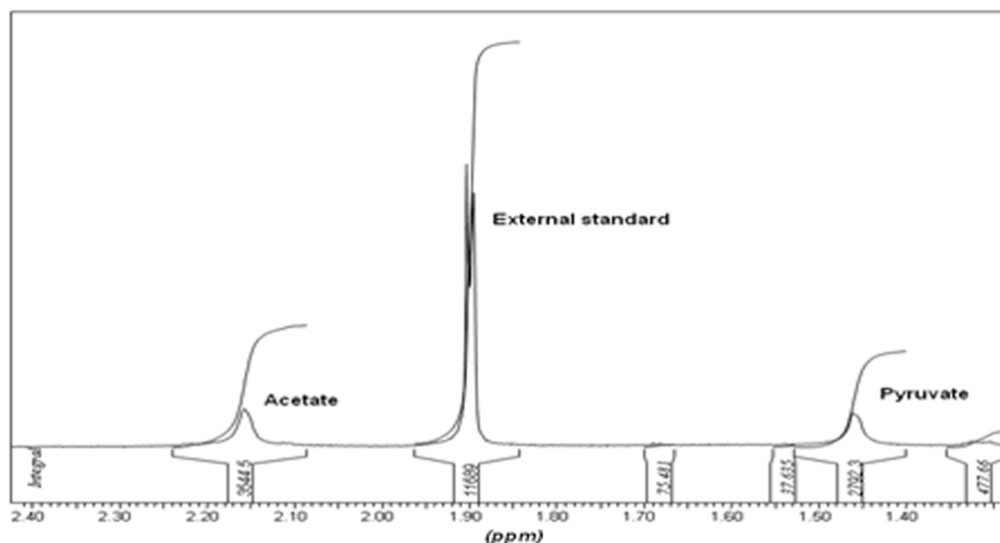
Figure II.3. Integrals of ^{1}H signals of acetate and pyruvate groups of xanthan (3 g/L) and of external standard (sodium acetate) for calculation of acetate and pyruvate degree of substitution.

From the integrals of ^{1}H signals corresponding to both substituents by reference to external standard protons one can calculate the number of the substituents (N_A, N_P)/gram of polysaccharide and, finally the number of acetate and pyruvate groups (n_A, n_P)/side chain of xanthan:

$$N_A = \frac{h_A}{h_E} \cdot \frac{c_E}{c_P} \qquad\qquad N_P = \frac{h_P}{h_E} \cdot \frac{c_E}{c_P} \qquad\qquad \text{(II.1)}$$

$$n_A = N_A \cdot 829 / (1 - 92 N_P - 42 N_A) \qquad n_P = N_P \cdot 829 / (1 - 92 N_P - 42 N_A) \qquad \text{(II.2)}$$

h_A, h_P, h_E - integrals of ^{1}H signals corresponding to acetate (h_A) and pyruvate (h_P) group, and to external reference (h_E), respectively; c_E, c_P - concentration of Na acetate (c_E, mole/L) and polysaccharide (c_P, g/L); 829 - molar weight of repeating unit of xanthan without acetate or pyruvate; 42 - molar weight of acetate group; 92 - molar weight of pyruvate group.

Table II.3. Acetate and pyruvate degree of native xanthan gum (starting material) per side chain. The values represent the mean of three replicates with standard deviation.

Sample	Acetate Degree (%)	Pyruvate Degree (%)
Native xanthan	44.4 ± 5.1	35.2 ± 2.6

1.2.1.4. Determination of molecular weight of native xanthan

The molecular weight (Mw) of xanthan gum used in this work was determined by size-exclusion chromatography (SEC). The samples were dissolved in an aqueous 0.1 M NaNO$_3$ solution (0.4% w/v). A PL-GPC 110 chromatograph was equipped with a pre-column PLaquagel-OH 15 µm and two SEC columns in series (PLaquagel-OH40 15 µm, 300 × 7.0 mm and PLaquagel-OH60 15 µm, 300 × 7.0 mm). The pre-column, the SEC columns, the injection system, and the refractive index detector were maintained at 36 ºC. The eluent (aqueous 0.1 M NaNO$_3$ solution) was pumped at a flow rate of 0.9 mL min^{-1}. The analytical columns were calibrated with pullulan standards (Polymer Laboratories, UK) in the range of 5.8-1600 kDa. The average molecular weight of xanthan gum was estimated as 152 kDa (Table II.4).

Table II.4. Molecular weight of native xanthan gum (starting material).

Sample	Mw (KDa)	Mn (KDa)	Mw/Mn
Native xanthan gum	152	174	0.87

1.2.2. Chemical modifications of xanthan gum

Xanthan is able to form self-supporting gels in the presence of ions, although they are not stable in the long term when placed in aqueous solutions. Within the scope of this PhD work, we have performed chemical modifications of xanthan to evaluate its potential to be used as cell encapsulation matrix.

1.2.2.1. Carboxymethylation

The first attempt to enhance the stability of xanthan hydrogels was to perform the carboxymethylation of xanthan to increase the amount of carboxylic groups (chapter III). Carboxymethyl xanthan (CMX) was prepared by adapting the carboxmethylation procedure used for chitosan described by Chen and Park [10]. 10 g of xanthan from *Xanthomonas campestris* and 13.5 g sodium hydroxide (Panreac, Spain) were mixed in 100 mL of solvent mixture of water/isopropanol (Fluka, Germany) using a top stirrer. The mixture was allowed to react at 50 ºC in a water bath (Thermostat IKA, Germany) for 1 h. Two solvent mixtures were used (1/1 and 1/4, v/v) to yield xanthan with different degrees of carboxymethylation designated by CMX1 and CMX2 respectively. Then, 15 g monochloroacetic acid, dissolved in 20 mL of isopropanol, were added dropwise to the reaction mixture for 30 min. The reaction was carried out for 4 h at the same temperature and stopped by adding 200 ml of ethanol 70% (Panreac, Spain). At the end, the obtained solid precipitate was filtered and rinsed with 70–90% of ethanol to desalt and dewater and further vacuum dried at room temperature.

1.2.2.2. Palmitoylation

Hydrophobized polysaccharides have been extensively studied in biomedical field due to their capability to spontaneously self-assemble in water into stable and functional structures. The possibility to generate and use this type of structures in cell friendly conditions, avoiding the use of potential harmful crosslinkers, together with the potential of xanthan to be used as cell encapsulating matrix, has motivated its hydrophobization with aliphatic palmitoyl on chapter IV. Xanthan was dissolved in distilled water (1 wt%) at room temperature in a round-bottom glass flask. The polymer solution was placed in an ice-water bath and vigorously stirred using a mechanical stirrer (IKA, Germany). Palmitoyl chloride was then added dropwise at different ratios, as shown in Table II.5. The reaction mixture was allowed to stand at room temperature under continuous stirring for 23 h. The reaction was stopped by the addition of excess of cold ethanol and filtered. The final product was dried at room temperature until constant mass.

Table II.5. Sample designation for each palmitoyl xanthan (PX) conjugate.

Sample designation	Xanthan (mmol)	Palmitoyl chloride (mmol)	Xanthan/Palmitoyl chloride ratio (w/w)
PX(X=0.50P)	0.58	1.18	**0.50**
PX(X=0.75P)	0.58	0.78	**0.75**
PX(X=1.40P)	0.58	0.42	**1.40**
PX(X=1.70P)	**0.58**	**0.35**	**1.70**

1.2.2.3. Phospholipid conjugation

Previously, the conjugation of simple hydrophobic alkyl chains to xanthan demonstrated to be quite effective on its amphiphilic self-assembly process and cell encapsulation. Based on these findings and following a more biomimetic approach, xanthan was conjugated/hydrophobized with a phospholipid (2-sn-glycero-phosphoetilamine, DOPE) by standard bioconjugation reaction with carbodiimides (chapter V).

Xanthan, with an average molecular weight of 152 kDa[11], was dissolved in 2-(*N*-morpholino)ethanesulfonic acid buffer solution (MES, Sigma), at 55 mM at room temperature. The xanthan solution was placed in an ice water bath, under inert atmosphere, and the pH was adjusted to 5.5. The N-hydroxysuccinimide (NHS) (with the same molarity of xanthan) was added under stirring, previously the addition of ethyl(dimethylaminopropyl)carbodiimide (EDC) at molar concentration of [NHS]/0.6. The pH was maintained at 5.5 and later DOPE was added at the same molarity of xanthan[12]. The reaction took place overnight (15 h) and was stopped by the addition of excess of cold ethanol. The precipitate was filtered and dried at room temperature until constant mass.

1.3. Alginate

Alginate, also known as alginic acid (if uronic acid groups are in –COOH) is an anionic polysaccharide that constitutes the cell wall of brown seaweeds. Alginates are linear unbranched copolymers containing β (1→4) linked D-mannuronic acid (M) and α (1→4) linked L-guluronic acid (G) residues [13]. These monomers are arranged in alginate molecules in regions made up exclusively of one unit or the other, or as regions in which monomers alternate in sequence. Alginate is well known for its ability to form stable gels with divalent cations such as Ca^{2+}.

Moreover, it has been widely studied for cell encapsulation purposes [14-15] and for this reason was selected for comparison purposes (control material) in chapter III.

The alginic acid used in the referred chapter is a sodium salt from brown algae and obtained from Fluka (Norway) with average Mw 100 kDa.

1.4. Poly-L-Lysine (PLL)

PLL is a polypeptide constituted of 25-30 L-lysine residues. Due to its polycationic character it has been widely used in cell microencapsulation to increase the strength of microcapsules and to control the membrane molecular weight cut-off[16].

In the present work, poly-L-lysine hydrobromide obtained from Sigma/Aldrich (USA) with Mw of 30-70 kDa was used to increase the strength of CMX, PX and xanthan-DOPE microcapsules (chapters III, IV and V).

1.5. Hyaluronan (HA)

Hyaluronan, also known as hyaluronic acid or hyaluronate, is one of a group of polysaccharides typically found in the connective tissues of vertebrates, known as glycosaminoglycans. It is an extremely large polymer made up of disaccharide repeating unit of N-acetylglucosamine and glucuronic acid linked together via alternating β-1,4 and β-1,3 glycosidic bonds (Figure II.5).

GlcNAc   GlcA
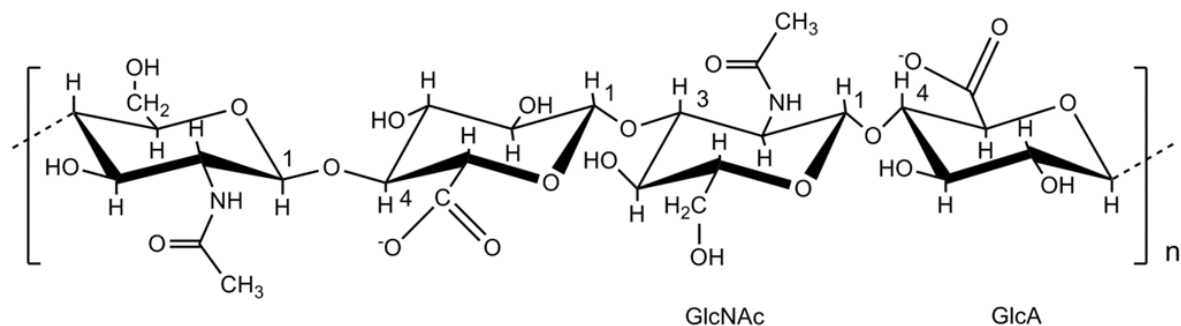
Figure II.5. Chemical structure of hyaluronan repeating unit.

HA exhibits a remarkable combination of properties, like polyanionic character, linear unbranched random-coil structure and large size, making HA solutions extremely elastoviscous. Moreover, the HA repeating unit disaccharide is identical in all species and all tissues and is therefore never itself recognized as immunologically foreign. Another important factor underlying the medical utility of HA derives from the magnitude and pathways available for systemic HA metabolism. In the normal body, the disposal of HA is almost entirely effected by the complete catabolism rather than excretion. HA is present in the extracellular matrix, on the cell surface,

and inside the cell and is therefore associated with numerous cellular processes such as signaling (cell adhesion and migration), inflammation and wound healing [17].

Based on the described characteristics and demonstrated biological properties of HA, this biopolymer (with an average molar mass of 2.0 MDa, Lifecore Biomedical, Inc, USA) was selected to fabricate bioactive self-assembled membranes (chapter VII).

1.5.1. HA fluorescent labelling

HA was labeled with 5-(Aminoacetamido) Fluorescein (Invitrogen, USA) using EDC chemistry as described elsewhere [18]. HA (50 mg) was dissolved in 20 mL of water to give 0.25% (w/v) solution. Then, a solution of 5 mg of dye in 20 mL of DMF was added. Next, 100 mg of NHS was added, and the solution pH was adjusted to 4.75 by adding 0.01 M HCl. Finally, 50 mg of EDC was added, and the solution pH was maintained at 4.75 by adding 0.01 M HCl. After 14 h, the solution was transferred to dialysis tubing and dialyzed exhaustively against 100 mM NaCl, followed by dialysis against distilled water. The solution was then lyophilized to give the fluorescent HA-dye.

1.6. Multidomain peptides

The multidomain $K_2(QL)_6K_2$ peptide (Figure II.6.A) consists of an ABA block motif [19] comprising a central block of glutamine-leucine (QL) repeats and two flanking positively charged lysines (K).
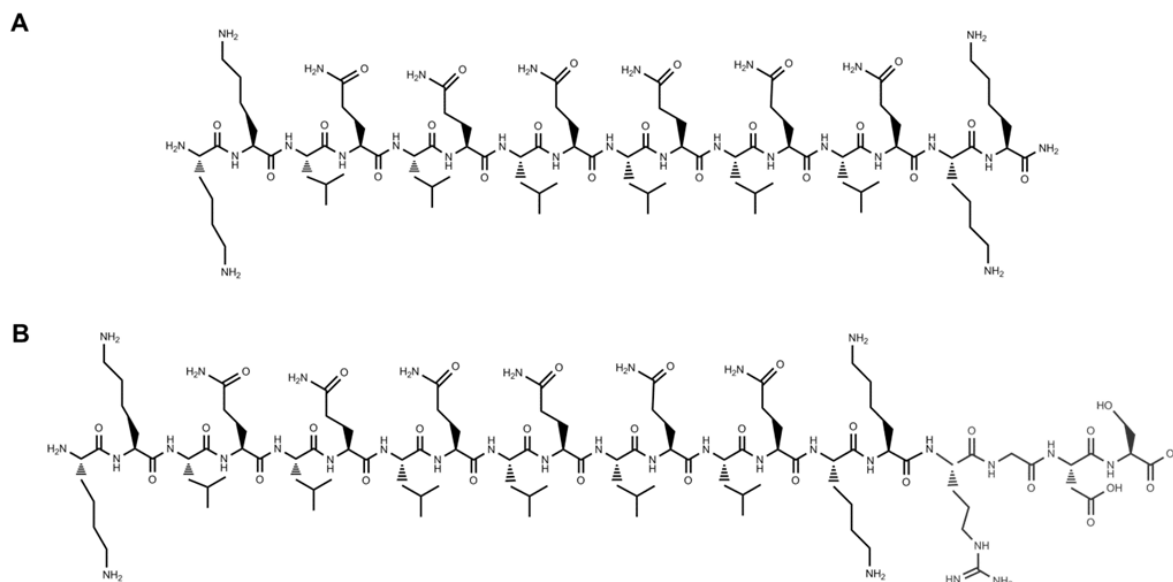
Figure II.6. Chemical structure of the self-assembling peptides used in this PhD work: $K_2(QL)_6K_2$ multidomain peptide without (A) and containing the cell adhesive RGDS sequence (B).

Different variations of these multidomain peptides [20-21] have been previously synthesized and demonstrated to self-assemble into well-defined nanofibers [19] with various bioactive epitopes [21-22].

1.6.1. Peptide synthesis

Peptides can be synthesized by conventional synthesis in solution or by solid phase (SP) chemistry [23]. This later method is based on the attachment of N-α-protected amino acid to an insoluble support (usually a resin). Subsequently, the N-α-blocking group is removed (deprotected) and the next amino acid coupled through a peptide bond. The deprotection/coupling cycle is repeated until the desired sequence of amino acids is generated.
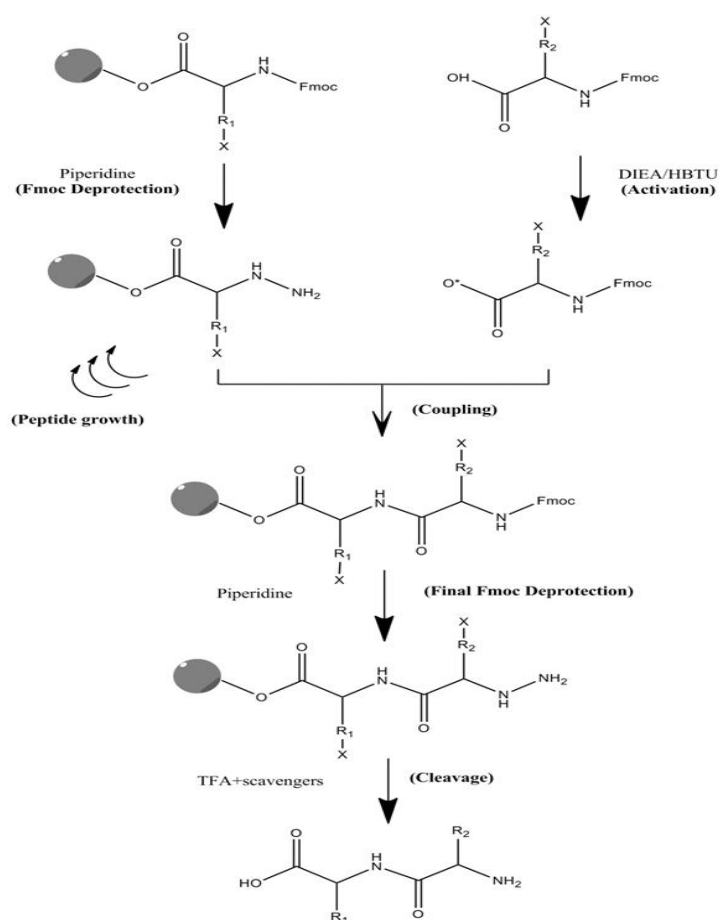
Figure II.7. Diagram of solid-phase synthesis of peptide molecules.

At the end, the peptide is cleaved from the resin to obtain the peptide as a free acid or amide, depending on the chemical nature of the resin (Figure II.7.). Solid phase peptide synthesis is advantageous comparatively to solution-phase methods, once it allows an easier separation of intermediates, reagents and by-products, being therefore less laborious.

Solid phase peptide synthesis was used to synthesize the following peptides: $K_2(QL)_6K_2$ (Figure II.6.A) and $K_2(QL)_6K_2RGDS$ (Figure II.6.B) described on chapters VI (for microcapsule formation with xanthan) and VII (for membrane fabrication with hyaluronic acid). The peptides were synthesized using standard 9-fluorenylmethoxycarbonyl (Fmoc) chemistry on an automated peptide synthesizer (CS Bio, USA) at 1 mmol scale on a 4-methylbenzhydrylamine (MBHA) rink amide resin. Once synthesized, cleavage of the peptide from the resin and deprotection of the protecting groups was carried out with a mixture of trifluoroacetic acid (TFA)/ triisopropylsilane (TIS)/ water (95/2.5/2.5) for 3 h at room temperature. After filtration of the cleavage mixture, excess TFA was removed by rotary evaporation. The resulting viscous peptide solution was triturated with cold diethylether. The white precipitate was collected by filtration, washed with cold ether, and allowed to dry under vacuum overnight. The solid powder was stored at -20 ºC for further characterization and purification.

1.6.2. Peptide characterization

1.6.2.1. Electron-spray ionization mass spectrometry (ESI-MS)

Mass spectrometry is an analytical technique that measures the mass/charge ratio (m/z) of ions and has been used to determine the exact mass of molecules and to study their structure[24]. It has been widely used in the characterization of peptides and proteins because of its accuracy and the relatively small amount of material required (fmols). The ESI-MS principle consists of ionizing chemical compounds to generate charged molecules or molecule fragments and measuring their mass/charge ratios. The mass of the synthesized peptides described on chapters VI and VII was determined by ESI-MS to verify their identity. Samples were dissolved in water/acetonitrile (0.1% TFA) and analyzed in HPLC-MS (Finnigan LXQ, USA).

1.6.2.2. High-pressure liquid chromatography (HPLC).

HPLC is a chromatographic technique with abiity to identify, quantify and purify the individual compounds of a mixture. The sample, which may have affinity for the liquid mobile phase or to the solid stationary phase, is injected and pumped to flow through a chromatographic column (that contains the stationary phase) under a high pressure, where the separation of the mixture compounds take place. Further, the separated analyte passes through an appropriate detector sensitive to the desired compound that provides a chromatogram where the characteristic retention time and the amount of the analyte can be appreciated. This technique is being widely used in the characterization of peptides and proteins due to excellent resolution for a wide range of chromatographic conditions for very closely related molecules as well as structurally quite

distinct molecules; facility to manipulate chromatographic selectivity through changes in mobile phase characteristics and the excellent reproducibility of repetitive separations [25].

Reverse phase (RP) HPLC was used in this PhD work to analyze the purity of the synthesized peptide molecules. HPLC was performed in a Smart Line analytical system from Knauer (Germany) using a water/acetonitrile gradient with 0.1% TFA (added to the mobile phase to improve solubility and peak resolution) at 1 mL/min. The peptides were run on a difunctionally bonded silica-based C18 column (Atlantis® T3, 4.6 x 150 mm, 5 µm, Waters, USA) and their detection made in an UV detector (Knauer, Germany) by absorbance at 220 nm.

Figure II.8. displays the MS spectra and HPLC traces of the synthesized peptides (crude samples). MS analysis confirmed their successful synthesis and the HPLC showed a main peak, corresponding to the peptide, as well as other minor peaks related with impurities present in the crude sample, indicating the need of further purification by HPLC methods.

1.6.3. Peptide purification

The peptides were then purified on a 2545 Binary Gradient (Waters, USA) HPLC system using a preparative reverse-phase C18 column (Atlantis Prep OBD T3 Column, 30 x 150 mm, 5 µm, Waters, USA) and a water/acetonitrile (containing 0.1% TFA) gradient at flow rate of 20 mL/min. The UV absorption was monitored at 220 nm in a Waters 2489 UV/visible detector.
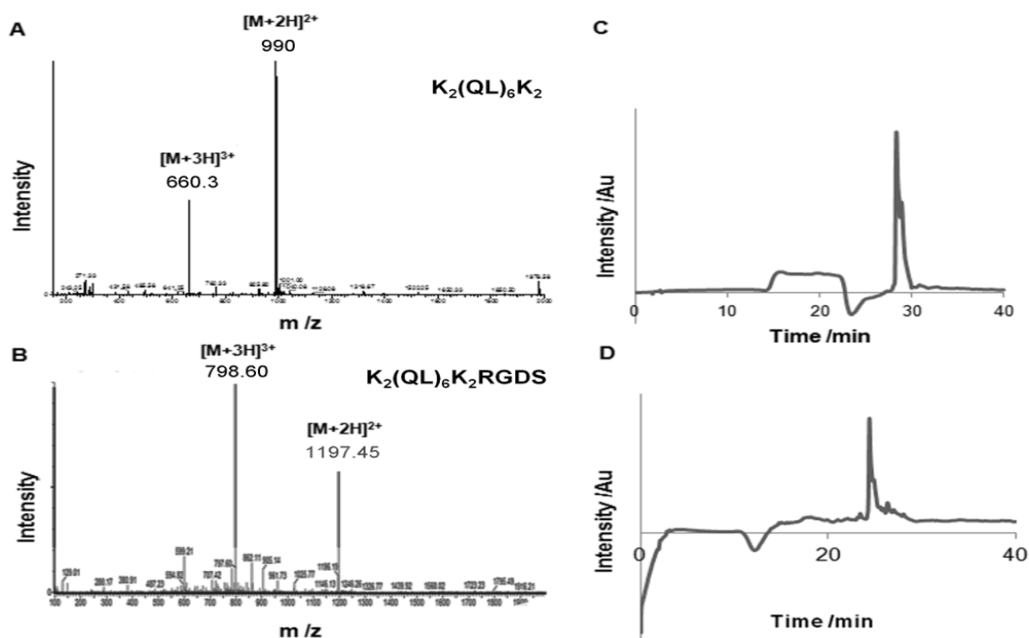
FigureII.8. MS (A, B) and HPLC (C and D) characterization of $K_2(QL)_6K_2$ and $K_2(QL)_6K_2RGDS$ peptides after purification. $K_2(QL)_6K_2$ expected mass: 1977.44; $[M+2H]^{2+}$: calculated 989.72, observed 990; $[M+3H]^{3+}$: calculated 660.15, observed 660.3. $K_2(QL)_6K_2RGDS$ expected mass: 2392,43; $[M+2H]^{2+}$: calculated 1197.22, observed 1197.45; $[M+3H]^{3+}$: calculated 798.48, observed 798.60.

The purified fraction(s) were verified using mass spectrometry and concentrated via rotary evaporation to remove the acetonitrile and lyophilized. TFA counter-ions were exchanged by sublimation from hydrochloric acid (0.1 M). Finally, the peptides were dialyzed against deionized water using dialysis tubing (500 MWCO, Spectrum Europe B.V., The Netherlands) to remove salts, lyophilized, to obtain a fluffy powder, and stored in closed containers at -20 ºC until use.

The purity and accurate mass of each peptide were verified using liquid chromatography/MS and the chromatogram and mass spectra are given in Figure II.8.

2. DEVELOPMENT AND APPLICATION OF MICROFABRICATION TECNHIQUES

Microfabrication techniques have been used to produce devices with dimensions in the micrometer to millimeter range. Key advantages of these techniques include small device size and sampling volume, and reproducibility. Therefore, one of the goals of this PhD research, was to use microtechnologies to guide the self-assembly across the scales to control the shape and structure of the final assemblies. Three distinct microfabrication techniques were developed and applied. A microdroplet generator and a microfluidic device were developed for cell encapsulation. The fabrication of micropatterned membranes was achieved through soft lithography processes.

2.1. Microdroplet generator
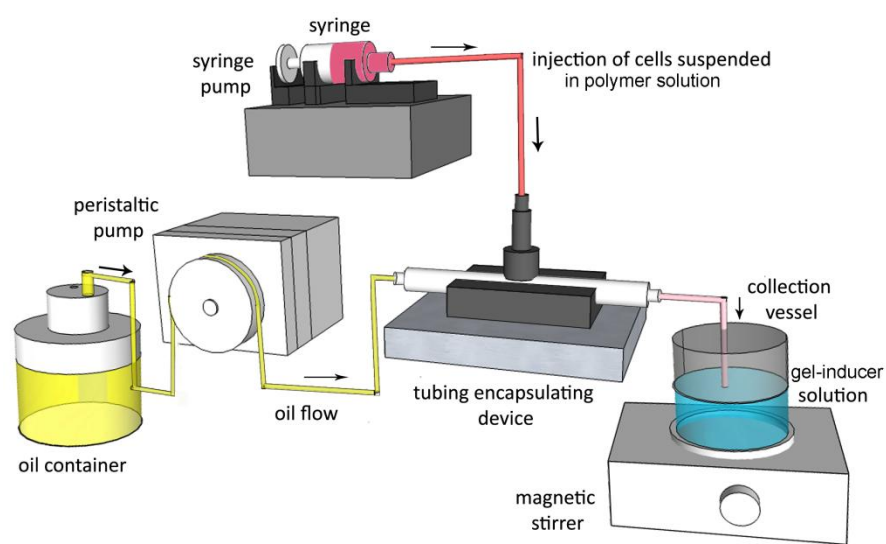
Figure II.9. Schematic representation of the microdroplet generator.

The microdroplet generator (Figure II.9.) is a simple device that was developed to generate spherical capsules at micrometer scale for cell encapsulation purposes[26]. This device was applied to fabricate microcapsules and encapsulate cells within carboxymethylated and palmitoyl xanthan, as described in chapters III and IV, respectively.

2.1.1. Microdroplet generator fabrication

This cell encapsulation device is based on micro-droplet generation inside of an autoclavable silicone tubing (Novosil, Fisher Scientific, USA) with 1 mm internal diameter, which is punctured with a blunt-ended syringe needle vertically and sealed with a silicone glue (Figure II.9). The injection of polymer solution is made through a syringe pump (Alladdin WPI, England) into a stream of mineral oil and results in the formation of a water-in-oil emulsion, because of immiscibility of two phases, and the generation of spherical droplets. The tubing system is also connected with a peristaltic pump (Ismatec, Switzerland) that pumps the mineral oil (Aldrich, Germany) from an oil reservoir to the other end of the tubing: a glass collector where the polymer droplets are cured in a gel inducer. A magnetic top stirring apparatus, made up of Teflon® with a magnet, was placed on the top of collector in order to stir solution without introducing a mechanical stress on the formed microcapsules. Providing a steady injection and flow rate of polymer solution and oil, respectively, the micro-droplets are produced in a narrow size distribution. The whole system is autoclavable and can be used many times after proper cleaning of setup [26].

2.1.2. Microcapsule preparation

Xanthan derivatives were first dissolved in the proper buffer solution at concentrations previously optimized (CMX powder was dissolved in DMEM at 5 wt% concentration and palmitoyl xanthan was dissolved in HEPES buffer solution (55 mM, pH 7.4, Sigma) supplemented with 0.1 M $CaCl_2$ at concentration of 1 wt %). Both solutions (CMX and PX) were injected in the microdroplet generator. The applied operation rate of peristaltic and syringe pumps were set at 0.35 mL/minute and 20 µL/min, respectively.

The CMX micro beads generated were collected into a solution containing 1.5% $CaCl_2$ (Merck Chemical Co., Germany) and 0.9% NaCl (Carlo Erba, Italy), while PX microbeads were collected in PBS (Sigma, USA), where the self-assembly into hollow micro-capsules took place. In both situations, 10 µL of Tween 80 was added to the collection solution as emulsifying agent. The CMX and PX capsules were gently stirred for 15 min and then washed with PBS in order to remove traces of mineral oil. Afterwards, the collected microcapsules were transferred into a

poly-L-lysine solution (0.1 wt%) for 10 min in order to strengthen the outer surface of the microcapsules

Similarly, alginate was used to produce microcapsules to serve as controls (chapter III). The alginate microcapsules were successively coated with the poly-L-lysine (0.05 wt%) for 5 min.

2.2. Microfluidics technology

Microfluidic devices have been recognized as a potential tool for the fabrication of micro-engineered hydrogels [27-28]. This fabrication process allows the generation of hydrogels with controlled size and shape by changing viscosity of polymer solution, flow rate and dimensions of micro channels. Small amounts of fluids can be manipulated using channels with dimensions of tens to hundred of micrometers. Moreover, it allows the manipulation of multiphase flows operating under laminar flow (without turbulence) enabling the generation of homogeneous structures using self-assembling materials for encapsulation of delicate biological agents and cells [27-29]. Moreover, it can provide a miniature and sterile platform without the need of a clean room making this fabrication process suited for cell encapsulation. Aiming to obtain microcapsules with lower size than those previously fabricated and considering the advantages versus suitability of microfluidics to be used with self-assembling materials[30-31], this technology was applied to fabricate microcapsules and encapsulate cells with xanthan-DOPE (chapter V) and xanthan-peptide (chapter VI).

2.2.1. Microfluidics device fabrication

The device design was made by CAD software and printed onto a transparency sheet by using a desk top laser printer. This pattern subsequently served as a mask for copper etching. The laser toner has been successfully exploited previously for applications as an etch mask for metal plates intended for microfluidics application [32]. A copper plate (1.5x1.5 cm, 0.675 mm thick, 0.99% annealed, Alfa Aesar, USA) was used as a substrate for developing microfluidic channels. The melted toner adheres to the copper and is insoluble in ferric chloride solution, allowing it to serve as an etch mask for microchannel fabrication. Initially, the copper plate surface was cleaned by rubbing thoroughly with a fine steel wool. The plate was then sonicated 5 min in a solution of acetone-water (50%). The cleaned plate was transferred onto a hot plate at 200 ^{o}C and incubated for 2 min. The heated plate was then transferred immediately to printed-face of transparency and a metal block weighing approximately 10 kg was placed onto copper plate to facilitate toner transfer. After 2 min, the copper plate and transparency was placed to a freezer (-20 ^{o}C) and incubated for 5 min. After cooling, the transparency was carefully peeled off from copper plate. The back and front surface of plate, where there is no toner, was covered

with plastic duct tape to protect unmasked region from etching process. The plate was etched in FeCl$_3$ solution (35%, 50 mL) in a glass beaker for 30 min at room temperature by manual shaking of the solution. The etching was stopped by removing the plate and washing it under running water. After removing duct tapes from the etched plate, the plate was placed into acetone-water solution (50%) and sonicated for 10 min to remove toner from the surface. Beside, a poly(dimethyl siloxane) (PDMS) seal was prepared at 1/10 crosslinker/monomer ratio (w/w) (SYLGARD® 184 silicone elastomer kit, Dow Corning, USA) and curing the mixture for 2 days at 37 °C in a rectangular mould. The seal was perforated at inlets and outlets of vertical and horizontal channels reserved for polymer-cell and oil flow, respectively (Figure II.11.A). A piece of poly(tetrafluoro ethylene) (TEFLON) block was also machined for securing and precise positioning of the perforated silicone seal and allowing the transfer of fluids by providing 4 adapters at the backside for connecting silicone tubing from peristaltic and syringe pump (Figure II.10.).
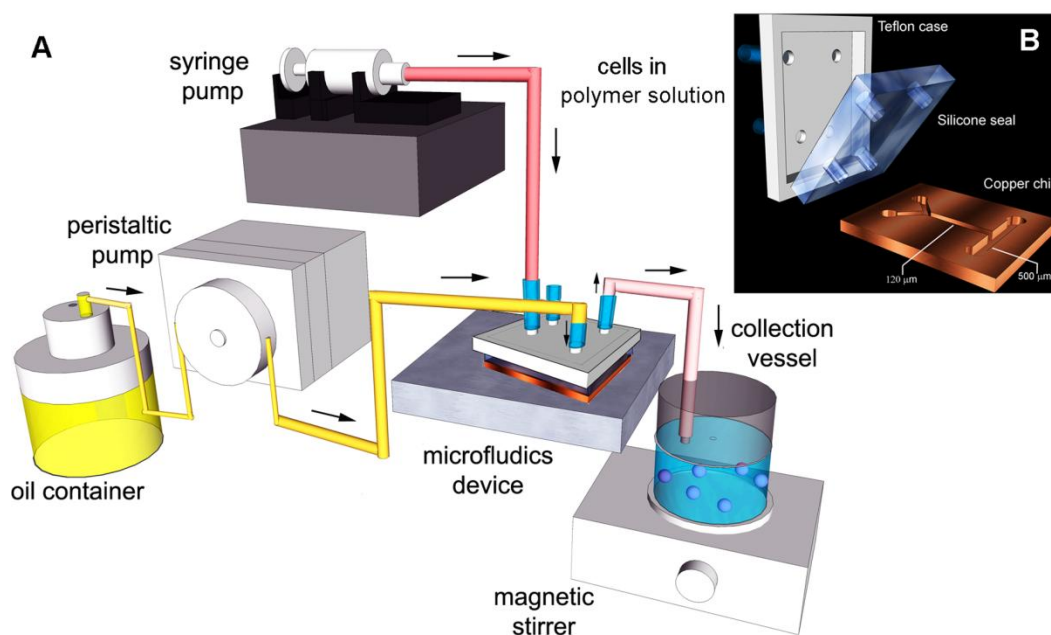
Figure II.10. Schematic representation of the microfluidics set-up for cell encapsulation (A) showing details of the microfluidics apparatus. View of dissembled microfluidics device which consists of a metal chip, silicone seal and TEFLON case (B).

2.2.2. Microcapsule preparation

The production of the xanthan-phospholipid (chapter V) and xanthan-peptide (chapter VI) microcapsules was done in the developed microfluidics.

Xanthan-DOPE (phospholipid) was dissolved in HEPES buffer solution (55 mM, pH 7.4) supplemented with 0. 1 M $CaCl_2$ at concentration of 1 wt% and native xanthan (1 wt%) was dissolved in PBS. The xanthan solutions were injected into the microfluidics device using a syringe pump. The polymer microdroplets were generated inside the microfluidics device by shear stress when entered into a stream of mineral oil. The formed homogenous microdroplets were collected in a collector vessel containing PBS (for xanthan-phospholipid microcapsules) and $K_2(QL)_6K_2$ solution (for xanthan-peptide microcapsules) at different concentration (0.1, 0.25 and 0.5 wt%). About 10 µL of Tween 80 was added as emulsifying agent. The self-assembly of xanthan-DOPE and xanthan-peptide into microcapsules took place in the collector vessel by gently stirring the polymer droplets for 15 minutes on a magnetic stirrer. To investigate the stability of the xanthan-DOPE microcapsules, they were also coated with poly-L-lysine solution (0.1 wt%) for 10 minutes for comparison purposes.

2.3. Soft photolitography

Despite the broad range of strategies to pattern polymers, photolithography has been the most widely used. It is a cost-effective high-throughput technique that is suitable for large-area surface patterning with good alignment, allowing high-resolution patterning, controlled topography with broad range of features [33-34]. At biological level, photolithographically generated polymer patterns have been demonstrated the ability to manipulate and control the localization of cells and the interactions of cell–cell and cell–substrate [33,35-38].

The integration of soft litograhy (top-down) with self-assembly (bottom-up) can offer new possibilities to fabricate miniaturized biomaterials, with high levels of precision and reproducibility, exhibiting increased bioactivity and hierarchical structure across the scales.

Soft photolithography was applied to create micropatterns on self-assembling membranes (chapter VII).

2.3.1. Fabrication of topographic PDMS molds

Molds comprising several microtopographical patterns were fabricated using a soft lithography process. The patterns were generated in SU8-10 photoresist (Microchem Corporation, USA) using conventional contact mode UV photolithography (Mask Aligner MJB4, SUSS Microtec, Germany) with a rigid chrome mask as follows. SU8-10 photoresist was spin coated onto a (111)-oriented silicon wafer (Siltronix) at 500 rpm for 5 s followed by 4000 rpm for 30 s, achieving a layer approximately 8 µm thick. The sample was baked at 65 ºC for 2 min and 95 ºC for 5 min prior to UV exposure (3.3 s at 30 mW.cm^{-2}) and baked post-exposure at 65 ºC for 1

min followed by 95 ºC for 5 min. The topographical patterns were then developed with SU8 developer (Microchem, USA). The resulting samples were silanized with trichloro(^{1}H,^{1}H,^{2}H,^{2}H-perfluorooctyl)silane (Sigma-Aldrich, USA) before being used as molds for the production of patterned PDMS substrates (Figure II.11.). The patterns were comprised of different geometries, channels (10 μm wide, 10 μm in separation, and 8 μm in height), posts (10 μm wide, 10 μm in separation, and 8 μm in height), and holes (10 μm wide, 10 μm in separation, and 8 μm deep), and posts and holes (20 μm wide, 20 μm in separation, and 8 μm in height).

2.3.2. Membrane fabrication

2.3.2.1. Smooth membranes

Smooth membranes were fabricated by casting hyaluronic acid solution (2 MDa, 1 wt% in water) on a polydimethylsiloxane (PDMS, Sylgard 184, Dow Corning, USA) substrate. The PDMS substrate was prepared by mixing the prepolymer and crosslinker at a 10:1 ratio, degassing for 10 min under vacuum and curing for 2 h at 65 ºC. The PDMS was oxygen plasma treated in a plasma cleaner (PDC-002, Harrick Cientific Corporation, USA), in order to increase the wettability of the surface. The $K_2(QL)_6K_2$ peptide (1 wt% in water) was next added on top of the HA, generating a membrane upon contact between the solutions. The membrane was allowed to age for either 4 or 24 h at 4, 21 and 50 ºC. The membranes were also prepared inverting the positions of the HA and peptide: peptide solution was cast onto the PDMS substrate with the HA added on top. The effects of time and temperature on the membranes were also analyzed. Membranes containing different amounts of the RGDS motif were prepared by mixing the $K_2(QL)_6K_2$ and $K_2(QL)_6K_2$RGDS peptides in different ratios (1:10 and 3:10) prior to the co-assembly with HA.

To get better insight into the self-assembly process, namely on the mixture of the components during membrane formation, fluorescently labeled HA (prepared as described in 1.5.1.) was used to prepare the self-assembled membranes. The membranes were prepared as described before, with variations in time, temperature and positioning of peptide and fluorescent HA.

2.3.2.2. Topographically patterned membranes

Topographically patterned membranes were fabricated by casting the peptide solution onto the hydrophilic PDMS molds followed by the addition of the HA on the top of peptide solution (Figure II.11.). The membranes were aged for 24 h at room temperature. The self-assembled membranes were removed from the patterned PDMS molds by immersion in ethanol (70%) and then characterized.
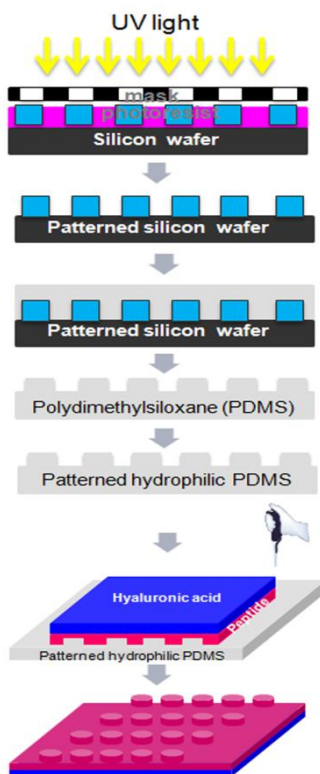
Figure II.11. Schematic representation of overall process to fabricate patterned membranes by soft photolithography.

3. METHODS AND TECHNIQUES FOR CHARACTERIZATION OF DEVELOPED MATERIALS AND MATRICES

3.1. Physico-chemical characterization of developed materials

3.1.1. Solubility analysis

Solubility is related with ability of a substance to dissolve and depends on the solvent as well as on the temperature and pressure. The solubility of each palmitoyl xanthan conjugate described on chapter IV was tested in water, ethanol, dimethyl sulfoxide, acetone, dichloromethane, tetrahydrofuran, by placing 10 mg of palmitoyl xanthan in 4 mL of each solvent. The suspension solution was mixed by vortex and placed in a water bath at 37 °C overnight. Solubility was examined visually for any undissolved solute particles [39].

3.1.2. Determination of the degree of substitution (DS)

The DS for xanthan derivatives can be defined as moles of substituent introduced per structural unit of the xanthan polymer being relevant on the chemical characterization of the

synthesized/modified xanthan based polymers. We have used two methods to determine the DS of xanthan derivatives.

3.1.2.1. Acid-base titration

The degree of substitution of CMX and xanthan-DOPE (Chapter III and V, respectively) was determined by acid-base titration. The polymers were dissolved in distilled water and the pH of the solutions adjusted to 2 with hydrochloric acid 0.2 M. The solutions of xanthan derivatives were titrated with NaOH and the volume of NaOH, as well as the pH values, were recorded. Three replicates were performed for each sample and DS was calculated following the procedure adapted from [40] as follows:

$$DS = \frac{M_{Xru} \times (n_{ep})}{m - (M_{ms} \times n_{ep})} \qquad \text{(II.3.)}$$

M_{Xru} is the molecular weight of xanthan repeating unity (851); n_{ep} is the number of moles of substituent introduced in the native structure of xanthan at the ending point of the titration; M_{ms} is the molecular weight of substituent inserted in the native structure of xanthan gum.

3.1.2.2. Elemental analysis.

The DS (fraction of hydroxyl groups modified per average of repeating unit of palmitoyl xanthan (X=1.7P) (chapter IV) was calculated on basis of %C from elemental analysis results. The elemental composition of palmitoyl xanthan was determined as described on 1.2.1. of this chapter for native xanthan. The results of elemental analysis are presented on Table II.6.

Table II.6 Elemental composition of palmitoyl xanthan (PX(X=1.7P)). The values represent the mean of two replicates with standard deviation.

Sample	%C	%H	%N	%O[a]
Palmitoyl xanthan	37.935 ± 0.148	5.895 ± 0.134	0.554 ± 0.019	55.617 ± 0.04

[a] by difference

Considering that each repeating unit of xanthan has 11 hydroxyl groups (Figure II.2), the maximum possible DS value would be 11 (100%). The DS values for palmitoyl xanthan were determined as shown in Table II.7.

Table II.7. Determination of palmitoyl xanthan DS.

Sample	Average Carbon/%	Mol number	DS
Xanthan (35 Carbon/molecule)	35.66[a]	(35.66/(35x12)= 0.0849	
Palmitoyl xanthan	37.93[a]	-	(0.0118)/0.0849)x100 = 13.9 %
Palmitoyl Chloride (16 Carbon/molecule)	2.275[b]	(2.275/(16x12)= 0.0118	(per repeating subunit)

[a] From elemental analysis (Tables II.1. and II.6.)

[b] Difference between palmitoyl xanthan and xanthan

3.1.3. Fourier transform infrared (FTIR) spectroscopy

FTIR is a spectroscopic technique that can provide information about the chemical structure of materials. It is based on the absorption of the infrared light by the material that may result in distinct molecular excitation/vibration. Once the energies provided by the molecular excitations are related with specific vibrational states of atomic and molecular units, they can be converted into a FTIR spectrum and the presence of the chemical groups can be identified.

FTIR was applied to characterize the xanthan derivatives (carboxymethylated xanthan, chapter III; palmitoyl xanthan, chapter IV; xanthan-DOPE, chapter V). Prior to analysis, potassium bromide (KBr, PIKE Techonologies, USA) pellets were prepared by mixing the xanthan derivative powder with KBr (Xanthan derivative/KBr, 1/10, wt/wt). The spectrum was taken with the average of 32 scans and a resolution of 4 cm^{-1} in an IR Prestige-21 (SHIMADZU, Japan) spectrophotometer.

3.1.4. Proton nuclear magnetic resonance (^{1}H NMR) spectroscopy

NMR is based on the fact that the nuclei have spin which is electrically charged. When a magnetic field is applied there is an energetic transition associated to a precise resonant frequency. The signal that matches this transfer is measured and converted into a NMR spectrum. Thus, for proton NMR (^{1}H NMR) spectroscopy, the information is provided concerning the hydrogen's atom environment in the molecule. Since protons from the solvent should not interfere in the analysis, deuterated solvents are usually preferred. This spectroscopic technique

was used in chapters IV and V to characterize the palmitoyl xanthan and xanthan-DOPE, respectively.

Samples containing different ratios of xanthan/palmitoyl chloride were dissolved at a concentration of 1 wt% in deuterated dimethylsulfoxide. Xanthan-DOPE was dissolved in deuterated water at the same concentration. Fully relaxed ^{1}H NMR spectra were acquired in a Varian Unity Plus 300 MHz spectrometer (USA).

3.1.5. Wide angle x-ray scattering (WAXS)

WAXS is an X-ray diffraction technique which can provide information about the macromolecular structure of the materials and thin films. This is based on the analysis of peaks provided by the Bragg´s law scattered to wide angles.

Palmitoyl xanthan (chapter IV) conjugates and xantha-DOPE (chapter V) were characterized by WAXS technique to verify any molecular organization after the introduction of hydrophobic molecules in the native xanthan structure. WAXS measurements were performed using a Bruker AXS NanoStar (USA) with a HiStar 2D detector with scattering angles from 5 to 60 º.

3.1.6. Differential scanning calorimetry (DSC)

DSC is a thermoanalytical technique that measures the temperatures and heat flows associated with transitions in materials as a function of time and temperature in a controlled atmosphere. These measurements provide quantitative and qualitative information about physical and chemical changes that involve endothermic or exothermic processes, or changes in heat capacity.

DSC analysis is described in chapter IV to investigate eventual transitions in palmitoyl xanthan conjugate and was performed in a calorimeter (TA instruments, USA) with a heating program of 10 ºC min^{-1} from 10 to 200 ºC under nitrogen at flow of 20 cm^3.min^{-1}.

3.1.7. Circular dichroism (CD)

CD spectroscopy is a form of light absorption spectroscopy that measures the difference in absorbance of right- and left-circularly polarized light in molecules [24]. It has been shown that CD spectra between 260 and 180 nm can be used to analyze the secondary structure of peptides and proteins (e.g. alpha helix, parallel and antiparallel beta sheet).

CD was used to study the effects of palmitoylation and the conjugation with DOPE on the secondary structure of native xanthan. Palmitoyl xanthan and xanthan-DOPE were dissolved in ultrapure water overnight at concentration of 0.1 wt%. The measurements were performed in a Stopped-flow circular dichroism spectropolarimeter (PiStar-180, Applied Photophysics, UK) at 25 ⁰C using Quartz cells with a 0.1 cm path length. The spectra were recorded from 300 to 180 nm with a scan rate of 100 nm/min and are an average of five accumulations.

3.1.8. Zeta potential measurements

Zeta potential is widely used for the quantification of the electrical charge of particles, polymers or proteins. Although the electrical charge is not measured directly, it can be calculated using established theoretical models.

Zeta potential measurements of xanthan, hyaluronan and peptide solutions (chapters IV, VI and VII) were performed at different pHs and temperatures using a Zetasizer NanoZS Instrument (ZEN 3600, Malvern Instruments, UK). Prior to the measurements, samples were dissolved at concentration of 0.1 wt% and their pH adjusted using 0.1 M HCl and 0.1 M NH_3OH. The solutions were filtered using a pyrogen free 0.45 µm disposable membrane filter (Schleicher and Schuell Bioscience, Germany**)**.

3.1.9. Quartz crystal microbalance with dissipation (QCM-D) monitoring

The QCM instrument operates with a quartz disc in contact with two electrodes. Since the quartz is a piezoelectric material, its excitation by an electric field produces an acoustic wave that propagates and makes the crystal oscillate. The resonance frequency is dependent on the total oscillating mass. The detection principle is based on the resonance frequency shifts due to addition or removal of mass on the crystal surface. Mass adsorption increases the frequency while mass losses induce decrease of frequency. The mass can be calculated by the Sauerbrey equation that correlates proportionally the frequency change with the mass adsorbs.

In order to study the interactions between xanthan and $K_2(QL)_6K_2$ peptide, QCM analyses were performed on chapter VI. QCM measurements were performed with an instrument with dissipation monitoring (QCM-D) from Q-Sense (Göteborg, Sweden). The experiments were performed at 24 ⁰C with 50 µL/min flow rate using gold coated crystals (model QSX301, Q-Sense, Göteborg, Sweden) previously cleaned with $H_2O_2(30\%)/NH_3(25\%)/H_2O$ (1:1:5) during 10 minutes at 75 ⁰C. The system was initially equilibrated with phosphate buffered saline (PBS) solution (10 mM, pH7.4) to obtain a stable frequency and dissipation baseline signal. Once the signals were stable, the buffer was replaced by a solution of xanthan (0.25 wt% in PBS) during

25 minutes. Then, the buffer was again introduced to remove weakly bound material. This step was followed by the introduction of the peptide solution (0.0025; 0.0625 or 0.125 wt% in H_2O) or BSA solution (0.5 mg/mL in PBS). Finally the system was rinsed with PBS solution.

Thickness was calculated by the Voigt model [41] incorporated in Q-Sense software using different overtones (7th; 9th, 11th, 13th). The layer viscosity values used in the model were between 0.001 and 0.01 $kg.ms^{-1}$, the layer shear modulus between 10 and 10^5 Pa, and layer thickness values were between 10^{-10} a 10^{-6} m. For xanthan, a fluid density of 1000 kg.m-^{3}, fluid viscosity of 0.001 $kg.ms^{-1}$ and layer density of 850 kg.m-^{3} were used. For the peptide modeling, a fluid density of 1300 kg.m-^{3}, fluid viscosity of 0.003 $kg.ms^{-1}$ and layer density of 1600 kg.m-^{3} were used. For BSA modeling, a fluid density of 1000 kg.m-^{3}, fluid viscosity of 0.001 $kg.ms^{-1}$ and layer density of 1500 kg.m-^{3} were used.

3.1.10. Scanning transmission electron microscopy (STEM)

Transmission electron microscopy (TEM) is a microscopy technique based on the interaction of a beam of electrons that are transmitted through a thin sample which enables high resolution at the nanoscale.

Samples of xanthan (control) and water-soluble PX conjugate (Chapter IV) for STEM observations were prepared by placing one drop of the polymer solution and (0.1 wt%) onto a 300-mesh copper grid coated with carbon film, followed by 1% (w/v) of uranyl acetate (Electron Microscopy Sciences) staining for 3 minutes. The samples were analyzed and photographed using a Hitachi Su electron microscope in S-TEM mode.

3.1.11. Polarized light microscopy

This is a simple technique that includes illumination of the sample with polarized light. This technique is commonly used with birrefringent samples where the polarized light interacts strongly with the sample and generates contrast with the background.

The morphology of xanthan-DOPE assemblies in aqueous conditions was also directly examined by polarized light microscopy. Native xanthan and xanthan-DOPE were dissolved in distilled water and the solution dropped onto a glass slide The samples were observed in a polarized light optical microscope (Olympus type BH-2) and recorded with a Olympus digital camera type DFC280.

3.2. Characterization of developed self-assembled matrices (microcapsules and membranes)

3.2.1. Microcapsules

3.2.1.1. Morphology

Bright field microscopy

In bright field microscopy, the sample is illuminated and some of the transmitted light is absorbed on its dense areas causing white light and contrast. A bright field microscopy image is a dark sample on a bright background.

Optical microscopy was used to assess the size, shape and morphology of the microcapsules on chapters III-VI in a bright field light microscope (AXIOVERT 40 CFL, Zeiss, Germany) equipped with a digital camera (Canon Power shot G8, Japan).

Scanning Electron Microscopy (SEM)

SEM is a microscopic technique that images a sample by scanning through a high energetic beam of electrons. Those electrons may interact with sample surface resulting in the emission of secondary electrons that is further converted in the micrographs [42]. Non-conductive samples are usually coated with a thin conductive metal layer in order to minimize charge accumulation.

SEM was used to evaluate the morphological details (at nano and microscale) of the developed microcapsules. Prior to the SEM observations, the microcapsules were fixed with glutaraldehyde (Electron Microscopy Sciences, USA) solution (3% v/v in PBS) at 4 ºC for 1 h. The samples were further dehydrated in a graded ethanol series followed by immersion in 100% hexamethyldisilazane (HMDS, Electron Microscopy Sciences, USA). Microcapsules were cut in half to expose the membrane cross-section and the internal surface of microcapsules. The microcapsules were mounted on aluminum stubs and sputter coated with Pt/Pd target (80/20) generating a thin film with 6 nm of thickness (208 HR High Resolution Sputter Coater, Cressington). The microcapsules were imaged on an ultra-high resolution field emission gun scanning electron microscope (FEG/SEM, FEI Nova 200 NanoSEM).

3.2.1.2. Permeability

The mass transport properties through an encapsulation membrane are crucial for the success of the encapsulating matrix. The influx of essential molecules, such as oxygen and nutrients and the efflux rate of therapeutic products and wastes are critical for cell survival. Additionally, the encapsulation membrane may avoid the influx of immune cells and antibodies, which might destroy the enclosed cells [14,43].

To assess the permeability of xanthan-DOPE and xanthan-peptide microcapsules, described on chapters V and VI respectively, to antibody molecules, the Immunoglobulin G (IgG, Mw = 146-155 KDa, Abcam, UK) was used. Prior use, IgG was labeled with fluorescein isothiocyanide (FITC) in order to determine the diffusion of the protein into microcapsules by fluorescence spectroscopy. The IgG was dissolved in sodium carbonate buffer (0.1 M, pH 9) at 2 mg/mL concentration. The fluorescein dye, dissolved in DMSO (1 mg/mL) was added per mL of protein solution and gentle mixed for 8 hour at 4 °C in the dark. Afterwards, the reaction was quenched by adding ammonium chloride to a final concentration of 50 mM. The solution was placed into dialysis tubing and dialysed against distilled water in the dark to remove unconjugated FITC. Finally, the dialyzed solution was freeze-dried in a light protected vessel. For permeability studies, equal volumes of microcapsules and IgG-FITC (15 mg/mL solution in NaCl 0.9%) were shaken in a water-shaker bath at 37 °C and aliquots of 5 μL were collected from 0 to 3 h. Concentrations of IgG-FITC were measured by fluorescence (485/528 nm) on a microplate reader (BIO-TEK, SYNERGIE HT, USA).

3.2.1.3. Mechanical stability

Microcapsule resistance to mechanical stress is another important criterion for the success of cell microencapsulation [14-15,44]. A microcapsule should be resistant enough to be durable during its production, handling and to resist to the mechanical stress without the loss of its membrane integrity [45]. Xanthan-DOPE and xantham-DOPE/PLL were subjected to agitation in saline solution (chapter V). For xanthan-peptide microcapsules (chapter VI) they were immersed in a hypotonic environment and later the microcapsules were exposed to PBS solution and agitated with glass microbeads to evaluate its mechanical strength in conditions resembling *in vivo* shear stress.

Induction of mechanical stress using agitation

The mechanical strength of xanthan-DOPE microcapsules was evaluated by agitating the microcapsules (uncoated and coated with PLL) in a flat rotator at maximum rate (about 240 rpm, DSR-2800V, Digisystem Laboratory Instruments Inc, Taiwan). The microcapsules were put in 24 well plates (10 per well) with 1 mL of PBS. At various time intervals (1, 2, 3, 6, and 24 h) the number of damaged capsules was counted by direct observation on light microscope and the percentage of ruptured capsules in function of time was determined.

Induction of mechanical stress using osmotic pressure

Aliquots of xanthan-peptide microcapsules were placed in 10 mL of water and incubated for 24 h at 37 ⁰C in a water shaker bath (procedure adapted from [44]). At various time intervals, the capsules were collected and observed in a bright field light microscope (AXIOVERT 40 CFL, Germany) equipped with a digital camera (Canon Power shot G8, Japan) and the number of ruptured capsules counted.

Induction of mechanical stress using bead agitation

Xanthan-peptide microcapsules were placed in flasks containing 20 glass beads (3 mm diameter, VWR Scientfic Products Corporation) and 30 mL of PBS solution in a flat rotator shaking at maximum rate (about 300 rpm) (DSR-2800V, Digisystem lab.instruments.inc). At various time intervals (2, 5, 7, 24 h) the number of ruptured capsules was counted by observation in a bright field light microscope (AXIOVERT 40 CFL, Germany) equipped with a digital camera (Canon Power shot G8, Japan). The percentage of ruptured capsules in function of time was determined (procedure adapted from [44]).

3.2.2. Membranes

3.2.2.1. Morphology

SEM

The morphology and uniformity of membrane surface and cross-section were investigated by SEM. The membranes for SEM analysis were prepared according with the procedure described in section 3.2.1.1. Then, they were mounted in a silicon wafer further sputtered coated with 20 nm of gold. The membranes were imaged on Nova NanoSEM microscope (FEI, Netherlands).

Confocal microscopy

In fluorescence microscopy, morphological details can be observed by the analysis of fluorescent samples through fluorescent light instead or additionally to reflection and absorption provided by the simple optical microscope.

The membranes prepared with fluorescein-HA were imaged using an SP2 confocal microscope (Leica Microsystems, Germany).

3.2.3. Biological assessment

3.2.3.1. Cell sources

Cell lines

Cell lines are immortalized cultures of cells genetically modified with ability to be subcultivated more than 70 times after the primary isolation without restriction [46]. In this PhD work, ATDC5 cell line was used in the encapsulation studies described in chapters III to VI. ATDC5 cells are a murine chondrocytic cell line that has been widely used as a monolayer culture system to study chondrogenic differentiation [47].

Primary cells

Primary cels are usually obtained directly from the parent tissue and have the same karyotype and chromosome number as those in the original tissue and subsequently are not immortalized. Mesenchymal stem cells have been shown the capability of self-renewal and differentiation into various connective tissue lineages [48]. Rat mesenchymal stem cells (rMSC) were used on the biological assessment of the membranes described in chapter VII to evaluate the effect of the developed bioactive patterned membranes on cell adhesion and morphology.

3.2.3.2. Culture and encapsulation ATDC5 cells on xanthan-based microcapsules

The murine ATDC5 chondrocyte cells were cultured in basic medium, consisted of Dulbecoo's Modified Eagle's Medium (DMEM, Sigma-Aldrich, USA) with phenol red, supplemented with 10% fetal calf serum (FCS, Biochrom AG, Germany), 5 mM L-Glutamine (Sigma, USA) and 1% of antibiotic-antimycotic mixture (Sigma, USA) and maintained at 37 °C in a humidified atmosphere of 5% CO_2. The medium was replaced every two days. At passage 7, cells were detached with trypsin/EDTA and counted in a hemacytometer for encapsulation.

The effect of xanthan based microcapsules on cellular metabolic activity was assessed by encapsulating ATDC5 cells using the microdroplet generator (chapters III and IV) and the microfluidics device (chapters V and VI). The cells were suspended in the mentioned polymers and microcapsules containing cells were produced according with the procedure described on the section 2.1.2. and 2.2.2. of this chapter for microcapsule preparation.

3.2.3.3. Seeding and culture of rat mesenchymal stem cells on fabricated membranes

Rat mesenchymal stem cells (rMSCs) isolated from bone marrow of rat tibia and femur, were provided by the Animal Research Center (SEA) of the Parc Científic Barcelona. Cells were expanded in Dulbecco's modified Eagle's medium (DMEM; Life Technologies, Spain) supplemented with fetal bovine serum (10%, FBS; Attendbio Research, Spain), L-glutamine (0.2 mM), penicillin (100 units ml^{-1}) and streptomycin (0.1 mg ml^{-1}) (Sigma-Aldrich, Spain).

rMSCs of passage 3–6 were suspended in serum-free DMEM and seeded at 12 500 cells cm^{-2} onto smooth and patterned membranes with and without the RGDS sequence (chapter VII). After 4 h of culture, all medium was replaced with DMEM containing 10% FBS to allow cell proliferation.

3.2.3.4. Cell viability and proliferation

To investigate the ability of xanthan based microcapsules (chapter III-IV) to support cell viability, encapsulated cells were examined using several biochemical analyses. Viability of cells was assessed by fluorescence microscopy using a live/dead assay and the metabolic activity of the encapsulated cells was analyzed by the AlamarBlue® assay.

Cell viability - Live/dead assay

The live/dead assay was used to evaluate the viability of the encapsulated cells. This is a two-color fluorescence assay that allows direct determination of live and dead cells by fluorescence. Live cells can be visualized through the conversion of the permeable non-fluorescent calcein acetomethyl (Calcein-AM) to the intensly fluorescent green calcein (excitation~495 nm/emission~515 nm). Dead cells have damaged membrane and consequently the propidium iodine (PI) enters in the damaged cells and becomes fluorescent when bound to nucleic acids. PI produces a bright red fluorescent in damaged or dead cells (excitation 488 nm/ emission 617 nm).

Calcein AM (Sigma, USA) solution (2/1000, v/v) was prepared in DMEM medium without FCS and phenol red. Propidium iodide (PI, Molecular Probes, Invitrogen, USA) solution was prepared by mixing 2 µL PI (1 mg/mL) with 20 µL (1 mg/mL) RNAse A (USB corporation, USA) and 2 mL PBS. The microcapsules with encapsulated cells and controls were collected from the culturing plates and incubated with calcein-AM and propidium iodide solutions at 37 ºC for 10 min protected from light. Samples were then observed under fluorescent microscopy using an Axioplan Imager Z1m microscope (Zeiss, Germany).

Metabolic activity - AlamarBlue® assay

This assay uses an oxidation-reduction indicator that both fluoresces and changes color in response to chemical reduction of growth medium resulting from metabolic activity. The cellular viability can be assessed by several methods based on the reduction of tetrazolium compounds such as Thiazolyl Blue Tetrazolium Bromide (MTT) or (MTS) [15]. Nevertheless, AlamarBlue® provides several advantages over the other methods: the proliferation and viability can be assessed, furthermore it is easy to implement and it is not toxic, which allow the concomitant

evaluation of the same culture at several time points, and by consequence their usage for additional assays.

The metabolic activity of encapsulated cells over time was assessed using the AlamarBlue® assay (AbD Serotec,UK). AlamarBlue® was added (10% of the volume of the well) to each well containing the encapsulated cells and the plate was incubated at 37 ºC for 20 hours protected from light. After incubation, 100 µL of solution was taken from each well and placed in a 96 well plate. The absorbance was read at 570 and 600 nm on a microplate reader (BIO-TEK, SYNERGIE HT, USA). The percentage of reduced AlamarBlue® was calculated according the manufacturer instructions.

Cell proliferation – DNA quantification assay

Cell proliferation was evaluated by quantifying the DNA content of the encapsulated ATDC5 cells over time. A fluorimetric dsDNA quantification kit (PicoGreen, Molecular Probes, Invitrogen, USA) was used that contains an ultra sensitive fluorescent nucleic acid stain for quantifying double-stranded DNA (dsDNA) in solution. For this purpose, the samples collected at days 1, 7, 14 and 21 were washed twice with sterile PBS (Sigma, USA) solution and transferred into 1.5 mL microtubes containing 1 mL of ultra-pure water. Capsules with and without cells were stored at -80 ºC until further analysis. Prior to DNA quantification, samples were thawed and broken by pipetting up and down using a syringe with a needle to cause material disruption and facilitate DNA extraction. 28.7 µL of each sample and standards (0-2 mg/mL) were transferred to an opaque 96 well plate. Then 71.3 µL of PicoGreen solution and 100 µL of Tris-EDTA buffer were added. Standards and samples were prepared in triplicate. The plate was incubated for 10 minutes in the dark and the fluorescence was measured using an excitation wavelength of 485 nm and emission of 528 nm. DNA amounts were calculated from the calibration curve.

3.2.3.5. Cell morphology

Bright field microscopy

Microscopy observations of the encapsulated cells were carried out over the course of the *in vitro* culture on chapters III-VI. A bright field light microscope (AXIOVERT 40 CFL, Zeiss, Germany) equipped with a digital camera (Canon Power shot G8, Japan) was used and images were acquired at 10x magnification.

Histology

Hematoxylin is a widely used nuclear stain, while eosin is used solely to enhance the contrast of the stain. H&E staining is based on a color change on the nucleus of cells in the tissue sections

from red to blue when there is a pH change (pH ~ 3). H&E staining was used on chapter III to examine the morphology of cells encapsulated within the microcapsules. Cell cultured microcapsules for histology were rinsed three times in PBS and then fixed in 3.7% formalin in PBS for 1 hour at room temperature. After fixation, samples were dehydrated in a graded ethanol series (70, 90, 95 and 100%) followed by immersion in xylene. Specimens were embedded in paraffin and cut in 4 µm-thick sections (MICROM HM355S Microtome, INOPAT, USA). Sections were then dewaxed and stained with Harris Hematoxylin (Sigma, USA) and eosin (H&E staining).

Immunostaining

In order to investigate the effect of the physical (topographies) and biochemical (RGDS) signals present in the developed self-assembling membranes (chapter VII) on cell adhesion and morphology, immunostaining was performed. After 18 h, the culture medium was removed and the samples were washed twice with PBS to remove any non-adherent cells. Cells were fixed with 4% (w/v) formalin (Sigma- Aldrich, Spain) in PBS for 30 min. To visualize the actin cytoskeleton, cells were stained with phalloidin-fluorescein isothiocyanate (phalloidin–FITC,Sigma-Aldrich, Spain) at a 1:500 dilution in PBS for 1h at room temperature. The remained phalloidin was removed and the nuclear fluorescent stain, 4',6-diamidino-2-phenylindole dihydrochloride (DAPI; Invitrogen, Spain), was added. Finally, the samples were placed in a glass slide with a droplet of Fluoro-Gel mountant (Aname, Spain). The cells were visualized using an SPE confocal microscope (Leica Microsystems, Germany).

SEM

Cells encapsulated within microcapsules and cultured on the membranes were examined under SEM to analyse cell morphology and its interactions with the matrices. Samples were prepared as described in section 3.2.2.1. of this chapter.

4. STATISTICAL ANALYSIS

A *Student's t-test* was used throughout this thesis to assess the statistical difference between two sample means. Results of DNA quantification and cell viability, zeta potential and membrane thickness were expressed as a mean ± standard deviation with n=3 for each group on chapters III to VII. Statistical significance of differences was determined using unpaired student's *t*-test multiple comparison procedure at a confidence level of 95% (p<0.05).

REFERENCES

1. Katzbauer B. Properties and applications of xanthan gum. Polymer Degradation and Stability 1998;59(1-3):81-84.

2. García-Ochoa F, Santos VE, Casas JA, Gómez E. Xanthan gum: production, recovery, and properties. Biotechnology Advances 2000;18(7):549-579.

3. Schorsch C, Garnier C, Doublier J-L. Microscopy of xanthan/galactomannan mixtures. Carbohydrate Polymers 1995;28(4):319-323.

4. Hamcerencu M, Desbrieres J, Popa M, Khoukh A, Riess G. New unsaturated derivatives of Xanthan gum: Synthesis and characterization. Polymer 2007;48(7):1921-1929.

5. Capron I, Brigand G, Muller G. About the native and renatured conformation of xanthan exopolysaccharide. Polymer 1997;38(21):5289-5295.

6. Rodd AB, Dunstan DE, Boger DV. Characterisation of xanthan gum solutions using dynamic light scattering and rheology. Carbohydrate Polymers 2000;42(2):159-174.

7. M. A. Coimbra, I. Delgadillo, K. W. Waldron, Selvendran RR. Isolation and Analysis of Cell Wall Polymers from Olive Pulp. Berlin: Springer-Verlag; 1996.

8. Blumenkrantz N, Asboe-Hansen G. New method for quantitative determination of uronic acids. Analytical Biochemistry 1973;54(2):484-489.

9. Ciucanu I, Kerek F. A simple and rapid method for the permethylation of carbohydrates. Carbohydrate Research 1984;131(2):209-217.

10. Chen X-G, Park H-J. Chemical characteristics of O-carboxymethyl chitosans related to the preparation conditions. Carbohydrate Polymers 2003;53(4):355-359.

11. Mendes AC, Baran ET, Nunes C, Coimbra MA, Azevedo HS, Reis RL. Palmitoylation of xanthan polysaccharide for self-assembly microcapsule formation and encapsulation of cells in physiological conditions. Soft Matter 2011;7(20):96-47.

12. Greg T H. 12 - Preparation of Liposome Conjugates and Derivatives. Bioconjugate Techniques. San Diego: Academic Press; 1996. p 528-569.

13. Gupta M, Raghava S. Smart systems based on polysaccharides. In: Reis R, Neves N, Mano J, Gomes M, Marques A, HS A, editors. Natural-based polymers for biomedical aplications. Cambridge: Woodhead Publishing; 2008.

14. Hernández RM, Orive G, Murua A, Pedraz JL. Microcapsules and microcarriers for in situ cell delivery. Advanced Drug Delivery Reviews 2010;62(7-8):711-730.

15. de Vos P, Bucko M, Gemeiner P, Navrátil M, Svitel J, Faas M, Strand BL, Skjak-Braek G, Morch YA, Vikartovská A and others. Multiscale requirements for bioencapsulation in medicine and biotechnology. Biomaterials 2009;30(13):2559-2570.

16. Juste S, Lessard M, Henley N, Ménard M, Hallé J-P. Effect of poly-L-lysine coating on macrophage activation by alginate-based microcapsules: Assessment using a new in vitro method. Journal of Biomedical Materials Research Part A 2005;72A(4):389-398.

17. Allison DD, Grande-Allen KJ. Review. Hyaluronan: a powerful tissue engineering tool. Tissue Eng 2006;12(8):2131-40.

18. Gajewiak J, Cai S, Shu XZ, Prestwich GD. Aminooxy Pluronics: Synthesis and Preparation of Glycosaminoglycan Adducts. Biomacromolecules 2006;7(6):1781-1789.

19. Dong H, Paramonov SE, Aulisa L, Bakota EL, Hartgerink JD. Self-assembly of multidomain peptides: Balancing molecular frustration controls conformation and nanostructure. Journal of the American Chemical Society 2007;129(41):12468-12472.

20. Aulisa L, Dong H, Hartgerink JD. Self-Assembly of Multidomain Peptides: Sequence Variation Allows Control over Cross-Linking and Viscoelasticity. Biomacromolecules 2009;10(9):2694-2698.

21. Galler KM, Aulisa L, Regan KR, D'Souza RN, Hartgerink JD. Self-Assembling Multidomain Peptide Hydrogels: Designed Susceptibility to Enzymatic Cleavage Allows Enhanced Cell Migration and Spreading. Journal of the American Chemical Society 2010;132(9):3217-3223.

22. Galler KM, Hartgerink JD, Cavender AC, Schmalz G, D'Souza RN. A Customized Self-Assembling Peptide Hydrogel for Dental Pulp Tissue Engineering. Tissue Engineering Part A 2012;18(1-2):176-184.

23. Bodanszky M. Principles of Peptide Synthesis: Springer-Verlag; 1993.

24. Hammes GG. Spectroscopy for the Biological Sciences. New Jersey: John Wiley & Sons, Inc; 2005.

25. Aguilar MI. Hplc of Peptides and Proteins: Methods and Protocols: Humana Press; 2004.

26. Baran ET, Mendes AC, Azevedo HS, Reis RL; DISPOSITIVO, MÉTODO E SISTEMA DE FABRICO DE MICROCÁPSULAS. Portugal. 2011.

27. Whitesides GM. The origins and the future of microfluidics. Nature 2006;442(7101):368-373.

28. Khademhosseini A, Langer R. Microengineered hydrogels for tissue engineering. Biomaterials 2007;28(34):5087-5092.

29. Tumarkin E, Kumacheva E. Microfluidic generation of microgels from synthetic and natural polymers. Chemical Society Reviews 2009;38(8):2161-2168.

30. Xu Y, Sato K, Mawatari K, Konno T, Jang K, Ishihara K, Kitamori T. A Microfluidic Hydrogel Capable of Cell Preservation without Perfusion Culture under Cell-Based Assay Conditions. Advanced Materials 2010;22(28):3017-3021.

31.   Aikawa T, Konno T, Takai M, Ishihara K. Spherical Phospholipid Polymer Hydrogels for Cell Encapsulation Prepared with a Flow-Focusing Microfluidic Channel Device. Langmuir 2011;28(4):2145-2150.

32.   Abdelgawad M, Wheeler AR. Rapid Prototyping in Copper Substrates for Digital Microfluidics. Advanced Materials 2007;19(1):133-137.

33.   Nie Z, Kumacheva E. Patterning surfaces with functional polymers. Nat Mater 2008;7(4):277-290.

34.   Smith KH, Tejeda-Montes E, Poch M, Mata A. Integrating top-down and self-assembly in the fabrication of peptide and protein-based biomedical materials. Chemical Society Reviews 2011;40(9):4563-4577.

35.   Park M, Harrison C, Chaikin PM, Register RA, Adamson DH. Block copolymer lithography: Periodic arrays of [sim]1011 holes in 1 square centimeter. Science 1997;276:1401-1404.

36.   Mata A, Hsu L, Capito R, Aparicio C, Henrikson K, Stupp SI. Micropatterning of bioactive self-assembling gels. Soft Matter 2009;5(6):1228-1236.

37.   Mata A, Kim EJ, Boehm CA, Fleischman AJ, Muschler GF, Roy S. A three-dimensional scaffold with precise micro-architecture and surface micro-textures. Biomaterials 2009;30(27):4610-4617.

38.   Tejeda-Montes E, Smith KH, Poch M, López-Bosque MJ, Martín L, Alonso M, Engel E, Mata A. Engineering membrane scaffolds with both physical and biomolecular signaling. Acta Biomaterialia (0).

39.   Jiang G-B, Quan D, Liao K, Wang H. Preparation of polymeric micelles based on chitosan bearing a small amount of highly hydrophobic groups. Carbohydrate Polymers 2006;66(4):514-520.

40.   Ge H-C, Luo D-K. Preparation of carboxymethyl chitosan in aqueous solution under microwave irradiation. Carbohydrate Research 2005;340(7):1351-1356.

41.   M V Voinova MR, M Jonson and B Kasemo. Viscoelastic Acoustic Response of Layered Polymer Films at Fluid-Solid Interfaces: Continuum Mechanics Approach. Physica Scripta 1999;59:391.

42.   Ratner BD. Biomaterials science : an introduction to materials in medicine. San Diego, Calif.; London: Elsevier Academic Press; 2004.

43.   Murua A, Portero A, Orive G, Hernández RM, de Castro M, Pedraz JL. Cell microencapsulation technology: Towards clinical application. Journal of Controlled Release 2008;132(2):76-83.

44.   Darrabie MD, Kendall Jr WF, Opara EC. Characteristics of Poly-l-Ornithine-coated alginate microcapsules. Biomaterials 2005;26(34):6846-6852.

45.   Mendes AC, Baran ET, Pereira RC, Azevedo HS, Reis RC. Encapsulation and Survival of a Chondrocyte Cell Line within Xanthan gum derivative. 2010.

46.   Minuth WW, Strehl R, Schumacher K. Tissue Engineering: Essentials for Daily Laboratory Work: Wiley-VCH; 2005.

47.   Tare RS, Howard D, Pound JC, Roach HI, Oreffo ROC. Tissue engineering strategies for cartilage generation--Micromass and three dimensional cultures using human chondrocytes and a continuous cell line. Biochemical and Biophysical Research Communications 2005;333(2):609-621.

48.   Deans RJ, Moseley AB. Mesenchymal stem cells: Biology and potential clinical uses. Experimental Hematology 2000;28(8):875-884.

Section 3

SELF-ASSEMBLED AND MICROFABRICATED STRUCTURES

Chapter III

ENCAPSULATION AND SURVIVAL OF A CHONDROCYTIC CELL LINE
WITHIN XANTHAN DERIVATIVE

ENCAPSULATION AND SURVIVAL OF A CHONDROCYTIC CELL LINE WITHIN XANTHAN DERIVATIVE

ABSTRACT

There is a renewed interest in using polymers of natural origin to obtain hydrogels for cell encapsulation, as they usually undergo gelation under mild conditions. The aim of this work was to investigate the potential of xanthan, a bacterial extracellular polysaccharide, as a new artificial matrix for the encapsulation of a chondrocytic cell line (ATDC5 cells) and to compare it with alginate, the most widely used material for encapsulation of living cells. Towards this goal, we have developed a novel micro-droplet generator to produce microcapsules. The system is based on a sterilizable silicone tubing which can be applied conveniently to almost every biology laboratory without using sophisticated microfabrication techniques of microfluidics. The prepared microcapsules were characterized according with their size, shape, surface morphology and stability. Microcapsules with an average diameter of 500 μm and homogenous size distribution were obtained. The morphology revealed by scanning electron microscopy showed microcapsules with a quite smooth surface and a capsule membrane of 5 μm with two distinct layers. ATDC5 cells encapsulated in carboxymethyl xanthan (CMX) microcapsules remained viable and were observed to proliferate for prolonged culture periods. When compared with alginate microcapsules, cells in CMX showed enhanced metabolic activity and proliferating rates. Furthermore, the cells exhibited a round morphology typical of chondrocytes, indicating that CMX promoted the retention of the chondrogenic phenotype and suggesting the potential of this matrix to be applied in cell-based therapies for cartilage tissue engineering approaches.

1.INTRODUCTION

Cell microencapsulation is a technology with enormous clinical potential for the treatment of a wide range of human diseases such as diabetes[1-3], hemophilia, anemia, hypoparathyroidism, renal failure [1,4-7], osteoarthritis [8-14] and also for constructing artificial organs [1]. In cell encapsulation, cells are protected from immune rejection by an artificial, semipermeable membrane, potentially allowing transplantation (allo- or xenotransplantation) without the need for immunosuppression [1,4-7,15-18]. For the clinical success of cell encapsulation, it is crucial to have a source of cells, a biocompatible, as well as mechanically and chemically stable membrane of suitable permeability, which is able to provide immune protection to the implant [1,4-6,15-16]. Although efforts have been made in order to accomplish these goals, the available systems still present limitations regarding their reproducibility during microcapsule preparation and long term viability of encapsulated cells. During the past decade, several polyelectrolytes, such as polysaccharides and polypeptides, have been widely used for the fabrication of capsules, due their ability to form gels through complexation with oppositely charged polymers (e.g. alginate/poly-L-lysine [3,17]) or by ionic crosslinking of the polyanionic biopolymer in the presence of a counterion (e.g. Ca^{2+}, Ba^{2+}). In these cases, the gelation processes is cell-compatible, since they do not require harsher chemicals, and the gels provide a highly hydrated three-dimensional network. Furthermore, these materials can be injected into the body, hence enabling the clinician to transplant the cell-polymer combination in a minimally invasive way [19].

Cell based therapies have demonstrated an enormous potential for the long term repair of cartilage defects [8-14] and the alginate-based hydrogels have been widely used as a convenient three-dimensional (3D) cell culture model system [9-11,13,20-21]. This system has demonstrated the ability to prevent chondrocytes from undergoing de-differentiation as well as restore cartilaginous phenotype to de-differentiated chondrocytes [22]. In addition, alginate systems have shown to promote the synthesis of cartilage matrix components, such as proteoglycans and collagen type II [21,23]. Although alginate/poly-L-lysine polyelectrolyte complexes have been widely investigated for cell encapsulation, they still present some drawbacks concerning their long-term mechanical performance and biocompability [7,24]

Xanthan gum is an extracellular polysaccharide produced by the bacterium *Xanthomonas campestris* [25-28]. The primary structure of xanthan consists of $\beta(1\rightarrow4)$-linked glucose units, similar to the structure of cellulose backbone, substituted at O-3 of alternate glucose residues, with a trisaccharide. The trisaccharide consists of one glucuronic acid unit between two mannose units (Figure III.1.A).

The terminal mannose moiety may carry pyruvate residues linked to the positions 4 and 6 with an unknown distribution. D-Mannose unit linked to the main chain contains an acetyl group at position O-6 [25-29]. The pyruvic acid content of xanthan can vary substantially depending on the strain of *X. campestris*, resulting in different viscosities of xanthan solutions. Molecular modelling studies suggest that xanthan gum can assume a helical structure, with the side branches positioned almost parallel to the helix axis and stabilizing the structure [25-27,29]. The presence of acetic and pyruvic acids is the main responsible for the polyanionic character of this polysaccharide. Xanthan forms very viscous solutions, and, at sufficiently high polymer concentration, it exhibits weak gel-like properties [25,30]. Furthermore, it was shown to be biocompatible [28], biodegradable and it is widely used in food, cosmetics and pharmaceuticals because of its encouraging reports on safety [25].
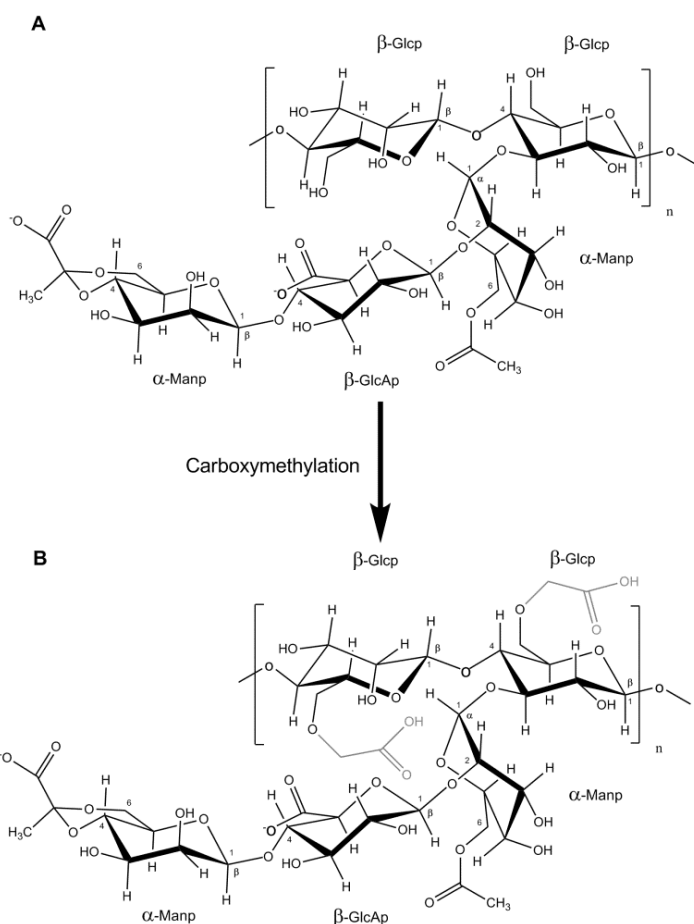
Figure III.1. Chemical structure of xanthan repeating unit (A) and carboxymethyl xanthan (B).

The application of other microbial polysaccharides with gelling properties, such as gellan gum, has been reported in the literature for the encapsulation of human chondrocytes for cartilage regeneration [31] but to the best of our knowledge, the use of xanthan gum as cell encapsulation matrix has only been described by our group [32]. Therefore, the present work aims to investigate the potential of a xanthan derivative (carboxymethyl xanthan, CMX) as a new matrix for the encapsulation of ATDC5 cell line which has been widely used as a model to study chondrogenic differentiation *in vitro* [33-37]. Furthermore, microcapsules made of alginate, a widely used material in cell encapsulation and in cartilage tissue engineering, were used for comparison purposes. To test our hypothesis, we have used a simple microdroplet generator, based on a tubing system, to produce microcapsules with homogenous size distribution and micrometer size favorable for

mass transfer and easy injects for cell therapy. *In vitro* studies were performed to evaluate the ability of the CMX mirocapsules to support cell viability, proliferation and cell functions.

2. MATERIALS AND METHODS

Materials

All chemicals, including xanthan gum from *Xanthomonas campestris*, monochloroacetic acid and poly-L-ysine (PLL), were obtained from Sigma/Aldrich unless otherwise indicated. The chemicals were used as received.

Determination of molecular weight of native xanthan

The average molecular weight (Mw) was determined by size-exclusion chromatography (SEC). The samples were dissolved in an aqueous 0.1 M $NaNO_3$ solution (0.4% w/v). A PL-GPC 110 chromatograph was equipped with a pre-column PLaquagel-OH 15 μm and two SEC columns in series (PLaquagel-OH40 15 μm, 300 × 7.0 mm and PLaquagel-OH60 15 μm, 300 × 7.0 mm). The pre-column, the SEC columns, the injection system, and the refractive index detector were maintained at 36 ºC. The eluent (aqueous 0.1 M $NaNO_3$ solution) was pumped at a flow rate of 0.9 mL min^{-1}. The analytical columns were calibrated with pullulan standards (Polymer Laboratories, UK) in the range of 5.8-1600 kDa. The average molecular weight of xanthan gum was estimated as 152 kDa[32].

Carboxymethyl xanthan (CMX) synthesis

Carboxymethyl xanthan was prepared by adapting the carboxmethylation procedure used for chitosan by Chen and Park [38]. 10 g of xanthan from *Xanthomonas campestris* and 13.5 g sodium hydroxide (Panreac, Spain) were mixed in 100 mL of solvent mixture of water/isopropanol (Fluka, Germany) using a top stirrer. The mixture was allowed to react at 50 ºC in a water bath (Thermostat IKA, Germany) for 1 h. Two solvent mixtures were used (1/1 and 1/4, v/v) to yield xanthan with different degrees of carboxymethylation designated by CMX1 and CMX2 respectively. Then, 15 g monochloroacetic acid, dissolved in 20 mL of isopropanol, were added dropwise to the reaction mixture for 30 min. The reaction was carried out for 4 h at the same temperature and stopped by adding 200 ml of ethanol 70% (Panreac, Spain). At the end, the obtained solid precipitate was filtered and rinsed with 70–90% of ethanol to desalt and dewater and further vacuum dried at room temperature.

CMX Characterization

Fourier Transform Infra Red spectroscopy (FTIR)

The chemical modification of xanthan was analysed by infrared spectroscopy in an IR Prestige-21(SHIMADZU, Japan) spectrophotometer. Prior to analysis, potassium bromide (KBr, PIKE Techonologies, USA) pellets were prepared by mixing the CMX powder with KBr (CMX/KBr, 1/10, wt/wt). The spectrum was taken with the average of 32 scans and a resolution of 4 cm^{-1}.

Determination of the degree of substitution (DS)

The degree of substitution of CMX was determined by acid-base titration. CMX (0.2 g) was dissolved in 40 mL of distilled water. The pH of the solution was adjusted to 2 with hydrochloric acid and then CMX was titrated with 0.1 N NaOH. The volume of added NaOH, as well as the pH values, were recorded. Three replicates were performed for each sample. DS was calculated following the calculation procedure used for carboxymethyl chitosan and described by Ge and co-authors[39] as follows:

$$DS = \frac{M_{Xru} \times (n_{ep})}{0.2 - (M_{CM} \times n_{ep})} \quad \text{(III.1)}$$

M_{Xru} is the molecular weight of Xanthan repeating unity (851); n_{ep} is the number of mol of carboxymethyl groups at the ending point of the titration; M_{CM} is the molecular weight of the carboxymethyl groups inserted in the native structure of Xanthan gum.

Cell culture and encapsulation

The murine ATDC5 chondrocyte cells were cultured in basic medium, consisted of Dulbecoo's Modified Eagle's Medium (DMEM, Sigma-Aldrich, USA) with phenol red, supplemented with 10% fetal calf serum (FCS, Biochrom AG, Germany), 5 mM L-Glutamine (Sigma, USA) and 1% of antibiotic-antimycotic mixture (Sigma, USA) and maintained at 37 °C in a humidified atmosphere of 5% CO_2. The medium was replaced every two days. At passage 7, cells were detached with trypsin/EDTA and counted in a hemacitometer for encapsulation.

The cells were encapsulated into CMX microcapsules using a novel in house micro-droplet generator[40] as illustrated in Figure III.2. A. In this system, an autoclavable tubing (Novosil, Fisher Scientific, USA) with 1 mm internal diameter was punctured with a blunt end needle in a vertical position and sealed with a silicone glue. This assembly can be autoclaved numerously and can be assembled with peristaltic pump (Ismatec, Switzerland) and syringe pump (Alladdin WPI,

England) as shown in Figure III.2.B. One end of the tubing was connected to an oil reservoir (Aldrich, Germany) and the other end to a glass collector where the droplets were cured in a crosslinker solution. A magnetic top stirring apparatus, made up of Teflon® with a magnet, was placed on the top of collector in order to stir solution without introducing a mechanical stress on the formed microcapsules. The operation rate of peristaltic and syringe pump was set at 0.35 mL/minute and 20 µL/min, respectively.
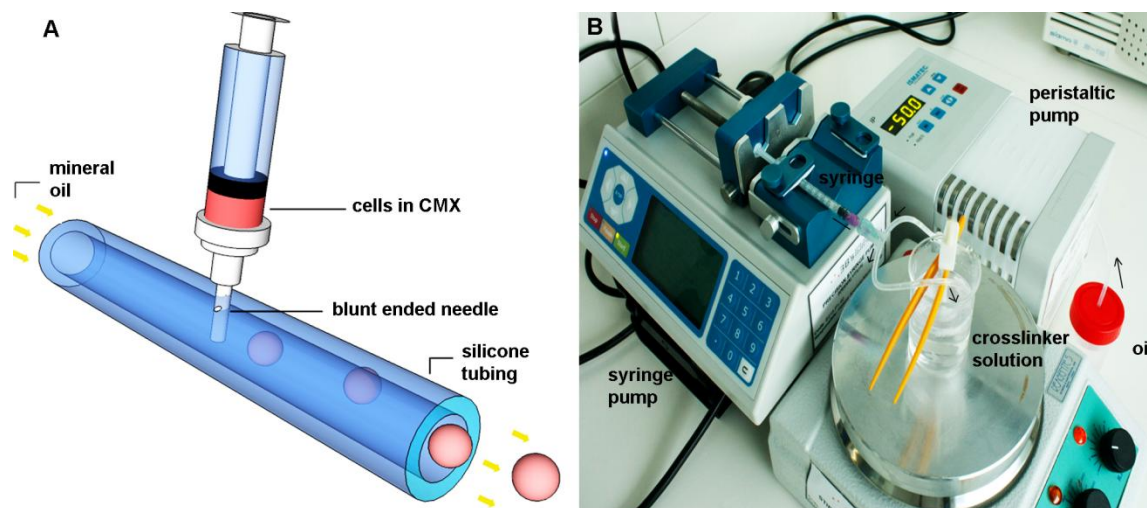
Figure III.2. (A) Schematic representation of the micro-droplet generator. (B) Photograph showing the apparatus used to produce the microcapsules

Prior to encapsulation, CMX powder (sterilized by autoclaving for 10 min at 121 $^{\circ}$C) was dissolved in DMEM (5 wt%) until obtaining a homogeneous solution. Subsequently, a cell suspension at cellular density of 10×10^6 cells/mL was mixed with aqueous CMX solution. The microdroplets generated by the device were fed into the crosslinker solution containing 1.5% $CaCl_2$ (Merck Chemical Co., Germany) and 0.9% NaCl (Carlo Erba, Italy) as shown in Figure III.2.B. The CMX capsules were stirred gently for 15 min and then washed with PBS (Sigma, USA) in order to remove traces of mineral oil. Afterwards, the collected microcapsules were transferred into a poly-L-lysine solution (0.1 wt%, 30-70 kDa) for 10 min in order to strengthen the outer surface of the microcapsules. Finally, the coated microcapsules were transferred to DMEM culture medium and cultured in a 24-well polystyrene plate, previously coated with agarose (4 wt% in PBS) to avoid the adhesion of non-encapsulated cells.

Alginate (alginic acid sodium salt from brown algae, average Mw 100 kDa, Fluka, Norway) was used to produce microcapsules to serve as controls. They were also produced following a procedure similar to the one described for CMX microcapsules. The alginate microcapsules

were successively coated with the poly-L-lysine (0.05 wt%) for 5 min. The encapsulated cells (n=3) were maintained *in vitro* culture for a period of 3 weeks in DMEM with media exchange every 2 days. Empty microcapsules were also maintained throughout the culture period to serve as controls.

Microcapsule Characterization

Light microscopy analysis

Microscopic observations of the encapsulated cells and controls were carried out over the course of the *in vitro* culture to examine the cell morphology and growth. A bright field light microscope (AXIOVERT 40 CFL, Zeiss, Germany) equipped with a digital camera (Canon Power shot G8, Japan) was used and images were acquired at 10x magnification.

Scanning Electron Microscopy (SEM) analysis

Prior to the SEM observations, the microcapsules were fixed with glutaraldehyde (Electron Microscopy Sciences, USA) solution (3% v/v in PBS) at 4 ºC for 1 h. The samples were further dehydrated in a graded ethanol series (20, 50, 60, 70, 80, 90 and 100%) followed by immersion in 100% hexamethyldisilazane (HMDS, Electron Microscopy Sciences, USA). Microcapsules were cut in half to expose the membrane cross-section and the internal surface of microcapsules. The specimens were mounted on aluminum stubs and sputter coated with Pt/Pd target (80/20) generating a thin film with 6 nm of thickness (208 HR High Resolution Sputter Coater, Cressington). The microcapsules were imaged on an ultra-high resolution field emission gun scanning electron microscope (FEG/SEM, FEI Nova 200 NanoSEM).

Cell viability and proliferation post-encapsulation

To investigate if the CMX microcapsules can support cell viability and proliferation, encapsulated cells were examined using several biochemical analyses. Viability of cells was assessed by fluorescence microscopy using a live/dead assay; the metabolic activity of the encapsulated cells was analyzed by the AlamarBlue® assay and cell proliferation evaluated by DNA quantification.

Live/dead cell assay

Calcein AM (Sigma, USA) solution (2/1000, v/v) was prepared in DMEM medium without FCS and phenol red. Propidium iodide (PI, Molecular Probes, Invitrogen, USA) solution was prepared by mixing 2 µL PI (1 mg/mL) with 20 µL (1 mg/mL) RNAse A (USB corporation, USA) and 2 mL PBS. The microcapsules with encapsulated cells and controls were collected from the culturing

plates and incubated with calcein-AM and propidium iodide solutions at 37 ºC for 10 min protected from light. Samples were then observed under fluorescent microscopy using an Axioplan Imager Z1m microscope (Zeiss, Germany).

Metabolic activity of encapsulated cells - AlamarBlue® assay

The metabolic activity of encapsulated cells over time was assessed using the AlamarBlue® assay (AbD Serotec,UK). AlamarBlue® was added (10% of the volume of the well) to each well containing the encapsulated cells and the plate was incubated at 37 ºC for 20 hours protected from light. After incubation, 100 µL of solution was taken from each well and placed in a 96 well plate. The absorbance was read at 570 and 600 nm on a microplate reader (BIO-TEK, SYNERGIE HT, USA). The percentage of reduced AlamarBlue® was calculated according the manufacturer instructions.

Cellular proliferation assay

ATDC5 proliferation within the capsules was determined using a fluorimetric dsDNA quantification kit (PicoGreen, Molecular Probes, Invitrogen, USA). For this purpose, the samples collected at days 1, 7, 14 and 21 were washed twice with sterile PBS (Sigma, USA) solution and transferred into 1.5 mL microtubes containing 1 mL of ultra-pure water. Capsules with and without cells were stored at -80 ºC until further analysis. Prior to DNA quantification, samples were thawed and broken by pipetting up and down using a syringe with a needle to cause material disruption and facilitate DNA extraction. 28.7 µL of each sample and standards (0-2 mg/mL) were transferred to an opaque 96 well plate. Then 71.3 µL of PicoGreen solution and 100 µL of Tris-EDTA buffer were added. Standards and samples were prepared in triplicate. The plate was incubated for 10 minutes in the dark and the fluorescence was measured using an excitation wavelength of 485 nm and emission of 528 nm. DNA amounts were calculated from the calibration curve.

Histology

Cell cultured microcapsules for histology were rinsed three times in PBS and then fixed in 3.7% formalin in PBS for 1 hour at room temperature. After fixation, samples were dehydrated in a graded ethanol series (70, 90, 95 and 100%) followed by immersion in xylene. Specimens were embedded in paraffin and cut in 4 µm-thick sections (MICROM HM355S Microtome, INOPAT USA). Sections were then dewaxed and stained with Harris Hematoxylin (Sigma, USA) and eosin (H&E staining).

Statistical analysis

Results of DNA quantification and cell viability are expressed as a mean ± standard deviation with *n*=3 for each group. Statistical significance of differences was determined using unpaired student's *t*-test multiple comparison procedure at a confidence level of 95 % ($p<0.05$).

3. RESULTS AND DISCUSSION

CMX Characterization

When designing materials for cell encapsulation, several properties should be considered. For instance, the amount and the character of functional groups contained in monomer units will influence the intermolecular interactions and consequently complex formation. Complexation is enhanced by the charge density in the polyanion, which depends on the chemical structure, the pKa of the polyelectrolyte, as well the pH of the solution. Xanthan by itself is able to form self-supporting gels in the presence of ions, although they are not stable in presence of aqueous solutions in the long term. For increasing gel stability, xanthan was carboxymethylated and its chemical composition was characterized in order to control capsule properties and performance in biological solutions. The chemical modification on xanthan was confirmed in FTIR spectra (Figure III.3.A) by the decrease of the C-O-H band intensity at 1425 cm^{-1} and O-H stretching at 3400 cm^{-1}.

In addition, the absorption band at 1616 cm^{-1}, attributed to C=O groups of pyruvate, was increased significantly after carboxymethylation, while the carbonyl peak, which is provided by the acetate at 1741 cm^{-1} in native xanthan, was not observed in CMX. This may indicate that the acetyl group was hydrolyzed by sodium hydroxide during carboxymethylation and consequently converted into carboxymethyl group.

Comparing the spectra of modified xanthans, CMX2 presents more evident changes than CMX1 when compared with native xanthan, indicating higher level of modification. To confirm this hypothesis, we determined the degree of substitution which was found to be higher for CMX2 (4.38) than for CMX1 (0.35) (Figure III.3.B). Due to the higher degree of substitution of CMX2 and its ability to form gels, we selected this carboxymethylated xanthan for subsequent encapsulation studies.
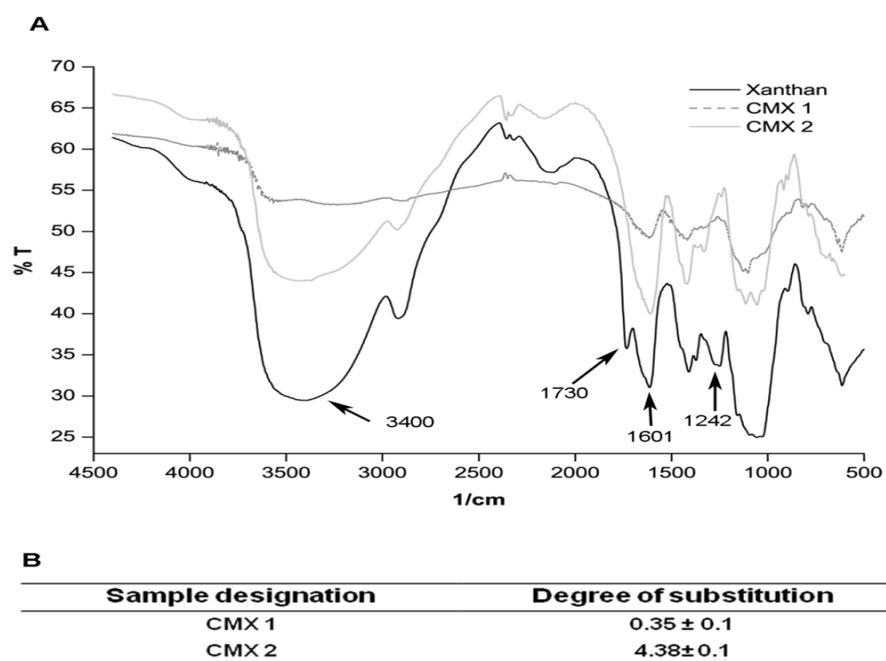
Figure III.3. (A) FTIR spectra of native xanthan and carboxymethylated xanthans with different degrees of modification (CMX1 and CMX2). (B) Degree of substitution obtained from acid-base titration.

Microcapsule preparation and encapsulation of cells

A simple microencapsulation process was developed by using a silicone tubing and blunt ended syringe needle which can be prepared in biology laboratories without need for advance techniques and skills which are required for preparation of microfluidic devices.

The size of microcapsules can be adjusted by using tubing at desired internal diameter that are commercially available in wide size range. The device can be sterilized by autoclaving and connected to pumps easily on aseptic conditions. The first step of microcapsule formation is the extrusion of the polymer solution through the micro-droplet generator which enables a homogenous size distribution. The microcapsules were then formed by crosslinking of generated droplets in a crosslinking solution while preserving physiological conditions for cells.

The morphology and microstructure of the microcapsules were analysed using scanning electron microscopy (Figure III.4).

Capsules with spherical shape and a diameter of 500 µm were obtained. At higher magnifications (Figure III.4.B,. C) the microcapsule external surface appears to be quite smooth. Their relatively small and uniform size (high surface to volume ratio) has been considered advantageous under a mass transport and immunological response perspectives [4,15-16,41]. At the

same time, capsules with rough surfaces should be avoided since they can elicit immunological reactions when implanted [15,41].
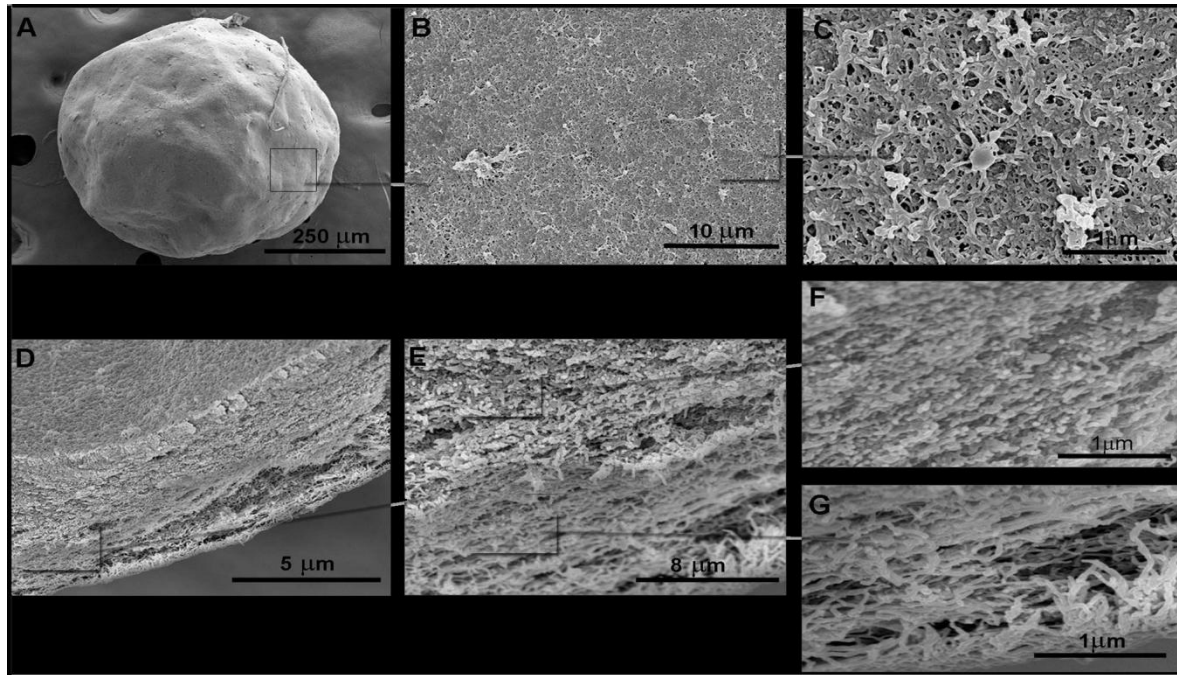
Figure III.4. SEM images showing the overall structure of CMX microcapsules (A), the microstructure of the microcapsule external surface (B, D) and cross-section of microcapsule membrane (D). (E) Zoom-in of (D) showing the interface between CMX and poly(L-lysine) complex (F, G) Magnified images revealing morphological details of CMX and poly(L-lysine) layers respectively.

SEM images of the microcapsule cross-sections (Figure III.4.D) reveal an amorphous membrane with thickness of about 5 µm and two layers with distinct morphologies. The magnified photos highlighted a fibrous structure which results in a porous matrix. The Image J software (NIH, USA) analysis showed that those structures have highly conserved dimension with the mean width of 35. 97 nm ± 6.3 (Figure III.4.C) and 29.89 ± 6.9 nm (Figure III.4.G) from capsule surface and cross sectioned area of microcapsule wall, respectively. This result may indicate that the complex formation between poly(L-lysine) and CMX might be affected by macromolecular tertiary structure of both biopolymers and as a result, reproducible tubular structures were formed. A successful capsule membrane for cell transplantation should allow rapid diffusion of nutrients, wastes, and important metabolic products. From those fibrous network structures it can be expected that the capsule wall can be quite permeable to nutrients and permit high viability conditions for encapsulated cells inside microcapsule. Moreover, it is expected that the permeability of the capsules can be controlled by changing the degree of modification of xanthan, the concentration and molecular weight of both polymers (xanthan and poly-L-lysine).

Cytotoxicity is an important criterion for any biomaterials used in tissue engineering. We analyzed the cytotoxicity of the CMX capsules over ATDC5 cells via MTS (3-(4,5-dimethylthiazol-2-yl)-2-(4-sulfophenyl)-2H-tetrazolium salt) assay (data not shown). Cells were exposed to the extracts from CMX capsules in contact with culture medium for 24, 48 and 72 h. Latex rubber extract and fresh complete culture medium were used respectively as negative and positive controls. The results showed that the CMX capsules do not cause any deleterious change in the metabolic activity of ATDC5 cells and consequently CMX capsules can be considered safe for cell encapsulation.

In vitro viability and proliferation of ATDC5 cells cultured within microcapsules

In vitro studies are necessary to ensure that CMX microcapsules did not cause cell death or inhibit cell proliferation. The morphology and viability of encapsulated cells were investigated after several days in culture (Figures III 5.A, .6.A).
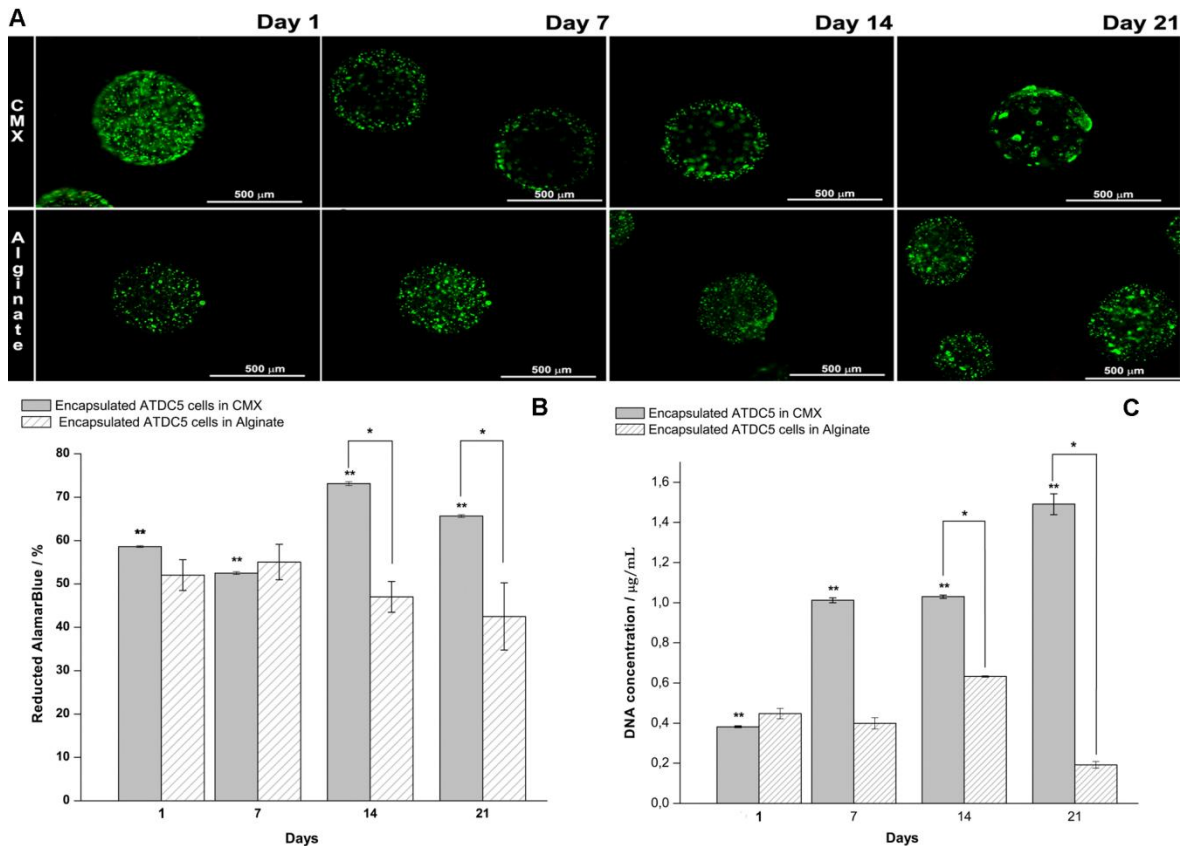
Figure III.5. *In vitro* viability and proliferation of ATDC5 cells cultured in CMX and alginate microcapsules. (A) Fluorescence microscopy images displaying the live/dead assay of encapsulated cells (green cells are live, red cells are dead) showing that the cells remain viable in the microcapsules up to 21 days of culture. (B) Metabolic activity and (C) proliferation of encapsulated cells determined by AlamarBlue® assay and DNA quantification. Results are expressed as means ± standard deviation with n=3. *Indicates a significant difference (p< 0.05) between CMX and alginate microcapsules for different time points. ** indicates significant difference (p< 0.05) between different time points for CMX microcapsules.

Cells formed small aggregates with strong green fluorescence observed inside the capsule (Figures III.5.A), demonstrating high viability of ATDC5 cells post-encapsulation. Furthermore, an even cell distribution can be observed throughout the culturing time (Figures III.5.A, .6.A) in alginate and CMX microcapsules, but in the latest times (14 and 21 days), ATDC5 cells encapsulated in CMX showed their tendency to form cellular aggregates (Figures III.5.A) demonstrating a potential chondrogenic phenotypic behaviour. Scanning electron microscopy also revealed the formation of cell aggregation inside the capsules (Figure III.7.D-E).

The metabolic activity of ATDC5 cells was investigated throughout the culturing period using AlamarBlue® assay (Figure III.5.B). The results showed that ATDC5 cells encapsulated in CMX matrix were able to reduce AlamarBlue® over the 21 days of *in vitro* culture (Figure III.5.B). Except for day 7, the cells encapsulated in the CMX microcapsules showed higher metabolic activity than the cells within alginate microcapsules. Although at the day 1 and 7 this difference was not significant ($p>0.05$), it was rather significant ($p<0.05$) for the latest time points (14 and 21 days).

To support the results provided from AlamarBlue® assay, cell proliferation was investigated by DNA quantification. DNA quantification (Figure III.5.C) revealed a steady and significant ($p<0.05$) increase in the DNA amounts with culturing time as a result of improved cellular proliferation in CMX microcapsules. When compared to the DNA values for cells encapsulated in alginate, significantly higher cellularity was observed ($p<0.05$) for CMX microcapsules in the latest days. It should be noted that at days 1 and 7, no statistical difference was observed between the cellularity level in both materials ($p>0.05$). A common limitation of polyelectrolyte complexes is lack of permeability to larger molecules, such as proteins, because these systems are normally characterized by a dense membrane structure [42]. The ATDC5 cells remained viable within microcapsules for up to 3 weeks in culture. The CMX microcapsules could therefore provide sufficient nutrient diffusion necessary for cell survival and proliferation.

ATDC5 is a very well established cell line known to be an excellent *in vitro* chondrogenic model for determining events during chondrogenesis [33-37]. Cell-matrix interactions during chondrogenesis are promoted by the three-dimensional (3D) environment [34]. In CMX microcapsules, ATDC5 cells retained their tendency to form cellular aggregates and they expressed higher metabolic activity than in alginate capsules used in our study.

H&E staining of cells encapsulated in the CMX microcapsules (Figure III.6.B) revealed that ATDC5 cells retained their rounded morphology throughout the culture and tend to form

cartilage nodule-like aggregates after 21 days of culture in the CMX microcapsules. This fact denotes that CMX microcapsules promoted the retention of the chondrocytic phenotype.
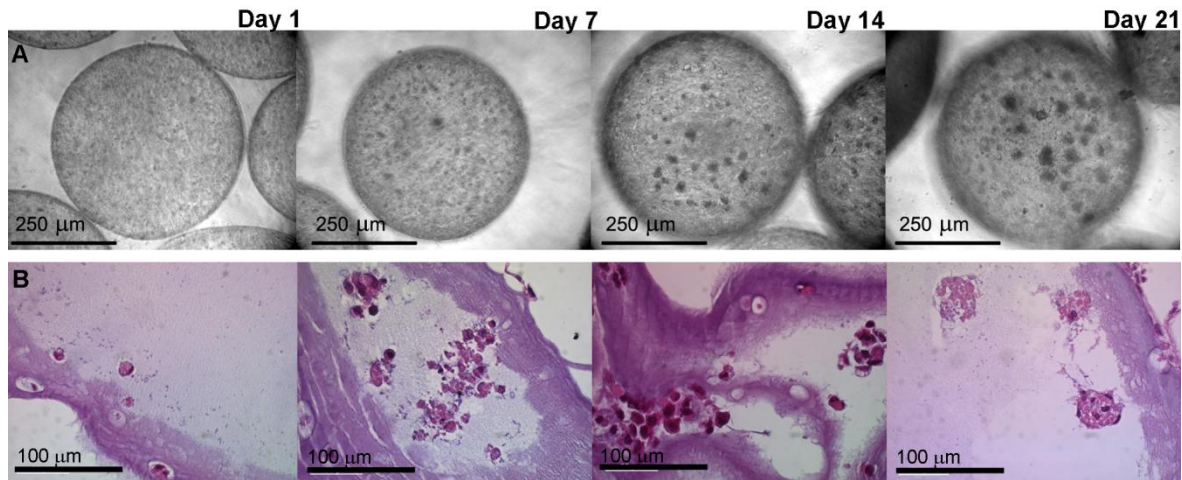
Figure III.6. Bright field light microscopy images of living cells encapsulated in CMX microcapsules (A) and microcapsule sections stained with H&E (B) after different culturing times.

SEM analysis on cell cultured microcapsules revealed that the cells attached on the internal microcapsule surface, interact with the surrounding matrix by their extended filopodias (Figure III.7.B, E) and tend to form small aggregates over 21 days (Figure III.7.D-E).
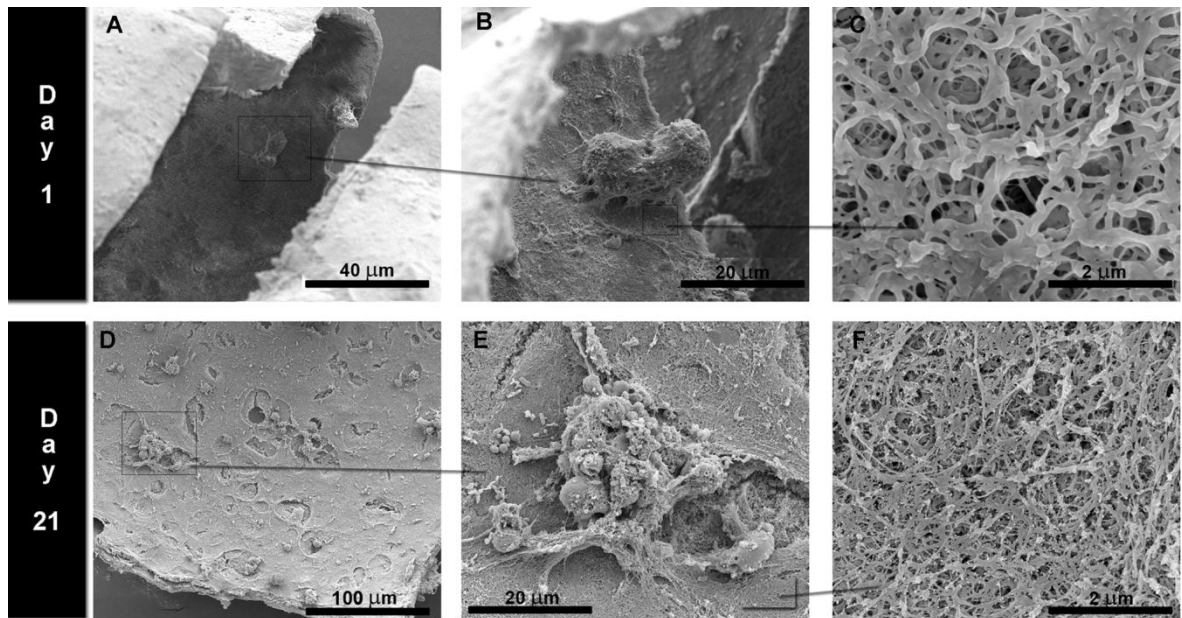
Figure III.7. SEM images showing the interior of the CMX microcapsules after 1 and 21 days of culture. (A, B) Morphological characteristics of the cells attached to the microcapsule inner surface. (D, E) Cell aggregates formed after 21 days of culture. (C, F) Microstructure of the microcapsule inner surface showing highly porous structure (F).

We speculate that the presence of ATDC5 cells and aggregates on the capsule wall may be a result of higher nutrient availability in these regions, since it is expected a better diffusion of nutrients near the capsule wall surface. At higher magnification, SEM image (Figure III.7.F) shows a fibrillar microstructure typical of natural ECM. Such fibrillar structure may offer additional advantages, when compared to the dense structure of other systems used for producing capsules, as it might allow a better control over capsule permeability.

In the current work, we have used a standard cell line to evaluate the ability of CMX microcapsules to support cell viability and proliferation. Given these encouraging preliminary results, we are undertaking encapsulation experiments with human articular chondrocytes in carboxymethyl xanthan to be applied as cell-based therapies in cartilage tissue engineering approaches.

4.CONCLUSIONS

This study presents a novel process that utilizes a micro-droplet generator to prepare microcapsules using the xanthan gum polysaccharide. The optimized process conditions enabled generating microcapsules with long-term stability and the encapsulation of a chondrocytic cell line. Encapsulated cells showed high viability (the cells survive in culture for at least three weeks) and retained the property of forming cell aggregates. In conclusion, our studies suggest that carboxymethyl xanthan can be an alternative to the current cell encapsulating materials, but *in vivo* studies are necessary to confirm our hypothesis. Nonetheless, CMX microcapsules may offer significant potential for long term cell culture in bioreactors for applications in cell therapies.

AKNOWLEDGEMENTS

REFERENCES

1.   Bhatia SR, Khattak SF, Roberts SC. Polyelectrolytes for cell encapsulation. Current Opinion in Colloid & Interface Science 2005;10(1-2):45-51.

2.   Maria-Engler SS, Mares-Guia M, Correa MLC, Oliveira EMC, Aita CAM, Krogh K, Genzini T, Miranda MP, Ribeiro M, Vilela L and others. Microencapsulation and tissue engineering as an alternative treatment of diabetes. Brazilian Journal of Medical and Biological Research 2001;34(6):691-697.

3.   Lim F, Sun AM. Microencapsulated islets as bioartificial endocrine pancreas. Science 1980;210(4472):908-910.

4.   Wilson JT, Chaikof EL. Challenges and emerging technologies in the immunoisolation of cells and tissues. Advanced Drug Delivery Reviews 2008;60(2):124-145.

5.   Orive G, Gascón AR, Hernández RM, Igartua M, Luis Pedraz J. Cell microencapsulation technology for biomedical purposes: novel insights and challenges. Trends in Pharmacological Sciences 2003;24(5):207-210.

6.   de Vos P, Bucko M, Gemeiner P, Navrátil M, Svitel J, Faas M, Strand BL, Skjak-Braek G, Morch YA, Vikartovská A and others. Multiscale requirements for bioencapsulation in medicine and biotechnology. Biomaterials 2009;30(13):2559-2570.

7.   Raschip IE, Yakimets I, Martin CP, Paes SS, Vasile C, Mitchell JR. Effect of water content on thermal and dynamic mechanical properties of xanthan powder: A comparison between standard and novel techniques. Powder Technology 2008;182(3):436-443.

8.   Wang N, Adams G, Buttery L, Falcone FH, Stolnik S. Alginate encapsulation technology supports embryonic stem cells differentiation into insulin-producing cells. Journal of Biotechnology 2009;144(4):304-312.

9.   Mo X-t, Guo S-c, Xie H-q, Deng L, Zhi W, Xiang Z, Li X-q, Yang Z-m. Variations in the ratios of co-cultured mesenchymal stem cells and chondrocytes regulate the expression of cartilaginous and osseous phenotype in alginate constructs. Bone 2009;45(1):42-51.

10.   Hsiao-Li M, Shih-Chieh H, Shan-Yang L, Yuh-Lien C, Wai-Hee L. Chondrogenesis of human mesenchymal stem cells encapsulated in alginate beads. Journal of Biomedical Materials Research 2003;64A(2):273-281.

11.   Hunziker EB. Articular cartilage repair: basic science and clinical progress. A review of the current status and prospects. Osteoarthritis and Cartilage 2002;10(6):432-463.

12.   Fan J, Gong Y, Ren L, Varshney RR, Cai D, Wang D-A. In vitro engineered cartilage using synovium-derived mesenchymal stem cells with injectable gellan hydrogels. Acta Biomaterialia;In Press, Corrected Proof.

13. Peter B, Meng D, Denis C, Michael G, Klaus-Peter G, Stefan F. Pellet culture elicits superior chondrogenic redifferentiation than alginate-based systems. Biotechnology Progress 2009;25(4):1146-1152.

14. Park H, Temenoff JS, Holland TA, Tabata Y, Mikos AG. Delivery of TGF-[beta]1 and chondrocytes via injectable, biodegradable hydrogels for cartilage tissue engineering applications. Biomaterials 2005;26(34):7095-7103.

15. Murua A, Portero A, Orive G, Hernández RM, de Castro M, Pedraz JL. Cell microencapsulation technology: Towards clinical application. Journal of Controlled Release 2008;132(2):76-83.

16. Uludag H, De Vos P, Tresco PA. Technology of mammalian cell encapsulation. Advanced Drug Delivery Reviews 2000;42(1-2):29-64.

17. Murua A, Orive G, Hernández RM, Pedraz JL. Xenogeneic transplantation of erythropoietin-secreting cells immobilized in microcapsules using transient immunosuppression. Journal of Controlled Release 2009;137(3):174-178.

18. Chang TMS. Therapeutic applications of polymeric artificial cells. Nature Reviews Drug Discovery 2005;4(3):221-235.

19. Pereira RC, Scaranari M, Castagnola P, Grandizio M, Azevedo HS, Reis RL, Cancedda R, Gentili C. Novel injectable gel (system) as a vehicle for human articular chondrocytes in cartilage tissue regeneration. Journal of Tissue Engineering and Regenerative Medicine 2009;3(2):97-106.

20. Benya PD, Shaffer JD. Dedifferentiated chondrocytes reexpress the differentiated collagen phenotype when cultured in agarose gels. Cell 1982;30(1):215-224.

21. Stevens MM, Qanadilo HF, Langer R, Prasad Shastri V. A rapid-curing alginate gel system: utility in periosteum-derived cartilage tissue engineering. Biomaterials 2004;25(5):887-894.

22. Francois L, Nathalie S, Caroline Le G, Sylvie D, Monique A. Dedifferentiated chondrocytes cultured in alginate beads: Restoration of the differentiated phenotype and of the metabolic responses to Interleukin-1&bgr. Journal of Cellular Physiology 1998;176(2):303-313.

23. Tare RS, Townsend PA, Packham GK, Inglis S, Oreffo ROC. Bcl-2-associated athanogene-1 (BAG-1): A transcriptional regulator mediating chondrocyte survival and differentiation during endochondral ossification. Bone 2008;42(1):113-128.

24. Vos PD, Haan BJD, Wolters GHJ, Strubbe JH, Schilfgaarde RV. Improved biocompatibility but limited graft survival after purification of alginate for microencapsulation of pancreatic islets. Diabetologia 1997;40(3):262-270.

25. Katzbauer B. Properties and applications of xanthan gum. Polymer Degradation and Stability 1998;59(1-3):81-84.

26. García-Ochoa F, Santos VE, Casas JA, Gómez E. Xanthan gum: production, recovery, and properties. Biotechnology Advances 2000;18(7):549-579.

27. Schorsch C, Garnier C, Doublier J-L. Microscopy of xanthan/galactomannan mixtures. Carbohydrate Polymers 1995;28(4):319-323.

28. Hamcerencu M, Desbrieres J, Popa M, Khoukh A, Riess G. New unsaturated derivatives of Xanthan gum: Synthesis and characterization. Polymer 2007;48(7):1921-1929.

29. Capron I, Brigand G, Muller G. About the native and renatured conformation of xanthan exopolysaccharide. Polymer 1997;38(21):5289-5295.

30. Rodd AB, Dunstan DE, Boger DV. Characterisation of xanthan gum solutions using dynamic light scattering and rheology. Carbohydrate Polymers 2000;42(2):159-174.

31. Oliveira JT, Santos TC, Martins L, Silva MA, Marques AP, Castro AG, Neves NM, Reis RL. Performance of new gellan gum hydrogels combined with human articular chondrocytes for cartilage regeneration when subcutaneously implanted in nude mice. Journal of Tissue Engineering and Regenerative Medicine 2009;3(7):493-500.

32. Mendes AC, Baran ET, Nunes C, Coimbra MA, Azevedo HS, Reis RL. Palmitoylation of xanthan polysaccharide for self-assembly microcapsule formation and encapsulation of cells in physiological conditions. Soft Matter 2011;7(20):96-47.

33. Shukunami C, Shigeno C, Atsumi T, Ishizeki K, Suzuki F, Hiraki Y. Chondrogenic differentiation of clonal mouse embryonic cell line ATDC5 in vitro: differentiation-dependent gene expression of parathyroid hormone (PTH)/PTH-related peptide receptor. J. Cell Biol. 1996;133(2):457-468.

34. Tare RS, Howard D, Pound JC, Roach HI, Oreffo ROC. Tissue engineering strategies for cartilage generation--Micromass and three dimensional cultures using human chondrocytes and a continuous cell line. Biochemical and Biophysical Research Communications 2005;333(2):609-621.

35. Atsumi T, Ikawa Y, Miwa Y, Kimata K. A chondrogenic cell line derived from a differentiating culture of AT805 teratocarcinoma cells. Cell Differentiation and Development 1990;30(2):109-116.

36. Akiyama H, Shukunami C, Nakamura T, Hiraki Y. Differential Expressions of BMP Family Genes during Chondrogenic Differentiation of Mouse ATDC5 Cells. Cell Structure and Function 2000;25(3):195-204.

37. Phornphutkul C, Wu K-Y, Yang X, Chen Q, Gruppuso PA. Insulin-like growth factor-I signaling is modified during chondrocyte differentiation. J Endocrinol 2004;183(3):477-486.

38. Chen X-G, Park H-J. Chemical characteristics of O-carboxymethyl chitosans related to the preparation conditions. Carbohydrate Polymers 2003;53(4):355-359.

39. Ge H-C, Luo D-K. Preparation of carboxymethyl chitosan in aqueous solution under microwave irradiation. Carbohydrate Research 2005;340(7):1351-1356.

40. Baran ET, Mendes AC, Azevedo HS, Reis RL; DISPOSITIVO, MÉTODO E SISTEMA DE FABRICO DE MICROCÁPSULAS. Portugal. 2011.

41. Ghidoni I, Chlapanidas T, Bucco M, Crovato F, Marazzi M, Vigo D, Torre M, Faustini M. Alginate cell encapsulation: new advances in reproduction and cartilage regenerative medicine. Cytotechnology 2008;58(1):49-56.

42. Ohkawa K, Kitagawa T, Yamamoto H. Preparation and Characterization of Chitosan-Gellan Hybrid Capsules Formed by Self-Assembly at an Aqueous Solution Interface. Macromolecular Materials and Engineering 2004;289(1):33-40.

Chapter IV

PALMITOYLATION OF XANTHAN POLYSSACCHARIDE FOR SELF-ASSEMBLY MICROCAPSULE FORMATION AND ENCAPSULATION OF CELLS IN PHYSIOLOGICAL CONDITIONS

PALMITOYLATION OF XANTHAN POLYSSACCHARIDE FOR SELF-ASSEMBLY MICROCAPSULE FORMATION AND ENCAPSULATION OF CELLS IN PHYSIOLOGICAL CONDITIONS

ABSTRACT

Hydrophobized polysaccharides have emerged as a promising strategy in biomedical field due to the versatility to design functional structures through the spontaneous self-assembly in cell-friendly conditions. Based on this concept, xanthan, a bacterial extracellular polysaccharide with potential as encapsulating matrix, was conjugated with hydrophobic palmitoyl groups to obtain an amphiphilic system able to form capsules by self-assembly processes. The conjugation of xanthan was performed at different xanthan/palmitoyl chloride ratios and Fourier transformed infra red, ^{1}H nuclear magnetic resonance spectroscopies, as well as wide angle X-ray diffraction, differential scanning calorimetry were performed to characterize the obtained conjugates. The results showed that the increase of the hydrophobic reactant promoted higher hydrophobic interaction and consequently higher molecular organization. At certain palmitoyl concentrations and through a proper balance between charge repulsion and hydrophobic interaction, the amphiphilic molecules showed to self-assemble into stable capsular hollow structures in the presence of physiological ion concentration and pH. Poly-l-lysine coated microcapsules with an average diameter of 450 μm and homogenous size distribution were obtained. The morphology revealed by scanning electron microscopy showed microcapsules with two distinct layers. The ability of Palmitoyl-Xanthan microcapsules to sustain viability and proliferation of encapsulated cells was confirmed by AlamarBlue and DNA assays. These findings suggest the application of Palmitoyl-Xanthan microcapsules as a potential material for cell encapsulation in cell-based therapies.

1. INTRODUCTION

Supramolecular chemistry makes use of non-covalent interactions to achieve the controlled assembly of molecular segments, providing a versatile tool for the spontaneous organization of molecules into stable and functional structures [1-2]. Self-assembly can occur through a change in temperature, pH or ion concentration or triggered by radiation [3]. Self-assembled structures can mimic aspects of biological systems such as artificial cell membranes, enzymes, channels which makes this methodology suitable to be applied for bottom-up fabrication of new biomaterial systems that can be used as artificial matrices for cell culture.

Hydrophobized polysaccharides have been extensively studied in biomedical field due to their capability to spontaneously self-assemble in water into functional nanostructures (bilayer membranes, micelles, tubes and vesicles) [4-8]. In general, such hydrophobized polymers consist of a water-soluble main chain, the polysaccharide, carrying a small number of hydrophobic groups. The polysaccharide backbone, presents numerous favorable characteristics such as biodegradability, low toxicity and abundance of functional groups for further modification. The amphiphilic nature imparted after hydrophobic modification gives them the possibility to be used in a wide range of applications such as emulsion stabilizers, surface modifiers for liposomes and nanoparticles [9-10] and as drug delivery vehicles [11-12].

Xanthan gum (Figure IV.1.A). is an anionic extracellular bacterial polysaccharide with the ability to organize into liquid crystaline phases at specific conditions [13-17] providing an anysotropic nature as a result of the helical structure. This biopolymer was shown to be biocompatible [17], biodegradable and exhibits gel-like properties, being widely used in food, cosmetic and pharmaceutical industries because of the encouraging reports on safety [15]. Recently, Mendes and co-workers [18] have reported the potential of this biopolymer as cell encapsulation matrix. They demonstrated that stable xanthan microcapsules were generated and encapsulated cells remained viable and were observed to proliferate for prolonged culture periods.

Herein, we present the synthesis of an amphiphilic polysaccharide, in which palmitoyl groups are attached to an anionic polysaccharide chain (xanthan gum) and demonstrate that the amphiphilic polysaccharide (palmitoyl xanthan) is able to self-assemble into capsules in saline solutions. The properties and performance of palmitoyl xanthan microcapsules were studied by exploiting the balance between the hydrophobic and ionic interactions. A second aim of this study was to evaluate the ability of these self-assembled matrices to support the viability, function, and proliferation of encapsulated cells.
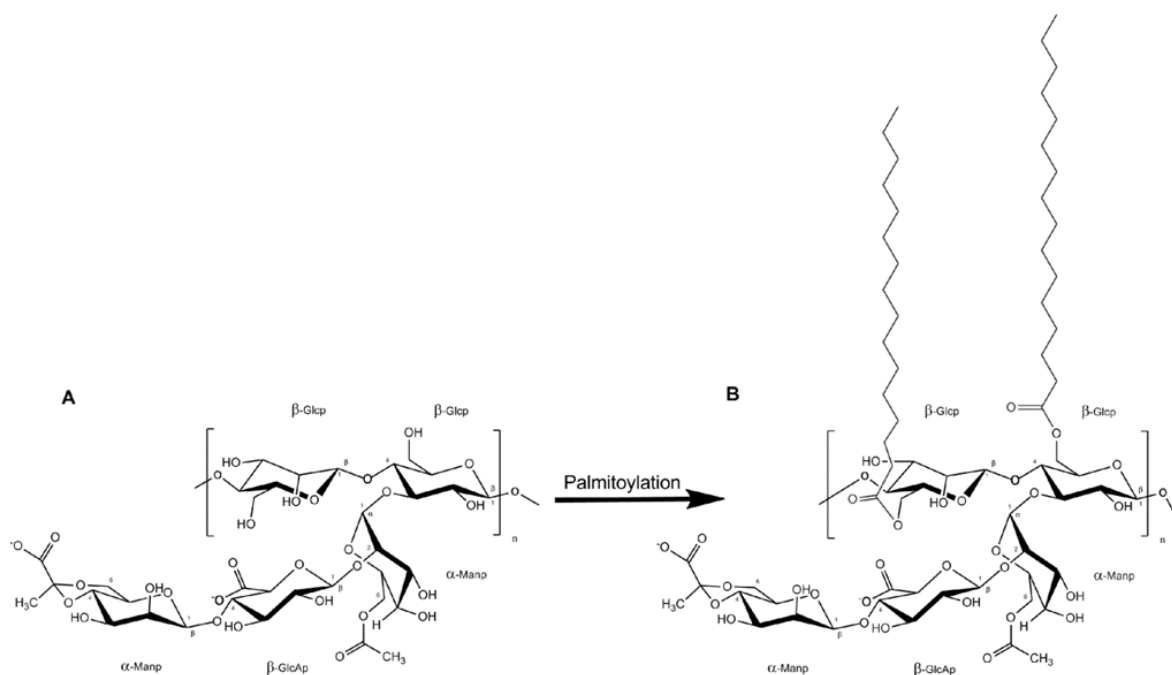
Figure IV.1. Chemical structure of xanthan repeating unit (A) and palmitoyl xanthan (B)

2. MATERIALS AND METHODS

Materials

All chemicals, including xanthan gum from *Xanthomonas campestris*, palmitoyl chloride and poly-l-ysine (PLL), were obtained from Sigma/Aldrich unless otherwise indicated. The chemicals were used as received. Characterization of native xanthan (elemental composition, degree of acetylation, molecular weight and monosaccharide content) is reported on experimental section of this thesis.

Preparation of palmitoyl xanthan (PX)

Xanthan was dissolved in distilled water (1 wt%) at room temperature in a round-bottom glass flask. The polymer solution was placed in an ice-water bath and vigorously stirred using a mechanical stirrer (IKA, Germany). Palmitoyl chloride was then added dropwise at different ratios as shown in Table IV.I. The reaction mixture was allowed to stand at room temperature under continuous stirring for 23 h. The reaction was stopped by the addition of excess of cold ethanol and filtered. The final product was dried at room temperature until constant mass.

Table IV.1. Sample designation for each palmitoyl xanthan conjugate.

Sample designation	Xanthan (mmol)	Palmitoyl chloride (mmol)	Xanthan/Palmitoyl chloride ratio (w/w)
PX(X=0.50P)	0.58	1.18	**0.50**
PX(X=0.75P)	0.58	0.78	**0.75**
PX(X=1.40P)	0.58	0.42	**1.40**
PX(X=1.70P)	**0.58**	**0.35**	1.70

Characterization of PX

Solubility

The solubility of each Palmitoyl-Xanthan conjugate was assessed in organic solvents by placing 10 mg of PX in 4 mL of each solvent. The suspension solution was mixed by vortex and placed in a water bath at 37 ºC overnight. Solubility was examined visually for any undissolved solute particles [19].

Fourier transform infrared (FTIR) spectroscopy.

The chemical modification of xanthan with palmitoyl was analysed by infrared spectroscopy. Prior to analysis, potassium bromide pellets were prepared by mixing the native xanthan and PXs powder with potassium bromide (KBr, PIKE Techonologies, USA) at 1/10 (wt/wt) PX/KBr ratio. The spectra were acquired on an IR Prestige-21 (SHIMADZU, Japan) spectrophotometer with the average of 32 scans and a resolution of 4 cm^{-1}.

^{1}H Nuclear magnetic resonance (NMR) spectroscopy

Samples containing different ratios of xanthan/palmitoyl chloride were dissolved at a concentration of 1 wt% in deuterated dimethylsulfoxide (d-DMSO). Fully relaxed ^{1}H NMR spectra were acquired in a Varian Unity Plus 300 MHz spectrometer.

Wide angle x-ray scattering (WAXS)

The PX conjugates were characterized by WAXS technique to verify any molecular orientation. WAXS measurements were performed using a Bruker AXS NanoStar with a HiStar 2D detector with scattering angles from 5 to 60 º.

Differential scanning calorimetry (DSC)

DSC analysis of PX conjugates were performed in a calorimeter (TA instruments, USA) with a heating program of 10 °C min^{-1} from 10 to 200 °C under nitrogen at flow of 20 cm^3.min^{-1}.

Circular dichroism (CD)

CD was used to study the effects of palmitoylation on the secondary structure of native xanthan. PX(X=1.7P) and native xanthan were dissolved in ultrapure water overnight at concentration of 0.1 wt%. The measurements were performed in a Stopped-flow circular dichroism spectropolarimeter (PiStar-180, Applied Photophysics, UK) at 25 °C using Quartz cells with a 0.1 cm path length. The spectra were recorded from 300 to 180 nm with a scan rate of 100 nm/min and are an average of five accumulations.

Dynamic light scattering (DLS) and zeta potential measurements

DLS and zeta potential measurements were performed using a Zetasizer NanoZS Instrument (ZEN 3600, Malvern Instruments, Worcestershire, UK). Prior the analyses, PX(X=1.7P) and xanthan solutions were prepared at concentration of 0.1 wt% and their pH was adjusted to 5, 6, 7 and 8 using 0.1 M HCl, and 0.1 M NH$_3$OH). The solutions were filtered using a pyrogen free 0.45 μm disposable membrane filter (Schleicher and Schuell Bioscience, Germany)**.**

Scanning transmission electron microscopy (STEM)

TEM samples of xanthan (control) and water-soluble PX conjugate were prepared by placing one drop of the polymer solution and (0.1 wt%) onto a 300-mesh copper grid coated with carbon film, followed by 1% (w/v) of uranyl acetate (Electron Microscopy Sciences) staining for 3 min. The samples were analyzed and photographed using a Hitachi Su electron microscope in S-TEM mode.

Microcapsule formation by self assembly and characterization

To study the capability of the palmitoyl-xanthan conjugates to form suitable capsules for cell encapsulation, we have selected PX(X=1.7P) conjugate having into account its solubility in aqueous solutions. Various concentrations of PX(X=1.7P) solutions (1-3%) were tested for microcapsule preparation. 1% solution provided smooth and spherical microcapsules and this concentration was further used in the subsequent studies. PX(X=1.7P) was dissolved in HEPES buffer solution (55 mM, pH 7.4, Sigma) supplemented with 0.1 M CaCl$_2$ at concentration of 1 wt% and further sterilized by UV light for 20 min in a laminar flow cabinet. Capsules were formed by extrusion of the polymer solution from a disposable plastic syringe with a 2.5 G diameter needle into a flask containing PBS.

Microcapsule morphology: scanning electron microscopy (SEM)

Previous to SEM observation, the capsules were fixed subsequently for 1 h with formaline 3.7% and 3% v/v of glutaraldehyde (Electron Microscopy Sciences) in PBS. The samples were further dehydrated in graded ethanol series (20, 50, 60, 70, 80, 90 and 100%) followed by immersion in 100% hexamethyldisilazane (HMDS, Electron Microscopy Sciences). The specimens were transferred and mounted on aluminum stubs and allowed to dry at room temperature. Microcapsules were cut in half to expose the membrane cross-section and the internal surface of microcapsules. Prior to observation, they were sputter coated with Pt/Pd target (80/20) generating a thin film with 6 nm of thickness (208 HR High Resolution Sputter Coater, Cressington). The microcapsules were imaged on an ultra-high resolution field emission gun scanning electron microscope (FEG/SEM, FEI Nova 200 NanoSEM).

Cell encapsulation and culture

To validate the utility of PX as cell encapsulating matrix, we carried out cell culture studies within the PX microcapsules. The murine ATDC5 chondrocyte cells were cultured in basic medium, consisted of Dulbecoo's Modified Eagle's Medium (DMEM, Sigma-Aldrich) with phenol red, supplemented with 10% fetal calf serum (FCS, Biochrom AG), 5 mM L-Glutamine (Sigma) and 1% of antibiotic-antimycotic mixture (Sigma) and maintained at 37 °C in a humidified atmosphere of 5% CO_2. The medium was replaced every two days. At passage 9, cells were detached with trypsin/EDTA and counted in a hemacytometer for encapsulation. A cell suspension ($5x10^6$ cells/ml, 0,5 ml) was mixed with PX(X=1.7P) solution (1.5 ml, 1 wt% final concentration). The cells were encapsulated into the PX(X=1.7P) matrix using a novel micro-droplet generator developed in our group as previously reported [18,20] (Figure IV.2.).

Briefly, an autoclavable tubing (Novosil, Fisher Scientific) with 1 mm internal diameter was punctured with a blunt end needle (12 G) in a vertical position and sealed with a silicone glue. This assembly was then connected to a peristaltic pump (Ismatec, Switzerland) for perfusion of mineral oil and syringe pump (Alladdin WPI, England) for gel-cell injection in a sterile laminar flow cabinet. One end of tubing was connected to an oil reservoir and the other end to a glass collector, where the micro droplets of gels can be self assembled in a PBS solution. The operation rate of peristaltic and syringe pump was set at 0.35 ml/minute and 0.50µl/min, respectively. The microcapsules were stirred in collection vessel for 15 min and then transferred into 0.1 wt% poly-L-lysine solution and stirred for 10 min. The coated microcapsules were transferred into tissue culture wells with DMEM and cultured in standard conditions (37 ºC and 5% CO_2) for 1, 7, 14 and 21 days. The medium was exchanged every 2 days.
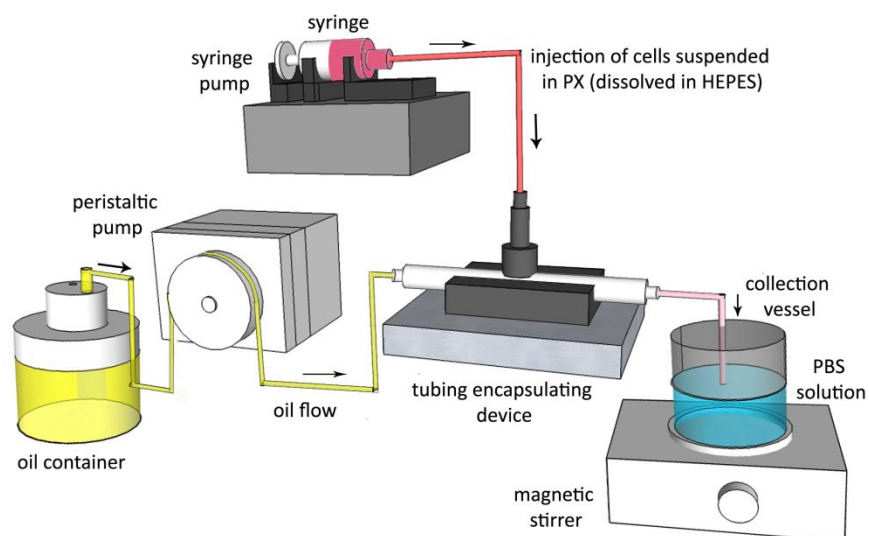
Figure IV.2. Schematic of the set-up for cell encapsulation showing details of the micro-droplet generator. A solution of palmitoyl xanthan, with or without cells, was injected into a stream of mineral oil resulting in the formation of spherical droplets and a water-in-oil emulsion due to the immiscibility of the two phases. The polymer microdroplets in oil were then carried into a gelling inducer solution (phosphate buffer solution, PBS). In PBS, the palmitoyl xanthan droplets self-assemble into capsular gel structure. The hollow capsules were then collected and treated with poly-L-lysine to strengthen the outer surface of the microcapsules.

Cell viability - live/dead cell assay

Calcein AM (Sigma) solution (2/1000, v/v) was prepared in DMEM medium without FCS and phenol red. Propidium iodide (PI, Molecular Probes, Invitrogen) solution was prepared by mixing 2 µL PI (1 mg/mL) with 20 µL (1 mg/mL) RNAse A (USB corporation) and 2 mL PBS. The microcapsules with encapsulated cells and controls (without cells) were collected from the culturing plates and incubated with calcein-AM and propidium iodide solutions at 37 ℃ for 10 min protected from light. Microcapsules were then observed under fluorescent microscopy using an Axio (Zeiss HAL 100/HBO 100; Axiocam MRc5 (Zeiss).

Metabolic activity of encapsulated cells - AlamarBlue® assay

The metabolic activity of encapsulated cells over time was assessed using the AlamarBlue® assay (AbD Serotec). AlamarBlue® was added (10% of the volume of the well) to each well containing the encapsulated cells and the plate was incubated at 37 ℃ for 20 hours protected from light. After incubation, aliquots were taken and transferred to a 96-well plate and the absorbance was measured at 570 and 600 nm on a microplate reader (BIO-TEK, Sʏɴᴇʀɢɪᴇ HT,

USA). The percentage of reduced AlamarBlue® was calculated according the manufacturer instructions.

Cellular proliferation assay – DNA quantification

ATDC5 proliferation within the capsules was determined using a fluorimetric DNA quantification kit (PicoGreen, Molecular Probes, Invitrogen). For this purpose, the samples collected at days 1, 7, 14 and 21 were washed twice with sterile PBS (Sigma, USA) solution and placed in 1 mL of ultra-pure water. Capsules with and without cells were stored at -80 ºC until further analysis. Prior to DNA quantification, samples were thawed and broken by pipetting up and down using a syringe with a needle to cause material disruption and facilitate DNA extraction. 28.7 µL aliquots and standards (0-2 mg/mL) were transferred to an opaque 96 well plate. Then 71.3 µL of PicoGreen solution and 100 µL of Tris-EDTA buffer were added. Standards and samples were prepared in triplicate. The plate was incubated for 10 minutes in the dark and the fluorescence was measured using an excitation wavelength of 485 nm and emission of 528 nm. DNA amounts were calculated from the calibration curve.

Statistical analysis

The results of DNA quantification and cell viability are expressed as a mean ± standard deviation with n=3 for each group. Statistical significance of differences was determined using unpaired student's t-test multiple comparison procedure at a confidence level of 95 % (p<0.05).

3. RESULTS AND DISCUSSION

The synthesis of palmitoyl xanthan was accomplished in a single-step reaction (Figure IV.1.). Hydrohobically-modified xanthans were prepared with different hydrophobic modification ratio (Table IV.I.).

Solubility analysis

The solubility of the palmitoyl/xanthan conjugates was tested in polar protic and aprotic solvents (Table IV.II.). PX(X=1.7P) Palmitoyl xanthan is the only conjugate that showed solubility in water which is a basic requirement for cell encapsulation in aqueous physiological buffer solutions. As shown in Table IV.2., all the PXs conjugates are soluble in DMSO, but PX(X=1.4P) and PX(X=1.7P) are also soluble in THF and PX(X=0.75P) also dissolves in DCM.

The conjugates soluble in organic solvents could be further used as biomaterials, in particular for the production of nano- and microparticles by using an emulsion and solvent

extraction/evaporation methods. In our study, however, the PX(X=1.7P) conjugate was selected as suitable conjugate for microencapsulation of mammalian cells as it provides an amphiphilic and self-assembly property in physiological pH and ionic strength.

Table IV 2. Solubility of PX conjugates in various polar aprotic (THF, DCM, Acetone, DMSO) and protic (ethanol and water) solvents.

Sample designation	Tetrahydro furane (THF) (DEC: 7.5)	Dichloromethane (DCM) (DEC: 9.1)	Acetone (DEC: 21)	Dimethyl Sulfoxide (DMSO) (DEC: 46.7)	Ethanol (DEC: 16.8)	Water (DEC: 80)
PX(X=0.50P)	Swelled	Swelled	-	Dissolved	-	-
PX(X=0.75P)	Swelled	Dissolved	-	Dissolved	-	-
PX(X=1.40P)	Dissolved	Swelled	-	Dissolved	Swelled	-
PX(X=1.70P)	Dissolved	Swelled	-	Dissolved	Swelled	Dissolved

- : not dissolved, nor swelled. DEC: Dielectric constant.

FTIR spectroscopy

FTIR spectrum (Figure III.3.A) of native xanthan shows carbonyl (C=O) band at 1725 cm^{-1} corresponding to acetate groups of an inner mannose unit. At 1606 cm^{-1}, the characteristic band of carboxylate of pyruvate group and glucuronic acid appears. Spectra of modified xanthans show a shift in the carbonyl band towards 1700 cm^{-1}. These changes may indicate the presence of additional ester groups and suggest that palmitoyl groups substituted the hydrogen atoms of hydroxyl groups in xanthan. It can also be noted the appearance of two absorption bands at 2914 and 2846 cm^{-1}, attributed to CH_3 and CH_2 vibrations from palmitoyl chains. The spectra show that the intensity of absorption bands is proportional to the palmitoyl content added during modification.

^{1}H NMR spectroscopy

^{1}H NMR spectra of palmitoyl xanthans (Figure IV.3.B) show peaks from the protons corresponding to the palmitoyl chain at 0.858 ppm (terminal methyl group), 1.062 ppm (13 methylene groups), 1.234 ppm (β-methylene group) and 2.380 ppm (α-methylene group) whose intensities are proportional to the amount of reacted palmitoyl.
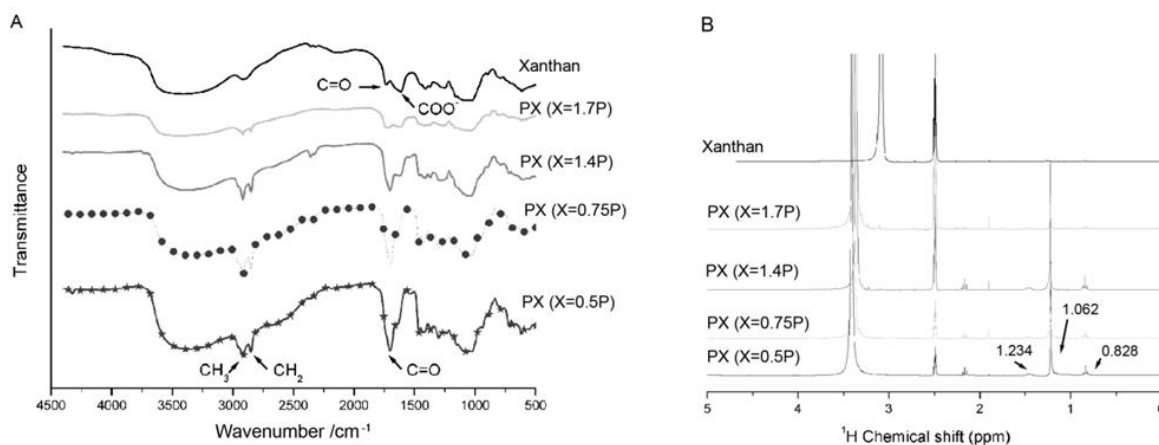
Figure IV.3. (A) FTIR and (B) ^{1}H NMR spectra of native xanthan and palmitoyl xanthan with various degrees of modification [PX(X=0.5P), PX(X=0.75P), PX(X=1.40P) and PX(X=1.70P)].

WAXS

To verify possible molecular organization after palmitoylation, we carried out WAXS experiments. Diffractograms of xanthan and palmitoyl/xanthan ratios (Figure IV.4.A), show the appearance of new peaks after modification, demonstrating that the native structure of xanthan has been modified after palmitoylation and this modification has induced a certain molecular organization. As expected, the peak intensity of palmitoyl xanthan increased proportionally with the feed ratio of palmitoyl chloride reactant (from PX(X=1.7P) to PX(X=0.5P)). This fact may be attributed to the higher amount of aliphatic chains (palmitoyl groups) that promotes higher hydrophobic interaction and consequently higher organization degree at structural level.

De Bragg's law gives the periodic distance, d-spacing values, that may correspond in this specific case to the distance for regularly molecular packing. Particularly, if the self-assemblies form bilayered structures with a same orientation, the d value should give the relative distance for the interdigitated hydrophobic interaction between alkyl chain groups, which is related to the hydrophobic interaction. Considering similarities between the main peaks, and comparing peak intensities as well as d-spacing, the intensities, as mentioned before, increase with increase of the amount of palmitoyl chains due the increase of hydrophobic interactions. Nevertheless, in all the samples, the distances between alkyl groups (d-spacing) does not change significantly with the amount of reacted palmitoyl chloride indicating that the arrangement of molecular packing should be the same independently of the intensity of hydrophobic forces (or amount of palmitoyl chains used in such reactions).
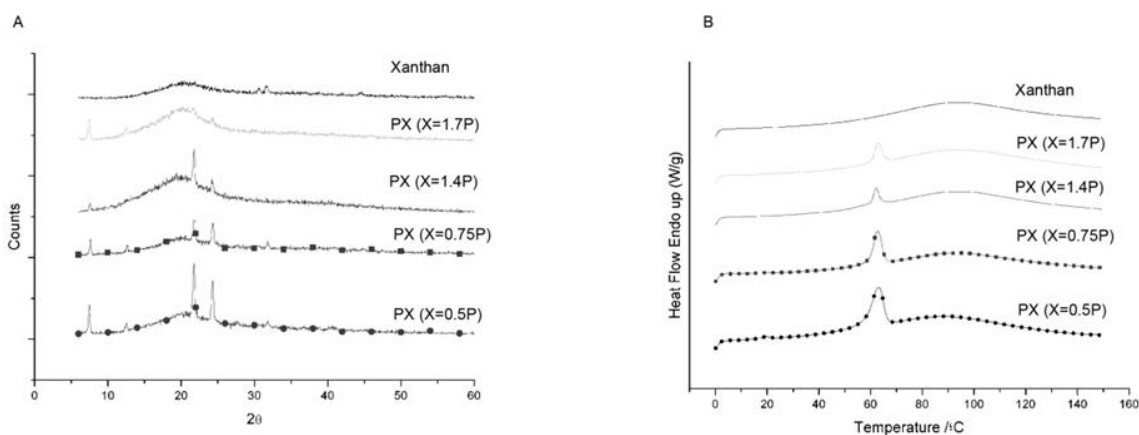
Figure IV.4. (A) WAXS diffractograms and (B) DSC thermograms of xanthan and palmitoyl xanthan(s).

Table IV.3. Wide angle x-ray diffraction data of palmitoylated xanthan in various conjugation ratios

Sample designation	Angle 2Θ	d-spacing Å
PX(X=0.50P)	7.48	11.82
	12.56	7.09
	21.80	4.15
	24.32	3.74
	31.84	2.92
PX(X=0.75P)	7.52	11.84
	12.60	7.06
	21.84	4.14
	24.28	3.74
	31.76	2.92
PX(X=1.40P)	7.52	11.84
	21.80	4.15
	24.28	3.74
PX7(X=1.7P)	7.32	12.12
	12.36	7.19
	21.60	4.18
	24.44	3.71
Xanthan	**31.60**	**2.94**

The main peaks of conjugate materials were detected at 21.8 and 24.32 2Θ values, which correspond to 4.15 and 3.74 Å respectively (Table IV.3.). The found d-values indicate that the ordered structures are near one and half and two palmitoyl chains length, as Benges et al observed in pure nanocrystals of palmitic acid (about 2 Å) [21]. As the palmitoylation was increased, the relative intensity ratio of 3.74 Å/4.15 Å was higher, showing that the palmitoyl chains are interacting more with opposite chains, which may induce stacking between aliphatic chains and shortening the packing distance.

DSC analysis

The DSC curves of palmitoyl xanthan (Figure IV.4.B) shows one endothermic phase transition at 61 ⁰C which is less intense as the amount of palmitoyl added to reaction is lower. In the DSC curve of native xanthan, no relevant transition was observed. These observations are corroborating the WAXS results. Such behaviour may be attributed to the increased hydrophobic interactions provided by the higher amounts of reacted palmitoyl that will supply a molecular rearrangement and consequently induce intermolecular organization.

Molecular conformation - CD spectroscopy

CD spectroscopy is suitable technique to predict molecular conformation in liquid state. We used CD to investigate changes in molecular structure of xanthan after palmitoylation, CD analyses of xanthan and PX(X=1.7P) were performed at 25 ⁰C in water. The spectrum of both polymers (Figure IV.5.A) showed an increase in peak height with maximum absorption wavelength at 196 nm (ordered state) and a decrease of the minimum with displacement at higher wavelengths at 220 nm (disordered state). Despite both materials present similar CD signatures, in PX(X=1.7P) the difference in absorption of left-hand and right-hand circularly polarized light is more accentuated, it can be deduced that the introduction of such hydrophobic tails are promoting a soft disruption of the organized structure. Considering that the palmitoylation was performed at low temperature (0 ⁰C), at which an ordered helicoidal structure on native xanthan is present, it is more probable that the palmitoyl chains reacted with the hydroxyl groups of the trissaccharide side chain due to the difficulty to access to the internal primary structure. Previously, the ordered conformation of xanthan was investigated thoroughly and indicated that native xanthan involves single or double helix structure and the solid state forms a helical structure with 5-fold symmetry [22]. As a result of conjugation of palmitoyl chains to hydroxyl groups, the disruption of hydrogen bonds, which are necessary for helicoidal structure formation, can be expected.

The native structure of xanthan has been reported in several studies which showed that this biopolymer could be stable when assuming helical structure [16], being also temperature dependent [13,15]. According to Lim and co-workers [23] for concentrations above 1 wt.%, xanthan may self-assemble into liquid crystalline regions. However, at around 0.5%, the structure is not liquid crystalline in nature but present networks formed by self-organization provided by hydrogen bonding. It has been studied before that xanthan forms gels in the presence of salts and those have the ability to stabilize the ordered conformation [13,15-16].

Dynamic light scattering and zeta potential measurements

The electrical charge (ζ-potential) of polymers is dependent on several factors such as the pH, polymer conformation, and polymer concentration.

Figure IV.5.B and C presents the zeta potential and particle size of PX(X=1.7P) and native xanthan as a function of pH.
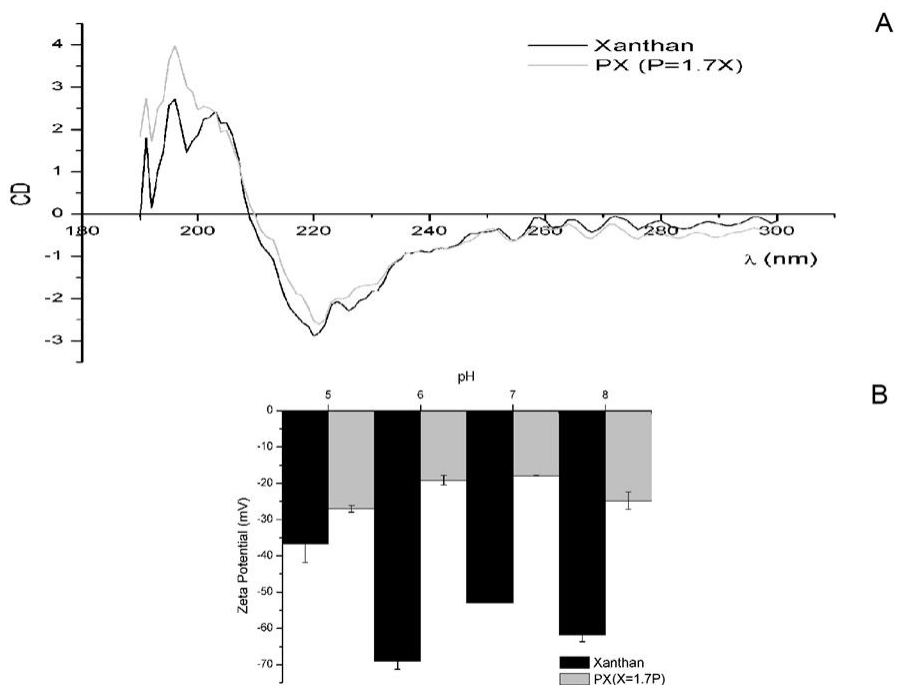
Figure IV.5. (A) CD spectra of xanthan and PX(X=1.70P) solutions (0.1 wt%) in distilled water (B) Zeta potential measurements and (C) particles size (diameter) of xanthan and PX(X=1.70P) xanthan conjugate aqueous solution as a function of pH.

After modification, a decrease in the negative zeta potential is observed when compared with native xanthan. At low pH (pH 5), PX(X=1.7P) exhibits a zeta potential value of -26 mV, which becomes less negative as the pH increase, reaching the minimum at pH 7 (-17 mV) and then increase again at pH 8. Nevertheless, these changes in zeta potential are not as evident as the ones observed for native xanthan, where the negatively charged carboxylic groups may be positioned without any stereochemical protection and consequently more sensitive to pH changes. In the case of PX(X=1.7P), the hydrophobic effect provided by the aliphatic chains of palmitoyl is improving the stabilization of molecules, being this maximum peak of stabilization

reached at pH 7. At this pH, the hydrophobic interaction between the palmitoyl groups took control, occurring the formation of particle aggregate, as can be noticed by the abrupt increase in particle size (533 nm) (Figure IV.5.C) while in native xanthan this effect was not observed. Given these preliminary results, pH 7 is considered as the transition pH for the self-assembly of the amphiphilic conjugate. At pH 7, PX(X=1.7P) was detected in the lowest charged state, in which the repulsion between charged groups is expected to be minimum, and this can enhance hydrophobic action between alkyl chains. Similarly, a recent study showed that a rapid hydrogelation of N-palmitoyl chitosan was occurred through a proper balance between charge repulsion and hydrophobic interaction by its environmental pH within a narrow range (pH 6-5-7.0) [24].

STEM analysis

In order to investigate the supramolecular rearrangement of palmitoyl xanthan in physiological conditions, namely in an ionic strength of 0.9 % NaCl and at pH 7.4, the casted solutions of conjugate was analyzed with scanning transmission electron microscope after negative staining with uranyl acetate. The conjugate which was not exposed to any ionic solution and dissolved in distilled water showed a random, thin, fibrous network structures as seen by STEM micrographs (Figure IV.8.). This fibrous network structure was also evident when the conjugate was dissolved in HEPES buffer. In that case, however, the thickness of fibrous structures was increased as determined by STEM micrographs at various magnifications. When the palmitoyl xanthan solution was incubated in PBS similar to microcapsule preparation, on the other hand, the lamellar structures were observed instead of fibrous networks. The magnified STEM images clearly show that the assembled structures were formed in an angular and lamellar morphology. In addition, the STEM micrographs of native xanthan did not indicate any visible ultra-structures which can interact with negative staining as seen in the micrographs.

Those results may indicate that there were light supromolecular organizations of palmitoyl xanthan molecules in aqueous environment without ions. This was even more pronounced in HEPES buffer solution by increased size of fibrous structures but still it was not sufficient for a major hydrophobic interaction resulting in stable assemblies. The aggregation of PX molecules in the ionic and pH milieu provided by PBS and the observation of lamellar structures were supporting the hypothesis that major hydrophobic transition occurred in physiological ion strength and pH.
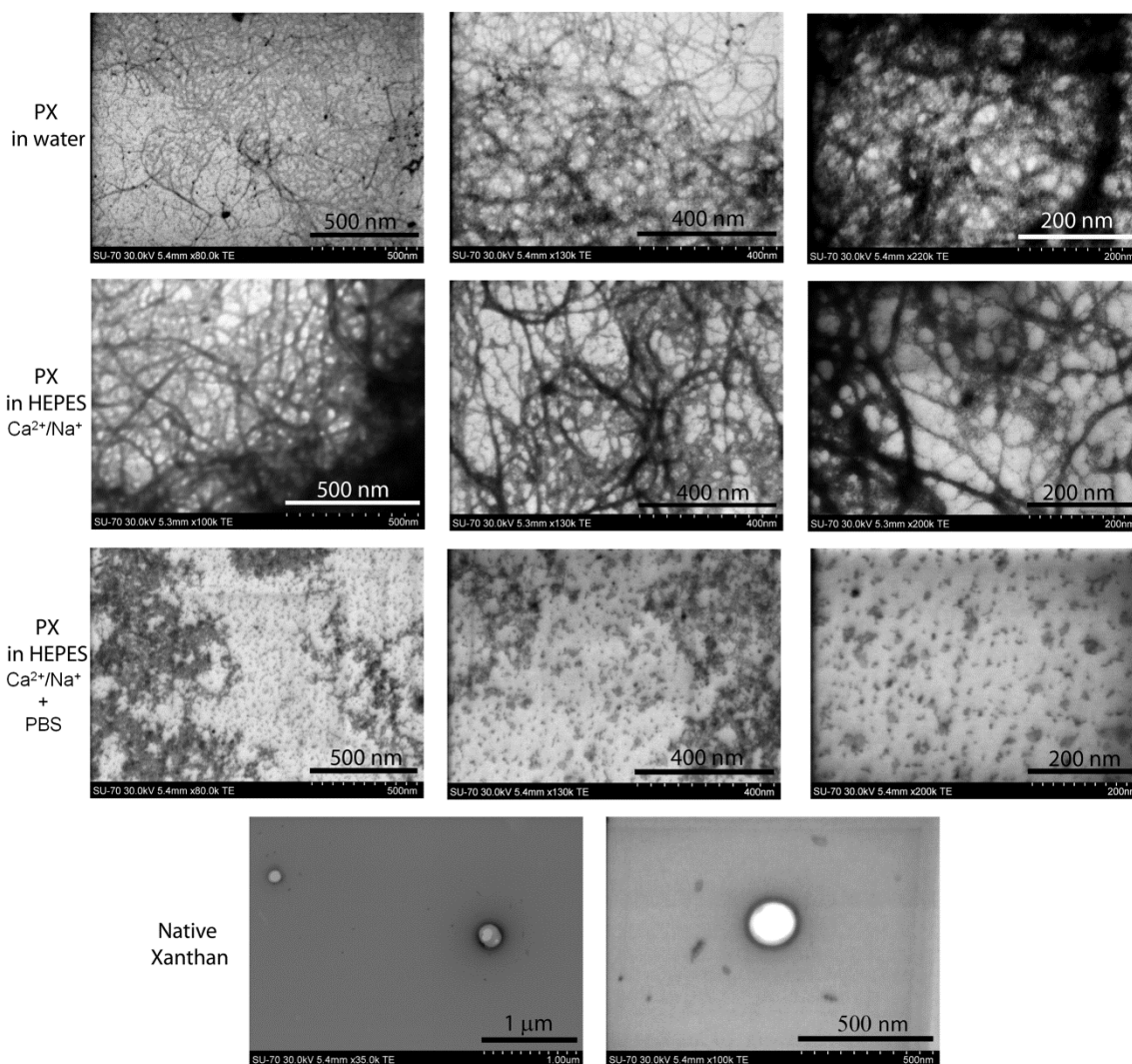
Figure IV.6. STEM images of palmitoyl-xanthan in 0.1 wt% solution. The samples were negatively stained with 1% (w/v) uranyl acetate.

SEM analysis

As the first attempt to produce capsules, we tried to extrude 1 and 3 wt% xanthan in PBS. Although capsules were able to be formed, they were not stable as they started to dissolve. Aiming to improve the stability of xanthan capsules, the procedure described previously was performed and successful with PX(X=1.7P), resulting in the hollow capsules showed in SEM micrographs (Figure IV.7.A.). SEM analysis of PX(X=1.7P) microcapsules have indicated that the external wall structure was constituted of nano-lamels which are overlapping each other with a layer thickness of about 52 nm as observed on surface and inside the wall cross-section (Figure IV.7.C, D, E and F).
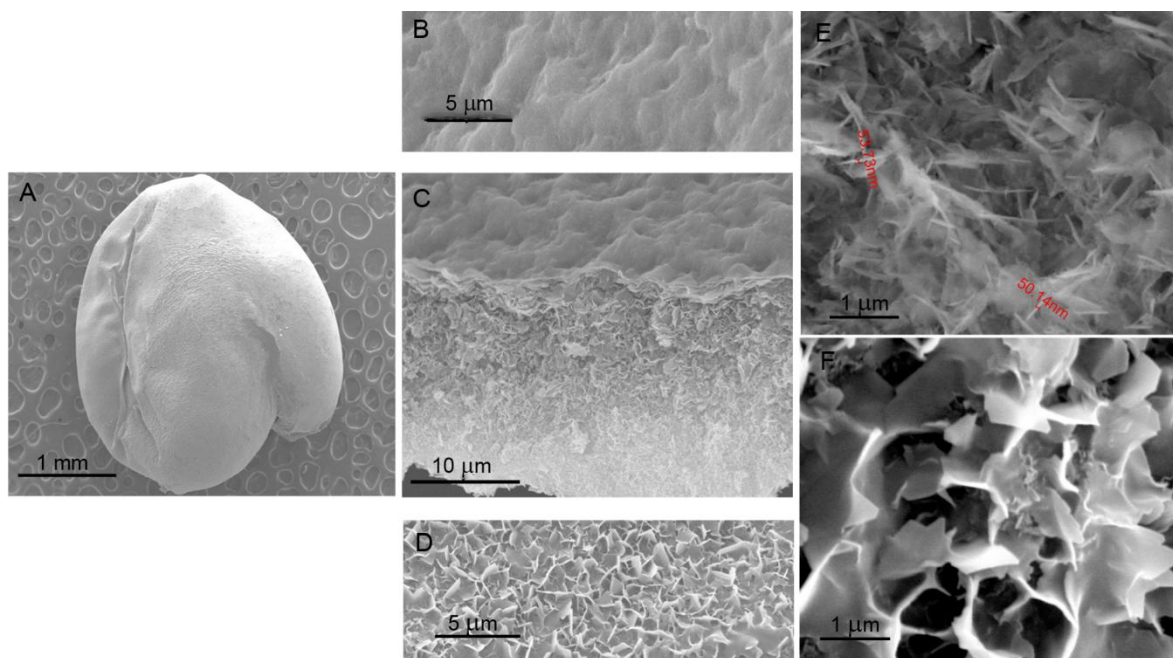
Figure IV.7. SEM images showing the overall structure of PX(X=1.70P) capsules performed manually (A), cross-section of microcapsule membrane (C and the microstructure of the capsule internal (B) and external surface (D). Magnified images revealing morphological details of the external surface of PX(X =1.70P) capsules (E and F).

Based on organization of ultra structures revealed by SEM, it can be hypothesized that salt addition result in the screening of electrostatic repulsion and the hydrophobic interaction between conjugated alkyl chains become the dominating forces leading to molecular packing (Figure IV.8.). The internal calcium in gel must diminish repulsion forces between carboxyl groups by ionic bridge formation and subsequently, the monovalent cations provided from PBS must interact with the polar groups of polysacharide backbone by decreasing their solvation with water molecules. As a result of those interactions, the hydrophobic forces between alkyl chains become a dominant force and a self organization of molecules resulted in multilayered lamellar structures. Those layered structures can further aggregate into piled up structures as polar-nonpolar repulsion between assembled alky chains and hydrophilic polysaccharide backbone. Non-covalent interactions are the main forces that hold supramolecular species together[2].

Despite of its weak nature, relatively to covalent interaction, when these interactions are used synergistically, a stable supramolecular complex could be formed. In this specific case, those interactions should create a synergistic effect and consequently, able to form and maintain a hollow structure with wall thickness of around 16.7 µm that is shown in Figure IV.7.C. We have formulated a possible mechanism for the self-assembly of palmitoyl xanthan amphiphile

(Figure IV.8.) into hollow capsular structures. The balance between charge repulsion and hydrophobic interaction in palmitoyl xanthan is sensitive to environmental pH and presence of salts. In absence of salts (water) the charge repulsion between the negatively charge carboxylic groups on xanthan is dominating. In PBS, the electrostatic repulsion resulting from the charged groups is suppressed by the accumulation of counter ions diffused from the PBS (screening effect), thus increasing the hydrophobic interaction.
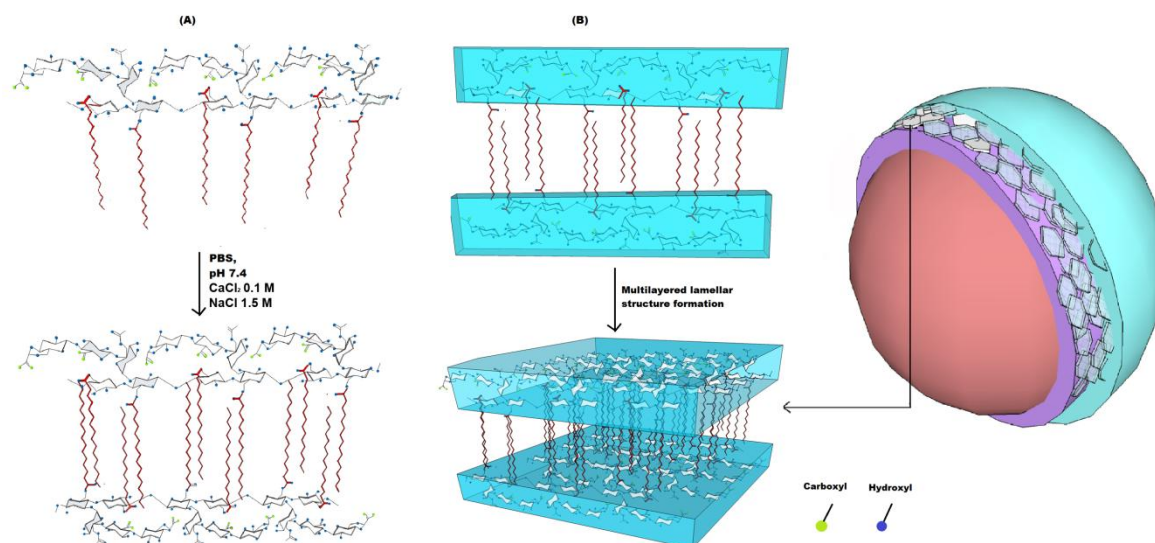
Figure IV.8. Schematic depiction of microcapsule formation mechanism by PBS induced self assembly of palmitoyl-xanthan amphiphile molecules (A) and the mechanism of microcapsule formation (B) by hydrophobic forces.

Xanthan-palmitoyl microcapsule formation and cell encapsulation

When designing materials for cell encapsulation, several properties should be considered for cell optimum biological functions. For instance, the amount and the character of functional groups contained in monomer units will influence the intermolecular interactions and also the interactions that lead to the capsule formation. As mentioned previously, palmitoyl xanthan by itself in physiological conditions is able to form self-supporting capsules in the presence of ions which are stable in long term. Although appropriate for cell encapsulation purposes, these capsules are not physically stable enough to enclosure cells and protect from immunotoxins. For this reason, the PX(X=1.7P) microcapsules, which have negatively charged carboxyl groups, were coated with cationic poly-l-lysine (PLL). The PLL is well studied in cell encapsulation and has showed satisfactory performance in the encapsulation of cells with xanthan based material [18].
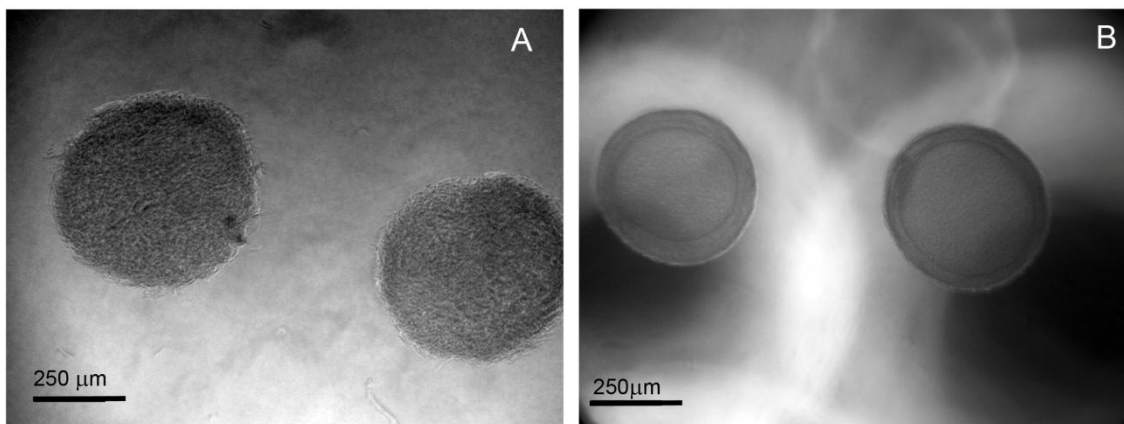
Figure IV.9. Bright field light microscopy images of PX(X=1.70P) microcapsules uncoated (A) and coated (B) with poly-l-lysine (external layer).

The microcapsules obtained in the present study were spherical and uniform in size with diameter size around 450 μm (Figure IV.9.). As it can be observed from the cross-section images, there are two distinct layers corresponding to PX(X=1.7P) matrix inside and poly-l-lysine cover at outside.

In vitro viability, proliferation and morphology of ATDC5 cells cultured within microcapsules

To assess the ability of PX(X=1.7P) microcapsules to sustain cell viability, we encapsulated ATDC5 cells, an immortalized chondrocytic cell line, within these self-assembled matrices. The morphology and viability of encapsulated cells in PX(X=1.7P) microcapsules were investigated.

Live/dead assay (Figure IV.10.A) shows that encapsulated cells remain viable up to 21 days of culture (viable cells depict a green fluorescence color), demonstrating the ability of palmitoyl xanthan self-assembled matrix to support cellular viability over prolonged time. Cell viability within the microcapsules is also confirmed by the results from the AlamarBlue® assay (Figure IV.10. B). Encapsulated cells were observed to reduce AlamarBlue® during 21 days of *in vitro* culture, exhibiting a slight increase in the metabolic activity from day 7 to day 21.

To validate the results from cell viability studies, cell proliferation was investigated by DNA quantification (Figure IV.10.C). A gradual increase of DNA quantity was observed from day 7 until day 21 as a result of improved cellular proliferation in PX(X=1.7P) microcapsules.

Cell viability and proliferation within the microcapsules indicate that palmitoyl xanthan microcapsules are permeable as they are able to provide sufficient oxygen and nutrients necessary for cell survival and proliferation. SEM images of the microcapsule (Figure IV.11.) show two layers with distinct morphologies that can be appreciated.
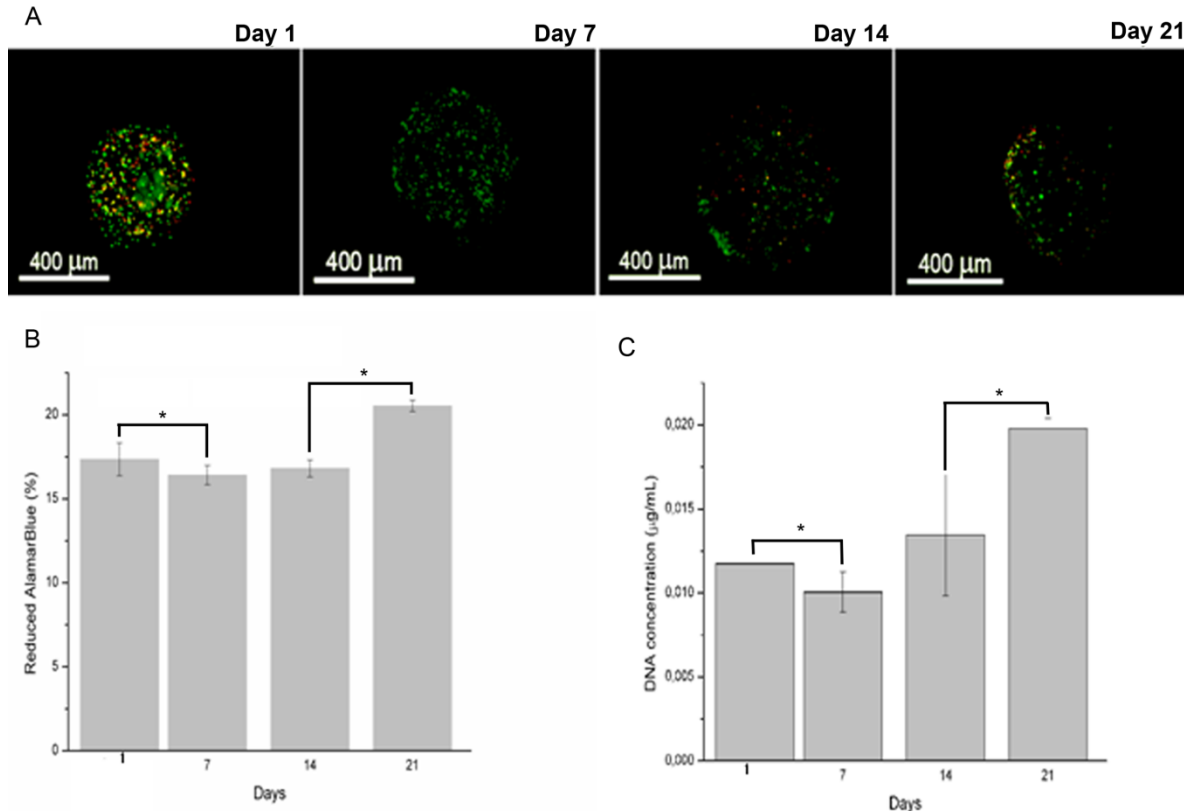
Figure IV.10. *In vitro* viability and proliferation of ATDC5 cells cultured in PX(X=1.70P)/PLL microcapsules. (A) Fluorescence microscopy images displaying the live/dead assay of encapsulated cells (green cells are live, red cells are dead) showing that the cells remain viable in the microcapsules up to 21 days of culture. (B) Metabolic activity and (C) proliferation of encapsulated cells determined by AlamarBlue® assay and DNA quantification. Results are expressed as means ± standard deviation with n=3. *Indicates a significant difference (p< 0.05) for different time points.

Most mammalian cells are anchorage dependent and therefore have to adhere to a surface to express their optimum metabolic functionality and viability [25]. SEM analysis on cell cultured microcapsules after 21 days revealed that the cells were partially entrapped on the internal side of the dense microcapsule wall (Figure IV.11.E and F) This may be explained by the fact that nutrients and oxygen are more readily available at the capsule surface than in the microcapsule core. This core shell type microcapsules, with partial embedding of cells on inner wall, might be superior to cell microencapsulation into firm gels, like into alginate beads formed by ionic

crosslinking, since the cells immobilized in the center of the gel would present decreased metabolic activity and proliferation as the diffusion of nutrients and oxygen would be more challenging at this location.
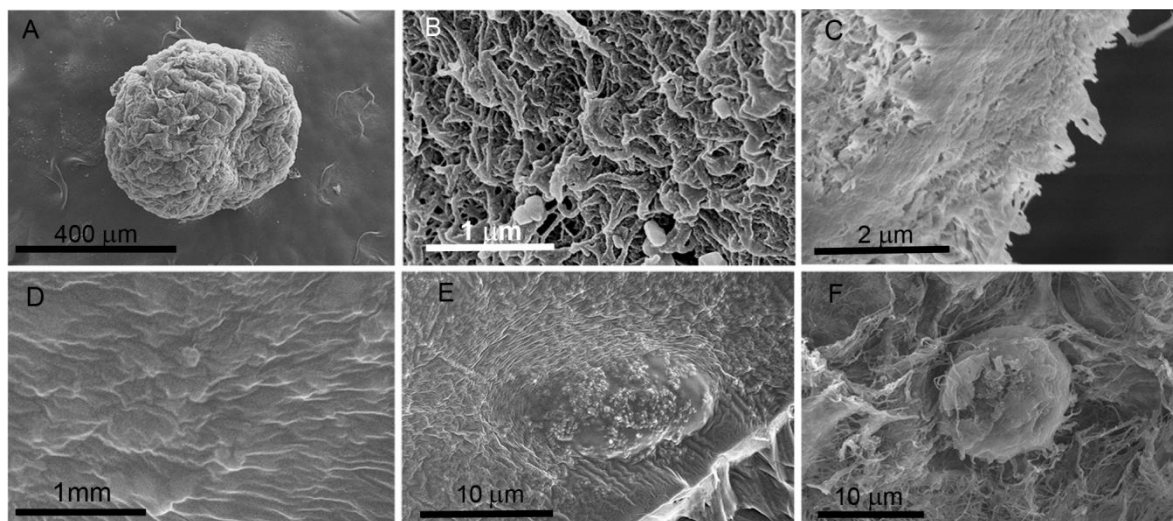
Figure IV.11. SEM images showing the overall PX(X=1.70P)/PLL microcapsule after 21 days of culture (A), the external surface (B) and the cross-section demonstrating the interface between PX(X=1.70P) and poly-l-lysine complex (C). Internal surface (D) and morphological characteristics of the cells attached to the microcapsule inner surface (E) and (F).

4. CONCLUSIONS

Palmitoyl xanthan with various conjugation ratios was successfully synthesized to obtain an amphiphilic polysaccharide. The amphiphilic character imparted to native xanthan only by certain palmitoyl ratio allows the self-assembly into stable hollow capsule structures in cell-friendly conditions, i.e., in the presence of physiological ion concentration and pH. Microcapsules with long-term stability and ability to support cell viability and proliferation *in vitro* over prolonged time were obtained using this self-assembling system. In summary, we have demonstrated the use of self-assembly to provide triggered activation for capsule formation. This approach provides an easy and versatile strategy for the construction of synthetic matrices capable of encapsulating living cells that could be applied in cell-delivery therapies.

REFERENCES

1. Chen P. Self-assembly of ionic-complementary peptides: a physicochemical viewpoint. Colloids and Surfaces A: Physicochemical and Engineering Aspects 2005;261(1-3):3-24.

2. Jonathan W. Steed DRT, Karl J. Wallace,. In: Sons JW, editor. Core concepts in supramolecular chemistry and nanochemistry; 1969.

3. Lowik DWPM, Leunissen EHP, van den Heuvel M, Hansen MB, van Hest JCM. Stimulus responsive peptide based materials. Chemical Society Reviews 2010;39(9):3394-3412.

4. Akiyoshi K, Kang EC, Kurumada S, Sunamoto J, Principi T, Winnik FM. Controlled Association of Amphiphilic Polymers in Water: Thermosensitive Nanoparticles Formed by Self-Assembly of Hydrophobically Modified Pullulans and Poly(N-isopropylacrylamides). Macromolecules 2000;33(9):3244-3249.

5. Hartgerink JD, Zubarev ER, Stupp SI. Supramolecular one-dimensional objects. Current Opinion in Solid State and Materials Science 2001;5(4):355-361.

6. Duval-Terrié C, Huguet J, Muller G. Self-assembly and hydrophobic clusters of amphiphilic polysaccharides. Colloids and Surfaces A: Physicochemical and Engineering Aspects 2003;220(1-3):105-115.

7. Bourov GK, Bhattacharya A. Brownian dynamics simulation study of self-assembly of amphiphiles with large hydrophilic heads. Journal of Chemical Physics 2005;122(4):1-6.

8. Akiyoshi K, Sunamoto J. Supramolecular assembly of hydrophobized polysaccharides. Supramolecular Science 1996;3(1-3):157-163.

9. Rouzes C, Durand A, Leonard M, Dellacherie E. Surface Activity and Emulsification Properties of Hydrophobically Modified Dextrans. Journal of Colloid and Interface Science 2002;253(1):217-223.

10. Cheng J, Zhu J-b, Wen N, Xiong F. Stability and pharmacokinetic studies of O-palmitoyl amylopectin anchored dipyridamole liposomes. International Journal of Pharmaceutics 2006;313(1-2):136-143.

11. Rodrigues JS, Santos-Magalhães NS, Coelho LCBB, Couvreur P, Ponchel G, Gref R. Novel core(polyester)-shell(polysaccharide) nanoparticles: protein loading and surface modification with lectins. Journal of Controlled Release 2003;92(1-2):103-112.

12. Rouzes C, Leonard M, Durand A, Dellacherie E. Influence of polymeric surfactants on the properties of drug-loaded PLA nanospheres. Colloids and Surfaces B: Biointerfaces 2003;32(2):125-135.

13. Schorsch C, Garnier C, Doublier J-L. Microscopy of xanthan/galactomannan mixtures. Carbohydrate Polymers 1995;28(4):319-323.

14.   Capron I, Brigand G, Muller G. About the native and renatured conformation of xanthan exopolysaccharide. Polymer 1997;38(21):5289-5295.

15.   Katzbauer B. Properties and applications of xanthan gum. Polymer Degradation and Stability 1998;59(1-3):81-84.

16.   García-Ochoa F, Santos VE, Casas JA, Gómez E. Xanthan gum: production, recovery, and properties. Biotechnology Advances 2000;18(7):549-579.

17.   Hamcerencu M, Desbrieres J, Popa M, Khoukh A, Riess G. New unsaturated derivatives of Xanthan gum: Synthesis and characterization. Polymer 2007;48(7):1921-1929.

18.   Mendes AC, Baran ET, Pereira RC, Azevedo HS, Reis RC. Encapsulation and Survival of a Chondrocyte Cell Line within Xanthan gum derivative. 2010.

19.   Jiang G-B, Quan D, Liao K, Wang H. Preparation of polymeric micelles based on chitosan bearing a small amount of highly hydrophobic groups. Carbohydrate Polymers 2006;66(4):514-520.

20.   Baran ET, Mendes AC, Azevedo HS, Reis RL; DISPOSITIVO, MÉTODO E SISTEMA DE FABRICO DE MICROCÁPSULAS. Portugal. 2011.

21.   Benages R, Bayes L, Cordobilla R, Moreno E, Calvet T, Cuevas-Diarte MA. A Comparative Study of Several Techniques to Obtain Fatty Acid Nanoparticles: Palmitic Acid. Crystal Growth & Design 2009;9(4):1762-1766.

22.   Millane RP, Wang B. A cellulose-like conformation accessible to the xanthan backbone and implications for xanthan synergism. Carbohydrate Polymers 1990;13(1):57-68.

23.   Timothy L, Jonathan TU, Robert KPh. Rheology of Self-Associating Concentrated Xanthan Solutions. Journal of Rheology 1984;28(4):367-379.

24.   Chiu Y-L, Chen S-C, Su C-J, Hsiao C-W, Chen Y-M, Chen H-L, Sung H-W. pH-triggered injectable hydrogels prepared from aqueous N-palmitoyl chitosan: In vitro characteristics and in vivo biocompatibility. Biomaterials 2009;30(28):4877-4888.

25.   Bhatia SR, Khattak SF, Roberts SC. Polyelectrolytes for cell encapsulation. Current Opinion in Colloid & Interface Science 2005;10(1-2):45-51.

Chapter V

GUIDED AND MICROFLUIDIC SELF-ASSEMBLY OF PHOSPHOLIPID-
XANTHAN MICROCAPSULES

GUIDED AND MICROFLUIDIC SELF-ASSEMBLY OF PHOSPHOLIPID-XANTHAN MICROCAPSULES

ABSTRACT

We report the synthesis of an amphiphilic polysaccharide, a phospholipid (1,2-dioleoyl-sn-glycero-phosphoetilamine (DOPE)) conjugated with the anionic xanthan gum, and its ability to spontaneously self-assemble into capsular structures under mild aqueous conditions for cell encapsulation. Moreover, this work also aimed to apply a microfluidic platform that can precisely generate micro-sized and monodispersed capsules. The properties (size, morphology, permeability) and performance (stability) of the obtained microcapsules were studied, as well their ability to support the viability, function, and proliferation of encapsulated cells. The self-assembly of the amphiphilic polysaccharide at certain concentrations in physiological ionic strength and pH resulted in the formation of stable hollow capsular structures. Using the microfluidic device, homogenous microcapsules were fabricated. ATDC5 cells were encapsulated within the capsules and shown to remain viable, evidencing an increased cellular metabolic activity over 21 days of *in vitro* culture. By combining self-assembly of xanthan-DOPE and microfluidic microencapsulation, we were able to fabricate microcapsules that provided an adequate environment for cells to survive and proliferate.

1. INTRODUCTION

Hydrophobic interactions have been recognized as one of the driving forces observed on the self-organization of biological structures. The cellular membrane, composed of phospholipid bilayer[1-2], is an example of self-assembled structure driven by hydrophobic effects. The phospholipids arrange themselves in such a way that their hydrophobic tails are projecting inwards while their polar head groups are projecting on the outside surfaces[1,3]. This organization of phospholipids in the cell membranes makes the latter selectively permeable to ions and molecules. Due to its biological importance, phospholipid membranes have been explored for preparing biomimetic capsular structures[4], mainly vesicles or liposomes, and also as a coating for water microdroplets[1]. In fact, lipids are common self-assembling molecules used by cells to compartmentalize biological processes. Liposomes, which are cell mimics lacking the internal cellular contents, are good candidates for the encapsulation of biological materials but their high sensitivity to osmotic pressure and mechanical stress has limited their application as cell encapsulation matrices. Furthermore, the water microdroplets coated with phospholiplips[2,5] have been investigated in order to overcome such problems and considered as suitable models of living cells, since the molecular organization of the phospholipids may be similar to the organization of the cytoplasmatic membrane[2]. Therefore, biomimetic microcapsules have been fabricated by applying lipids and proteins as assembly pairs[6] for cell encapsulation. Self-assembling hydrophobized polysaccharides have been considered to provide opportunities in molecular design of biomaterials. A hydrophobized polysccharide consists mainly in a water-soluble main chain, the polysaccharide, carrying a small number of hydrophobic groups. The use of these materials is appealing, once the polysaccharide backbone presents numerous favorable characteristics such as biodegradability, low toxicity, protein rejecting ability, receptor interaction through specific sugar moieties, and abundance of functional groups for modification or functionalization[7-8]. Afterwards, the amphiphilic nature imparted to the polysaccharides after hydrophobic modification gives them the ability to self-assemble in cell friendly conditions into functional nanostructures [9-13] that can be used in a wide range of biomedical application such as emulsion stabilizers, surface modifiers for liposomes and nanoparticles[14-15] and as drug delivery vehicles[16-17]. Self-assembly of an amphiphilic polysaccharide into microcapsules in aqueous solution for cell encapsulation has been demonstrated in our group as an alternative path to the current ion crosslinkable systems[18]. In this work, we describe the conjugation of the phospholipid 1,2-dioleoyl -sn-glycero-phosphoetilamine (DOPE) with xanthan (Figure V.1.), a bacterial extracellular polysaccharide with a known potential as encapsulating matrix[18-19], to obtain an amphiphilic system able to form hollow capsules by self-assembly obviating the need of core removal, like in the approach of layer-by-layer assembly on colloidal templates. For reproducibly

generating capsules with controlled spherical shape and micro-size range, we have employed microfluidic technique. The structure and properties of phospholipid xanthan microcapsules are described and their potential for application in cell encapsulation.
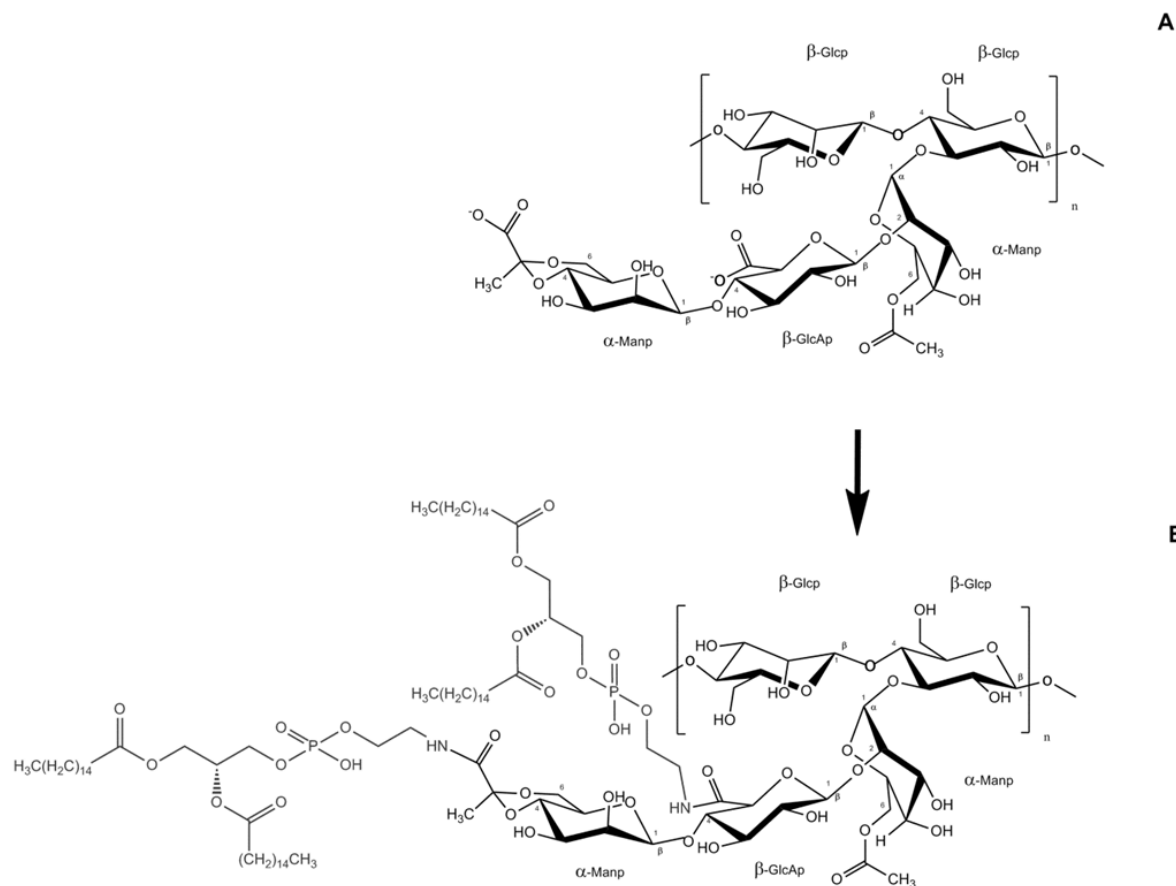
Figure V.1. Chemical structure of xanthan repeating unit (A) and xanthan-DOPE (B) with DOPE molecules (shown in red) conjugated in the carboxylic groups of xanthan.

2. MATERIALS AND METHODS

Materials

All chemicals, including xanthan gum from *Xanthomonas campestris,* 1,2-dioleoyl-sn-glycero-3-phosphoethylenoamine (DOPE) and poly-L-lysine (PLL, 30-70 KDa) were obtained from Sigma/Aldrich (USA) unless otherwise indicated, and used as received. Calcium and sodium chloride were provided from Merck (Germany) and Carlo Erba (Italy) respectively. Ethanol was obtained from Panreac (Spain).

Synthesis of xanthan-DOPE

Xanthan, with an average molecular weight of 152 kDa[18], was dissolved in 2-(*N*-morpholino)ethanesulfonic acid buffer solution (MES, Sigma), at 55 mM at room temperature. The xanthan solution was placed in an ice water bath, under inert atmosphere, and the pH was adjusted to 5.5. The N-hydroxysuccinimide (NHS) and ethyl(dimethylaminopropyl)carbodiimide (EDC) (NHS/EDC molar ratio = 0.6) was added to xanthan under stirring condition. Equimolar amount of EDC was used to activate carboxyl group of xanthan which contains two units per repeating pentasaccharide. Later, DOPE was added at the same molarity of carboxyls[20] and the pH was monitored and maintained at 5.5 during half an hour by adding HCl. The reaction took place overnight (15 h) and was stopped by the addition of excess of cold ethanol (70 %). The precipitate was washed by ethanol repeatedly on a filter and dried at room temperature until constant mass.

Characterization of xanthan-DOPE

Fourier transformed infra red (FTIR) spectroscopy

The structural modification of xanthan-DOPE was followed by FTIR spectroscopy using an IR Prestige-21 (SHIMADZU, Japan) spectrophotometer. Prior the analysis, potassium bromide pellets were prepared by mixing the native xanthan and xanthan-DOPE powder with KBr (X/KBr and X-D/KBr, 1/10, wt/wt). The spectra were taken with the average of 32 scans and a resolution of 4 cm^{-1}.

^{1}H nuclear magnetic resonance (NMR) spectroscopy

Xanthan and xanthan-DOPE powders were dissolved at a concentration of 1.0 wt% in deuterated water (D_2O). Fully relaxed ^{1}H NMR spectra were acquired in a Varian Unity Plus 300 MHz spectrometer at 25 and 60 ºC.

Determination of the degree of substitution (DS)

The DS of the carboxylic groups of native xanthan with DOPE was determined by acid-base titration based on the method applied in[19,21]. Xanthan-DOPE (0.01 g) was dissolved in 40 mL of distilled water. The pH of the solution was adjusted to 2 with hydrochloric acid and then xanthan-DOPE was titrated with 0.02 N NaOH. The volume of added NaOH, as well as the pH values were recorded. Three replicates were performed for each sample. DS was calculated as following:

$$DS = \frac{M_{Xru} \times (n_{ep})}{m - (M_D \times n_{ep})} \qquad (V.1.)$$

M_{Xru} is the molecular weight of xanthan repeating unity (851); n_{ep} is the number of mol of carboxyll groups at the ending point of the titration; M_D is the molecular weight of the reacted DOPE molecules grafted in the native structure of xanthan gum.

Wide angle X-ray scattering (WAXS)

WAXS technique was employed to obtain the X-ray diffraction patterns of native xanthan and xanthan-DOPE. Dry powders were placed in the sample holder and the WAXS patterns were obtained in a Bruker AXS NanoStar diffractometer with a HiStar 2D detector with scattering angles from 5 to 60°.

Circular dichroism (CD) spectroscopy

Xanthan and xanthan-DOPE were dissolved in ultrapure water at concentration of 0.1 wt%. The measurements were performed in a Stopped-flow circular dichroism spectrometer (PiStar-180 spectrometer, Applied Photophysics, UK) at 25 °C using quartz cells with 0.1 cm path length. The spectra were recorded from 300 to 180 nm with scan rate of 100 nm min^{-1} and are an average of five accumulations.

Polarized light microscopy

The morphology of xanthan-DOPE assemblies in aqueous conditions was also directly examined by polarized light microscopy. Native xanthan and xanthan-DOPE were dissolved in distilled water and the solution dropped onto a glass slide The samples were observed in a polarized light optical microscope (Olympus type BH-2) and recorded with a Olympus digital camera type DFC280.

Microcapsule preparation

Xanthan-DOPE was dissolved in HEPES buffer solution (55 mM, pH 7.4) supplemented with 0. 1 M CaCl$_2$ at concentration of 1 wt% and injected through the polymer microchannel of microfluidics device using a syringe pump (Alladdin WPI, England) (Figure V.4.C). Simultaneously, the flow of mineral oil was provided to the oil microchannel from an oil reservoir by using a peristaltic pump (Ismatec, Switzerland). The operation rate of peristaltic and syringe pump was set at 0.35 mL/minute and 20 µL/min, respectively. The xanthan-DOPE microdroplets were generated inside the microfluidics device by shear stress when the polymer solution in vertical microchannel entered into the stream of mineral oil in larger horizontal microchannel. The formed homogenous droplets of the xanthan-DOPE were collected in a collector vessel containing PBS solution and about 10 µL of Tween 80 as emulsifying agent. The self-assembly

of the amphiphilic xanthan in the aqueous PBS took place with subsequent microcapsule formation by gently stirring of droplets for 15 min. Separately, for coating purpose, some batches of self assembled microcapsules were transferred into 0.1wt% of poly-L-lysine solution and stirred gently for 10 min. Afterwards, the xanthan-DOPE and xanthan-DOPE-PLL microcapsules were washed in PBS before transferring them into cell culture plate 12 wells.

Microcapsule characterization

Microcapsule morphology by light microscopy analysis

Microscopic observations of the microcapsules were carried out to examine the microcapsule and eventually cell morphology. At predetermined time points, micrographs of microcapsules were acquired in a bright field light microscope (AXIOVERT 40 CFL, Germany) equipped with a digital camera (Canon Power shot G8, Japan).

Microcapsule microstructure by scanning electron microscopy (SEM) analysis

Prior to SEM observation, the capsules were fixed with 3% v/v of glutaraldehyde (Electron Microscopy Sciences) in PBS for 1 h. The samples were further dehydrated sequentially by immersing microcapsules in graded ethanol series (20, 50, 60, 70, 80, 90 and 100%) for 10 min followed by immersion (three times for 10 min) in hexamethyldisilazane (Electron Microscopy Sciences). The specimens were transferred and mounted on aluminum stubs and allowed to dry at room temperature. Microcapsules were then frozen quickly in liquid nitrogen and cut in half by using a razor blade to expose the membrane cross-section and the internal surface of microcapsules. Prior to observation, they were sputter coated with Pt/Pd target (80/20) generating a thin film with 6 nm of thickness (208 HR High Resolution Sputter Coater, Cressington). The microcapsules were imaged on an ultra-high resolution field emission gun scanning electron microscope (FEG/SEM, FEI Nova 200 NanoSEM).

Microcapsule permeability to Imoglobine G (IgG) antibody

In order to assess IgG (Mw = 146-155 KDa, Abcam, UK) diffusion into the microcapsule interior, IgG was labelled with fluorescent dye (fluorescein isothiocyanate, FITC) which allows measuring protein sensitively. IgG was dissolved in sodium carbonate buffer (0.1 M, pH 9) at 2 mg/mL concentration. The fluorescein dye, dissolved in DMSO (1 mg/mL) was added into protein solution (1/1, v/v) and gently mixed for 8 hour at 4 $^{\circ}$C in a dark room. Afterwards, the reaction was quenched by adding of ammonium chloride to final concentration of 50 mM. The solution

was dialyzed against distilled water in the darkness to remove unconjugated FITC. Finally, the dialyzed solution was freeze-dried in a light protected vessel.

Equal volumes of xanthan-DOPE and xanthan-DOPE\PLL microcapsules (400 µL) and IgG-FITC (400 µL, 15 mg/mL solution in 0.9% NaCl) were shaken in a water-shaker bath at 37 ºC and aliquots of 5 µL were collected from 0 to 3h. Concentrations of The fluorescence (485/528 nm excitation/emission) of IgG-FITC in aliquots were measured on a microplate reader (BIO-TEK, SYNERGIE HT, USA) and their concentrations were calculated after constructing a standard curve from IgG standards.

Mechanical stability

The mechanical strength of xanthan-DOPE microcapsules was evaluated by agitating 100 microcapsules (uncoated and coated with PLL) in a flat rotator at maximum rate (about 240 rpm, DSR-2800V, Digisystem Laboratory Instruments Inc., Taiwan). The microcapsules were distributed in 24 well plates (10 per well) with 1 mL of PBS. At various time intervals (1, 2, 3, 6, and 24 h) the number of ruptured capsules was counted by observation on a light microscope and the percentage of ruptured capsules in function of time was determined.

Cell culture and encapsulation

Cell expansion prior to encapsulation

The murine ATDC5 chondrocyte cells were cultured in basic medium, consisting on Dulbecoo's Modified Eagle's Medium (DMEM, Sigma-Aldrich) with phenol red, supplemented with 10% fetal calf serum (FCS, Biochrom AG), 5 mM L-Glutamine (Sigma) and 1% of antibiotic-antimycotic mixture (Sigma) and maintained at 37 °C in a humidified atmosphere of 5% CO_2. The medium was replaced every two days. At passage 10, cells were detached with trypsin/EDTA and counted in a hemacytometer for encapsulation. A cell suspension (5×10^6 cells/mL, 0.1 mL) was mixed with xanthan-DOPE solution (1.9 mL, 1 wt% final concentration). The microcapsules were fabricated as described previously for microcapsule preparation.

Cell viability

Live/dead cell assay

Calcein AM (Sigma) solution (2/1000, v/v) was prepared in DMEM medium without FCS and phenol red. Propidium iodide (PI, Molecular Probes, Invitrogen) solution was prepared by mixing 2 µL PI (1 mg/mL) with 20 µL (1 mg/mL) RNAse A (USB corporation) and 2 mL PBS. The

microcapsules with encapsulated cells and controls (without cells) were collected from the culturing plates and incubated with calcein-AM and propidium iodide solutions at 37 ºC for 10 min protected from light . Microcapsules were then observed under fluorescent microscopy using an Axioplan Imager Z1m (Zeiss, Germany) microscope.

AlamarBlue® assay

The metabolic activity of encapsulated cells over time was assessed using the AlamarBlue® assay (AbD Serotec). AlamarBlue® was added (10% of the volume of the well) to each well containing the encapsulated cells and the plate was incubated at 37 ºC for 20 hours protected from light. After incubation, the absorbance was read at 570 and 600 nm on a microplate reader (BIO-TEK, SYNERGIE HT, USA). The percentage of reduced AlamarBlue® was calculated according the manufacturer instructions.

Cellular proliferation assay – DNA quantification

ATDC5 proliferation within the capsules was determined using a fluorimetric dsDNA quantification kit (PicoGreen, Molecular Probes, Invitrogen). For this purpose, the microcapsules collected at days 1, 7, 14 and 21 were washed twice with sterile PBS (Sigma, USA) solution and placed in 1 mL of ultra-pure water. Capsules with and without cells were stored at -80 ºC until further analysis. Prior to DNA quantification, samples were thawed and broken by pipetting up and down using a syringe with a hypotonic needle (21 G) to disrupt the material and facilitate DNA extraction. 28.7 µL of each sample and standards (0-2 mg/mL) were transferred to an opaque 96 well plate. Then 71.3 µL of PicoGreen solution and 100 µL of Tris-EDTA buffer were added. Standards and samples were prepared in triplicate. The plate was incubated for 10 minutes in the dark and the fluorescence was measured using an excitation wavelength of 485 nm and emission of 528 nm. DNA amounts were calculated from the calibration curve obtained by dsDNA standards (Molecular Probes, Invitrogen).

Statistical analysis

The results of DNA quantification and cell viability are expressed as a mean ± standard deviation with n=3 for each group. Statistical significance of differences was determined using unpaired student's t-test multiple comparison procedure at a confidence level of 95 % (p<0.05).

3. RESULTS AND DISCUSSION

This study addresses the use of a phospholipid polysaccharide that spontaneously self-assembles into capsular structures for the encapsulation of cells in a microfluidic device. To

obtain an amphiphilic polysaccharide, DOPE phospholipid was conjugated to the anionic and pH sensitive xanthan macromolecule (Figure V.1.A) so that hydrophobic forces can be engaged in the self-assembly process upon charge screening of xanthan by pH changes or electrolyte addition. Xanthan has hydroxyl and carboxyl groups available for chemical modification for obtaining xanthan derivatives. The chemical modification performed in this study is represented in Figure V.1.B and the obtained derivative was characterized by spectroscopy and microscopy techniques.

Fourier Transformed Infra Red spectroscopy

FTIR spectrum of xanthan-DOPE (Figure V.2.A) shows an increase in the intensity of the bands at 1735 and 1624 cm^{-1} assigned to the carbonyl groups. These bands derive from the acetate and pyruvate groups present in xanthan in addition to carbonyl from DOPE. Bands at 2935 and 2856 cm^{-1} indicated the presence of the aliphatic DOPE chains (-CH_3 and -CH_2 respectively). In addition, the appearance of bands at 1166, 1081and 977 cm^{-1}, representative of the stretch vibrations of P=O, P-OH and P-O of phosphate group, respectively, was also observed. Taken together, these observations indicate that DOPE was successfully grafted into xanthan.
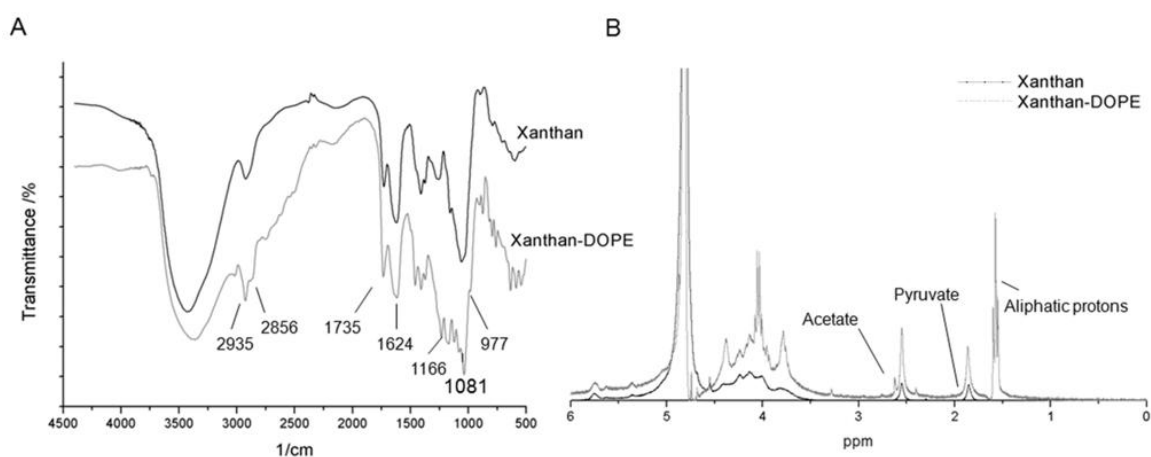
Figure V.2. FTIR (A) and ^{1}H NMR at 60 °C (B) spectra of native xanthan and xanthan-DOPE.

[1]H Nuclear Magnetic Ressonance spectroscopy

^{1}H NMR spectrum of xanthan-DOPE (Figure V.2.B) shows the appearance of new signals in the range of 1-1.5 ppm attributed to aliphatic protons from DOPE. Moreover, it displays new signals in the range of 3.3-3.7 ppm and also the increase on the intensity of the protons from pyruvate and acetate groups, demonstrating the changes in the native structure of xanthan.

Degree of substitution

As determined by potentiometric titration, a degree of substitution (DS) about 1.16 ± 0.024 was obtained considering the two carboxylic acid groups present in the xanthan repeating unit.

Wide Angle X-ray Scattering

To determine whether there were any ordered structures after phospholipid conjugation, we carried out WAXS experiments. Comparing the diffractograms of xanthan and xanthan-DOPE (Figure V.3.A) the appearance of new peaks on xanthan-DOPE pattern at 17.7, 20.66, 21.51, 24.11 and 25.84° suggests the presence of ordered molecular arrangement.

When comparing with X-ray diffraction of palmitoyl xanthan measurements described in our recent study[18], it is apparent that xanthan-DOPE presents more diffraction points with higher intensities. It can be deduced that the hydrophobic effect in xanthan-DOPE is stronger and consequently the intermolecular interactions resulted from the self-assembly could expected to be higher due to the higher degree of substitution and higher number of hydrophobic chains (two alkyl chains per unit of DOPE grafted).

Molecular conformation – Circular Dichroism spectroscopy

CD spectroscopy is a suitable technique to predict molecular conformation in liquid state. We used CD to investigate changes in molecular structure of xanthan after the hydrophobization of xanthan with DOPE.

The spectrum of both polymers (Figure V.3.B) showed an increase in peak height with maximum absorption wavelength at 196 nm (ordered state) and a decrease of the minimum with displacement at higher wavelengths at 220 nm (disordered state)[18]. Despite both polymers present similar CD signatures, for xanthan-DOPE the difference in absorption of left-hand and right-hand circularly of polarized light is less accentuated, suggesting that introduction of such hydrophobic tails are improving stability of the native structure of xanthan.

Polarized light microscopy

By polarized light microscopy, the birefringence dispersion in xanthan-DOPE (Figure V.3.C) allows the detection of organized structures disposed with same orientation as a result of the hydrophobic self-assembly of the xanthan amphiphile, while in native xanthan for the same conditions this scenario cannot be visualized.
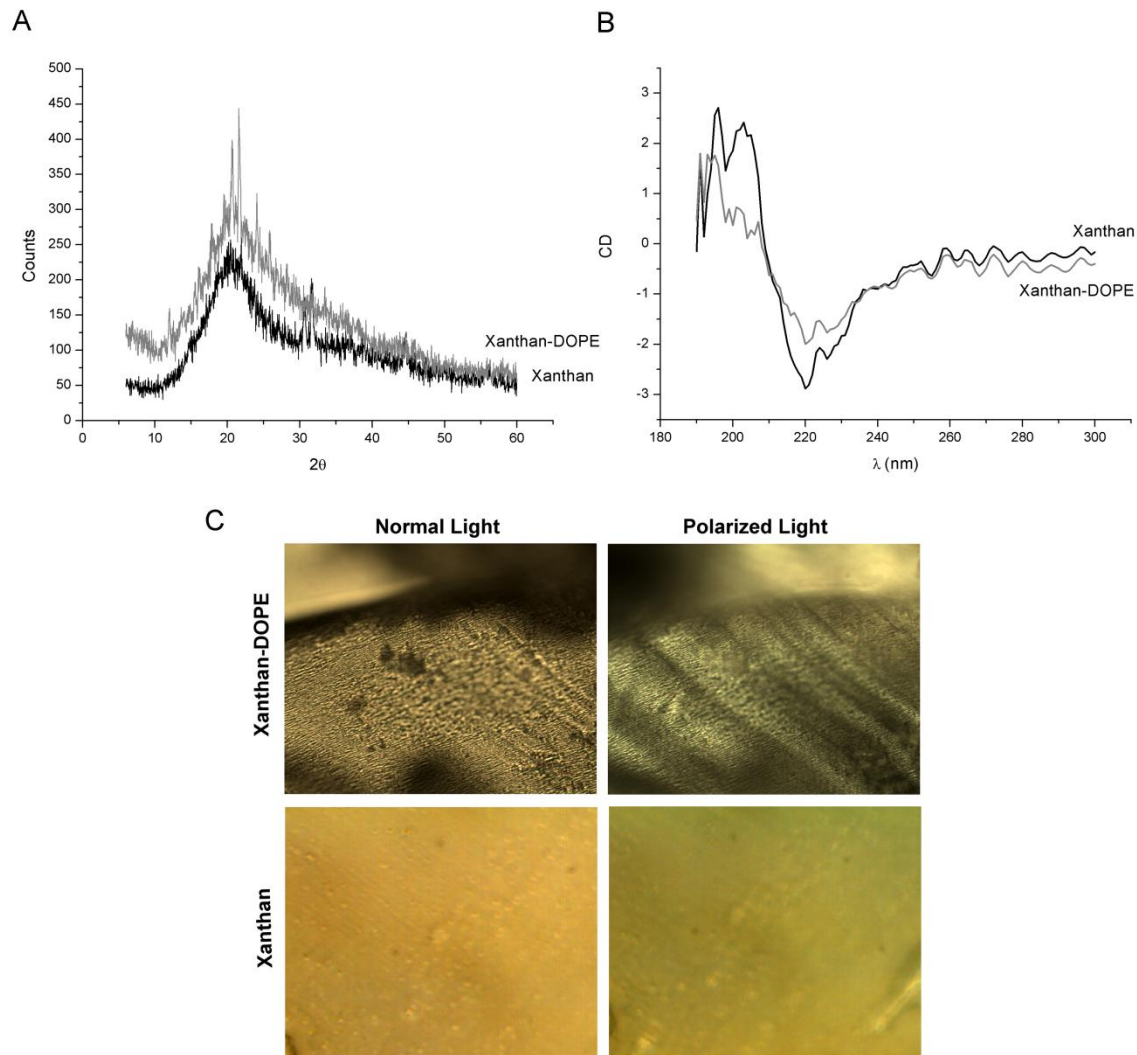
Figure V.3. Characterization of native xanthan and xanthan-DOPE by WAXS (A), CD at 0.1 wt% (B) and polarized light microscopy in the aqueous state (C).

Polarized light microscopy in combination with WAXS and CD analyses revealed the presence of organized structures. It is believed that the hydrophobic nature imparted to native xanthan after phospholipd conjugation is the main driving force for the observed molecular organization.

A key challenge in cell encapsulation consists in obtaining reproducible monodisperse microcapsules with a minimum number of fabrication steps. After investigating the physicochemical properties of xanthan-DOPE, we used microfluidic technology (Figure V.4) to realize the self-assembly of the lipid-polymer (xanthan-DOPE) into microcapsules for cell encapsulation.
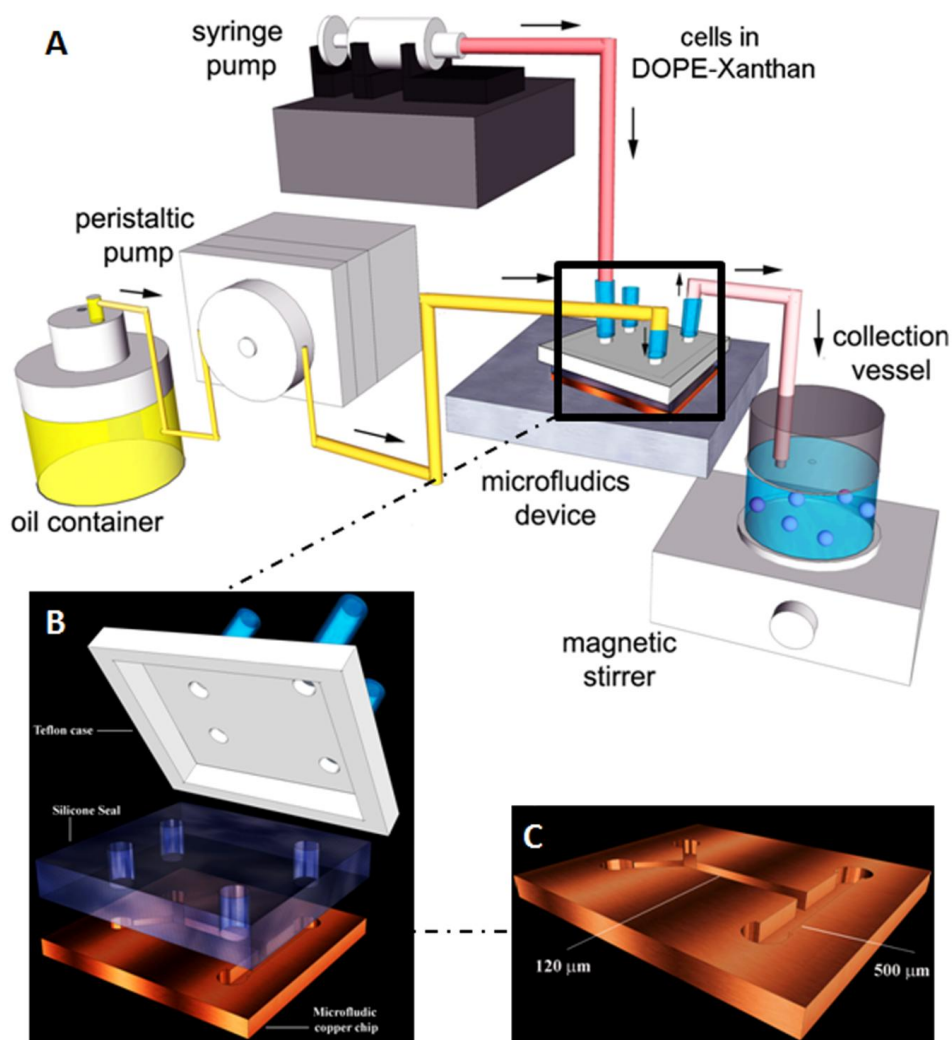
Figure V.4. Schematic representation of the set-up for cell encapsulation (A) showing details of the microfluidics assembly (B) and copper chip device (C).

The morphology and microstructure of the developed microcapsules were investigated using optical and electron microscopy. Their permeability, mechanical resistance and ability to encapsulate cells was also assessed.

Bright Field Microscopy

Figure V.5.A displays images of the obtained microcapsules (uncoated and coated with PLL) observed by bright field microscopy showing their spherical shape and uniform size. The shape and size of both microcapsules remained constant over time, confirming their stability. Uncoated microcapsules present a diameter size around 530 μm, but when coated with PLL the diameter

size decreased for 350 µm. This could be a consequence of polyelectrolyte complexation at which the electrostatic forces may lead to stronger gel formation, thereby less swelling[22] in aqueous media as compared to self-assembled gel that is based on relatively weaker hydrophobic forces.
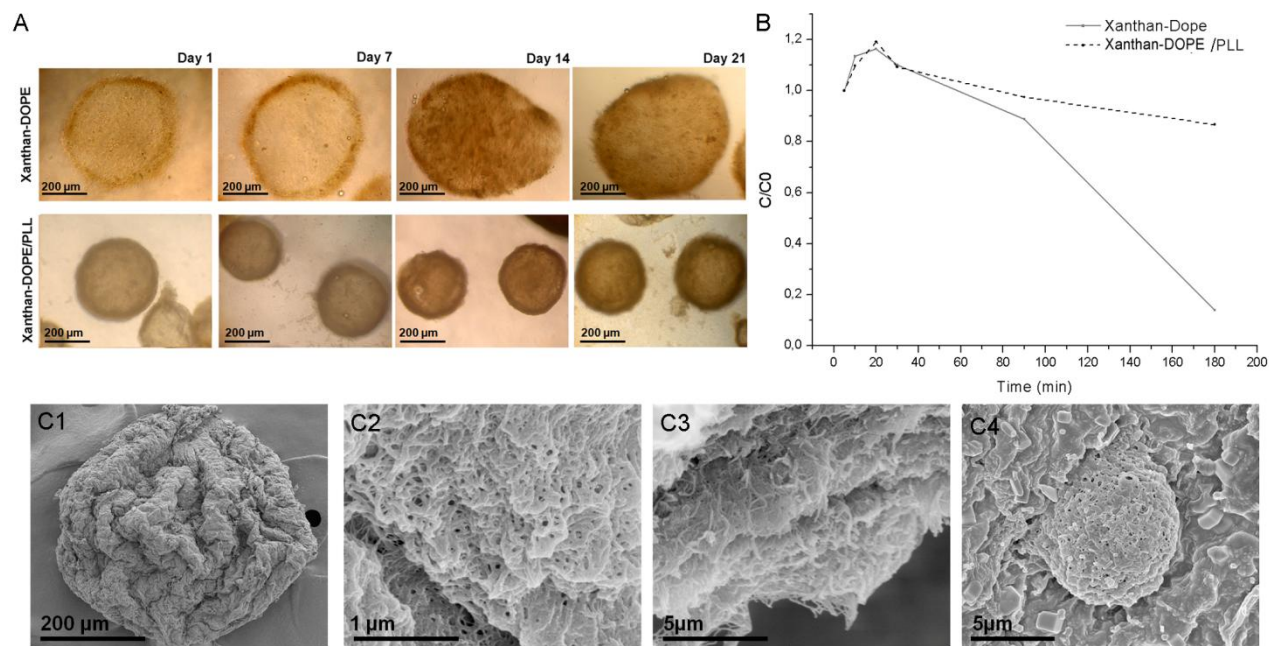
Figure V.5. (A) Bright field light microscopy images of xanthan-DOPE and xanthan-DOPE microcapsules coated with PLL. (B) Permeability of xanthan-DOPE and xanthan-DOPE/PLL microcapsules, assessed by IgG (Mw=146-155 KDa) diffusion, where C is the IgG concentration at different time points and C_o initial concentration. (C) SEM images showing the overall structure of xanthan-DOPE/PLL microcapsules (C1), external surface (C2), cross-section (C3) and inner wall with morphological feature of a cell attached to the microcapsules surface (C4).

Microcapsule permeability and stability

The permeability of the microcapsules to oxygen and nutrients and its impermeability to immune cells and antibodies is one of the crucial criteria to be considered when developing microcapsules for cell encapsulation purposes[23-24]. The required immunoisolation for a successful transplantation of encapsulated cells depends on the selective permeability property of the microcapsules[23,25].

The permeability of xanthan-DOPE and xanthan-DOPE/PLL microcapsules was assessed by immersing microcapsules in a labeled IgG solution and the diffusion of the protein from surrounding medium to the microcapsule interior was evaluated. Both microcapsules are permeable to IgG (Figure V.5.B), but as expected, the PLL coated microcapsules are more

effective on protecting encapsulated cells from immunotoxins, since the diffusion of the antibody is lower when compared with the uncoated ones.

To ensure that the developed microcapsules maintain their structural integrity when dispersed in aqueous media, we have performed mechanical stability tests[26]. Both types of microcapsules demonstrated to be resistant to rupture, when subjected to strong agitation in PBS (data not shown). This result showed the efficiency of self-assembly process by phospholipid-conjugated polysaccharide in preserving microcapsule structure for prolonged periods in vitro. Nevertheless, PLL coated xanthan-DOPE microcapsules are expected to have higher mechanical strength since it was demonstrated before in literature that PLL coating improved the mechanical strength of alginate microcapsules[26]

Scanning Electron Microscopy

SEM images of the microcapsules coated with PLL (Figure V.5.C) confirmed the spherical shape and revealed a porous outer layer and a denser inner layer. The cross-section evidences a porous and fibrillar structure as a result of the self-assembly of xanthan-DOPE and further interactions with PLL. SEM analysis on cell cultured microcapsules after 21 days revealed that the cells were partially entrapped on the internal side of the dense microcapsule wall. This may be explained by the fact that nutrients and oxygen are more readily available at the capsule surface than in the microcapsule core.

Live/dead assay

The fluorescence microscopy images displaying the live/dead assay of encapsulated cells showed that the cells remained viable and well distributed within the microcapsules during the 21 days of *in vitro* culture (Figure V.6.A). While most cells appear to be viable, in the PLL coated microcapsules few non-viable cells (red cells) were also observed.

AlamarBlue® assay

In order to quantify the cellular metabolic activity of encapsulated cells, the AlamarBlue® assay was performed. Figure V.6.B shows that the encapsulated ATDC5 cells were able to reduce AlamarBlue® during 21 days of *in vitro* culture with slight increase over time. Furthermore, ATDC5 cells encapsulated in uncoated xanthan-DOPE microcapsules exhibited significantly higher metabolic activity ($p < 0.05$) for the initial time points than in those coated with PLL. Nevertheless, at the end of 21 days the cells encapsulated in xanthan-DOPE/PLL presented higher metabolic activity than the uncoated ones, but not statistically significant.
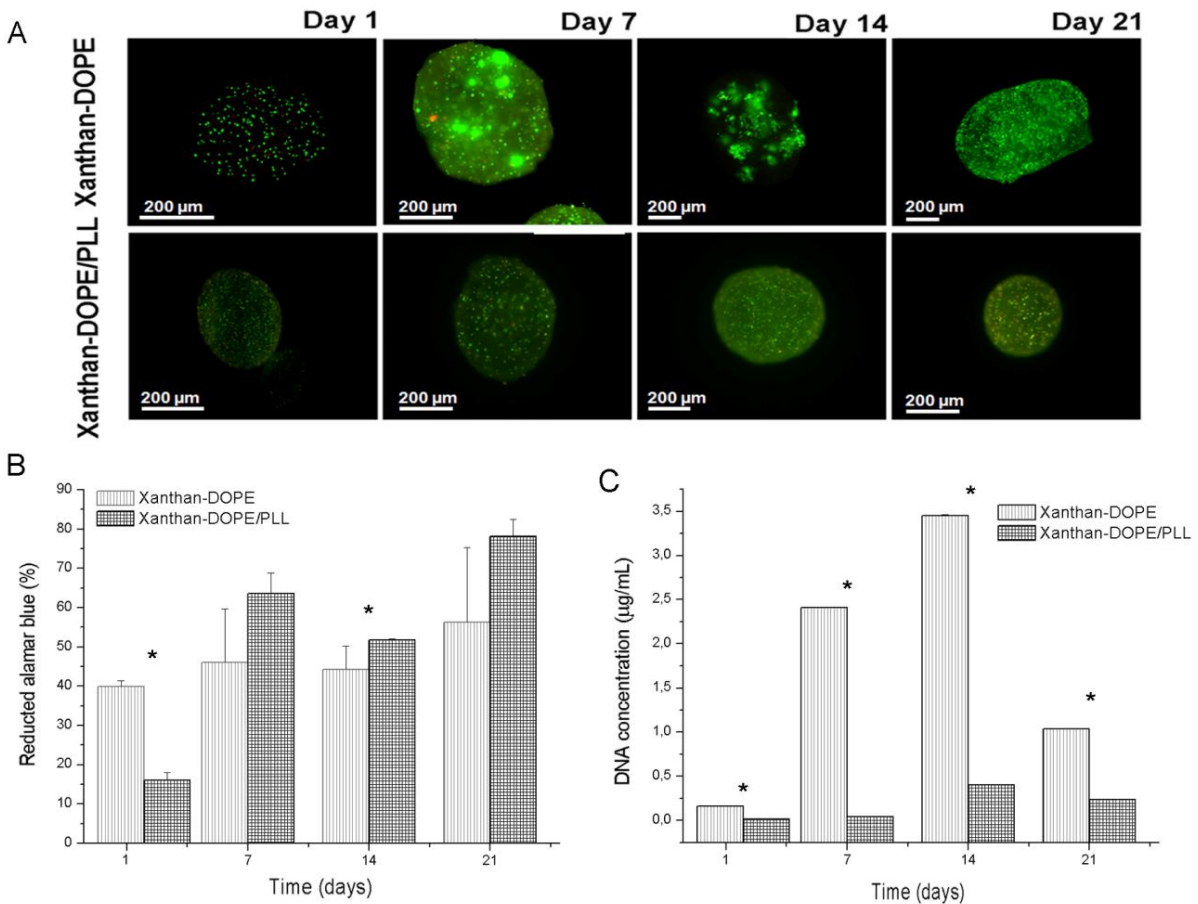
Figure V.6. *In vitro* viability and proliferation of ATDC5 cells cultured in xanthan-DOPE and xanthan-DOPE-PLL microcapsules. (A) Fluorescence microscopy images displaying the live/dead assay of encapsulated cells (green cells are live, red cells are dead) showing that the cells remain viable in the microcapsules up to 21 days of culture. (B) Metabolic activity and (C) proliferation of encapsulated cells determined by AlamarBlue® assay and DNA quantification. Results are expressed as means ± standard deviation with *n*=3. *Indicates a significant difference (*p*< 0.05) between xanthan-DOPE and xanthan-DOPE/PLL microcapsules for different time points.

When comparing ATDC5 cells within xanthan-DOPE/PLL microcapsules with the same cells encapsulated in palmitoyl xanthan/PLL[18], although the methodology for fabricating microcapsules was different (microfluidics and micro-droplet generator, respectively) the cellular metabolic activity seems to be apparently higher when cells are encapsulated in Xanthan-DOPE matrix. These observations are evincing the potential of phospholipids to be used to form unique and organized structures, the microcapsules in this specific case, through the spontaneous self-assembly, simultaneously with its advantage of the inherent biocompatibility of the lipids as a component of the cytoplasmatic membrane in biomimetic systems[1]. However, regarding the permeability results, the uncoated microcapsules were more permeable to antibodies than those

containing PLL, suggesting that those within PLL are more effective for prolonged time periods in terms of immunoisolation and able to maintain or even enhance the cellular viability.

Proliferation assay: DNA quantification

The quantification of DNA over the culture time revealed (Figure V.6.C) a gradual and significant increase of DNA ($p<0.05$) as a result of improved cellular proliferation in both microcapsule types (uncoated and PLL-coated microcapsules). Curiously, the cells within xanthan-DOPE-PLL are expressing significantly ($p<0.05$) lower cellularity comparatively to the uncoated ones. We believe that the lower cellularity observed in the coated microcapsules may be related with the higher rigidity of the wall membrane and decreased permeability to nutrients provided by the interactions between PLL and xanthan-DOPE. The cells were found to be entrapped in the microcapsule wall (Figure V.5.C) that may result in a decreased mobility and ability to proliferate. Additionally, in previous works[27], it was demonstrated that the cell growth may be inhibited by the reduced volume inside microcapsules as it may happen in the case of coated capsules with PLL.

The use of PLL as coating matrix in alginate microcapsules containing transplanted islets has shown to cause inflammatory responses when transplanted[28] which poses concerns for their application *in vivo*. Even low concentrations of PLL[29], necrosis effect was observed on islet transplants[26].

4. CONCLUSIONS

An amphiphilic xanthan derivative (xanthan-DOPE) was successfully synthesized which allowed its self-assembly into stable hollow capsular structures when subjected to physiological pH and ion concentrations. We have demonstrated that using a microfluidic device, stable self-assembled and size-controlled spherical microcapsules were obtained, and cells could be encapsulated within the xanthan-DOPE microcapsules with enhanced metabolic activity for prolonged time, without the need of any external coat such as the potential immunogenic poly-L-lysine. In summary, these results suggest that xanthan-DOPE microcapsules might provide a biomimetic environment for cells to grow and thus be useful in cell-based transplantation therapies.

AKNOWLEDGEMENTS

REFERENCES

1. Collier JH, Messersmith PB. PHOSPHOLIPID STRATEGIES IN BIOMINERALIZATION AND BIOMATERIALS RESEARCH. Annual Review of Materials Research 2001;31(1):237-263.

2. Hase M, Yamada A, Hamada T, Baigl D, Yoshikawa K. Manipulation of Cell-Sized Phospholipid-Coated Microdroplets and Their Use as Biochemical Microreactors. Langmuir 2006;23(2):348-352.

3. Gazit E. Self-assembled peptide nanostructures: the design of molecular building blocks and their technological utilization. Chemical Society Reviews 2007;36(8):1263-1269.

4. Vonarbourg A, Passirani C, Desigaux L, Allard E, Saulnier P, Lambert O, Benoit J-P, Pitard B. The encapsulation of DNA molecules within biomimetic lipid nanocapsules. Biomaterials 2009;30(18):3197-3204.

5. Yamada A, Yamanaka T, Hamada T, Hase M, Yoshikawa K, Baigl D. Spontaneous Transfer of Phospholipid-Coated Oil-in-Oil and Water-in-Oil Micro-Droplets through an Oil/Water Interface. Langmuir 2006;22(24):9824-9828.

6. He Q, Cui Y, Li J. Molecular assembly and application of biomimetic microcapsules. Chemical Society Reviews 2009;38(8):2292-2303.

7. Besheer A, Hause G, Kressler J, Mader K. Hydrophobically modified hydroxyethyl starch: Synthesis, characterization, and aqueous self-assembly into nano-sized polymeric micelles and vesicles. Biomacromolecules 2007;8(2):359-367.

8. Lemarchand C, Gref R, Couvreur P. Polysaccharide-decorated nanoparticles. European Journal of Pharmaceutics and Biopharmaceutics 2004;58(2):327-341.

9. Akiyoshi K, Kang EC, Kurumada S, Sunamoto J, Principi T, Winnik FM. Controlled Association of Amphiphilic Polymers in Water: Thermosensitive Nanoparticles Formed by Self-Assembly of Hydrophobically Modified Pullulans and Poly(N-isopropylacrylamides). Macromolecules 2000;33(9):3244-3249.

10. Hartgerink JD, Zubarev ER, Stupp SI. Supramolecular one-dimensional objects. Current Opinion in Solid State and Materials Science 2001;5(4):355-361.

11. Duval-Terrié C, Huguet J, Muller G. Self-assembly and hydrophobic clusters of amphiphilic polysaccharides. Colloids and Surfaces A: Physicochemical and Engineering Aspects 2003;220(1-3):105-115.

12. Bourov GK, Bhattacharya A. Brownian dynamics simulation study of self-assembly of amphiphiles with large hydrophilic heads. Journal of Chemical Physics 2005;122(4):1-6.

13. Akiyoshi K, Sunamoto J. Supramolecular assembly of hydrophobized polysaccharides. Supramolecular Science 1996;3(1-3):157-163.

14. Rouzes C, Durand A, Leonard M, Dellacherie E. Surface Activity and Emulsification Properties of Hydrophobically Modified Dextrans. Journal of Colloid and Interface Science 2002;253(1):217-223.

15. Cheng J, Zhu J-b, Wen N, Xiong F. Stability and pharmacokinetic studies of O-palmitoyl amylopectin anchored dipyridamole liposomes. International Journal of Pharmaceutics 2006;313(1-2):136-143.

16. Rodrigues JS, Santos-Magalhães NS, Coelho LCBB, Couvreur P, Ponchel G, Gref R. Novel core(polyester)-shell(polysaccharide) nanoparticles: protein loading and surface modification with lectins. Journal of Controlled Release 2003;92(1-2):103-112.

17. Rouzes C, Leonard M, Durand A, Dellacherie E. Influence of polymeric surfactants on the properties of drug-loaded PLA nanospheres. Colloids and Surfaces B: Biointerfaces 2003;32(2):125-135.

18. Mendes AC, Baran ET, Nunes C, Coimbra MA, Azevedo HS, Reis RL. Palmitoylation of xanthan polysaccharide for self-assembly microcapsule formation and encapsulation of cells in physiological conditions. Soft Matter 2011;7(20):96-47.

19. Mendes AC, Baran ET, Pereira RC, Azevedo HS, Reis RC. Encapsulation and Survival of a Chondrocyte Cell Line within Xanthan gum derivative. 2010.

20. Greg T H. Preparation of Liposome Conjugates and Derivatives. Bioconjugate Techniques. San Diego: Academic Press; 1996. p 528-569.

21. Ge H-C, Luo D-K. Preparation of carboxymethyl chitosan in aqueous solution under microwave irradiation. Carbohydrate Research 2005;340(7):1351-1356.

22. Thu B, Bruheim P, Espevik T, Smidsrød O, Soon-Shiong P, Skjåk-Bræk G. Alginate polycation microcapsules: II. Some functional properties. Biomaterials 1996;17(11):1069-1079.

23. Hernández RM, Orive G, Murua A, Pedraz JL. Microcapsules and microcarriers for in situ cell delivery. Advanced Drug Delivery Reviews 2010;62(7-8):711-730.

24. Murua A, Portero A, Orive G, Hernández RM, de Castro M, Pedraz JL. Cell microencapsulation technology: Towards clinical application. Journal of Controlled Release 2008;132(2):76-83.

25. Briscaronscaronová M, Lacík I, Powers AC, Anilkumar AV, Wang T. Control and measurement of permeability for design of microcapsule cell delivery system. Journal of Biomedical Materials Research 1998;39(1):61-70.

26. Darrabie MD, Kendall Jr WF, Opara EC. Characteristics of Poly-l-Ornithine-coated alginate microcapsules. Biomaterials 2005;26(34):6846-6852.

27. Breguet V, Gugerli R, von Stockar U, Marison I. CHO immobilization in alginate/poly-l-lysine microcapsules: an understanding of potential and limitations. Cytotechnology 2007;53(1):81-93.

28. Horcher A, Zekorn T, Siebers U, Klock G, Frank H, Houben R, Bretzel RG, Zimmermann U, Federlin K. Transplantation of microencapsulated islets in rats: evidence for induction of fibrotic overgrowth by islet alloantigens released from microcapsules. Transplant Proc 1994;26(2):784-6.

29. Strand BL, Ryan L, Veld PI, Kulseng B, Rokstad AM, Skj, aring, k-Braek G, Espevik T. Poly-L-Lysine Induces Fibrosis on Alginate Microcapsules via the Induction of Cytokines. Cell Transplantation 2001;10(3):263-275.

Chapter VI

MICROFLUIDICS FABRICATION OF SELF-ASSEMBLED PEPTIDE-POLYSSACCHARIDE MICROCAPSULES AS 3D ENVIRONMENTS FOR CELL CULTURE

MICROFLUIDICS FABRICATION OF SELF-ASSEMBLED PEPTIDE-POLYSSACCHARIDE MICROCAPSULES AS 3D ENVIRONMENTS FOR CELL CULTURE

ABSTRACT

We report a mild cell encapsulation method based on self-assembly and microfluidics technology. Xanthan gum, an anionic polysaccharide, was used to trigger the self-assembly of a positively charged multidomain peptide. The self-assembly results in the formation of a nanofibrous matrix and using a microfluidic device, microcapsules with homogenous size were fabricated. The properties and performance of xanthan-peptide microcapsules were optimized by changing peptide/polysaccharide ratio and their effects on the microcapsule permeability and mechanical stability were analyzed. The effect of microcapsule formulation on viability and proliferation of encapsulated chondrocytic (ATDC5) cells were also investigated. The encapsulated cells were metabolically active, showing an increased viability and proliferation over 21 days of *in vitro* culture, demonstrating the long-term stability of the self-assembled microcapsules and their ability to support and enhance the survival of encapsulated cells over prolonged time. Self-assembling materials combined with microfluidics demonstrated to be an innovative approach in the fabrication of cytocompatible matrix for cell micro-encapsulation and delivery.

1. INTRODUCTION

Molecular self-assembly relies on the design of molecular segments that interact with each other in a coordinated way to form large and more complex supramolecular assemblies[1] with defined morphologies (tubes, spheres, fibrils) and can occur through a change in temperature, pH or ion concentration, or triggered by radiation[2]. Self-assembling is, therefore, an appealing methodology for the bottom-up fabrication of new biomaterials allowing to achieve very high accuracy in positioning small components (nanometer resolution) with signaling functionality. In spite of its importance in the bottom-up fabrication of functional nanomaterials, the use of self-assembly processes has been limited by a lack of temporal and spatial control[3]. Most self-assembling materials are macroscopically disordered which can limit their bulk properties and consequently their functionality/performance. Alignment of nanostructures provides a strategy to control materials properties and macro-scale behavior by tuning the directionally of interactions at the nano-scale. Different strategies have been investigated to control order in materials and several factors may play a significant role on the dynamics and kinetics of self-assembly, including, concentration gradients, diffusion/mobility of molecules and supramolecular aggregates that can be generated under specific processing environments (temperature, mechanical agitation, electrical fields, spatial confinement)[4-5]. Some of these techniques are based on the effects that spatial confinement has on the behavior of materials to guide micro- or nano-scale ordering. There is a growing recognition that the physical properties of materials can also regulate biological responses. For example, the *in vivo* performance of particle materials are dependent on their size and shape[6]. It is known that particle size controls their transport and adhesion in specific body regions such as in blood vessels and airways[6-7]. In addition, shape assumes an important role in the regulation/modulation of cellular responses[6,8]. Although there are numerous techniques and methods for microcapsule formation, the integration of self-assembly nanofabrication into existing microtechnologies can still offer new possibilities to fabricate complex capsular structures with increased level of bioactivity. Microfluidic devices have been recognized as a potential tools for the fabrication of micro-engineered hydrogels[9-10]. This fabrication process allows the generation of hydrogels with controlled size and shape by changing viscosity of polymer solution, flow rate and dimensions of micro-channels. Small amounts of fluids can be manipulated using channels with dimensions of tens to hundred

of micrometers. Manipulation of multiphase flows in microfluidics, where the viscous and surface tension forces are used to create homogeneous structures and operating under laminar flow without turbulence, is an appealing technology to be used with self-assembling materials for encapsulation of delicate biological agents and cells[9-11]. Moreover, it can provide a miniature and

sterile platform without the need of a clean room making this fabrication process suited for cell encapsulation.

Biomaterials that can undergo self-assembly in conditions that are cell-compatible and be injected into the body in a minimally invasive way can find numerous applications, including controlled growth of cell populations for cell therapies or to promote regenerative processes *in vivo*[12-13]. In this context, peptides are excellent building blocks to form complex nanostructures by self-assembly processes. They can self-assemble into fibril nanostructures, thus recreating some of the architectural features of the natural extracellular matrix[14]. Another intrinsic advantage of using peptides as structural units is the ability to incorporate into their structure known biological signals that are recognized by cell receptors and thus mediate cell specific functions[15] (e.g. adhesion, proliferation, differentiation).

Hartgerink's group has proposed multi-domain peptides based on ABA block motif[16-17] in which forces favoring self-assembly into a nanofiber versus those favoring disassembly could be easily modified by balancing the forces of block A against B. These peptides consist of a central block of glutamine-leucine repeats (B block, with ability to induce the assembly into β-sheets) and two flanking positively charged lysine (A blocks). They have shown that for example the $K_2(QL)_6K_2$ peptide (Figure VI.1.B) has the ability to self-assemble into organized nanostructures (e.g. nanofibers) and form self-supporting gels when the charge is screened (e.g. in presence of multivalent anions such as phosphate)[16].
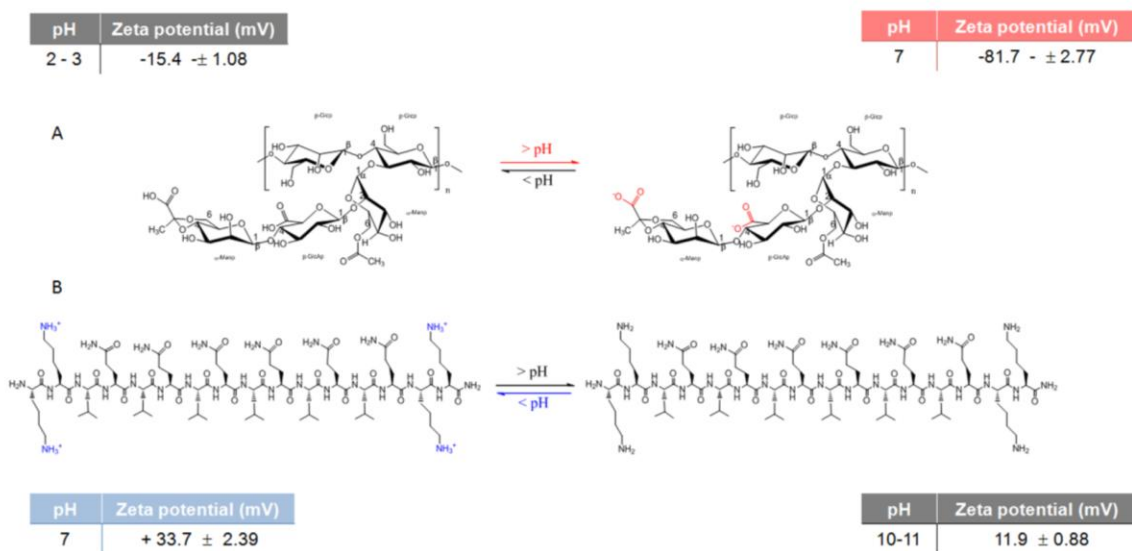
Figure VI.1. Chemical structure of xanthan repeating unit (A) and $K_2(QL)_6K_2$ peptide (B). Zeta potential of both component solutions (0.1 wt%) was measured at different pHs to demonstrate the nature of ionizable groups in the self-assembling components.

Our group has been investigating xanthan gum (Figure VI.1.A), an anionic extracellular bacterial polysaccharide, as a potential cell encapsulation matrix. We have used different strategies, carboxymethylation[18] and palmitoylation[19] of xanthan, to drive the assembly of this polysaccharide into capsular structures with controlled properties. Following these studies, we thought on using xanthan gum to drive the self-assembly of the $K_2(QL)_6K_2$ multi-domain peptide, proposed by Hartgerink group, and microfluidic technology to convert the self-assembled structures into spherical microcapsules for cell encapsulation.

The self-assembly between peptide amphiphiles and polysaccharides has been reported previously[20-21], showing the formation macroscopic structures with highly organized architecture at the nanoscale. In this work, the properties and microcapsule performance of xanthan-peptide microcapsules were optimized by changing peptide/polysaccharide ratio and their effects on the membrane permeability, microcapsule stability and cell function (viability and proliferation) of encapsulated chondrogenic cell line were investigated.

2. MATERIALS AND METHODS

Materials

All chemicals, including xanthan gum from *Xanthomonas campestris*, were obtained from Sigma/Aldrich (USA) unless otherwise indicated. The chemicals were used as received. The average molecular weight (Mw) of xanthan was estimated by size-exclusion chromatography as 152 KDa[22].

Peptide synthesis and purification

All amino acids and Rink MBHA resin were purchased from Novabiochem Corporation (USA). $K_2(QL)_6K_2$ peptide was synthesized by solid-phase peptide synthesis in a automated peptide synthesizer (CS Bio, USA) using Fmoc strategy. After synthesis, the peptide was cleaved from the resin using a cocktail of trifluoroacetic acid (TFA), triisopropylsilane, and water (95:2.5:2.5). The mass of the peptide (Mw = 1977.44 g.mol^{-1}) was confirmed by mass spectrometry (see supplementary information) and its isolation from impurities was achieved by purification of the crude product in a 2545 Binary Gradient preparative high-performance liquid chromatography (Waters, USA) with 2489 UV/Visible Detector (Waters, USA) using C18 column (Atlantis Prep OBD T3 Column, Waters, USA) and a water/acetonitrile (0.1% trifluoroacetic acid) gradient. TFA counter-ions were exchanged by sublimation from 0.1 M hydrochloric acid. Finally, the peptides were dialyzed against deionized water using 500 MWCO dialysis tubing (Spectrum Europe B.V.,

The Netherlands) to remove salts, lyophilized, to obtain a fluffy powder, and stored in closed containers at -20 ºC until use.

Characterization of peptide-xanthan interactions

Zeta potential

Zeta potential measurements of polymer and peptide solutions were performed at 25 ºC using a Zetasizer NanoZS Instrument (ZEN 3600, Malvern Instruments, Worcestershire, UK). Xanthan and $K_2(QL)_6K_2$ solutions were prepared at a concentration of 0.1 wt% with ultrapure water and its pH adjusted to the desired value by adding HCl (0.1 M) and NH_4OH (0.1 M).

Quartz crystal microbalance (QCM) with dissipation monitoring

QCM measurements were performed with an instrument with dissipation monitoring (QCM-D) from Q-Sense (Göteborg, Sweden). The experiments were performed at 24 ºC with 50 μL/min flow rate using gold coated crystals (model QSX301, Q-Sense, Göteborg, Sweden) previously cleaned with $H_2O_2(30\%)/NH_3(25\%)/H_2O$ (1:1:5) during 10 minutes at 75 ºC. The system was initially equilibrated with phosphate buffered saline (PBS) solution (10 mM, pH7.4) to obtain a stable frequency and dissipation baseline signal. Once the signals were stable, the buffer was replaced by a solution of xanthan (0.25 wt% in PBS) during 25 minutes. Then, the buffer was again introduced to remove weakly bound material. This step was followed by the introduction of the peptide solution (0.0025; 0.0625 or 0.125 wt% in H_2O) or BSA solution (0.5 mg/mL in PBS). Finally the system was rinsed with PBS solution.

Thickness was calculated by the Voigt model[23] incorporated in Q-Sense software using different overtones (7th; 9th, 11th,13th). The layer viscosity values used in the model were between 0.001 and 0.01 kg.ms^{-1}, the layer shear modulus between 10 and 10^5 Pa, and layer thickness values were between 10^{-10} a 10^{-6} m. For xanthan, a fluid density of 1000 kg.m-^{3}, fluid viscosity of 0.001 kg.ms^{-1} and layer density of 850 kg.m-^{3} were used. For the peptide modeling, a fluid density of 1300 kg.m-^{3}, fluid viscosity of 0.003 kg.ms^{-1} and layer density of 1600 kg.m-^{3} were used. For BSA modeling, a fluid density of 1000 kg.m-^{3}, fluid viscosity of 0.001 kg.ms^{-1} and layer density of 1500 kg.m-^{3} were used.

Microfluidic device fabrication

The device design was made by CAD software and printed onto a transparency sheet by using a desk top laser printer. This pattern subsequently served as a mask for copper etching. The laser

toner has been successfully exploited previously for applications as an etch mask for metal plates intended for microfluidics application[24]. A copper plate (1.5x1.5 cm, 0.675 mm thick, 0.99% annealed, Alfa Aesar, USA) was used as a substrate for developing microfluidic channels.
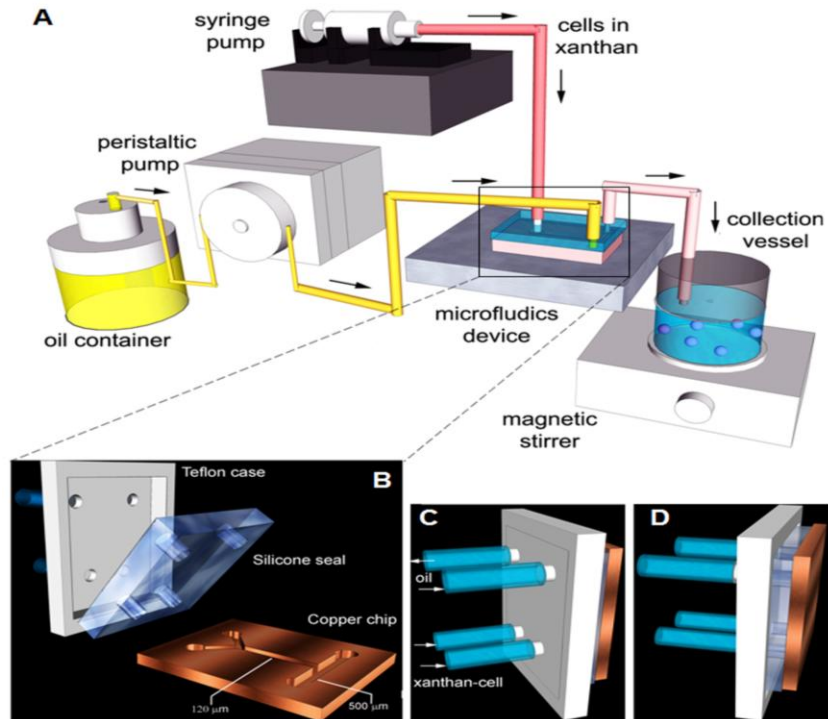
Figure VI.2. Schematic representation of the set-up for cell encapsulation (A) showing details of the micro-fluidics apparatus (B- view of disasembled microfluidics device which consists of a metal chip, silicone seal and TEFLON case). Side views of combined microfluidic device enabling fluid flows by backside adapters (B, C).

The melted toner adheres to the copper and is insoluble in ferric chloride solution, allowing it to serve as an etch mask for microchannel fabrication. Initially, the copper plate surface was cleaned by rubbing thoroughly with a fine steel wool. The plate was then sonicated 5 min in a solution of acetone-water (50%). The cleaned plate was transferred onto a hot plate at 200 ^{o}C and incubated for 2 min. The heated plate was then transferred immediately to printed-face of transparency and a metal block weighing approximately 10 kg was placed onto copper plate to facilitate toner transfer. After 2 min, the copper plate and transparency was placed to a freezer (-20 ^{o}C) and incubated for 5 min. After cooling, the transparency was carefully peeled off from copper plate. The back and front surface of plate, where there is no toner, was covered with plastic duct tape to protect unmasked region from etching process. The plate was etched in FeCl$_3$ solution (35%, 50 mL) in a glass beaker for 30 min at room temperature by manual

shaking of the solution. The etching was stopped by removing the plate and washing it under running water. After removing duct tapes from the etched plate, the plate was placed into acetone-water solution (50%) and sonicated for 10 min to remove toner from the surface. Beside, a poly(dimethyl siloxane) (PDMS) seal was prepared at 1/10 crosslinker/monomer ratio (w/w) (SYLGARD$^{®}$ 184 silicone elastomer kit, Dow Corning, USA) and the mixture was cured for 2 days at 37 ^{o}C in a rectangular mould. The seal was perforated at inlets and outlets of vertical and horizontal channels reserved for polymer-cell and oil flow, respectively (Figure VI.2.).

A piece of poly(tetrafluoro ethylene) (TEFLON) block was also machined for securing and precise positioning of the perforated silicone seal and allowing the transfer of fluids by providing 4 adopters at the backside for connecting silicone tubing from peristaltic and syringe pump (Figure VI.2.B-D).

Microcapsule preparation

Xanthan (1 wt%) was dissolved in PBS. The xanthan solution was injected into the microfluidics device using a syringe pump. The polymer microdroplets were generated inside the microfluidics device by shear stress when entered into a stream of mineral oil. The formed homogenous microdroplets were collected in a collector vessel containing $K_2(QL)_6K_2$ solution at different concentration (0.1, 0.25 and 0.5 wt%). About 10 µL of Tween 80 was added as emulsifying agent. The self-assembly of xanthan-peptide into microcapsules took place in the collector vessel by gently stirring of the polymer droplets over 15 minutes on a magnetic stirrer.

Microcapsule characterization

Light microscopy analysis.

Microscopic observations of the microcapsules were carried in a bright field light microscope (AXIOVERT 40 CFL, Germany) equipped with a digital camera (Canon Power shot G8, Japan).

Scanning Electron Microscopy (SEM) analysis

Prior to the SEM observations, the microcapsules were fixed with glutaraldehyde (Electron Microscopy Sciences, USA) solution (3%, v/v in PBS) at 4 ^{o}C for 1 h. The samples were further dehydrated in a graded ethanol series (20, 50, 60, 70, 80, 90 and 100%) followed by immersion in 100% hexamethyldisilazane (HMDS, Electron Microscopy Sciences, USA). Microcapsules were cut into half to expose the membrane cross-section and the internal surface of microcapsules. The specimens were mounted on aluminum stubs and sputter coated with Pt/Pd

target (80/20) generating a thin film with 6 nm of thickness (208 HR High Resolution Sputter Coater, Cressington). The microcapsules were imaged on an ultra-high resolution field emission gun scanning electron microscope (FEG/SEM, FEI Nova 200 NanoSEM).

Microcapsules permeability to Immunoglobulin G (IgG) antibody

IgG (Mw = 146-155 KDa, Abcam, UK) was labeled with fluorescein isothiocyanide (FITC) in order to determine the diffusion of the protein into the microcapsules using a highly sensitive techniques such as fluorescence spectroscopy. The IgG was dissolved in sodium carbonate buffer (0.1 M, pH 9) at 2 mg/mL concentration. The fluorescein dye, dissolved in DMSO (1 mg/mL) was added per mL of protein solution and gentle mixed for 8 hours at 4 °C in the dark. Afterwards, the reaction was quenched by adding ammonium chloride to a final concentration of 50 mM. The solution was placed into dialysis tubing and dialyzed against distilled water in the dark to remove unconjugated FITC. Finally, the dialyzed solution was freeze-dried in a light protected vessel. For permeability studies, equal volumes of microcapsules and IgG-FITC (15 mg/mL solution in NaCl 0.9%) were shaken in a water-shaker bath at 37 °C and samples of 5 μL were collected from 0 to 3 h. Concentrations of IgG-FITC were measured by fluorescence (485/528 nm) on a microplate reader (BIO-TEK, SYNERGIE HT, USA).

Mechanical stability

The mechanical testing used in this study were adapted from the work described for Darrabie and co-authors[25].

Induction of mechanical stress using osmotic pressure

Aliquots of xanthan-peptide microcapsules were placed in 10 mL of water and incubated for 24 h at 37 °C in a water shaker bath. At various time intervals, the capsules were collected and observed in a bright field light microscope (AXIOVERT 40 CFL, Germany) equipped with a digital camera (Canon Power shot G8, Japan) and the number of ruptured capsules counted.

Induction of mechanical stress using bead agitation

Xanthan-peptide microcapsules were placed in flasks containing 20 glass beads (3 mm diameter, VWR Scientific Products Corporation) and 30 mL of PBS solution in a flat rotator shaking at maximum rate (about 300 rpm) (DSR-2800V, Digisystem Laboratory Instruments Inc, Taiwan). At various time intervals (2, 5, 7, 24 h) the number of ruptured capsules was counted by observation in a bright field light microscope (AXIOVERT 40 CFL, Germany) equipped with a

digital camera (Canon Power shot G8, Japan). The percentage of ruptured capsules in function of time was determined.

Cell culture and encapsulation

The murine ATDC5 chondrocyte cells were cultured in basic medium, consisted of Dulbecoo's Modified Eagle's Medium (DMEM) with phenol red, supplemented with 10% fetal calf serum (FCS, Biochrom AG, Germany), 5 mM L-Glutamine and 1% of antibiotic-antimycotic mixture and maintained at 37°C in a humidified atmosphere of 5% CO_2. The medium was replaced every two days. At passage 8, cells were detached with trypsin/EDTA and counted in a hemacytometer for encapsulation. The production of the xanthan-peptide microcapsules and the encapsulation of the ATDC5 cells were done in the developed microfluidics device which was connected to syringe and peristaltic pump for transferring xanthan-cell and mineral oil, respectively (Figure 2). Xanthan (1 wt%), previously sterilized in an autoclave (10 min, 121 °C) was dissolved in PBS and mixed subsequently with a cell suspension ($5x10^6$ cells/mL). Xanthan solution and cell suspension in xanthan solution were injected by syringe pump (Alladdin WPI, England) into the polymer microchannel of microfluidics device (Figure 2). Simultaneously, the flow of mineral oil was provided from an oil reservoir by using a peristaltic pump (Ismatec, Switzerland). The operation rate of peristaltic and syringe pump was set at 0.35 mL/minute and 20 µL/min, respectively. The xanthan microdroplets were generated inside the microfluidics device by shear stress when the polymer-cell suspension in vertical microchannel entered into the stream of mineral oil in larger horizontal microchannel. The formed homogenous droplets of polysaccharide-cell were collected in a collector vessel containing $K_2(QL)_6K_2$ solutions at different percentages (0.1, 0.25 and 0.5 wt%) and about 10 µL of Tween 80 as emulsifying agent. The self-assembly of the polysaccharide with peptide, and the subsequent microcapsule formation took place after the contact between both components by gently stirring the polymer droplets for 20 min on a magnetic stirrer. Afterwards, the xanthan-peptide microcapsules were washed in PBS and transferred to tissue culture plate containing DMEM for further cellular studies. The encapsulated cells (n=3) were maintained *in vitro* culture for a period of 3 weeks in DMEM with media exchange every 2 days. Empty microcapsules were also maintained throughout the culture period to serve as controls.

Viability and proliferation of microencapsulated cells

To investigate the ability of the xanthan-peptide microcapsules to support cell viability and proliferation in respect to various peptide concentrations, the live/dead and AlamarBlue® assays (viability) and DNA quantification (proliferation) were performed.

Metabolic activity assay

AlamarBlue® (AbD Serotec,UK) was added (10% of the volume of the well) to each well containing the encapsulated cells and the plate was incubated at 37 ºC for 20 hours protected from light. After incubation, 100 μL of solution was taken from each well and placed in a 96 well plate. The absorbance was read at 570 and 600 nm on a microplate reader (BIO-TEK, SYNERGIE HT, USA). The percentage of reduced AlamarBlue® was calculated according the manufacturer instructions.

Live/dead cell assay

Calcein AM (Sigma, USA) solution (2/1000, v/v) was prepared in DMEM without FCS and phenol red. Propidium iodide (PI, Molecular Probes, Invitrogen, USA) solution was prepared by mixing 2 μL PI (1 mg/mL) with 20 μL (1 mg/mL) RNAse A (USB corporation, USA) and 2 mL PBS. The microcapsules with encapsulated cells and controls were collected from the culturing plates and incubated with calcein-AM and propidium iodide solutions at 37 ºC for 10 min protected from light. Samples were then observed under fluorescent microscopy using an Axio (Zeiss HAL 100/HBO 100; Axiocam MRc5 (Zeiss).

DNA quantification assay

ATDC5 proliferation within the microcapsules was determined using a fluorimetric DNA quantification kit (PicoGreen, Molecular Probes, Invitrogen, USA). For this purpose, the samples collected at days 1, 7, 14 and 21 were washed twice with sterile PBS (Sigma, USA) solution and transferred into 1.5 mL microtubes containing 1 mL of ultra-pure water. Capsules with and without cells were stored at -80 ºC until further analysis. Prior to DNA quantification, samples were thawed and broken by pipetting up and down using a syringe with a needle and crushed with a glass tube to cause material disruption and facilitate DNA extraction. 28.7 μL of each sample and standards (0-2 mg/mL) were transferred to an opaque 96 well plate. Then 71.3 μL of PicoGreen solution and 100 μL of Tris-EDTA buffer were added. Standards and samples were prepared in triplicate. The plate was incubated for 10 minutes in the dark and the fluorescence was measured using an excitation wavelength of 485 nm and emission of 528 nm. DNA amounts were calculated from the calibration curve.

Statistical analysis

The results of DNA quantification and cell viability are expressed as a mean ± standard deviation with n=3 for each group.

Statistical significance of differences was determined using unpaired student's *t*-test multiple comparison procedure at a confidence level of 95 % ($p < 0.05$).

3. RESULTS AND DISCUSSION

We have hypothesized that the presence of anionic groups in the xanthan chain at pH 7 (Figure VI.1.A) could trigger the self-assembly of a positively charged multidomain peptide (Figure VI.1.B) into macroscopic assemblies by electrostatic interactions, as reported in previous studies using hyaluronic acid [20] or alginate [21] combined with a different peptide molecule. Moreover, we thought on using microfluidics (Figure VI.2.) to precisely generate micro-sized and monodispersed capsules for cell encapsulation in physiological conditions. To test our hypotheses, we have analyzed the peptide-xanthan interactions, as well the structures formed from these interactions in certain assembling conditions.

Peptide-xanthan interaction studied by QCM

QCM detection principle is based on the resonance frequency shifts due to addition or removal of mass on a piezoelectric material (typically quartz crystal) [26]. In this study, QCM measurements were performed with an instrument with dissipation monitoring (QCM-D). Dissipation monitoring allows analyzing the viscoelastic properties of the adhered layers and their interaction with layers previously deposited on the crystal surface [27]. In order to verify the specificity of the interactions between the peptide and xanthan, the interaction of BSA with xanthan was also analyzed as a control test. Figure VI.3.A shows that the change in the frequency related with the BSA interaction is lower than the one obtained for all peptide concentrations.

The frequency signal (Figure VI.3.A) in the initial stage for all the peptide concentrations presents a similar behavior: a fast decrease as a result of the fast and high interaction of the peptide with xanthan. After the fast decrease, the frequency signal presented an instable behavior probably due to rearrangements between the two layers and finally the signal stabilized, indicating that the interaction reached the equilibrium.

After the addition of PBS (about 102 min) the frequency of signal decreased. PBS is more viscous than water, thus it is expected to induce an increase in dissipation, as it was observed in Figure VI.3.B and at the same time a decrease in the frequency (Figure VI.3.A). It can be noticed that the layer created by the interactions between peptide and xanthan was stable in PBS, since no increase in frequency signal was observed, indicating no mass loss. The final frequency change indicates, as expected, that the total mass adsorbed was higher for the higher peptide concentrations (Figure VI.3.A).

Figure VI.3.B shows that the dissipation changes associated with the peptide-xanthan interactions present a parallel behavior with the frequency change. For the higher peptide concentration, a fast increase in the dissipation followed by a slower decrease was observed. This behavior is indicative of the formation of a highly viscoelastic layer during the beginning of the interaction, that slowly reorganizes and becomes less viscous with the time. For the lowest peptide concentration, the dissipation initially increases, then presents some instability and finally increases slowly until a stable signal. This behavior indicates that the interaction initially increases highly the viscosity, passes through a rearrangement step that decreases the viscosity and finally stabilizes increasing again the viscosity (Figure VI.3.B). The final dissipation for the two lower concentrations is similar indicating similar structural character.
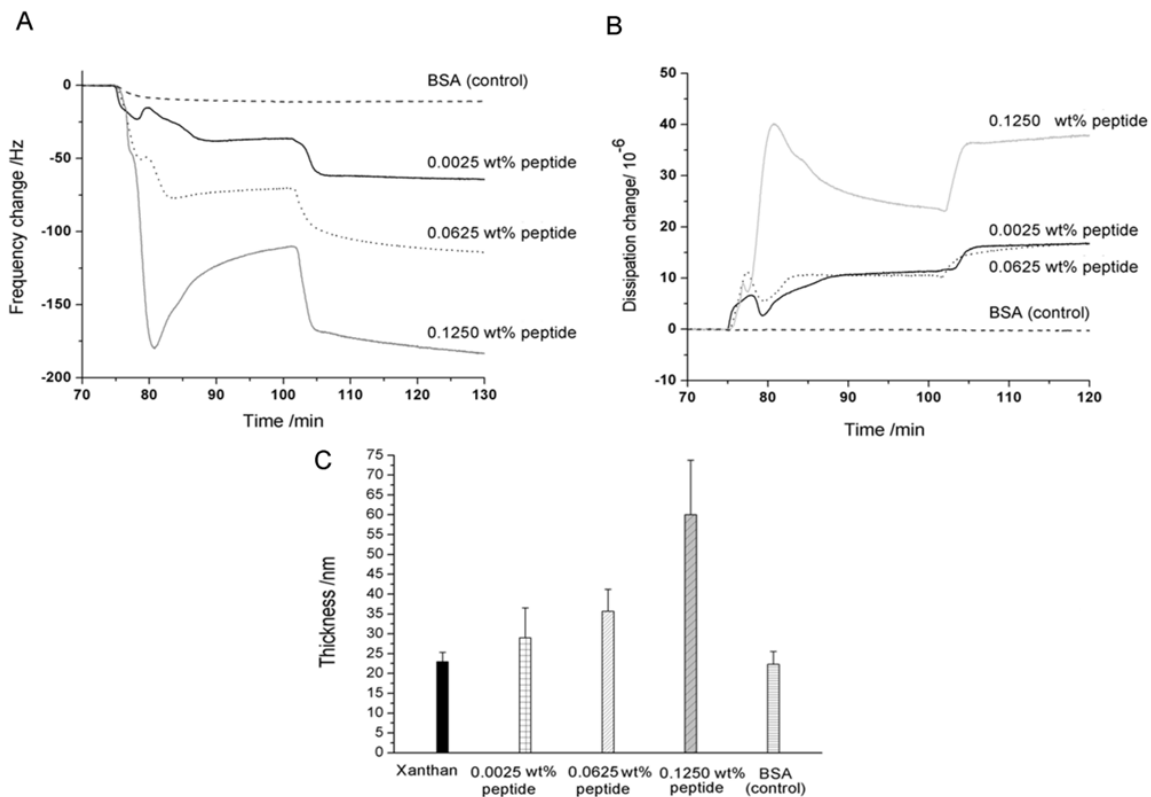
Figure VI.3. Visco-elastic properties, frequency (A) and dissipation (B) from the 9th overtone and thickness (C) of the films of xanthan-$K_2(QL)_6K_2$ monitored by QCM.

The thickness of the xanthan-peptide layer was determined by applying the viscoelastic model (based on Voigt model) incorporated in Q-Sense software. For all the different peptide concentrations there was an increase in the thickness as compared to the xanthan initial thickness, being this increase proportional to the peptide concentration as it is demonstrated in

Figure VI.3.C. The highest peptide concentration presents a thickness of about 60 nm, two times higher than the thickness revealed by the lowest peptide concentration (30 nm).

Microcapsule morphology and microstructure

The morphology and microstructure of the microcapsules were analysed using bright field and scanning electron microscopy (Figure VI.4. and 5.). From these observations, it can be noticed that size and morphologies are dependent on the peptide concentration.
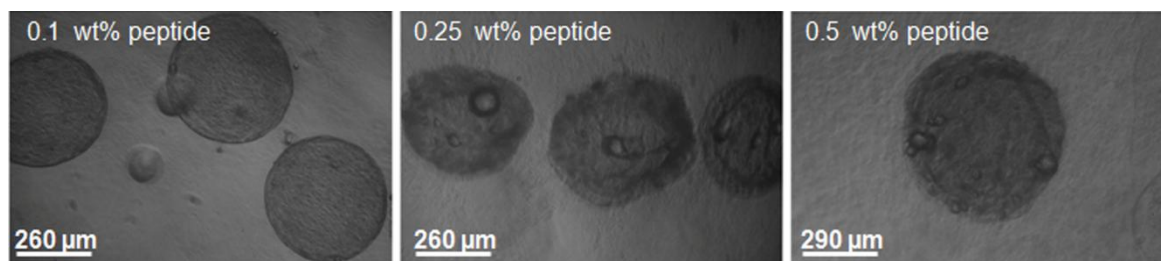
Figure VI.4. Bright field light microscopy photographs of xanthan-$K_2(QL)_6K_2$ microcapsules prepared with three peptide concentrations (0.1, 0.25 and 0.5 wt%).

Nevertheless, all the obtained capsules are hollow, as noticed by microscopy analyses, present spherical shape and their diameter varies from 390 ± 8 µm when 0.1 wt% of peptide was used to 585 ±18 µm for 0.5 wt% peptide (Table VI.1.).

Table VI.1. Effect of peptide concentration on the size and membrane thickness of peptide-xanthan microcapsules.

Peptide / wt%	d-Size/µm	Membrane thickness / µm
0.1	390± 8	5.6± 0.5
0.25	417± 8	-
0.5	585± 18	10.7± 0.33

Additionally, the microcapsule external surface appears to be quite smooth in the case of the capsules fabricated with the lowest peptide concentration (0.1 wt%), while for the highest concentrations the surface morphology appears to be rougher (Figure VI.4.).

SEM images of the microcapsule cross-sections (Figure VI.5.A and C) reveal an amorphous and dense membrane with thickness ranging from 5.6 μm to 10.7 μm for the microcapsules prepared with 0.1 and 0.5 wt% of peptide, respectively. Those results are corroborating the differences in the thickness found in QCM results (Figure VI.3.C), that increasing the peptide concentration five times, the thickness of the resulted complex would duplicate. Moreover, nanofibrilar structures are observed in the in internal side of the microcapsules (Figure VI.5.D) as a result of the self-assembly of the peptide with xanthan.
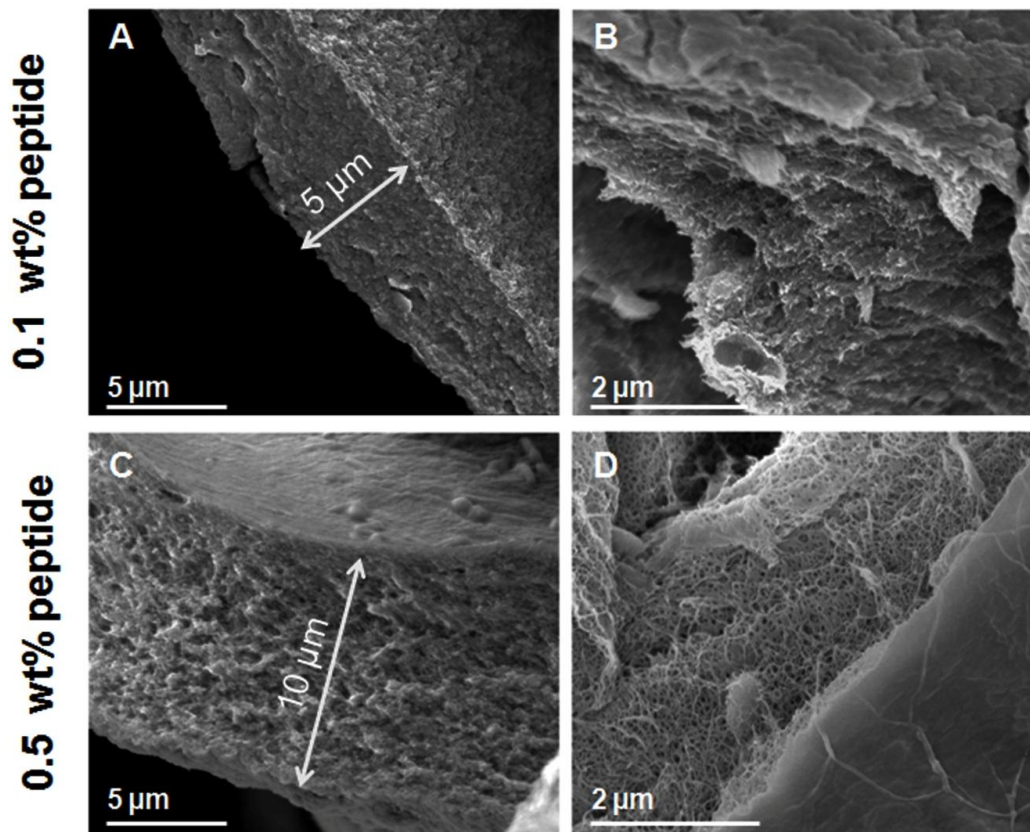
Figure VI.5. SEM micrographs showing the cross-section of xanthan-peptide microcapsule membrane (A and C) and the interior of microcapsules (B and D).

Stupp and co-workers[21] have reported the formation of uniform microcapsules with an average diameter of 25 μm using capillary picospray and interfacial self-assembly between alginate and a peptide amphiphile molecule. The microcapsules exhibited a nanofibrous surface and a liquid core (alginate) that could be gelled upon addition of Ca^{2+} ions to increase their mechanical resistance. They have shown that the thickness of the microcapsule membrane was dependent

on the incubation time of the alginate microcapsules in the peptide solution. Here we showed that the microcapsule diameter and membrane thickness (Table VI.1.) can be controlled by varying the peptide concentration.

Permeability to IgG.

The mass transport properties through an encapsulation membrane are crucial for the success of the encapsulating process. The influx of essential molecules, such as oxygen and nutrients, are critical for cell survival. On the other hand, the efflux rate of therapeutic product and wastes would determine the extent of the encapsulated cell viability. Additionally, the encapsulation membrane may avoid the influx of immune cells and antibodies, which might destroy the enclosed cells[28-29].

Microcapsules were placed into the IgG solution and the protein diffused from the dispersing medium, outside the peptide-xanthan microcapsules, to the inner part of the microcapsules was measured. In Figure VI.6.A it can be noticed that although IgG was able to diffuse in the microcapsules, this permeability was lower for those microcapsules prepared with the highest peptide concentration. This fact may be related with the membrane thickness, which is higher for the microcapsules prepared with 0.5 wt% peptide. It has been shown that higher membrane thickness result in higher resistance to protein diffusion[30-31].

Mechanical stability

Microcapsule resistance is another important criterion for the success of cell microencapsulation[25,28,30]. A microcapsule should be resistant enough to be durable during its production and handling and to resist to the mechanical stress without the loss of its membrane integrity[32]. Moreover, by increasing the strength and resistance of the capsules, the durability of the transplant will also increase *in vivo*[30]. Initially, in order to understand the effect of peptide concentration in the mechanical strength of the xanthan-peptide microcapsules, the microcapsules were immersed into a hypotonic environment. This assay was carried out by incubating the microcapsules in water under shaking over 24 h. At the end of the assay, none of microcapsules were observed broken by osmotic pressure. The low susceptibility of the microcapsules to collapse and burst under these conditions is quite unusual having into account their hollow structure. This may be related with the dense microcapsule wall observed in Figure VI.5. and with the stable visco-elastic interactions (Figure VI.3.B) that may cause reduced swelling of the microcapsules and consequently increased mechanical strength. The capsules with reduced swelling rate are less prone to rupture and to induce inflammatory responses which

may result in an enhanced mechanical strength and biocompatibility[25]. Nevertheless, in order to resemble *in vivo* shear stress, the microcapsules were exposed to PBS solution and agitated with glass micro beads over 24 h. Although in the initial time points the capsules with the lowest peptide concentration were showed to be more resistant (Figure VI.6.B) at 24 h less breakage rate was found for the microcapsules prepared with 0.5 wt% of peptide. This was an expected result, considering the differences in the membrane thickness found (in QCM and SEM measurements) for the distinct peptide concentrations and from the literature which reported that the membrane thickness is an significant indicator of the strength and permeability[33].
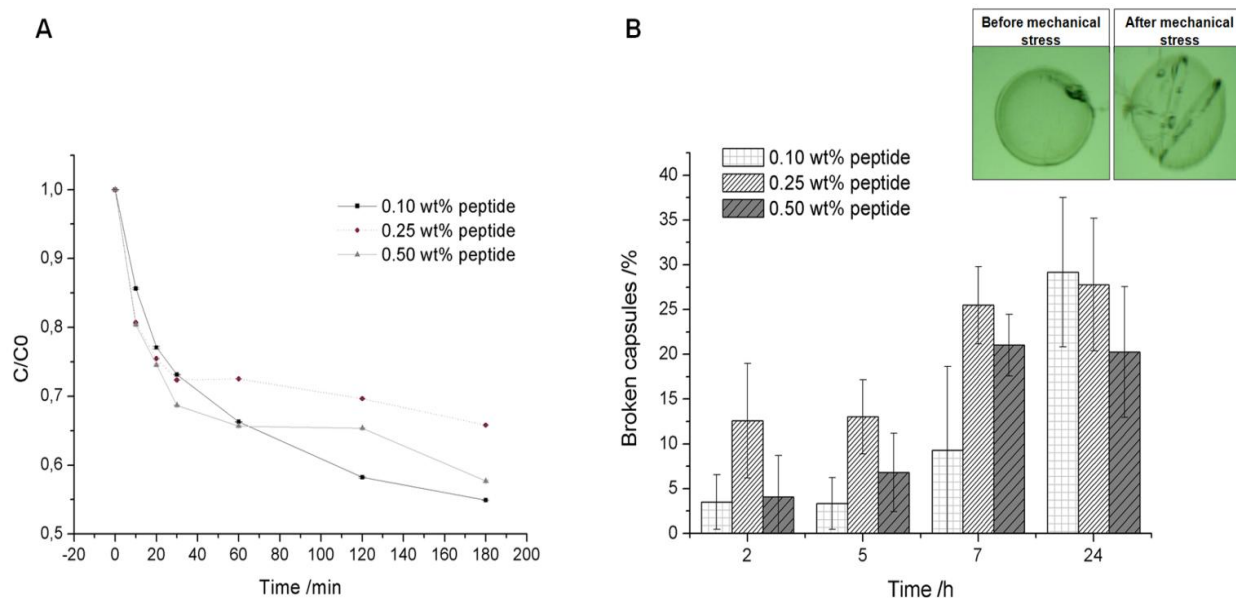
Figure VI.6. (A) Microcapsule permeability, assessed by IgG (Mw=146-155 KDa) diffusion, and (B) mechanical resistance of the xanthan-peptide microcapsules as function of peptide concentration.

In vitro viability and proliferation of ATDC5 cells cultured within microcapsules

The potential of xanthan-peptide microcapsules and the effects of peptide concentration in the cellular metabolic activity of encapsulated ATDC5 cells were investigated by using AlamarBlue®, live/dead and DNA quantification assays (Figure VI.7.).

The results showed that ATDC5 cells encapsulated in xanthan-peptide microcapsules were able to reduce AlamarBlue® over the 21 days of *in vitro* culture (Figure VI.7.A), with a slight increase as a result of the increased cellular viability. Additionally, it can be noticed that the ATDC5 cells within the capsules prepared with the highest peptide concentration were expressing significantly ($p<0.05$) higher viability than those encapsulated in the microcapsules with the

lowest peptide concentration. The highest viability of encapsulated cells in xanthan-peptide microcapsules was also confirmed by the live/dead assay (Figure VI.7.B) which showed that encapsulated cells remained viable up to 21 days of culture (viable cells depict a green fluorescence color), demonstrating the ability of this self-assembled matrix to support cellular viability over prolonged time. Moreover it can be noticed that the cells are well distributed within the microcapsule.
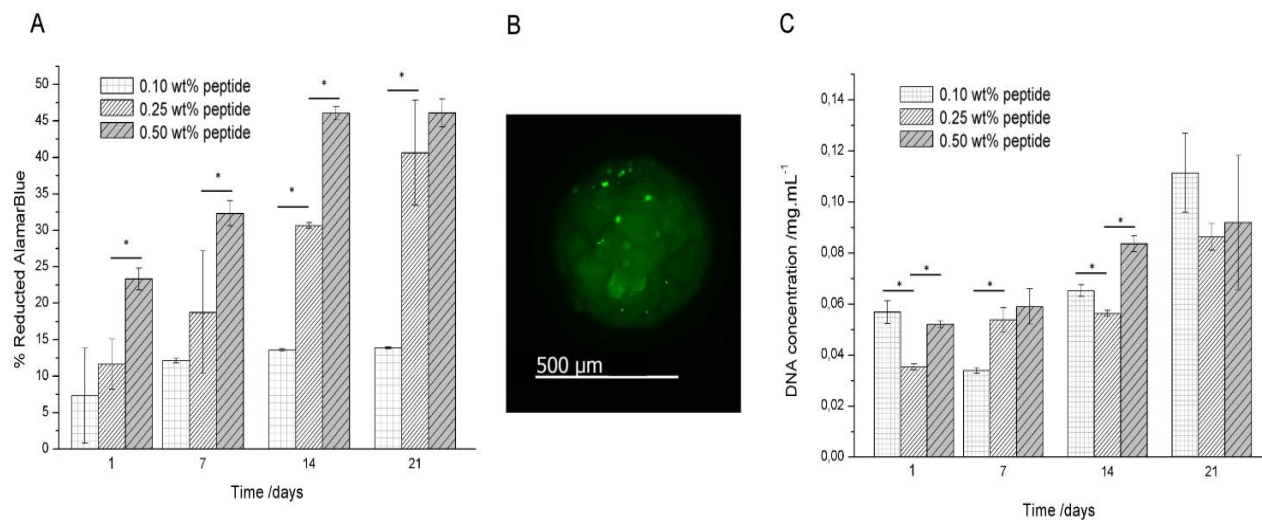
Figure VI.7. *In vitro* viability and proliferation of ATDC5 cells cultured within the xanthan- peptide microcapsules. Metabolic activity (A) and fluorescence microscopy image (B) displaying the live/dead assay of encapsulated cells (green cells are live, red cells are dead) showing that the cells remain viable in the microcapsules (0.5 wt% peptide) up to 21 days of culture. Proliferation of encapsulated cells determined by DNA quantification (C). Results are expressed as means ± standard deviation. * indicates significant difference ($p < 0.05$) between different time points for xanthan-peptide with different peptide concentrations.

To assess cell proliferation within the microcapsules, the DNA of encapsulated cells was quantified along the culture time (Figure VI.7.C). A gradual increase in the DNA concentration was observed for all xanthan-peptide microcapsules as a result of cell proliferation. Although the cells in the capsules prepared with 0.1 wt% peptide showed lower metabolic activity (Figure VI.7.A) the number of cells in these capsules at day 21 was found to be higher than those in the capsules of higher peptide concentration (Figure VI.7.C). This might be related with the available space within the hollow capsules and the distribution of cells in the microcapsule interior. These factors are expected to influence cell-cell contact and cell-matrix interactions and thus cell activities, including their metabolism and proliferation.

While in this study a non-bioactive peptide was used, the possibility to incorporate biological epitopes into the peptide sequence is diverse and several examples of peptide-based matrices used for cell encapsulation have been reported in the literature. In an early study on chondrocyte encapsulation, ionic self-complementary peptide gels were found to support cell survival and maintain chondrogenic phenotype expression and increased production of glycosaminoglycans and type II collagen[34]. Increased gene expression of chondrogenic markers was also reported in peptide gels as compared to agarose gels, and expression of osteogenic and adipogenic markers were found constant or decreased during 15 days in culture in a study with bone marrow stromal cells[35]. Furthermore, in a recent study, peptide amphiphile molecules designed to form nanofibers for cartilage regeneration by displaying a high density of binding epitopes to transforming growth factor beta-1 (TGF beta-1) showed that these materials can promote regeneration of articular cartilage in a full thickness chondral defect with or even without the addition of exogenous growth factor[36].

4. CONCLUSIONS

Combining self-assembling materials with microfluidic technology appears to be a promising alternative to the conventional biomaterials employed in cell encapsulation due the simplicity and size-control property of fabrication. We were able to develop robust microcapsules using an alternative to the conventional gelation methods, by employing a negatively charged polysaccharide to screen and drive the self-assembly of a positively charged peptide. The control of the properties of xanthan-peptide microcapsules can be achieved by changing peptide concentration, once the concentration plays an important role in the morphology, size, and permeability of the microcapsules. The optimized processing conditions enabled generating homogenous-size microcapsules with long-term stability and the ability to support the survival and function of encapsulated cells over prolonged time.

ACKNOWLEDGMENTS

REFERENCES

1. Gazit E. Self-assembled peptide nanostructures: the design of molecular building blocks and their technological utilization. Chemical Society Reviews 2007;36(8):1263-1269.

2. Lowik DWPM, Leunissen EHP, van den Heuvel M, Hansen MB, van Hest JCM. Stimulus responsive peptide based materials. Chemical Society Reviews 2010;39(9):3394-3412.

3. Gazit E. Bioinspired chemistry: Diversity for self-assembly. Nat Chem 2010;2(12):1010-1011.

4. Zhang S, Greenfield MA, Mata A, Palmer LC, Bitton R, Mantei JR, Aparicio C, de la Cruz MO, Stupp SI. A self-assembly pathway to aligned monodomain gels. Nat Mater 2010;9(7):594-601.

5. Hung AM, Stupp SI. Simultaneous Self-Assembly, Orientation, and Patterning of Peptide−Amphiphile Nanofibers by Soft Lithography. Nano Letters 2007;7(5):1165-1171.

6. Mitragotri S, Lahann J. Physical approaches to biomaterial design. Nat Mater 2009;8(1):15-23.

7. Kohane DS. Microparticles and nanoparticles for drug delivery. Biotechnology and Bioengineering 2007;96(2):203-209.

8. Champion JA, Katare YK, Mitragotri S. Particle shape: A new design parameter for micro- and nanoscale drug delivery carriers. Journal of Controlled Release 2007;121(1-2):3-9.

9. Whitesides GM. The origins and the future of microfluidics. Nature 2006;442(7101):368-373.

10. Khademhosseini A, Langer R. Microengineered hydrogels for tissue engineering. Biomaterials 2007;28(34):5087-5092.

11. Tumarkin E, Kumacheva E. Microfluidic generation of microgels from synthetic and natural polymers. Chemical Society Reviews 2009;38(8):2161-2168.

12. Stupp SI. Self-Assembly and Biomaterials. Nano Letters 2010;10(12):4783-4786.

13. Huebsch N, Mooney DJ. Inspiration and application in the evolution of biomaterials. Nature 2009;462(7272):426-432.

14. Collier JH, Rudra JS, Gasiorowski JZ, Jung JP. Multi-component extracellular matrices based on peptide self-assembly. Chemical Society Reviews 2010;39(9):3413-3424.

15. Matson JB, Zha RH, Stupp SI. Peptide self-assembly for crafting functional biological materials. Current Opinion in Solid State & Materials Science 2011;15(6):225-235.

16. Dong H, Paramonov SE, Aulisa L, Bakota EL, Hartgerink JD. Self-Assembly of Multidomain Peptides: Balancing Molecular Frustration Controls Conformation and Nanostructure. Journal of the American Chemical Society 2007;129(41):12468-12472.

17.   Aulisa L, Dong H, Hartgerink JD. Self-Assembly of Multidomain Peptides: Sequence Variation Allows Control over Cross-Linking and Viscoelasticity. Biomacromolecules 2009;10(9):2694-2698.

18.   Mendes AC, Baran ET, Pereira RC, Azevedo HS, Reis RL. Encapsulation and Survival of a Chondrocyte Cell Line within Xanthan gum derivative. Macromolecular Bioscience 2012;12(3):350-359.

19.   Mendes AC, Baran ET, Nunes C, Coimbra MA, Azevedo HS, Reis RL. Palmitoylation of xanthan polysaccharide for self-assembly microcapsule formation and encapsulation of cells in physiological conditions. Soft Matter 2011;7(20):96-47.

20.   Capito RM, Azevedo HS, Velichko YS, Mata A, Stupp SI. Self-Assembly of Large and Small Molecules into Hierarchically Ordered Sacs and Membranes. Science 2008;319(5871):1812-1816.

21.   Rożkiewicz DI, Myers BD, Stupp SI. Interfacial Self-Assembly of Cell-like Filamentous Microcapsules. Angewandte Chemie International Edition 2011;50(28):6324-6327.

22.   Mendes AC, Baran ET, Nunes C, Coimbra MA, Azevedo HS, Reis RL. Palmitoylation of xanthan polysaccharide for self-assembly microcapsule formation and encapsulation of cells in physiological conditions. Soft Matter 2011.

23.   M V Voinova MR, M Jonson and B Kasemo. Viscoelastic Acoustic Response of Layered Polymer Films at Fluid-Solid Interfaces: Continuum Mechanics Approach. Physica Scripta 1999;59:391.

24.   Abdelgawad M, Wheeler AR. Rapid Prototyping in Copper Substrates for Digital Microfluidics. Advanced Materials 2007;19(1):133-137.

25.   Darrabie MD, Kendall Jr WF, Opara EC. Characteristics of Poly-l-Ornithine-coated alginate microcapsules. Biomaterials 2005;26(34):6846-6852.

26.   Sauerbrey G. Verwendung von Schwingquarzen zur Wägung dünner Schichten und zur Mikrowägung. Zeitschrift für Physik 1959;155:206-222

27.   Hook F, Kasemo B, Nylander T, Fant C, Sott K, Elwing H. Variations in Coupled Water, Viscoelastic Properties, and Film Thickness of a Mefp-1 Protein Film during Adsorption and Cross-Linking:‚Äâ A Quartz Crystal Microbalance with Dissipation Monitoring, Ellipsometry, and Surface Plasmon Resonance Study. Analytical Chemistry 2001;73(24):5796-5804.

28.   Hernández RM, Orive G, Murua A, Pedraz JL. Microcapsules and microcarriers for in situ cell delivery. Advanced Drug Delivery Reviews 2010;62(7-8):711-730.

29. Murua A, Portero A, Orive G, Hernández RM, de Castro M, Pedraz JL. Cell microencapsulation technology: Towards clinical application. Journal of Controlled Release 2008;132(2):76-83.

30. de Vos P, Bucko M, Gemeiner P, Navrátil M, Svitel J, Faas M, Strand BL, Skjak-Braek G, Morch YA, Vikartovská A and others. Multiscale requirements for bioencapsulation in medicine and biotechnology. Biomaterials 2009;30(13):2559-2570.

31. Briscaronscaronová M, Lacík I, Powers AC, Anilkumar AV, Wang T. Control and measurement of permeability for design of microcapsule cell delivery system. Journal of Biomedical Materials Research 1998;39(1):61-70.

32. Mendes AC, Baran ET, Pereira RC, Azevedo HS, Reis RC. Encapsulation and Survival of a Chondrocyte Cell Line within Xanthan gum derivative. 2010.

33. Thu B, Bruheim P, Espevik T, Smidsrød O, Soon-Shiong P, Skjåk-Bræk G. Alginate polycation microcapsules: II. Some functional properties. Biomaterials 1996;17(11):1069-1079.

34. Kisiday J, Jin M, Kurz B, Hung H, Semino C, Zhang S, Grodzinsky AJ. Self-assembling peptide hydrogel fosters chondrocyte extracellular matrix production and cell division: Implications for cartilage tissue repair. Proceedings of the National Academy of Sciences 2002;99(15):9996-10001.

35. Kopesky PW, Vanderploeg EJ, Sandy JS, Kurz B, Grodzinsky AJ. Self-Assembling Peptide Hydrogels Modulate In Vitro Chondrogenesis of Bovine Bone Marrow Stromal Cells. Tissue Engineering Part A 2009;16(2):465-477.

36. Shah RN, Shah NA, Del Rosario Lim MM, Hsieh C, Nuber G, Stupp SI. Supramolecular design of self-assembling nanofibers for cartilage regeneration. Proceedings of the National Academy of Sciences 2010;107(8):3293-3298.

Chapter VII

CO-ASSEMBLED AND MICROFABRICATED BIOACTIVE MEMBRANES

CO-ASSEMBLED AND MICROFABRICATED BIOACTIVE MEMBRANES

ABSTRACT

We report on the fabrication of hierarchical and bioactive self-supporting membranes, integrating physical and biomolecular elements, in a single-step process that combines molecular self-assembly with soft lithography. A positively charged multi-domain peptide (with or without the cell-adhesive sequence RGDS) self-assembles with hyaluronic acid (HA), an anionic biopolymer. Optimization of the assembling conditions enable the realization of membranes with well-controlled and easily tunable features at multiple size scales including peptide sequence, building-block co-assembly, membrane thickness, bioactive epitope availability, and topographical pattern morphology. Membrane structure, morphology, and bioactivity are investigated according to temperature and assembly time as well as experimental setup variations. Furthermore, in order to evaluate the physical and biomolecular signaling of the self-assembled microfabricated membranes, rat mesenchymal stem cells are cultured on membranes exhibiting various densities of RGDS and different topographical patterns. Cell adhesion, spreading, and morphology are significantly affected by the surface topographical patterns and the different concentrations of RGDS. The versatility of the combined bottom-up and top-down fabrication processes described here may permit the development of hierarchical macrostructures with precise biomolecular and physical properties and the opportunity to fine tune them with spatio-temporal control.

1. INTRODUCTION

As a bottom-up fabrication technique, self-assembly facilitates the development of new biomaterials with molecular resolution by precisely controlling the positioning of high quantities of small building-blocks [1]. This level of precision enables the capacity to generate nanoarchitectures similar to those found in the natural extracellular matrix (ECM) that additionally exhibit biomolecular ligands capable of controlling biological processes [2]. However, a major limitation of current self-assembling systems is the lack of structural and functional control at the micro and macroscopic levels, which significantly limits the bulk properties of the material and consequently its practicality, functionality, and overall performance.

In order to overcome this limitation, a number of groups are focusing efforts on developing strategies that facilitate molecular assembly at higher size-scales. One approach relies on molecules that incorporate by design the "code" to guide their assembly across scales. For example, Hartgerink *et al.* have developed a strategy that employs electrostatic interactions to guide the self-assembly of heterotrimeric triple helices designed to replicate the self-assembly of collagen, from peptide chain to triple helix formation to nanofiber and finally to a hydrogel [3]. Stupp and co-workers have reported the formation of hierarchically structured macroscopic sacs and membranes obtained by the co-assembly of positively charged small peptide molecules (peptide amphiphiles) and a large negatively charged polymer (hyaluronic acid) with a millimeter size scale [4-6]. Another example of hierarchical organization was provided by Chung *et al.* who used self-templating assembly of chiral colloidal particles (phage particles) to produce long-range ordered supramolecular films [7]. While these mechanisms are highly biomimetic and generate materials with improved macroscopic properties, there is still a great need to develop novel fabrication schemes that reproducibly control molecular assembly at higher scales. On the other hand, controlled multiscale self-assembly has been investigated by incorporating top-down methods that offer high reproducibility, micro/nano precision over large areas, and batch fabrication capabilities[8]. For example, building on the work of Zhang and colleagues[9], soft lithography techniques have been widely used to fabricate material surfaces with molecular patterns at various scales[10]. However, limited biocompatibility and capacity to generate three-dimensional structures has hampered the practicality of this approach in applications such as tissue engineering and regenerative medicine. The present work aims to integrate both of these approaches to provide an additional level of hierarchical order and a higher degree of functionality.

Soft lithography has been used to precisely manipulate and localize cells, control cell–cell and cell–substrate interactions, guide cell behavior, and facilitate the fundamental study of many

biological processes[11-15]. These studies have thoroughly demonstrated the possibility to modulate cell morphology[16-17], adhesion[18], migration[19], proliferation[14,20], and differentiation[21-22] through precise nano- and microstructures using large variety of biocompatible materials such as polydimethylsiloxane[14,20], polylactic acid[23], hyaluronic acid[24], or poly-ε-caprolactone[25]. Generating self-assembling materials with such well-controlled topographical features would not only improve hierarchical order, but would also provide a higher level of bioactivity by enabling the opportunity for cell interaction on various size scales. For example, Mata *et al*[13], reported on the possibility to enhance osteoblastic differentiation when presenting cells with a combination of bioactive self-assembling nanofibers and well-defined 40 µm diameter, 4 µm deep holes. The possibility to fabricate materials with such well-defined topographical patterns using increasingly complex self-assembling systems represents an attractive approach to generate biomimetic and easily tunable materials with improved spatio-temporal control of bioactive signals.

Synthetic membranes would benefit significantly from this kind of top-down/bottom-up approach. In the human body, membranes play critical roles supporting cell attachment and function, regulating nutrient and waste transfer, and providing boundaries between tissues and organs [26]. The possibility of using artificial membranes as *in vitro* or *in vivo* scaffolds capable of exhibiting specific signals, tunable properties, and cell guiding features would be broadly useful in tissue engineering and regenerative medicine applications. For example, membranes have been investigated for bone and cartilage regeneration[27], cornea repair[28], skin engineering[29], reconstruction of the abdominal wall[30] and cardiac tissue replacement[31]. Natural (e.g. OSSIX™ PLUS™, Tutodent®, Bio-Gide® and Chondro-Gide®)[32], and synthetic materials have been used, isolated or in combination, to fabricate membranes using methods such as solvent casting, electrospinning, polyelectrolyte complexation, or compression molding[33]. Although intense research efforts have been devoted to develop functional membranes as scaffolds for tissue engineering, limited work has been focused on developing membranes that exhibit a level of biomimetic complexity more similar to the *in vivo* environment.

The formation of membranes at the interface between two aqueous solutions, one containing a megadalton polymer and the other small self-assembling molecules bearing opposite charge, was previously demonstrated[4] The structure-property relationship of these kinds of membranes has been studied[5] and the effect of electric fields on the self-assembly process forming the membranes has been recently investigated[34]. Inspired by this remarkable self-assembling system, we propose here a single-step bottom-up (self-assembly) and top-down (soft lithography) fabrication technique to create hybrid multifunctional membranes that, in addition to displaying biomimetic nanofibers and biomolecular elements, exhibit specific surface

topographies that can be easily modified to elicit desirable biological responses. We have selected the natural polymer hyaluronic acid (HA), an anionic polysaccharide typically found in the connective tissues of vertebrates, to drive the self-assembly of a multi-domain peptide, previously proposed by Hartgerink and co-workers[35]. The resulting peptide/HA co-assembled membranes exhibited a hierarchical structure of nanofibers and surface microtopographies with various densities of RGDS. Furthermore, we investigate the effect of temperature, time, and experimental setup on the structural characteristics of the membranes.

2. MATERIALS AND METHODS

Peptide synthesis and purification

Two similar peptides were synthesized in this study, having the following amino acid sequences: $K_2(QL)_6K_2$ and $K_2(QL)_6K_2RGDS$. The structure of $K_2(QL)_6K_2$ is shown in Figure VII.1.A.
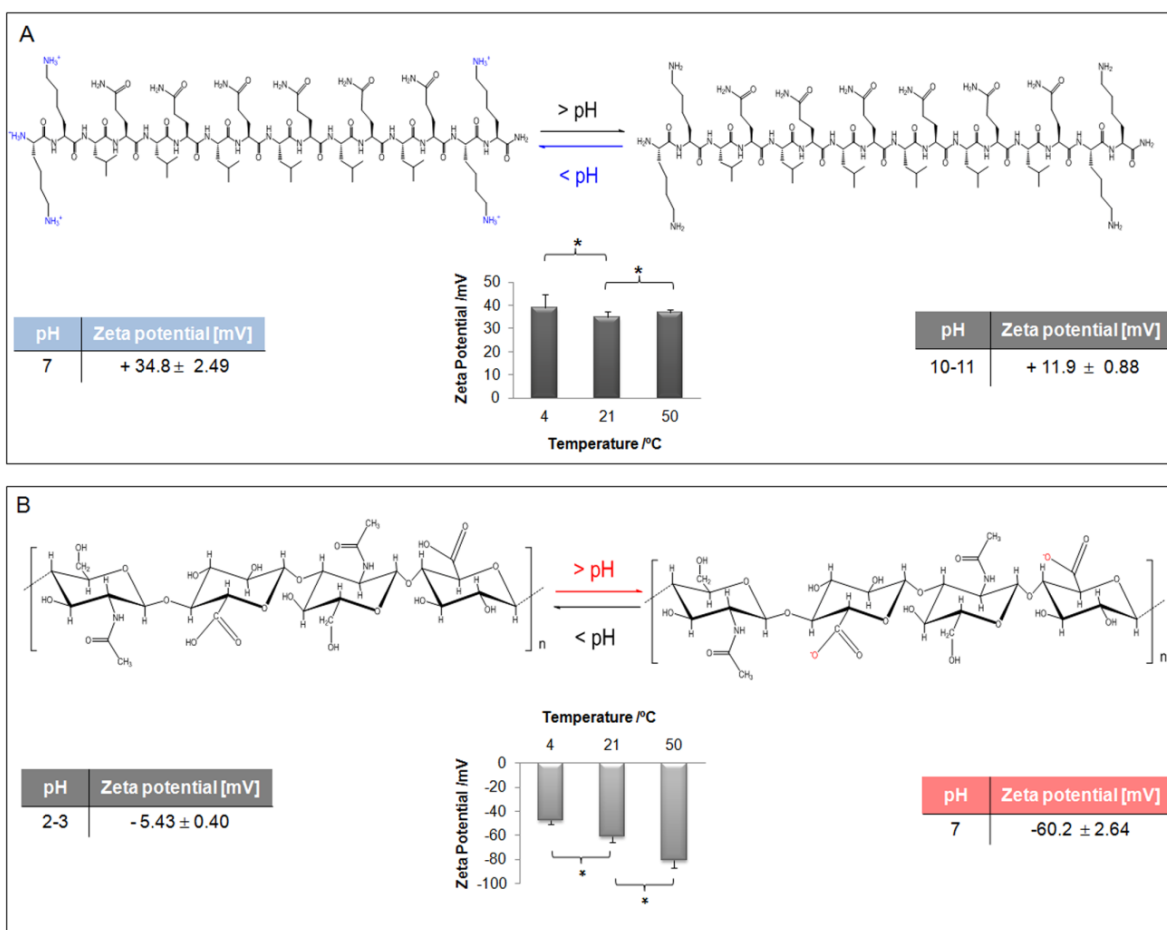
Figure VII.1. Chemical structure of the self-assembling components used in this study: multidomain $K_2(QL)_6K_2$ peptide (A) incorporating alternating hydrophilic/hydrophobic amino acid residues (QL) and two flanking positively charged lysines (K) required for self-assembly in presence of negatively charged high molecular weight polymer hyaluronic acid (B). Zeta potential of both component solutions (0.1 wt%) was measured at different temperatures (pH 7) and pHs (21 ºC) to demonstrate the nature of ionizable groups in the self-assembling components (* indicates a significant difference ($p < 0.05$) between conditions).

The peptides were produced by solid-phase peptide synthesis using standard 9-fluorenylmethoxycarbonyl (Fmoc) chemistry on an automated peptide synthesizer (CS Bio, USA) at 1 mmol scale on a 4-methylbenzhydrylamine (MBHA) rink amide resin. Fmoc-protected amino acids and MBHA rink amide resin were purchased from Novabiochem (USA) and O-(benzotriazol-1-yl)-N,N,N',N'-tetramethyluronium (HBTU) from Carbosynth (UK). N-N-diisopropylethylamine (DIEA), piperidine and all other reagents were obtained from Sigma-Aldrich (USA).

Once synthesized, cleavage of the peptide from the resin and deprotection of the protecting groups was carried out with a mixture of trifluoroacetic acid (TFA)/ triisopropylsilane (TIS)/ water (95/2.5/2.5) for 3 h at room temperature. After filtration of the cleavage mixture, excess TFA was removed by rotary evaporation. The resulting viscous peptide solution was triturated with cold diethylether. The white precipitate was collected by filtration, washed with cold ether, and allowed to dry under vacuum overnight. The peptide mass was confirmed by electrospray ionization mass spectrometry (ESI-MS, Finnigan LXQ, USA). The peptide was then purified on a Waters 2545 Binary Gradient high-performance liquid chromatography (HPLC) system using a preparative reverse-phase C18 column (Atlantis Prep OBD T3 Column, Waters) and a water/acetonitrile (0.1% TFA) gradient. TFA counter-ions were exchanged by sublimation from hydrochloric acid (0.1 M). Finally, the peptides were dialyzed against deionized water using dialysis tubing (500 MWCO, Spectrum Europe B.V., The Netherlands) to remove salts, lyophilized, to obtain a fluffy powder, and stored in closed containers at -20 ºC until use. The purity and accurate mass of each peptide were verified using liquid chromatography/MS and the HPLC.

Zeta potential analysis

Zeta potential measurements of the peptide and hyaluronic acid (2 MDa, Lifecore Biomedical, Inc, USA) solutions (0.1 wt%) were performed at distinct pHs (T = 21 ºC) and different temperatures (pH 7) using a Zetasizer Instrument (NANO-ZS ZEN3600, Malvern Instruments, UK).

Membrane fabrication

Smooth membranes were fabricated by casting hyaluronic acid solution (2 MDa, 1 wt% in water) on a polydimethylsiloxane (PDMS, Sylgard 184, Dow Corning, USA) substrate. The PDMS substrate was prepared by mixing the prepolymer and crosslinker at a 10:1 ratio, degassing for 10 min under vacuum and curing for 2 h at 65 ºC. The PDMS was oxygen plasma treated in a plasma cleaner (PDC-002, Harrick Cientific Corporation, USA), in order to increase the

wettability of the surface. The $K_2(QL)_6K_2$ peptide (1 wt% in water) was next added on top of the HA, generating a membrane upon contact between the solutions. The membrane was allowed to age for either 4 or 24 h at 4, 21 and 50 ºC. The membranes were also prepared inverting the positions of the HA and peptide: peptide solution was cast onto the PDMS substrate with the HA added on top. The effects of time and temperature on the membranes were also analyzed. Membranes containing different amounts of the RGDS motif were prepared by mixing the $K_2(QL)_6K_2$ and $K_2(QL)_6K_2RGDS$ peptides in different ratios (1:10 and 3:10) prior to the co-assembly with HA.

Topographically patterned membrane fabrication

Fabrication of topographic PDMS molds

Molds comprising several micro topographical patterns were fabricated using a soft lithography process. The patterns were generated in SU8-10 photoresist (Microchem Corporation, USA) using conventional contact mode UV photolithography (Mask Aligner MJB4, SUSS Microtec, Germany) with a rigid chrome mask as follows. SU8-10 photoresist was spin coated onto a (111)-oriented silicon wafer (Siltronix) at 500 rpm for 5 s followed by 4000 rpm for 30 s, achieving a layer approximately 8 µm thick. The sample was baked at 65 ºC for 2 min and 95 ºC for 5 min prior to UV exposure (3.3 s at 30 mW.cm^{-2}) and baked post-exposure at 65 ºC for 1 min followed by 95 ºC for 5 min. The topographical patterns were then developed with SU8 developer (Microchem, USA). The resulting samples were silanized with trichloro(1H,1H,2H,2H-perfluorooctyl)silane (Sigma-Aldrich, USA) before being used as molds for the production of patterned PDMS substrates (Figure VII.4.A). The patterns were comprised of different geometries, channels (10 µm wide, 10 µm in separation, and 8 µm in height), posts (10 µm wide, 10 µm in separation, and 8 µm in height), and holes (10 µm wide, 10 µm in separation, and 8 µm deep), and posts and holes (20 µm wide, 20 µm in separation, and 8 µm in height).

Fabrication of topographic membranes

Topographically patterned membranes were fabricated by casting the peptide solution onto the hydrophilic PDMS molds followed by the addition of the HA on the top of peptide solution (Figure VII.4.B). The membranes were aged for 24 h at room temperature. The self-assembled membranes were removed from the patterned PDMS molds by immersion in ethanol (70%) and then characterized.

Membrane characterization

Scanning Electron Microscopy (SEM): The morphology and uniformity of membrane surface and cross-section were investigated by SEM. Prior to the SEM observations; the membranes were fixed with glutaraldehyde (Electron Microscopy Sciences, Spain) solution (2.5%, v/v in 0.1 M phosphate buffer solution, pH 7.4) for 1 h. The samples were then dehydrated in a graded ethanol series (50, 70, 90, 96 and 100%) followed by immersion in hexamethyldisilazane (HMDS, Sigma-Aldrich, Spain). The membranes were sputter-coated with 20 nm of gold and then visualized using a Nova nano SEM (FEI, Netherlands).

Confocal microscopy: To get better insight into the self-assembly process, namely on the mixture of the components during membrane formation, HA was labeled with 5-(aminoacetamido) Fluorescein (Life Technologies, USA) according to a procedure described elsewhere[36]. The membranes were prepared as described previously, with variations in time, temperature and positioning of peptide and fluorescent HA. They were then imaged using an SP2 confocal microscope (Leica Microsystems, Germany).

Biological assessment

Cell seeding and culture on the fabricated membranes

Rat mesenchymal stem cells (rMSCs) isolated from bone marrow of rat tibia and femur, were provided by the Animal Research Center (SEA) of the Parc Científic Barcelona. Cells were expanded in Dulbecco's modified Eagle's medium (DMEM; Life Technologies, Spain) supplemented with fetal bovine serum (10%, FBS; Attendbio Research, Spain), L-glutamine (0.2 mM), penicillin (100 units ml^{-1}) and streptomycin (0.1 mg ml^{-1}) (Sigma-Aldrich, Spain). rMSCs of passage 3–6 were suspended in serum-free DMEM and seeded at 12 500 cells cm^{-2} onto smooth and patterned membranes with and without the RGDS sequence. After 4 h of culture, all medium was replaced with DMEM containing 10% FBS to allow cell proliferation.

Cell adhesion

After 18 h, the culture medium was removed and the samples were washed twice with PBS to remove any non-adherent cells. Cells were fixed with formaldehyde (4%, v/v, Sigma-Aldrich, Spain) in PBS for 30 min at RT. To visualize the actin cytoskeleton, cells were stained with phalloidin-fluorescein isothiocyanate (phalloidin–FITC, Sigma-Aldrich, Spain) at a 1:500 dilution in PBS for 1 h at room temperature. They were then counterstained with 4',6-diamidino-2-phenylindole dihydrochloride (DAPI; Sigma-Aldrich, Spain) for observation of the nuclei. Finally,

the samples were mounted on glass slides with a drop of Fluoro-Gel mountant (Aname, Spain). The cells were visualized using an SPE confocal microscope (Leica Microsystems, Germany).

SEM observations

Cells cultured on the membranes were examined under SEM to analyze cell morphology and its interactions with the membranes at the nano and microscale. Samples were fixed and dehydrated as described above.

Statistical analysis

The results of zeta potential and membrane thickness are expressed as a mean $\pm$ standard deviation with n = 3 for each condition. Statistical significance of differences was determined using the unpaired Student's t-test multiple comparison procedure at a confidence level of 95% ($p < 0.05$).

3. RESULTS AND DISCUSSION

The self-assembling building blocks used in this study were a positively charged multidomain peptide, with or without the RGDS cell-adhesive peptide sequence, and a high molecular weight (2 MDa) negatively charged biopolymer. The peptides, $K_2(QL)_6K_2$ and $K_2(QL)_6K_2RGDS$, were synthesized and purified successfully (MS and HPLC spectra provided in the supporting information). The multidomain $K_2(QL)_6K_2$ peptide (Figure VI.1.A) consists of an ABA block motif[35] comprising a central block of glutamine-leucine (QL) repeats and two flanking positively charged lysines (K). Different variations of these multidomain peptides[37-38] have been previously synthesized and demonstrated to self-assemble into well-defined nanofibers[35] with various bioactive epitopes.[38-39] On the other hand, HA (Figure VII.1.B) was selected due to its intrinsic polyanionic nature, linear unbranched random-coil structure, biocompatibility, low immunogenicity, and large size[40]. Furthermore, its presence in the natural ECM of many tissues and role in cellular signaling and wound healing makes it a highly attractive molecule to serve as a building block of a self-assembled biomimetic scaffold.

Fabrication of Smooth Membranes

When the $K_2(QL)_6K_2$ peptide solution (1 wt%) was added at a 1:1 ratio (v/v) to the high molecular weight hyaluronic acid solution (1 wt%), a membrane was obtained at the interface between the two solutions. However, the order in which the two solutions were combined (HA over the peptide or vice-versa) resulted in strikingly different types of membranes (Figures VII.2. and .3.).

Furthermore, time and temperature variations during the self-assembly and incubation of the membranes were also investigated and resulted in significant variations.

As expected, combining the viscous HA solution with the peptide solution enabled the continuous growth of a self-assembled membrane, with its thickness increasing over time from 4 to 24 h after initial contact (Figure VII.2).
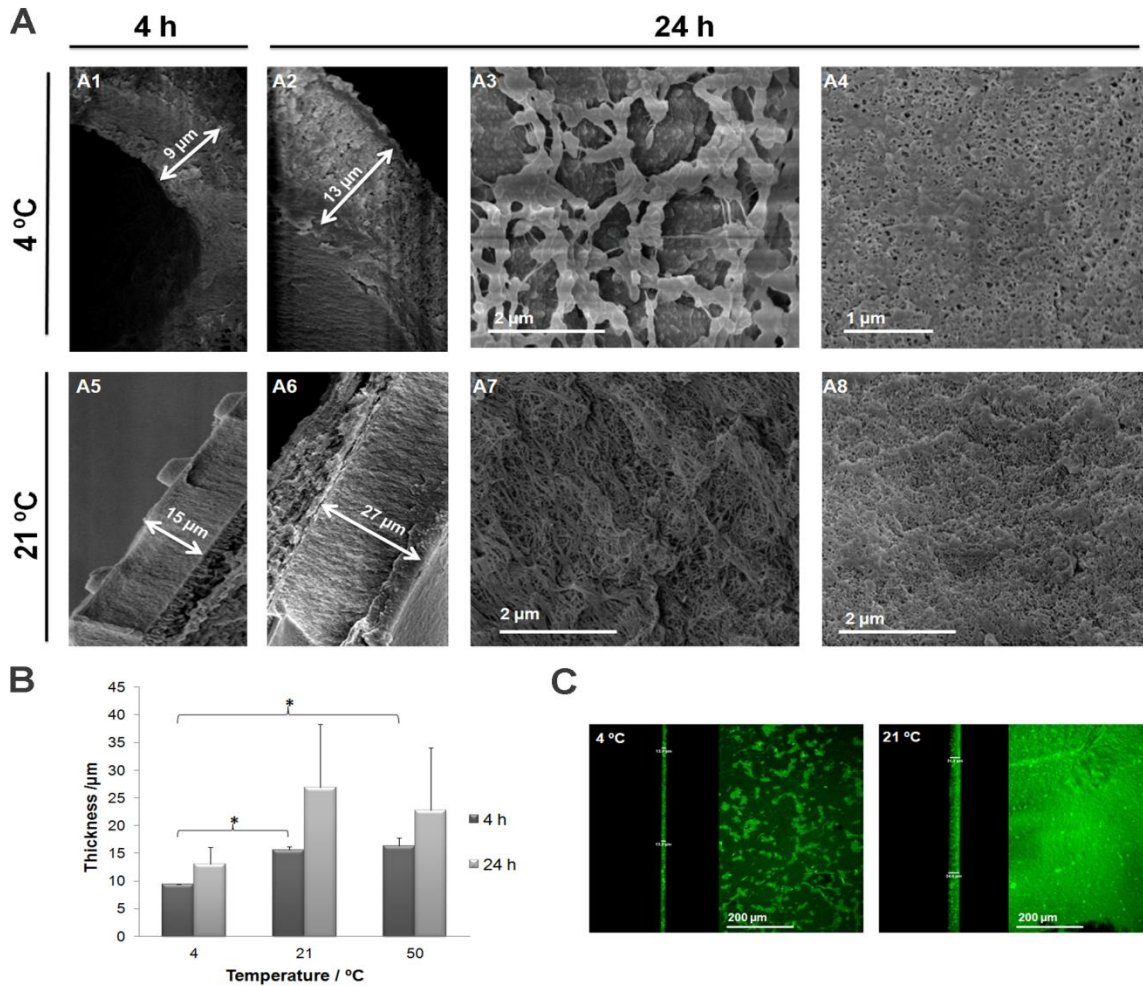
Figure VII.2. SEM images of membranes fabricated with peptide on top of hyaluronic acid solution showing the membrane cross-sections at 4 ⁰C (A1, A2) and 21 ⁰C (A5, A6) after 4 and 24 h of incubation and surface morphology on the HA side (A3, A7) and peptide side (A4, A8). Graph in B shows the increase in membrane thickness, measured by SEM, with increasing time and temperature (* indicates a significant difference $p < 0.05$) between conditions). C are confocal microscopy images of the membranes with fluorescein-HA formed after 4 h of incubation showing the distribution of fluorescent labeled HA over the membrane as well as the increase in the membrane thickness with temperature.

This time-dependency is consistent with that reported by Capito et al., when mixing HA with a different self-assembling peptide[4]. When the HA solution was positioned on top of the peptide, 4 h after initial contact, the membranes exhibited an increase in thickness from 4 °C (9.37 ± 0.064 µm) up to 21 °C (15.55 ± 0.70 µm) to 50 °C (16.34 ± 1.40 µm) (Figure VII.2.B). A similar increase was observed 24 h after contact from 4 °C (13.06 ± 2.99 µm) to 21 °C (26.84 ± 11.48 µm), but not from 21 °C to 50 °C (22.82 ± 11.21 µm). In addition, SEM observations revealed distinct surface morphologies on both sides of the membrane depending on the temperature. The surface of the HA-side at 4 °C (Figure VII.2.A3) exhibited a higher heterogeneity associated with the presence of HA aggregates compared to the HA-side of membranes at 21 °C (Figure VII.2.A7). This increase in surface homogeneity of the HA side and membrane thickness from 4 °C to 21 °C may be a result of better diffusion and consequent enhanced interaction between HA and peptide molecules owing to the higher temperature during the self-assembly. Furthermore, confocal microscopy of membranes assembled with a fluorescently tagged HA enabled visualization of the distribution of HA through the membrane cross-section. The images in Figure VII.2.C show that membranes assembled at 4 °C exhibited less fluorescence, suggesting an incomplete mixing of the components due to restricted mobility of the HA at lower temperatures. At 50 °C (data not shown), the membranes presented similar surface morphology and statistically similar thickness to those obtained at 21 °C, supporting our hypothesis.

Assuming the significance of electrostatic interactions on the self-assembly of the $K_2(QL)_6K_2$ peptide, we investigated the zeta potential of HA and peptide solutions at the different temperatures. It was found that at neutral pH the zeta potential of the peptide tended to decrease with an increase in temperature from 4 °C to 21 °C (Figure VII.1.A, from 21 to 50 °C no significant change was observed), while the value for hyaluronic acid increased considerably across the whole temperature range (Figure VII.1.B). The zeta potential is associated with the stability of charged aggregates in solution, and in this case should correlate to the total electrostatic charge of the molecules[4]. The greater values of the zeta potential obtained at higher temperatures, may indicate that at 21 °C and 50 °C the mobility of the HA chains is increased, allowing better diffusion of the two components into each other, resulting in thicker and more robust membranes. Similarly, Capito and co-workers[4] found that their self-assembled sacs were formed with greater physical integrity when both solutions had strong zeta potentials of opposite charge.

In addition to temperature and time, the experimental setup (e.g. peptide solution cast on top of HA solution or vice-versa), played a crucial role in the surface and cross-section morphology of the assembled membranes. When the peptide solution was positioned on top of the more viscous HA solution, a thin film was initially formed at the interface between the components,

due to limited diffusion of the peptide into the viscous HA solution. This phenomenon would be accentuated at 4 $^{\circ}$C because of the reduction in mobility of the molecules, resulting in a membrane with two distinct layers (Figure VII.3.A1).
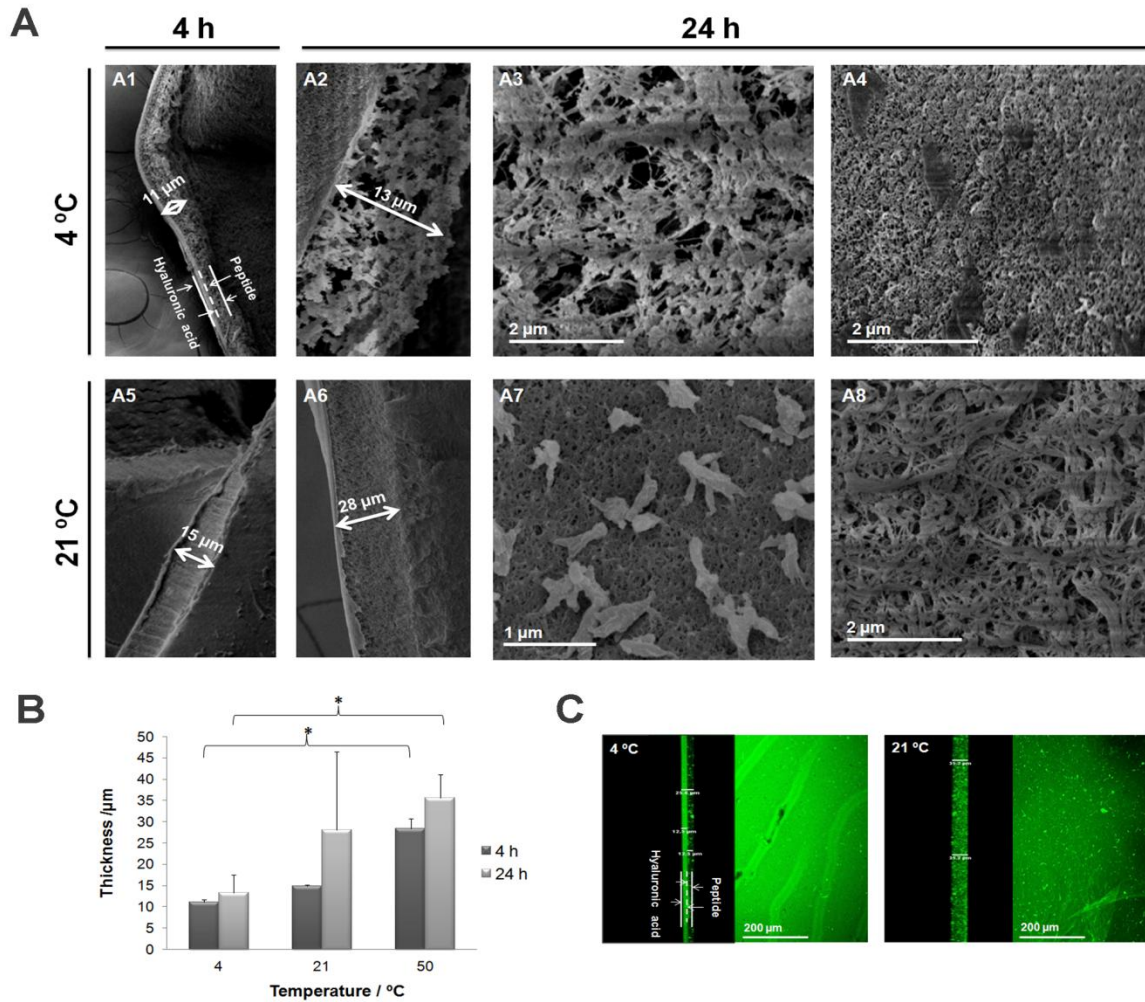
Figure VII.3. SEM images of membranes fabricated with hyaluronic acid on top of the peptide solution showing the membrane cross-sections at 4 $^{\circ}$C (A1, A2) and 21 $^{\circ}$C (A5, A6) after 4 and 24 h of incubation and surface morphology on the HA side (A3, A7) and peptide side (A4, A8). Graph in B shows the increase in membrane thickness, measured by SEM, with increasing time and temperature (* indicates a significant difference, $p < 0.05$) between conditions). C are confocal microscopy images of the membranes with fluorescein-HA formed after 4 h of incubation showing the distribution of fluorescent labeled HA over the membrane as well as the increase in membrane thickness with temperature.

The bilayer membrane obtained at 4 $^{\circ}$C was confirmed by confocal microscopy, where a dense, green layer of fluorescent HA can be distinguished from a darker region attributed to the peptide layer (Figure VII.3.C). When the temperature was increased to 21 $^{\circ}$C, although the presence of

nano-fibers was observed, confirming a degree of self-assembly occurred; HA fragments could still be seen on one side of the membrane (Figure VII.3.A7).

Based on these findings, it was hypothesized that by applying the more viscous HA solution over the less viscous peptide, faster and more efficient diffusion of the HA into the peptide would occur. This would result in membranes with a more homogenous structure. Figure VII.2. shows SEM and confocal images of the cross-sections of membranes formed in this manner. As expected, the membranes consist of a single uniform layer made up of densely packed nano-fibers.

The optimum time and temperature for the membrane fabrication process were therefore considered to be 24 h, 21 °C, respectively, with the addition of the HA solution to the top of the peptide solution used as the experimental setup. These conditions were subsequently selected for the preparation of membranes for further studies.

Topographically Patterned Membranes

The two-dimensional (2D) patterning of self-assembling peptides has been previously described in the literature[41-42], Mata *et al*[13], proposed a three-dimensional (3D) patterning method applied to peptide amphiphiles that resulted in substrates capable of enhancing osteoblastic differentiation of MSCs. However, this fabrication process required further chemical modification of the peptide to enable photo-crosslinking in order to form the desired patterns. More recently, we reported on a drop casting/evaporation technique to create thin bioactive membranes based on recombinant elastin-like polymers[15]. While this process allowed the generation of self-supporting structures and the incorporation of both physical and biomolecular signals, it also required chemical cross-linking and lacked the biomimetic nanofibrous architecture. The present study aimed to overcome these limitations by relying solely on molecular co-assembly and soft lithography, resulting in precise biomimetic nanofibers, bioactive microtopographies, and self-supporting macroscopic membranes. Considering the lower resistance provided by the peptide solution (less viscous) to the diffusion of the HA molecules, we decided to cast first the peptide solution onto the hydrophilic patterned PDMS in order to guarantee that the solution would fill all the spaces in the molds, which in turn can guide their self-assembly, resulting in effective transference of the patterns (Figure VII.4.C).
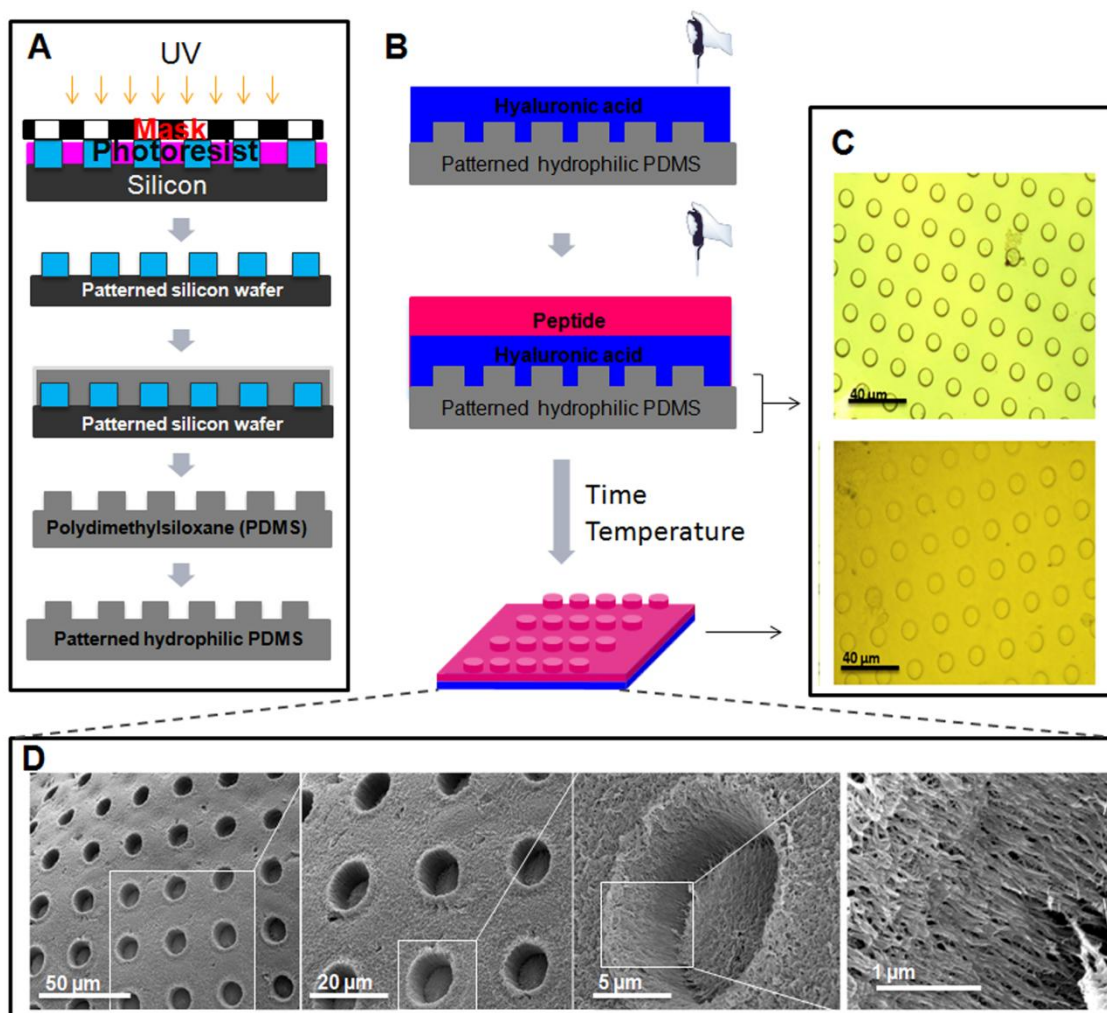
Figure VII.4. (A) SU8-10 photoresist-coated Si wafer patterned by photolithography and the following steps of the microfabrication process; (B) Membrane fabrication over the patterned PDMS mold; (C) Images obtained by bright field microscopy of the patterned PDMS mold and patterned peptide–HA membrane after removal from the mold confirming the success of the transference of the patterns; (D) SEM images and zoom-in of the patterned membrane surface demonstrating the fibrilar network resulting from the self-assembly of the $K_2(QL)_6K_2$ peptide triggered by HA.

Using this approach, membranes displaying posts (Figure VII.5.A and D), holes (Figure VII.4.-D and Figure VII.5.E), channels (Figure VII.5.C), and pores (Figure VII.5.F) ranging from 10 to 20 μm in lateral dimension were successfully produced. Figure VII.5. (B) shows an image of the cross section of a membrane demonstrating the absence of distinct regions. The fabrication of patterned membranes with the peptide cast on top of the HA was also attempted, however the structures exhibited distortions and the quality was considerably inferior. In this case, the use of a top mold to press the setup from above may be necessary to improve the lithographic process.
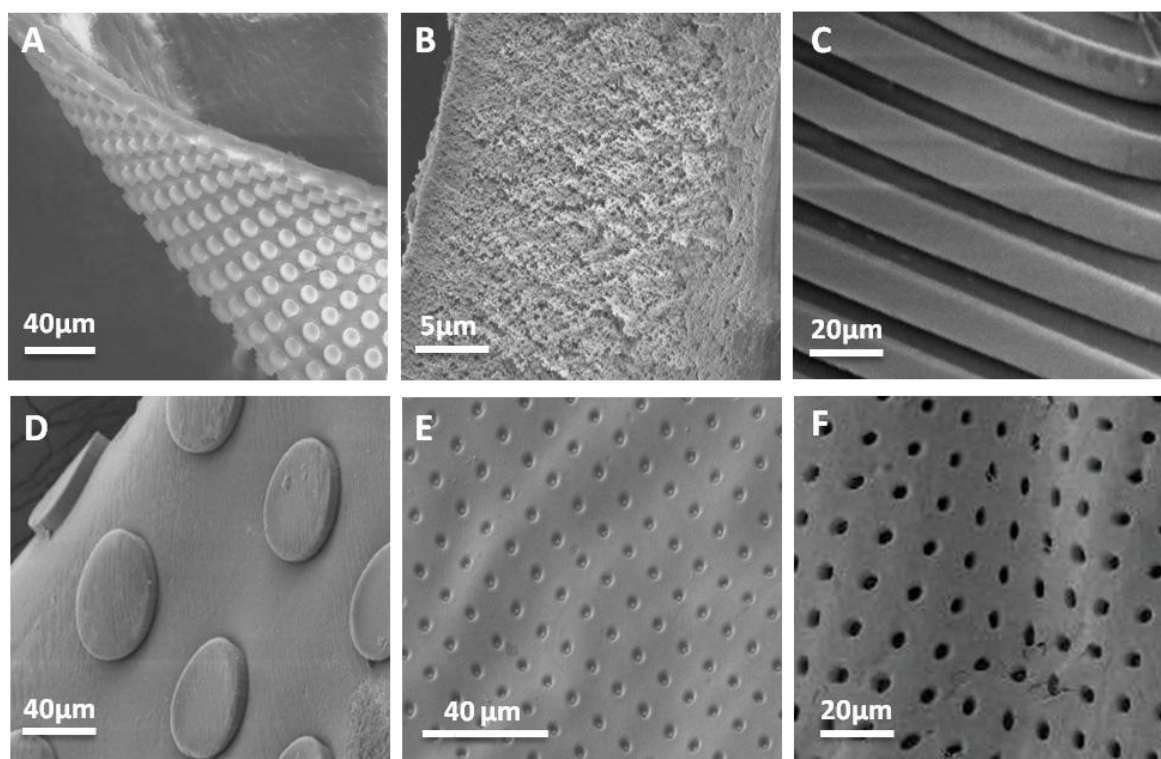
Figure VII.5. SEM micrographs showing membranes with different patterned geometries: posts 10 (A) and 20 (D) µm in diameter, channels (C), pores 5 µm in diameter (F), B displays an image of a membrane cross-section confirming the absence of distinct regions, E is a high magnification image of a post and (inset) the nanofibrilar membrane structure.

Control of membrane thickness is recognized as being of extreme importance in the application of bioengineered scaffolds for tissue engineering applications[43]. We show here that it is possible to vary membrane thickness by changing the time and/or temperature during the molecular co-assembly process. Moreover, the membrane complexity can be increased by the combination of top-down and bottom-up methodologies. Examples of this have previously been reported in the literature[13,15], however, for the membranes presented in this work, the topographical patterns are incorporated into the membrane structure during the self-assembly process. The versatility of these membranes to incorporate a variety of geometrical shapes is of extreme relevance, as it opens up the possibility to include specific physical signals that can be tailored to the specific application and designed to interact with cells on different length scales. Reproducible patterns were obtained over large regions of the membranes, which is a major criterion in the development of tissue engineered scaffolds, where sizeable surface areas are desirable for enhancing cell interactions[15].

Biological Assessment

In order to investigate the effects of the physical guidance provided by topographies and the biomolecular signaling by the incorporated RGDS, rat mesenchymal stem cells (rMSCs) were cultured on the membranes. The difference in cell adhesion on the HA side versus the peptide side for smooth membranes was analyzed. In addition, the effect of different proportions of the RGDS sequence within the peptide component of the membranes was assessed, as well as, the effect of the topographical patterns.

Rat MSCs were observed to adhere to both sides of the membrane, as well as to interact with the RGDS-containing peptide nanofibers, as shown in Figure VII.6..
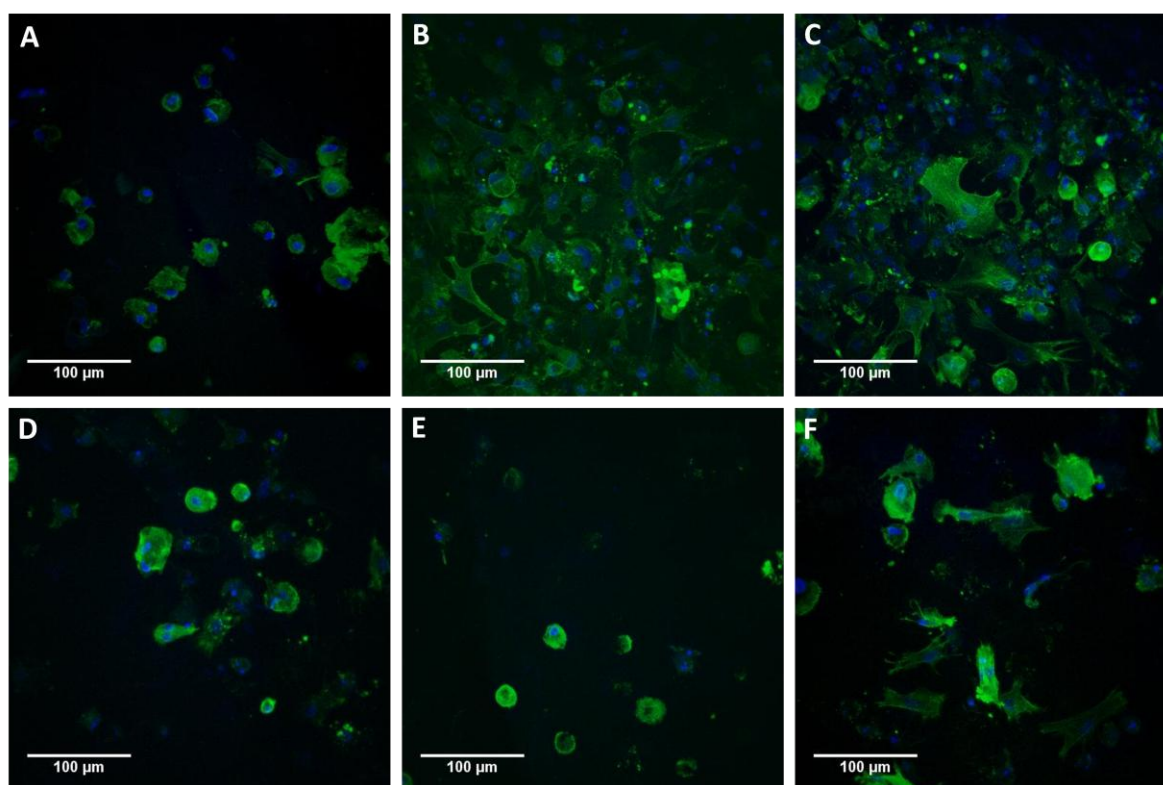
Figure VII.6. Confocal microscopy images showing the actin cytoskeleton (green) and nuclei (blue) of rMSCs cultured for 18 h on the surface of smooth membranes with different percentages of RGDS: (A-C) peptide side, (D-F) hyaluronic acid side. (A,D) no RGDS, (B,E) 10% RGDS and, (C,F) 30% RGDS.

Without the RGDS cell binding sequence, the cells remained round without a well-defined actin cytoskeleton, appearing similar on both sides of the membrane. However, for the membranes containing the RGDS motif rMSCs tended to attach and spread when cultured on the peptide side, exhibiting a well defined actin cytoskeleton (Figure VII.6.A). In contrast, on the HA side

they maintained a rounded morphology (Figure VII.6.B) and a lower number of attached cells were evident. Interestingly, for the membranes prepared with 30% RGDS, there was a slight increase in the degree of spreading of the cells cultured on the HA side. It is possible that a small quantity of the peptide solution diffused completely through the HA during the assembly process, and due to the high RGDS concentration in this instance, a proportion of the adhesion motif was displayed on the HA surface.

Although hyaluronic acid has previously been considered as a mediator of cell adhesion[44], it is clearly not as effective as the RGDS sequence. It has been demonstrated that a number of cell-surface integrins have the ability to recognize the RGD peptide sequence[45-47], and there is a great deal of evidence showing strong cell adhesion to substrates displaying this peptide motif as has been demonstrated in the present study. This particular peptide motif was used in this work as a proof of principle. However, owing to the peptide molecular design, it would be extremely easy to incorporate an alternative signaling sequence in order to elicit more specific cellular responses.
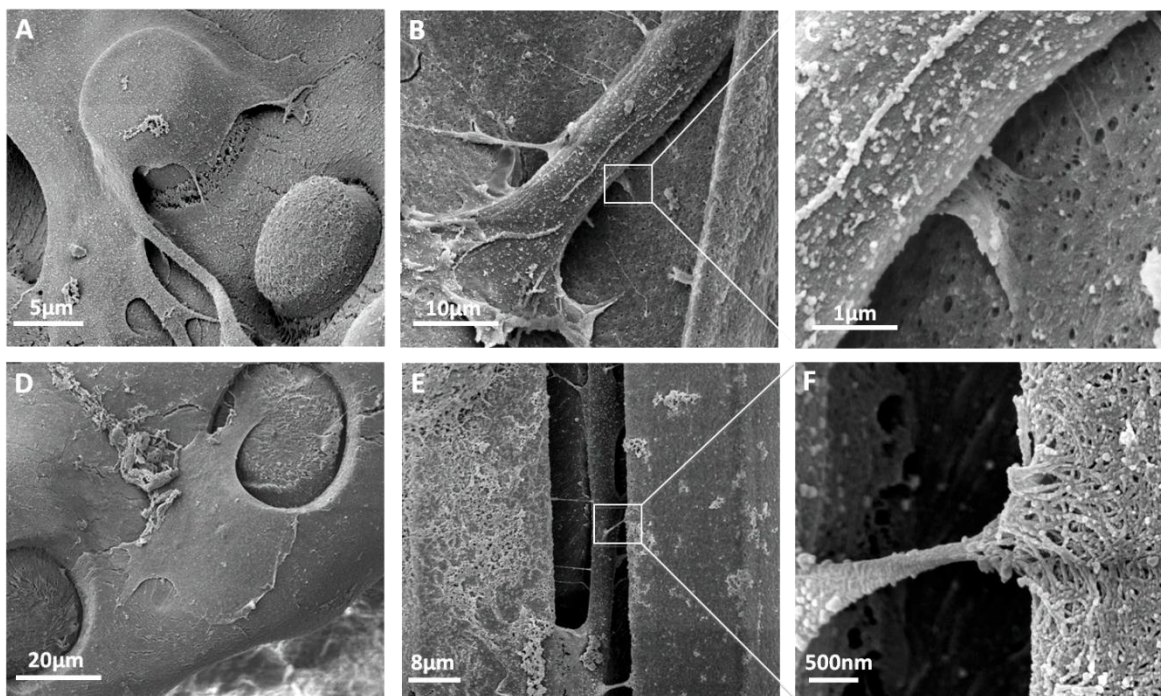
Figure VII.7. SEM micrographs showing differences in cell morphology when cultured on smooth membranes and those patterned with different topographies: (A) posts 10 µm in diameter, (B,C) smooth, (D) holes 20 µm in diameter and (E,F) channels 10 µm across.

It is well known that cell morphology can not only be modulated by epitope availability, but that physical signaling provided by topographical surface patterns can also have a noticeable effect. In this work, rMSCs were cultured on smooth and patterned membranes and their morphologies were assessed. In Figure VII.7., SEM images show that cells on the smooth membrane were randomly oriented. In contrast, when cells were seeded on membranes patterned with channels, they tended to align and spread along them, growing both on the ridges and within the channels. Cells also adapted their morphology when cultured on posts or holes. Similar behavior was observed by Tejeda and co-workers when culturing rMSCs on elastin like-polymer (ELP) membranes[15] with patterned channels. Figure VII.7 also contains high magnification images showing the cell filopodia attached to the membrane fibers.

These results confirm the potential of combining both biomolecular and physical features to act synergistically to elicit specific biological responses, such as cell proliferation or differentiation. Moreover, we have produced a membrane intrinsically containing these properties: fibrilar nanostructure (as a result of self-assembly), epitope availability (biomolecular signals), and micro-patterns (topographic signals). The fabrication process for producing these membranes enables each of these features to be incorporated in a single step, without the need for additional chemical modifications of the molecules or post-assembly treatments.

4. CONCLUSIONS

In summary, a self-supporting bioactive membrane was produced through the self-assembly of a positively charged multidomain peptide triggered by a negatively charged high molecular weight polymer. The growth and structure of the membranes were seen to be affected by assembly time and temperature in addition to the positioning of components (peptide on top or bottom of HA). A biomolecular signaling motif was incorporated into the membranes, and the proportion of this could be easily controlled by varying the composition of the peptide solution prior to assembly. Topographical features could be incorporated into the membrane structure during its formation, removing the requirement for post-assembly fabrication steps. Rat MSCs were observed to recognize the RGDS cell adhesion sequence and the topographical patterns, varying their morphology depending on the concentration of binding motif or specific physical features that were cultured on. The simultaneous integration of bottom-up and top-down fabrication processes described here permit the development of hierarchical macrostructures made from well-defined nanofibers and microtopographies that together provide precise biomolecular and physical properties. The numerous possibilities to better tune them with spatio-temporal and biomimetic control provide a broad spectrum of potential applications in tissue engineering and regenerative medicine.

ACKNOWLEDGEMENTS

REFERENCES

1. Sanchez C, Arribart H, Guille MMG. Biomimetism and bioinspiration as tools for the design of innovative materials and systems. Nature Materials 2005;4(4):277-288.

2. Huebsch N, Mooney DJ. Inspiration and application in the evolution of biomaterials. Nature 2009;462(7272):426-432.

3. O'Leary LER, Fallas JA, Bakota EL, Kang MK, Hartgerink JD. Multi-hierarchical self-assembly of a collagen mimetic peptide from triple helix to nanofibre and hydrogel. Nature Chemistry 2011;3(10):821-828.

4. Capito RM, Azevedo HS, Velichko YS, Mata A, Stupp SI. Self-assembly of large and small molecules into hierarchically ordered sacs and membranes. Science 2008;319(5871):1812-1816.

5. Carvajal D, Bitton R, Mantei JR, Velichko YS, Stupp SI, Shull KR. Physical properties of hierarchically ordered self-assembled planar and spherical membranes. Soft Matter 2010;6(8):1816-1823.

6. Chow LW, Bitton R, Webber MJ, Carvajal D, Shull KR, Sharma AK, Stupp SI. A bioactive self-assembled membrane to promote angiogenesis. Biomaterials 2011;32(6):1574-1582.

7. Chung WJ, Oh JW, Kwak K, Lee BY, Meyer J, Wang E, Hexemer A, Lee SW. Biomimetic self-templating supramolecular structures. Nature 2011;478(7369):364-368.

8. Smith KH, Tejeda-Montes E, Poch M, Mata A. Integrating top-down and self-assembly in the fabrication of peptide and protein-based biomedical materials. Chemical Society Reviews 2011;40(9):4563-4577.

9. Zhang SG, Yan L, Altman M, Lassle M, Nugent H, Frankel F, Lauffenburger DA, Whitesides GM, Rich A. Biological surface engineering: a simple system for cell pattern formation. Biomaterials 1999;20(13):1213-1220.

10. Xia YN, Whitesides GM. Soft lithography. Annual Review of Materials Science 1998;28:153-184.

11. Nie ZH, Kumacheva E. Patterning surfaces with functional polymers. Nature Materials 2008;7(4):277-290.

12. Park M, Harrison C, Chaikin PM, Register RA, Adamson DH. Block copolymer lithography: Periodic arrays of similar to 10(11) holes in 1 square centimeter. Science 1997;276(5317):1401-1404.

13. Mata A, Hsu L, Capito R, Aparicio C, Henrikson K, Stupp SI. Micropatterning of bioactive self-assembling gels. Soft Matter 2009;5(6):1228-1236.

14.   Mata A, Kim EJ, Boehm CA, Fleischman AJ, Muschler GF, Roy S. A three-dimensional scaffold with precise micro-architecture and surface micro-textures. Biomaterials 2009;30(27):4610-4617.

15.   Tejeda-Montes E, Smith KH, Poch M, Lopez-Bosque MJ, Martin L, Alonso M, Engel E, Mata A. Engineering membrane scaffolds with both physical and biomolecular signaling. Acta Biomaterialia 2012;8(3):998-1009.

16.   Teixeira AI, Abrams GA, Bertics PJ, Murphy CJ, Nealey PF. Epithelial contact guidance on well-defined micro- and nanostructured substrates. Journal of Cell Science 2003;116(10):1881-1892.

17.   Teixeira AI, McKie GA, Foley JD, Berticsc PJ, Nealey PF, Murphy CJ. The effect of environmental factors on the response of human corneal epithelial cells to nanoscale substrate topography. Biomaterials 2006;27(21):3945-3954.

18.   Craighead HG, James CD, Turner AMP. Chemical and topographical patterning for directed cell attachment. Current Opinion in Solid State & Materials Science 2001;5(2-3):177-184.

19.   Mata A, Boehm C, Fleischman AJ, Muschler G, Roy S. Analysis of connective tissue progenitor cell behavior on polydimethylsiloxane smooth and channel micro-textures. Biomedical Microdevices 2002;4(4):267-275.

20.   Mata A, Boehm C, Fleischman AJ, Muschler GF, Roy S. Connective tissue progenitor cell growth characteristics on textured substrates. International Journal of Nanomedicine 2007;2(3):389-406.

21.   Dalby MJ, Gadegaard N, Tare R, Andar A, Riehle MO, Herzyk P, Wilkinson CDW, Oreffo ROC. The control of human mesenchymal cell differentiation using nanoscale symmetry and disorder. Nature Materials 2007;6(12):997-1003.

22.   McMurray RJ, Gadegaard N, Tsimbouri PM, Burgess KV, McNamara LE, Tare R, Murawski K, Kingham E, Oreffo ROC, Dalby MJ. Nanoscale surfaces for the long-term maintenance of mesenchymal stem cell phenotype and multipotency. Nature Materials 2011;10(8):637-644.

23.   Wang GJ, Hsueh CC, Hsu SH, Hung HS. Fabrication of PLGA microvessel scaffolds with circular microchannels using soft lithography. Journal of Micromechanics and Microengineering 2007;17(10):2000-2005.

24.   Suh KY, Seong J, Khademhosseini A, Laibinis PE, Langer R. A simple soft lithographic route to fabrication of poly(ethylene glycol) microstructures for protein and cell patterning. Biomaterials 2004;25(3):557-563.

25.   Steedman MR, Tao SL, Klassen H, Desai TA. Enhanced differentiation of retinal progenitor cells using microfabricated topographical cues. Biomedical Microdevices 2010;12(3):363-369.

26.   LeBleu VS, MacDonald B, Kalluri R. Structure and function of basement membranes. Experimental Biology and Medicine 2007;232(9):1121-1127.

27.   Malizos KN, Papatheodorou LK. The heating potential of the periosteum Molecular aspects. Injury-International Journal of the Care of the Injured 2005;36:13-19.

28.   Lawrence BD, Marchant JK, Pindrus MA, Omenetto FG, Kaplan DL. Silk film biomaterials for cornea tissue engineering. Biomaterials 2009;30(7):1299-1308.

29.   MacNeil S. Progress and opportunities for tissue-engineered skin. Nature 2007;445(7130):874-880.

30.   Shi CY, Chen W, Zhao YN, Chen B, Xiao ZF, Wei ZL, Hou XL, Tang J, Wang ZX, Dai JW. Regeneration of full-thickness abdominal wall defects in rats using collagen scaffolds loaded with collagen-binding basic fibroblast growth factor. Biomaterials 2011;32(3):753-759.

31.   Gao J, Liu JZ, Gao Y, Wang C, Zhao YN, Chen B, Xiao ZF, Miao Q, Dai JW. A Myocardial Patch Made of Collagen Membranes Loaded with Collagen-Binding Human Vascular Endothelial Growth Factor Accelerates Healing of the Injured Rabbit Heart. Tissue Engineering Part A 2011;17(21-22):2739-2747.

32.   Warnke PH, Douglas T, Sivananthan S, Wiltfang J, Springer I, Becker ST. Tissue engineering of periosteal cell membranes in vitro. Clinical Oral Implants Research 2009;20(8):761-766.

33.   Stamatialis DF, Papenburg BJ, Girones M, Saiful S, Bettahalli SNM, Schmitmeier S, Wessling M. Medical applications of membranes: Drug delivery, artificial organs and tissue engineering. Journal of Membrane Science 2008;308(1-2):1-34.

34.   Velichko YS, Mantei JR, Bitton R, Carvajal D, Shull KR, Stupp SI. Electric Field Controlled Self-Assembly of Hierarchically Ordered Membranes. Advanced Functional Materials 2012;22(2):369-377.

35.   Dong H, Paramonov SE, Aulisa L, Bakota EL, Hartgerink JD. Self-assembly of multidomain peptides: Balancing molecular frustration controls conformation and nanostructure. Journal of the American Chemical Society 2007;129(41):12468-12472.

36.   Gajewiak J, Cai S, Shu XZ, Prestwich GD. Aminooxy Pluronics: Synthesis and Preparation of Glycosaminoglycan Adducts. Biomacromolecules 2006;7(6):1781-1789.

37. Aulisa L, Dong H, Hartgerink JD. Self-Assembly of Multidomain Peptides: Sequence Variation Allows Control over Cross-Linking and Viscoelasticity. Biomacromolecules 2009;10(9):2694-2698.

38. Galler KM, Aulisa L, Regan KR, D'Souza RN, Hartgerink JD. Self-Assembling Multidomain Peptide Hydrogels: Designed Susceptibility to Enzymatic Cleavage Allows Enhanced Cell Migration and Spreading. Journal of the American Chemical Society 2010;132(9):3217-3223.

39. Galler KM, Hartgerink JD, Cavender AC, Schmalz G, D'Souza RN. A Customized Self-Assembling Peptide Hydrogel for Dental Pulp Tissue Engineering. Tissue Engineering Part A 2012;18(1-2):176-184.

40. Allison DD, Grande-Allen KJ. Review. Hyaluronan: A powerful tissue engineering tool. Tissue Engineering 2006;12(8):2131-2140.

41. Biesalski MA, Knaebel A, Tu R, Tirrell M. Cell adhesion on a polymerized peptide-amphiphile monolayer. Biomaterials 2006;27(8):1259-1269.

42. Stroumpoulis D, Zhang HN, Rubalcava L, Gliem J, Tirrell M. Cell adhesion and growth to peptide-patterned supported lipid membranes. Langmuir 2007;23(7):3849-3856.

43. Uygun BE, Bou-Akl T, Albanna M, Matthew HWT. Membrane thickness is an important variable in membrane scaffolds: Influence of chitosan membrane structure on the behavior of cells. Acta Biomaterialia 2010;6(6):2126-2131.

44. Cohen M, Joester D, Geiger B, Addadi L. Spatial and temporal sequence of events in cell adhesion: From molecular recognition to focal adhesion assembly. Chembiochem 2004;5(10):1393-1399.

45. Salinas CN, Anseth KS. The influence of the RGD peptide motif and its contextual presentation in PEG gels on human mesenchymal stem cell viability. Journal of Tissue Engineering and Regenerative Medicine 2008;2(5):296-304.

46. Frith JE, Mills RJ, Cooper-White JJ. Lateral spacing of adhesion peptides influences human mesenchymal stem cell behaviour. Journal of Cell Science 2012;125(2):317-327.

47. Ruoslahti E. RGD and other recognition sequences for integrins. Annual Review of Cell and Developmental Biology 1996;12:697-715.

Section 4

CONCLUSIONS AND OUTLOOK

Chapter VIII

GENERAL CONCLUSIONS AND FUTURE PERSPECTIVES

Cell encapsulation technology holds promise in various areas of medicine and some important applications are, for example, treatment of diabetes and production of biologically important therapeutics. The hope that encapsulated cells might be used as a therapeutic strategy is increasingly being recognized and is expected to have enormous potential in medicine in the near future. However, to be a viable complement to the current methods of cell transplantation therapy, encapsulation technology has to fulfill the strict requirements necessary to these types of therapeutic strategies, like performance, biosafety, biocompatibility, stability, availability, purity, characterization and cost. It is widely understood that in order to encapsulate living cells within an artificial matrix, the encapsulating conditions must not damage the living cells and the matrix material must be biocompatible and at the same time provide a natural microenvironment for cells to sustain their viability, function, and growth. The mechanical strength of the encapsulating matrix is also critical, particularly when long-term implantation is envisaged. The mechanical strength is essential for maintaining the matrix integrity and to withstand manipulations associated with *in vitro* culture, implantation and *in vivo* existence. Moreover, it is essential that the matrix should be permeable to ensure sufficient diffusion of nutrients and the removal of secreted metabolic waste products, to sustain the survival and function of encapsulated cells. Thus, there is a need for relatively mild cell encapsulation methods, which offers control over properties of the encapsulating matrix. An exciting approach for cell delivery is the use of materials that can self-assemble in conditions that are cell-compatible and into structures that can be injected into the body (e.g. microcapsules). Self-assembly can occur through a change in temperature, pH or ion concentration or be triggered by radiation. This approach enables the clinician to transplant the cell and material combination in a minimally invasive way.

Although xanthan gum has been widely used in food and pharmaceutical industry, because of the encouraging reports on xanthan biosafety, the use of this polysaccharide has not been fully explored as a biomaterial. We have, thus, hypothesized that its unique chemical structure could offer very interesting rheological and functional properties in cell encapsulatitechnology. The overall goal of the work presented in this thesis was to develop novel biomaterial systems, microcapsules and membranes, for cell encapsulation and culture, respectively. Bottom-up and top-down approaches, based on self-assembly and microfabrication methods, were combined and explored to develop the proposed systems.

To obtain stable microcapsules, we have investigated the potential of xanthan gum and its derivatives to form encapsulating matrices in physiological conditions, and capsule-forming devices (micro-droplet generator and micro-fluidics) for reproducibly generating capsules with controlled shape and micro-size range. The materials and microcapsules were characterized and evaluated for their biological response *in vitro*. The results of these studies show that cells can be encapsulated, remaining viable within the developed microcapsules. To the best of our knowledge, this dissertation is the first work to report the use of xanthan gum as cell encapsulating matrix. It was also hypothesized that microscale features, incorporated on self-assembled membranes exhibiting simultaneously biomolecular signals (RGDS cell-adhesive sequence), could provide instructive cues to cells. Cell adhesion, spreading, and morphology were significantly affected by the surface topographical patterns and the different densities of RGDS.

It is object of the present chapter to summarize the significant findings in the experiments presented in the preceding chapters and describe how the conclusions address the aforementioned hypotheses.

Xanthan is able to form self-supporting gels in the presence of ions, although they are not stable in the long term when placed in aqueous solutions. In the present PhD investigation, we have performed chemical modification of xanthan to evaluate its potential as a cell encapsulation matrix. In a first attempt, xanthan was carboxymethylated (carboxymethyl xanthan, CMX) to increase the number of carboxylic groups available for ionic crosslinking. Simultaneously, a simple micro-droplet generator (as alternative to the common sophisticated microfluidic systems) was developed to produce CMX microcapsules with reduced size (comparatively to capsules obtained manually) and spherical shape. The microcapsules generated from xanthan in its carboxymethylated form were shown to be stable in the long-term and able to encapsulate chondrocytic cells. Encapsulated cells showed enhanced viability, proliferation and retained the property of forming cell aggregates comparatively to the ones encapsulated in alginate microcapsules produced in similar conditions. In conclusion, these studies suggest that CMX can be an alternative to the current cell encapsulating materials, but *in vivo* studies are necessary to confirm our hypothesis.

Most of the biological systems found in the Nature are hierarchically structured and organized at nano, micro and meso scale, presenting unique and multi-functional properties. Molecular self-assembly provides the opportunity to design reproducible biomimetic materials with known and controllable chemistry, organized at nano-scale, being an appellative approach for cell encapsulation. In that respect, xanthan based amphiphilic systems were developed to self-

assemble into hollow capsular structures in physiological conditions and encapsulate cells. In one attempt, the hydrophilic xanthan was reacted with hydrophobic palmitoyl chloride in a single step. The amphiphilic character imparted to native xanthan only by certain palmitoyl ratio allowed the supramolecular rearrangement of palmitoyl xanthan into nano-fibrilar structures when placed in aqueous media. Palmitoyl xanthan was able to form stable and robust hollow capsules by self-assembly in physiological ion concentration and pH. The capsule morphology was revealed to be highly organized in lamellar nanostructures. Capsules with uniform spherical shape and micro-size were then obtained using the micro-droplet generator previously developed. Cells encapsulated in the palmitoyl xanthan microcapsules were shown to remain viable and proliferate for longer periods of time. The developed micro-droplet generator demonstrated high versatility to be used as microcapsule generator device allowing working with a variety of polymer systems and the generation of microcapsules by different processes (ionic cross-linking, self-assembly) in physiological conditions for encapsulation of cells. Knowing the amphipathic nature of phospholipids and their role in biological membranes, the second attempt consisted on using a similar strategy to attach 1,2-Dioleoyl-*sn*-glycero-3-phosphoethanolamine (DOPE) phospholipid to xanthan through the standard carbodiimide chemistry. Xanthan-DOPE amphiphile was successfully synthesized with ability to self-assemble into stable hollow capsular structures when subjected to physiological ion concentrations. In this case, the self-assembled phospholipid-xanthan structures were converted into spherical microcapsules by means of microfluidics technology. Stable microcapsules were obtained with ability to support and enhance cellular metabolic activity *in vitro*. A particular advantage of this system relies on the fact that the phospholipid-xanthan microcapsules did not require an external coat with poly-L-Lysine, as described for the CMX and palmitoyl xanthan microcapsules, avoiding potential immunological problems. The successful self-assembly of amphiphilic xanthan and their conversion into stable microcapsules using microfluidics encouraged us to explore new self-assembling systems. Following this approach, robust microcapsules were developed when combining the negatively charged xanthan with a positively charged self-assembling peptide. The properties of the self-assembled microcapsules, generated by microfluidics technology, were controlled by changing peptide concentration. It was demonstrated that the concentration played an important role in the morphology, size, and permeability of the microcapsules. The optimized processing conditions enabled generating homogenous-size microcapsules with long-term stability and the ability to support the survival and function of encapsulated cells over prolonged time. This set of experiments and data show that several aims proposed in this thesis were satisfactorily achieved, namely i) the use of xanthan gum as potential cell encapsulation

matrix and ii) production of microcapsules with homogeneous size distribution and micrometer size favorable for mass transfer and easy injects for cell therapy, mentioned in Chapter II.

Still within the same strategy, a bioactive membrane was developed through self-assembly of a positively charged multidomain peptide triggered by the negatively charged hyaluronic acid. The growth and structure of the membranes were seen to be affected by assembly time and temperature in addition to the positioning of components (peptide on top or bottom of HA). A biomolecular signaling motif was incorporated into the membranes, and the proportion of this could be easily controlled by varying the composition of the peptide solution prior to assembly. Topographical features could be incorporated into the membrane structure during its formation, removing the requirement for post-assembly fabrication steps. Rat MSCs were observed to recognize the RGDS cell adhesion sequence and the topographical patterns, varying their morphology depending on the concentration of binding motif or specific physical features that were cultured on. The simultaneous integration of bottom-up and top-down fabrication processes described here permit the development of hierarchical macrostructures made from well-defined nanofibers and microtopographies that together provide precise biomolecular and physical properties. The numerous possibilities to better tune them with spatio-temporal and biomimetic control provide a broad spectrum of potential applications in tissue engineering and regenerative medicine.

The present thesis incrementally expanded the current scientific knowledge on considering the use of xanthan gum polysaccharide as a biomaterial. We have proposed several chemical modifications on xanthan (carboxymethylation, palmitoylation and conjugation with phospholipids) and its combination with self-assembling peptides to obtain distinct assembling pathways (ionic crosslinking, self-assembly) for the formation of stable capsules indented for cell encapsulation. In the process of developing these systems, an attempt was made to better understand the fundamental aspects of their design on their resulting functionality and performance *in vitro*. The obtained results are promising and can enhance the applicability of xanthan gum in the biomaterial field. The same approaches, described herein, can also be applied for other polysaccharides in general. Self-assembly was used in this PhD project as a nanofabrication technique. Self-assembly allows the spontaneous organization of individual building blocks into ordered and stable nanostructures by noncovalent interactions. We have used negatively charged polysaccharides with self-assembling peptides of opposite charge to direct their self-assembly into cylindrical nanostructures (nanofibers). The nanofibers had diameters as small as 10 nm (significantly smaller that those obtained by electrospinning, a top-down fabrication technique). Furthermore, the peptide structures were designed to display bioactive sequences to foster the adhesion of cells. Nevertheless, since most of the self-

assembling materials are macroscopically disordered and this may limit their performance, micro-fabrication methods were applied within the scope of this PhD work to fabricate biomaterial systems with well-defined features at micro-scale. Several examples presented in this thesis proved that combining self-assembling materials with microfabrication technologies can be an effective approach to fabricate microcapsules and membranes with increased level of control over their structure, shape, bioactivity and overall performance.

A number of valuable results were obtained in this research project which will hopefully be of utility in future investigations. The development of amphiphilic xanthan systems is one the most significant contributions of this thesis. The combination of polysaccharides with self-assembling peptides of opposite charge has also contributed to the understanding on the self-assembly between large and small molecules and revealed new potential applications. In addition, the results reported in this thesis provide a deeper understanding on the properties of xanthan derivatives and their use as encapsulating matrix. While extensive work has been presented in this thesis, further studies must be performed to confirm the potential of the developed biomaterial systems, including:

- Study the *in vitro* degradation of the developed systems (microcapsules and membranes);

- Perform cell encapsulation studies with primary cells (e.g. human articular chondrocytes, stem cells) to validate the performance of the developed microcapsules;

- Undertake *in vivo* studies to assess the biocompatibility, stability and performance of the developed microcapsule systems;

- Evaluate the mechanical properties of the micropatterned self-assembled membranes and perform advanced cell culture studies to investigate in detail cell-membrane interactions, cell spreading and differentiation;

- Increase the level of biochemical complexity of the fabricated patterned membranes, such as including mineral-attracting sequences for inducing biomineralization and/or growth-factor binding sequences for directing cell differentiation, to develop truly biomimetic synthetic periosteum membranes, for example.